NASA CONTRACTOR REPORT

NASA CR-1056

NASA CR-1056

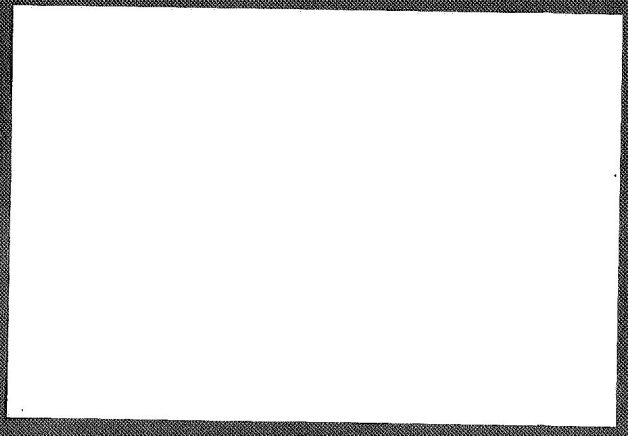

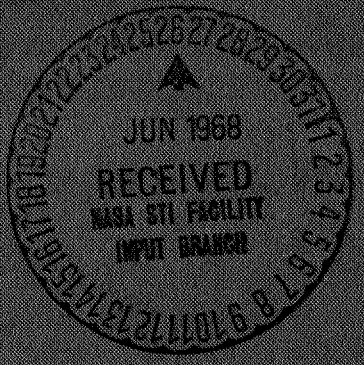

A STUDY OF TURBOFAN-ENGINE COMPRESSOR-NOISE-SUPPRESSION TECHNIQUES

by Alan H. Marsh, I. Elias, J. C. Hoehne, and R. L. Frasca

Prepared by
McDONNELL DOUGLAS CORPORATION, AIRCRAFT DIVISION
Long Beach, Calif.
for Langley Research Center

NATIONAL AERONAUTICS AND SPACE ADMINISTRATION • WASHINGTON, D. C. • JUNE 1968

NASA CR-1056

A STUDY OF TURBOFAN-ENGINE COMPRESSOR-NOISE-SUPPRESSION TECHNIQUES

By Alan H. Marsh, I. Elias, J. C. Hoehne,
and R. L. Frasca

Prepared under Contract No. NAS 1-5256 by
MCDONNELL DOUGLAS CORPORATION, AIRCRAFT DIVISION
Long Beach, Calif.

for Langley Research Center

NATIONAL AERONAUTICS AND SPACE ADMINISTRATION

For sale by the Clearinghouse for Federal Scientific and Technical Information
Springfield, Virginia 22151 – CFSTI price $3.00

CONTENTS

ILLUSTRATIONS

ILLUSTRATIONS (Continued)

LIST OF TABLES

LIST OF TABLES (Continued)

A STUDY OF TURBOFAN-ENGINE COMPRESSOR-NOISE-SUPPRESSION TECHNIQUES

By Alan H. Marsh, I. Elias,
J. C. Hoehne, and R. L. Frasca

SUMMARY

Preliminary engineering designs of nacelle acoustical treatments applicable to operational jet transports have been studied. The treatments are intended to be used to suppress compressor noise, especially during the landing approach. Studies were limited to the P&WA JT3D turbofan engine series as installed on the Douglas DC-8 airplane; however, the principles developed are applicable to other installations as well.

Concepts were investigated involving application of narrow-band resonators and wide-band acoustical absorbers to the walls of the fan-discharge and inlet ducts. The concept of choked engine inlets was also considered. A broadband resonator concept for duct lining was developed offering the potential for high absorptivity over a wide frequency range with minimal weight and drag penalties. This concept uses a thin, porous fiber metal surface (typically 0.040-in. thick) backed by a cavity. The cavity can be filled with acoustical absorbing material (e.g., fiberglass or compressed open-cell polyurethane foam).

Analytical aerodynamic studies and wind tunnel model tests evaluated inlets with lightbulb-shaped centerbodies to provide narrower duct dimensions, and increased surface area for the addition of acoustical treatment.

Sound pressure levels on the order of 150 to 160 dB at blade-passage frequencies were measured at the wall of an inlet duct and of a fan-discharge duct on a full-scale JT3D engine. Tests were run to determine the flow resistance and the normal-incidence acoustical impedance and absorption coefficient of various duct-lining treatment configurations. Subsequently, transmission loss tests were conducted at Pratt & Whitney Aircraft Company in East Hartford, Connecticut to determine the attenuation produced by several of these duct lining configurations. Five sections of full-scale JT3D ducts (two fan-discharge and three inlet duct models) were tested. Attenuations of 15 to 20 dB from 1600 to 6300 Hz were obtained with the fan-discharge duct models at 300 ft/sec and from 8.5 to 15 dB in the same frequency range with the lightbulb inlet duct models at 465 ft/sec.

Inlet and fan-discharge duct lining design recommendations for the JT3D engine series are made which use the broadband resonator concept. Estimates are given of the reduction in flyover noise level and the effects on airplane performance. Recommendations are given for additional tests to verify predictions of this preliminary study and for further development of effective nacelle acoustical treatments.

INTRODUCTION

The use of turbine-engine-powered commercial transport aircraft has created neighborhood noise problems in communities near major airports. These noise problems occur during takeoff, landing, and ground runup operations, and are produced by two principal sources of noise, namely, the jet exhaust stream and the rotating pressure fields associated with the compressor or the turbine rotors. The jet exhaust stream, by shearing action with the surrounding air, produces a sound with energy distributed over a broad range of frequencies, and an amplitude, in any frequency band, that has a random distribution. Jet exhaust noise is quite directional with maximum directivity occurring at an angle of about 45° to the direction of the jet exhaust, for the engines on most of the current commercial aircraft. The major source of sound associated with the rotors is essentially a discrete frequency sound ("pure tone") with energy only at certain fundamental blade-passage frequencies, and harmonics thereof, related to the number of blades on the rotor stage and its rotational speed. Typical fundamental frequencies occur in the frequency range between 1800 and 3700 Hz. There is also a broadband, random noise generated by the rotating blades due to vortices shed by the blades. This broadband noise, in conjunction with the jet exhaust noise, forms a background noise to mask the discrete tones. In many cases, however, the discrete tones become very intense and are distinctly heard above the background noise.

The first jet transports to enter commercial service used turbojet engines and were equipped with jet exhaust noise suppressors which reduced the noise levels during takeoff, but which had no effect on the noise during landing. (See references 1 through 4 for descriptions of these suppression devices.) On turbojet-powered transports, jet-exhaust noise tends to mask the high-frequency pure tones during takeoff.

The introduction of the turbofan-powered jet transports in 1959 improved the community noise problem in some respects and made it worse in others. First, since the primary jet exhaust velocity is lower on the turbofan engines, the broadband noise produced by the jet exhaust is greatly reduced, with the largest reductions occurring in the frequency range below 1000 Hz. Secondly, for airplanes of equal gross weights, the greater takeoff thrust of the turbofan engines (compared to the early turbojet engines) permits airplanes equipped with these engines to attain a higher altitude over communities at a given distance from the start of takeoff roll and thereby produce even lower noise levels. However, the compressor noise radiated from the fan stage(s) is more intense and more noticeable than that generated by the turbojet engines. Even at high engine power settings the pure tones are quite noticeable. Finally, studies of the perceived noisiness of sounds (references 5 and 6) showed that human beings are most sensitive to sounds in the frequency range from 2000 to 7000 Hz, with the greatest sensitivity (or the most annoyance) occurring around 3500 Hz. This frequency range encompasses the range of most of the pure tones produced by current large turbofan engines.

On a turbofan engine the compressor noise from the fan stages (fan noise or fan whine) is directed out through the fan-discharge ducts and engine inlet (or fan inlet duct). The noise directed to the rear of the engine is often more

intense, and propagates through shorter distances to ground observers than the noise radiated forward which is radiated at shallow angles relative to the thrust axis. Thus, the compressor noise from the fan-discharge ducts of current large turbofan engines dominates during a flyover-type operation.

Many studies have been made to obtain a better understanding of the compressor-noise problem (e.g., references 7 through 16). These studies have been primarily concerned with the mechanisms for noise generation, propagation and radiation. The propagation and radiation studies have been restricted to pressure fields confined in cylindrical or annular ducts and are of limited usefulness in fan-discharge duct studies. Moreover, the studies of noise generation offered little help in reducing the noise of an existing engine which was already in service on hundreds of airplanes, although they may offer the designers of new engines valuable guidelines for the best combinations of blade and vane numbers, rotor-stator spacings, rotor tip speeds, etc.

The purpose of the investigations described in this report was to develop preliminary engineering designs for practical acoustical treatments to be applied to the nacelles of the large turbofan engines installed on current operational commercial jet transport aircraft. The nacelle treatments (1) were intended to reduce the discrete-frequency compressor noise radiated from the fan-discharge and fan-inlet duct(s), (2) were to be particularly effective during the landing operation, and (3) were not intended to be effective in controlling the wide-band, random noise from the primary jet exhaust.

The engines were to be in the thrust class producing at least 15 000 lb of thrust on a sea-level standard day. There are only two turbofan engines currently in service that meet this condition; namely, the Pratt & Whitney Aircraft Company (P&WA) JT3D-1 (or JT3D-3B) front-fan turbofan and the General Electric Company (GE) CJ805-23D aft-fan turbofan. Furthermore, since the GE CJ805-23D engine is only installed on the Convair CV-990 airplanes and only 37 CV-990 airplanes were sold, most of which operate outside the United States, the studies described herein are limited to the P&WA JT3D turbofan engine. The Rolls Royce RCo-12 and RCo-15 bypass engines are, for the purposes of this study, considered to be in the turbojet and not the turbofan engine class because their bypass ratio is so low. The bypass ratio (ratio of the weight flow of the fan exhaust to the weight flow of air through the gas generator) at takeoff conditions on a standard day at sea level is about 0.3 for the RCo-12 compared to about 1.4 for the JT3D. Moreover, the studies are restricted to the short fan-discharge duct installation of this engine on the Douglas DC-8 airplane, because this was the installation most familiar to and most readily available to the contractor. However, there is no fundamental reason why the acoustical principles and design techniques described herein could not be applied to similar or different installations of either current turbofan engines or future higher-bypass-ratio turbofan engines.

Various nacelle treatments were considered in the study including the use of choking, resonators, and absorbent devices. Although the literature contains many references on the subject of acoustically lined ducts (e.g., references 17 through 28), most of the treatments discussed and the theories developed cannot be applied directly to the development of flyable hardware. This is due principally to (1) the presence of rather high mean airflow velocities, (2) the nature of the various kinds of spinning modes set up in the ducts by the rotating pressure fields, and (3) the design requirement that

the nacelle treatments produce only the barest minimum of performance penalties in order to be economically acceptable for commercial use.

Recent developments in the field of fiber metallurgy have provided promising materials suitable for use in practical in-flight noise suppression systems. This report discusses the aerodynamic and acoustical development work on various techniques for installing these noise suppression systems. The results of aerodynamic wind-tunnel tests are presented along with estimates of the performance penalties incurred by use of various systems under various operational conditions. The acoustical tests consisted of laboratory measurements of the acoustical properties (flow resistance and acoustical impedance) of various duct liners, measurement of the sound pressures incident on the wall of a JT3D engine inlet duct and fan-discharge duct, and a series of acoustic transmission-loss measurements using a special dual-reverberant-chamber facility located at the Pratt & Whitney Aircraft Company in East Hartford, Connecticut. With this facility, transmission loss values of acoustically treated ducts were determined for various duct airflow speeds. Test conditions included high intensity sound propagation in the same direction as the airflow or opposite to it, depending on whether it was a fan-discharge duct or an inlet duct that was being studied.

Acknowledgment

The successful completion of the part of this program involving the transmission-loss tests and the acoustical evaluation of the duct models is due to the diligent efforts of the Pratt & Whitney Aircraft Company's Sound Research Group (especially Mr. E. A. Burdsall) in East Hartford, Connecticut. Their assistance and support are gratefully acknowledged.

SYMBOLS

A_2	area at throat of venturi meter, ft^2
A_E	engine compressor face area, ft^2
A_L	engine face area at local radius, ft^2
CF	ceramic fiber
CPF	compressed polyurethane foam
C_A	acoustic compliance, cm^3/dyne
C_p	incompressible pressure coefficient
C_{p_o}	incompressible pressure coefficient, referred to the velocity at the minimum area inlet station
C_V	venturi meter velocity discharge coefficient
dB	decibel, a unit for the level of a quantity

EPR	engine pressure ratio, ratio of total pressure at the compressor inlet to the total pressure at the turbine discharge
FG	fiberglass
FM	fibermetal
G	acoustical conductivity of the opening or channel in a resonant structure, ft
Hz	unit for frequency, second $^{-1}$
IGV	inlet guide vanes
M_A	acoustic mass, gram/cm^2
M_1	inlet Mach number (at the minimum area of the inlet lip)
P	local static pressure, lb/ft^2 or inches of Hg
P_t	local total (stagnation) pressure, lb/ft^2 or inches of Hg
P_{to}	total (reference) pressure in the test chamber, lb/ft^2
ΔP_t	total pressure loss (reference minus local), lb/ft^2
ΔP	pressure difference, dynes/cm^2 for the flow resistance apparatus, and lb/ft^2 or inches of H_2O for the model duct transmission-loss tests
PNdB	perceived-noise decibels
PNL	perceived noise level, in units of PNdB
R	universal gas constant, ft-lb/lb-° Rankine
Re	unit Reynolds number (based on inlet-lip-station velocity and full-scale size), per foot full scale
R_A	dynamic acoustic resistance, rayls or dyne-sec/cm^3
R_f	static air flow resistance, rayls or dyne-sec/cm^3
R_1	specific air flow resistance, rayls/inch
S	area of sample in air flow resistance apparatus, cm^2
S/N	signal-to-noise ratio, dB
SPL	sound-pressure level, dB re 0.0002 dynes/cm^2 or 0.0002 microbars
SWR	standing wave ratio

T_t	stagnation temperature, degrees Rankine
T	static temperature, degrees Rankine
TL	transmission loss, dB
U	volume velocity of air flow through the flow resistance apparatus, cm^3/sec
V	volume of air in the cavity of a resonant structure, ft^3
W	weight flow of air through the model ducts, lb/sec
X_A	acoustic reactance, $\omega M_A - 1/\omega C_A$, rayls
Y	porosity of an acoustical material, $1 - \left(\sigma_s / \sigma_f\right)$ for fibermetal
Y_a	adiabatic expansion factor for a venturi meter
Z	specific acoustic impedance ratio, $Z_A/\rho_o c$
Z_A	specific acoustic impedance (acoustic impedance per unit area), $R_A + jX_A$, rayls
Z_o	characteristic impedance of air at standard pressure and temperature, rayls
c	speed of sound, cm/sec or ft/sec
d	duct cross dimension, ft
g	acceleration due to gravity, ft/sec^2
p	root-mean-square sound pressure, $dynes/cm^2$
q_1	dynamic pressure at inlet station, lb/ft^2
t	thickness of sample used in flow resistance tests, inches
u	linear particle velocity of air flow, cm/sec
v	steady-flow model duct velocity, ft/sec
α_N	normal-incidence acoustical absorption coefficient
α_R	random-incidence acoustical absorption coefficient
β	ratio of venturi meter throat diameter to upstream pipe diameter
γ	ratio of the specific heats
λ	wavelength of a sound wave, ft

ρ static density of the air in a model duct, slugs/ft^3

ρ_o density of the air at standard (ambient) temperature and pressure, g/cm^3 or slugs/ft^3

σ_f weight density of the fibers used in a porous acoustical absorber, lb/ft^3

σ_s weight density of the sample of a porous acoustical absorber, lb/ft^3

ω angular frequency, radians/sec

DESCRIPTION OF THE NOISE SOURCE

The turbofan engine was developed from the axial-flow turbojet engine by the addition of one or two stages of rotating blades. The additional stages, the fan stages, can be either compressor or turbine stages. An engine with fan stages added to the compressor is called a front-fan turbofan engine. When the fan stage is added to the turbine section, it is called an aft-fan engine. In either case, the fan stages are larger in diameter than the adjacent stages and, if they are on the same shaft, have higher blade tip Mach numbers. Figure 1 shows a cutaway view of the P&WA JT3D front-fan turbofan engine. At sea level on a standard day, statically, the JT3D-3B version of this engine produces 18 000 lb total thrust; the primary gas generator part of the engine produces slightly more than half the total thrust, the fan produces the balance.

As shown in figure 1, the first two compressor rotor stages are the fan stages. In front of the first fan stage there is a set of stator or inlet guide vanes (IGV). There is a set of stator vanes between the two fan stages and a set of outlet guide vanes downstream of the second fan rotor stage. A flow splitter is located downstream of the outlet guide vanes to separate the air which entered the engine through the inlet cowl into two parts: fan air and primary engine air. The engine air is exhausted through a round, conical nozzle at the rear of the engine. The fan air (on all Douglas DC-8 series 50 and model 61 airplanes) is exhausted through bifurcated, short fan-discharge ducts — on on each side of the engine. On Douglas DC-8 model 62 and 63 airplanes, which enter commercial service in 1967, the short fan-discharge ducts will be replaced by longer ducts to bring the fan air back to the rear of the engine where it will be exhausted through a round nozzle concentric with the primary nozzle. This report concentrates on applications intended for the short fan-discharge ducts, although the techniques could be easily applied to the long ducts.

Figure 2 shows the installation of a JT3D-3B engine on an inboard pylon of a DC-8-55 airplane. The side view of the engine, figure 2a, shows the engine inlet (about 4 ft long), the nacelle access doors, the mechanism to reverse the direction of the fan air, the primary engine-air reverser, and the primary exhaust nozzle. The total length of the engine is about 19.5 ft. The primary engine reverser ring is shown translated aft to

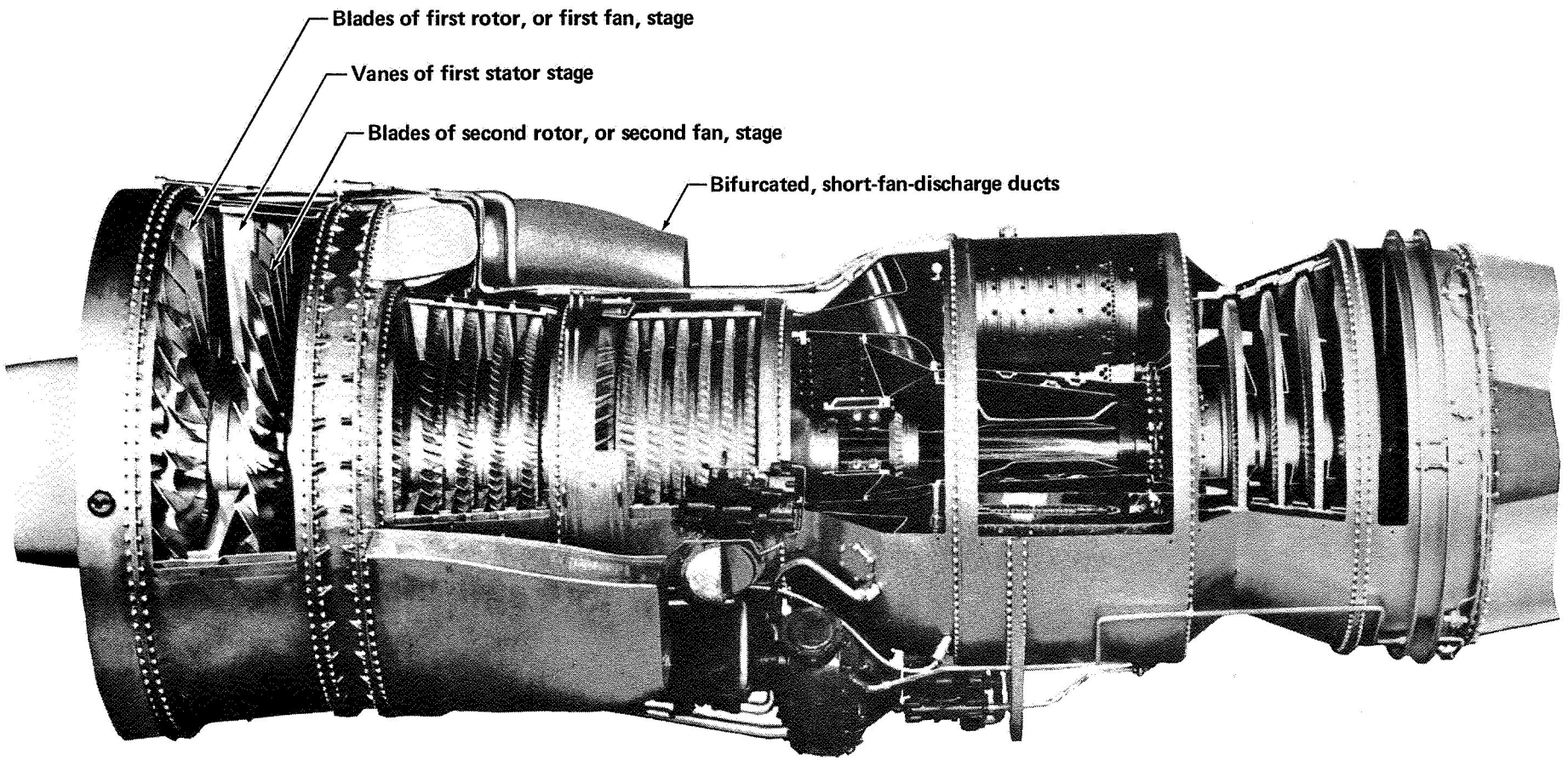

Figure 1. - Cutaway view of Pratt & Whitney Aircraft JT3D turbofan engine.

expose the louvered openings through which the primary air is forced when the reverser buckets inside the tailpipe are closed.

The path length along the fan-discharge duct from the discharge plane to the nozzle exit is about 2 feet; a typical duct cross dimension (radially) is about 6.5 inches. There are four full-length splitters in each duct to direct the airflow; these splitters divide each duct into three approximately equal portions (figure 2b): a central portion with no splitter and two end portions with a splitter. The short piece visible (figure 2b) in the central portion on the horizontal centerline at the nozzle exit is not intended to act as a splitter; it is merely a structural tie across the duct.

Views of the inlet to the engine are given in figures 2c and 2d. The minimum cowl diameter (throat diameter) is about 46 inches; the bullet (centerbody) diameter is about 18 inches at the IGV station. The inlet guide vanes and the blades of the first rotor stage can be seen in figure 2d; there are 23 IGV and 35 first rotor stage blades on all hush-kit equipped JT3D engines. (The hush kit was a development by P&WA for the JT3D engine intended to reduce the noise levels during landing approach and consisted of revisions to the numbers of blades and vanes and to the axial spacing of the various fan stages. The hush kit was incorporated as a production change early in the JT3D program and was offered as a design improvement to all airlines using JT3D-1 engines without hush kits as a retrofit item.)

NOISE-CONTROL METHODS

Background

There are, essentially, two ways to reduce the compressor noise produced by a jet engine. The first is to reduce the noise at the source. This involves making fundamental modifications to the engine, such as changing the aerodynamic loading on the rotating blades, varying the number of blades or vanes on the various rotors and stators, varying the spacing between rotor and stator, etc. All of these modifications affect engine performance (usually adversely), are costly and difficult to incorporate on engines already in service, and, for the JT3D-series turbofan engines, have been rather thoroughly investigated and incorporated by the engine manufacturer.

The second way is to reduce the noise output of the engine by the addition of various external devices. Modification of the fan-inlet duct and/or the fan-discharge duct is the only method available to an airframe manufacturer. In general terms, these modifications consist of various schemes to: (1) make use of reactive mufflers with resonant chambers tuned to absorb sound energy at certain frequencies, (2) make use of dissipative mufflers with air passages lined with acoustically absorptive materials, (3) partially or completely block the "line-of-sight" to the rotating blades both through the inlet and through the fan-discharge ducts, and (4) produce sonic (Mach 1) or near-sonic flow in the engine inlet.

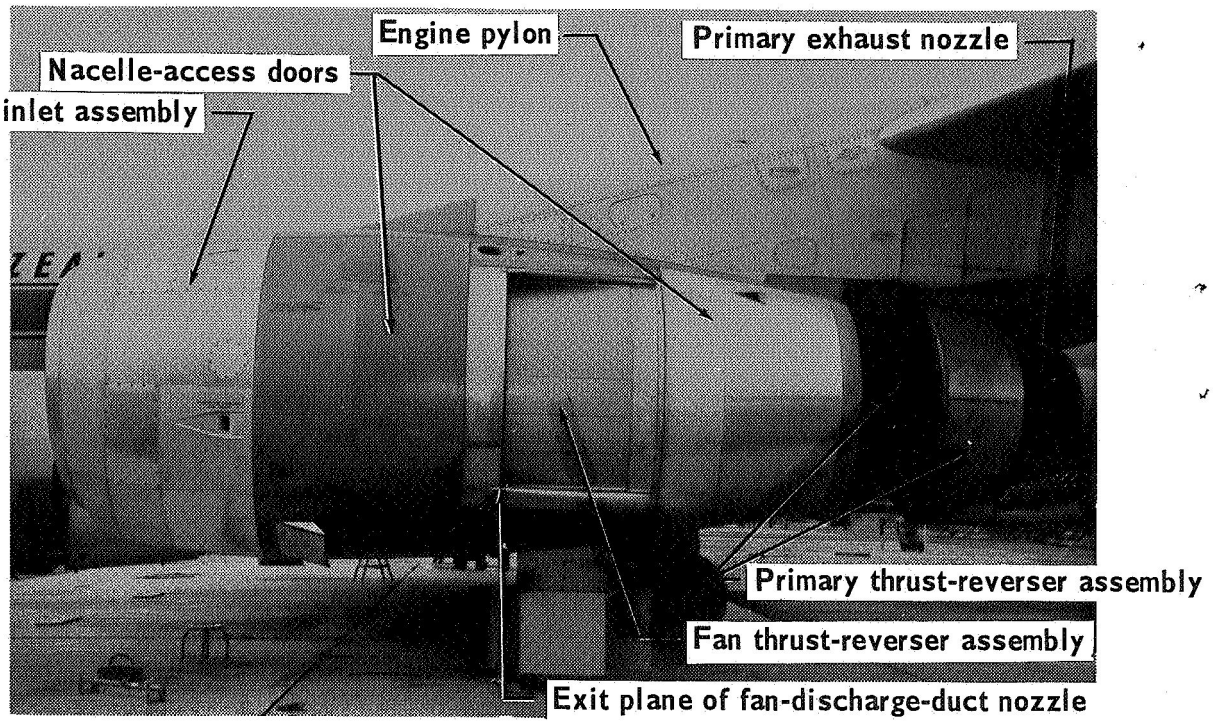

(a) Side view of left-hand inboard engine.

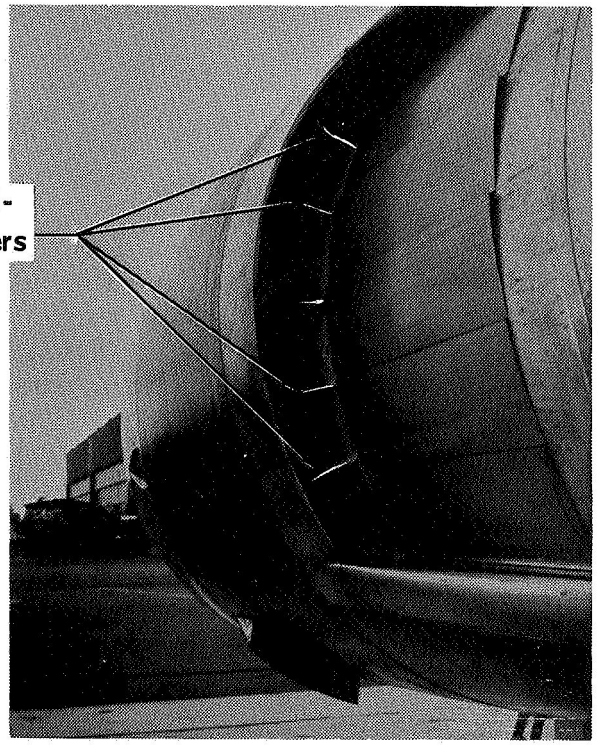

(b) View looking forward at the exit of the left-hand fan-discharge duct.

Figure 2.- P & WA JT3D-3B turbofan engine as installed on Douglas DC-8-55 airplane with short fan-discharge ducts and standard inlet.

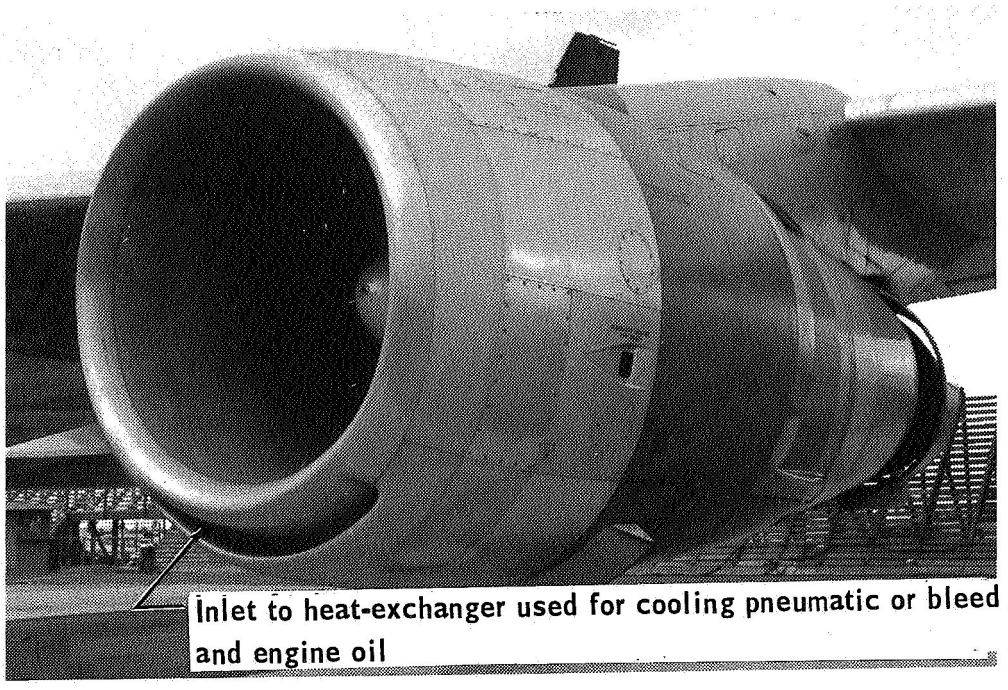

(c) 3/4 front view.

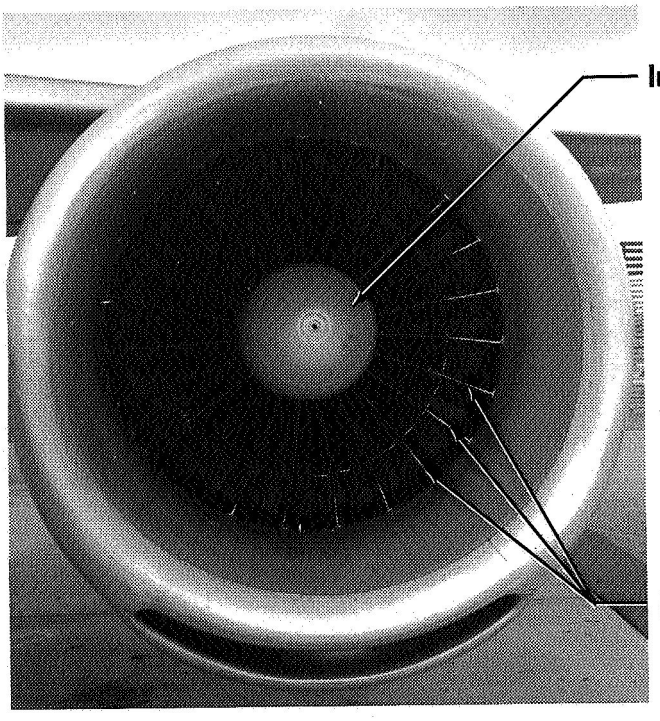

(d) Front view looking aft into engine inlet showing inlet guide vanes (IGV), and blades of first rotor stage. There are 23 IGV and 35 first stage blades.

Figure 2.- Concluded.

Using these general methods, several practical and rather effective noise suppression devices have been developed for use during ground runup operations. None of the ground runup suppressors are readily adaptable for use as in-flight devices, primarily because of the extremely high airplane performance penalties that would be incurred. However, as a result of certain recent innovations in the fields of fiber metallurgy and aerodynamics, it should now be possible to develop practical acoustical treatments to control discrete frequency compressor noise.

Design Requirements

In order to install practical and flyable acoustical treatments into the nacelles of the engines on a commercial jet transport, certain unique design requirements must be fulfilled. The installation must satisfy the following (not necessarily in order of importance):

- Meet a design goal as to the amount of noise reduction
- Produce a minimum performance loss and weight penalty
- Avoid impairment of the safety or reliability of the airplane
- Maintain the noise reduction and the minimum performance losses over the life of the airplane
- Provide means and provisions for anti-icing compatible with available engine bleed-air capacity, if required
- Fit within the established envelope of the nacelle and inlet cowl
- Be simple, reliable, and easy to maintain
- Not be too expensive to manufacture
- Be able to withstand all the rigors of the environment to which it may be exposed, such as temperatures ranging from +250°F to -65°F and the scrubbing effect of air flowing over the surface at speeds up to about 1100 ft/sec.

The following sections describe the acoustical and aerodynamic design concepts that were considered for this study.

Acoustical Considerations

Choking. — It has been demonstrated by several investigators that reducing the flow area at the inlet throat to the point of choking the flow (producing sonic velocity) dramatically reduces the noise propagated forward from the compressor face. With the inlet choked, noise may only be transmitted in the thin boundary layer region next to the skin. From the standpoint of suppressing sound radiated forward out the inlet, the choked

inlet solution offers the maximum potential. Also it is known that complete choking (M = 1) is not required to obtain some noise reduction. A certain amount of suppression is achieved if the average throat Mach number is raised to 0.8.

On the other hand, choking the inlet does nothing to reduce fan noise radiated out the fan-discharge ducts and there is some evidence, reference 10, to indicate that the fan-discharge noise might even be increased due to the passage of the more disturbed air through the fan. As pointed out previously, the noise radiated from the fan-discharge ducts (for the short-duct JT3D installation) dominates the perceived noise level during a flyover operation (takeoff or landing). Thus, it would be futile to consider the use of a choked inlet unless an effective fan-discharge noise suppressor were already developed.

There are several practical operational and performance problems (involving aspects of safety and reliability) associated with choked inlets that tend to preclude the use of this type of device on a commercial jet transport. This is not to say that development of a choked inlet is impossible; only that other solutions may be more attractive. The major problems associated with inlet choking are related to the wide range of engine power settings or airflows that may be encountered during representative approach conditions for a typical subsonic jet transport. Figure 3 shows the reductions in inlet area necessary to choke the flow at the inlet throat at approach conditions for the JT3D turbofan-powered DC-8, considering the extremes in landing weights possible, different flap settings permissible during approach, range of rates of descent, and possibility of an inoperative engine. Note that area reductions from 30 percent to near 70 percent of the basic inlet area must be provided. The area reduction obtained by translating a standard-type (existing) nose bullet to the throat is only 15 percent. To provide the required range of inlet areas, a "lightbulb"-type bullet might be necessary with a relatively complex control system to set the bullet at the appropriate positions. If area reductions of from 50 to 70 percent are to be obtained without excessive lengthening of the inlet, then diffuser angles of near 40° would be encountered aft of the throat. These high diffuser angles would lead to serious flow separations and associated total pressure distortions at the engine face, and possibly result in intolerable engine surge and stall.

Elimination of the inlet separation and associated surge and stall problems would require lengthening the inlet to reduce the diffuser angles. To obtain a diffuser angle of 7° would necessitate increasing the length of the inlet by a factor of 5 to 7 relative to a normal inlet for 50 percent and 70 percent blockage, respectively. The drag and weight of this additional nacelle length would result in unacceptable increases in aircraft fuel consumption.

Other practical considerations which tend to eliminate the movable-bullet choked-inlet solution include the facts that:

- The loads on the bullet are such that on failure of the actuation system the bullet could go to a forward position. This would lead to an excessive loss in thrust at high power and possibly result in an unsafe condition.

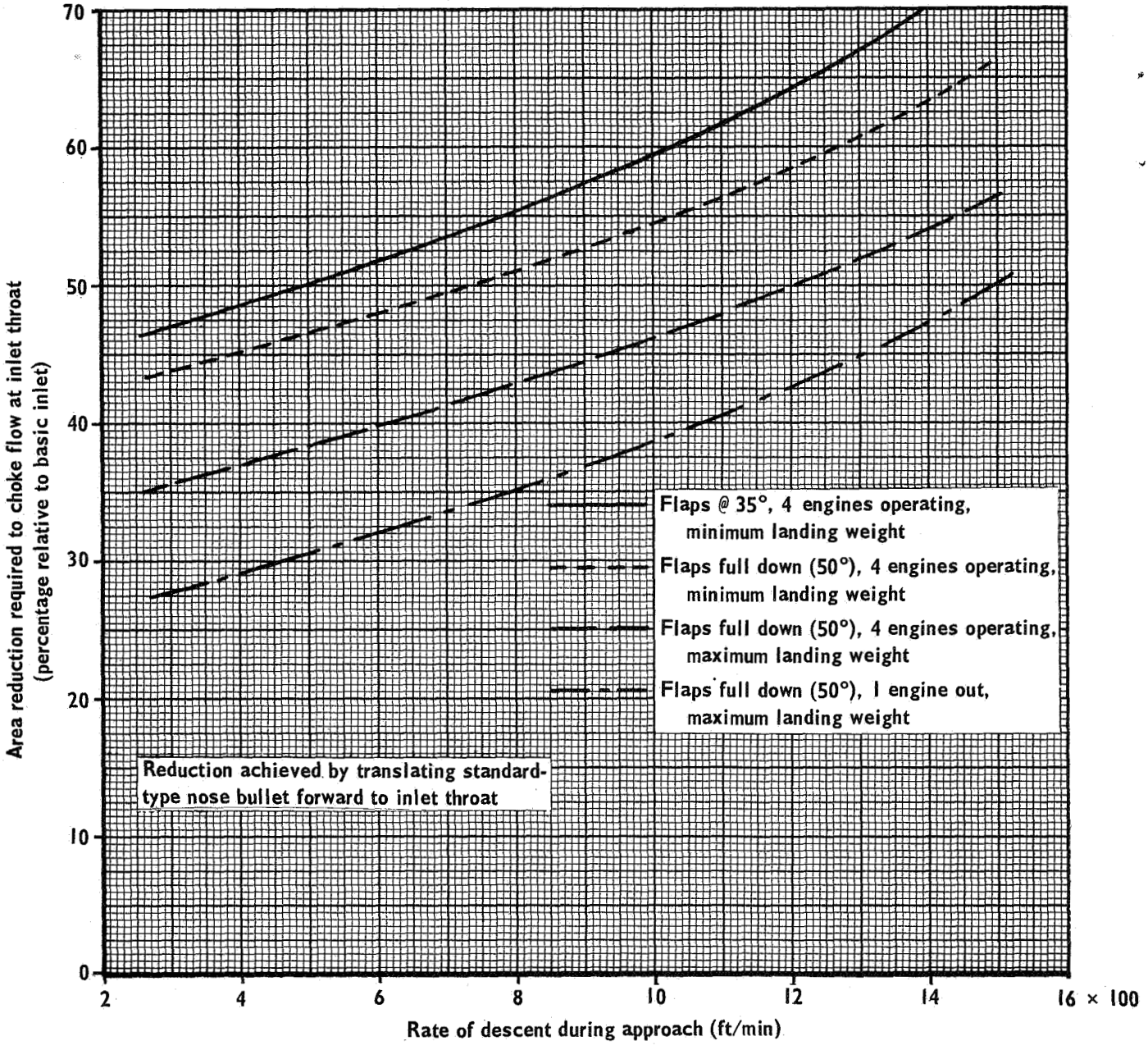

Figure 3.- Area reduction required to choke inlet on approach.

- There is a large increase in noise level when the airflow through the blades is turbulent. Thus, choking the inlet may increase the noise radiated out the fan and aggravate rather than reduce the neighborhoodl noise problem.

Therefore, it was considered that development of a choked inlet device would be outside the scope of this program and no experiments to demonstrate the effect of choking on inlet noise were carried out. It is felt that choking is not an acoustical design problem since it is known to be effective; it is an engineering development problem, though a very complex one, with some difficult decisions to be made about the magnitude of the penalties involved and the possible effects on the safety and reliability of the aircraft.

Resonators. — A resonator is defined as a device of the Helmholtz type which usually has strong selective absorption (i.e., it is absorptive only in a narrow band of frequencies) and which, in combination with other acoustical elements, is often used in reactive mufflers. A resonator consists of a trapped volume of air which is connected to the external medium by some kind of channel.

Rayleigh, reference 29, gives a derivation for the frequency of resonance. With the usage of reference 22, the frequency is

$$f_{res} = \frac{c}{2\pi}\sqrt{\frac{G}{V}} \qquad (1)$$

where f is the frequency in Hertz (or cycles/second), c is the speed of sound in ft/sec, G is the conductivity of the opening to the resonator in feet, and V is the trapped volume in ft^3.

The conductivity is related to the acoustic mass of air contained in the channel connecting the volume to the medium. The volume of the cavity is proportional to the acoustic compliance. Resonance occurs between the kinetic energy of the acoustic mass of air oscillating in the channel under the influence of the imposed sound field and the potential energy stored in the compliance of the volume where the air acts like a spring.

A resonator of this type absorbs energy principally by two mechanisms: friction or viscous losses in or near the connecting channel, and energy storage at resonance. The resonator is assumed to have little or no acoustic damping and thus can only respond to the frequency to which it is tuned. However, when it does respond at the resonance frequency, the energy storage is very large and the absorption is very great. There are two problems with the use of this concept as a duct lining. The first is that it is difficult to get the acoustic energy to enter the resonator since there are many duct modes which carry energy in axial or circumferential modes compared to the radial modes which would have a perpendicular or normal incidence and thus a better coupling to the resonator. The second problem results from the requirement that a practical suppression device be absorptive over a broad frequency band in order to be effective not only against the fundamental frequency but also against the second and higher harmonics of the fundamental over a range of engine operating conditions.

In order to broaden the bandwidth of the absorption spectrum, some type of acoustic resistance must be added. For maximum effectivity the resistive material should be added where the acoustic particle velocities are highest, i.e., near the opening to the channels. However, addition of resistive material decreases the amount of absorption attained. Thus, the real difficulty and the major design problem lies in the proper and practical choice of the resistance.

Perforated panels spaced in front of rigid back walls can be analyzed by an extension of the theory of single resonators, with certain restrictions (reference 22), and can be designed to have rather high absorptivity (greater than 50 percent) over a rather broad frequency band (two octaves). However, in order to have low aerodynamic friction drag, the perforations must be very small. The panel should be thin to reduce the weight penalty. Moreover, the choice of the size of the perforations is dependent upon knowledge of the behavior of the resistance of the perforations as the particle velocity of the air molecules increases. Increasing the particle velocity of the airflow through an orifice raises the effective resistance of the orifice above that measured under low flow conditions due to turbulence, acoustic streaming, and other nonlinear phenomena. As the particle velocity approaches the speed of sound, flow in the perforations approaches a choked condition and the acoustic resistance becomes infinite. Bies and Wilson, reference 30, showed that the resistance of an orifice starts to increase, above its linear laminar flow value, at an equivalent sound pressure level of 138 to 140 dB (i.e., at a sound pressure corresponding to the steady flow particle velocity).

Bies and Wilson conducted their experiments in an unconvected, stationary medium. In a turbofan engine, the medium is convected and typical SPL's are on the order of 150 to 160 dB. Therefore, the effective resistance of a perforated resonator is undoubtedly much greater than that calculated from classical small-amplitude theory and the determination of the proper design becomes a matter for empirical determination requiring simulation of the actual full-scale environment.

In summary, utilization of the perforated panel type of resonators as a noise suppression technique did not seem worthwhile because:

- Resonators have too narrow an absorption bandwidth
- A high value of absorption over a wide range of frequencies is needed (at least two octaves)
- The direction of propagation and modal structure of the sound field in the engine ducts makes it difficult to effectively couple the sound energy into resonators installed on the duct walls
- A wide absorption bandwidth requires the addition of acoustically resistive material
- The resistance of the perforations or the channel into the resonator increases nonlinearly with increasing particle velocity starting at sound pressure levels of about 140 dB
- The required acoustic damping is hard to predict and requires considerable full-scale empirical effort to select an optimum value

- Friction Drag of the design might be high.

Absorbers. — Absorbers are defined here as a class of acoustical materials which absorb energy through viscous resistance to the motion of the air molecules. The acoustic energy is converted into heat which is dissipated in the air and in the material. An example of this material is the low-density rockwool or fiberglass batt commonly used for insulation in air conditioning ducts. These materials can be made to absorb well over 80 percent of the incident acoustic energy in a band of frequencies three octaves wide, for frequencies greater than 1000 Hz. However, these materials have to be porous to admit the acoustic pressure oscillations and to absorb the energy. The low-density (0.6 lb/ft^3) fiberglass of the type commonly used in aircraft insulation is over 99-percent porous; i.e., less than 1 percent of a given volume of a sample is glass fibers, the rest is air.

Use of these materials as duct linings alone was not considered to be feasible because:

- The material would erode away rapidly due to the high-velocity stream of air in the duct
- The porous materials would wick the various fluids that might be present in a duct (fuel, oil, water, etc.)
- Water retained in the material would freeze and possibly cause damage. It might also tend to corrode the structure of the duct
- Fuel or other flammable fluid retained in the material would present a fire hazard.

The use of acoustical absorbers can be considered for duct linings if a suitable facing material can be found. The facing material would prevent erosion of the material. Drains could be provided to drain away liquids. Warm bleed air, if needed and if available, could be circulated to prevent freezing damage. However, considerable detailed engineering design work would be needed before these materials could be utilized in an actual installation.

Broadband resonator. — The most promising noise suppression technique consists of lining the walls of the fan inlet duct and the fan-discharge ducts with a broadband resonator. Such a resonator consists of sheets of porous metal installed over a fixed cavity.

There are several requirements which can be specified to guide the selection of an acoustical material suitable for lining a duct wall for the application intended. The acoustic impedance of the porous surface should approach a pure resistance with almost no reactive components. The resistance of the resonator should be almost independent of frequency, maintaining a nearly constant value as frequency is increased. The lining should be comparatively smooth, so that friction losses may be held to a minimum.

The lining would replace part of the existing sheet-aluminum duct lining and would be backed up by a cavity. (It is the compliance of the volume of the cavity resonating with the distributed reactance of the air in the pores of the liner that produces the broadband resonator.) Wirt, references 31 and 32, showed the feasibility of this approach for small gas-turbine exhaust muffler applications.

A lining material which meets the requirements stated above has recently been developed. It is a fibermetal product made from short metal fibers arranged in a random manner by a felting operation. The fibers are arranged in a sheet form, then put into an oven where sinter bonds between interlocking fibers are created in a heated hydrogen atmosphere. The density, thickness, and flow resistance are controlled in rolling operations. The most suitable product available in time for the test program was one was made from drawn stainless steel (type 347) wires. The diameter of the wire fibers in the products tested was nominally 0.004 inch. A stainless steel, 18-mesh, box weave screen, made from 0.009-inch wires, was sintered and rolled into the sheets of felted fibers to increase the strength of the sheet and to reduce the tendency for very short fibers to bend up (nap) and produce a rough surface.

The cavity behind the fibermetal lining can be either air-filled or filled with a porous absorbent material. Addition of a porous acoustical absorber in the cavity was expected to fill in any valleys in the absorption spectrum and produce greater attenuations over a wider frequency range. A product made from compressed open-cell polyurethane foam also seemed attractive because it had high acoustical absorptivity without being subject to an erosion problem — though it would act like a good sponge. This product is available in various thicknesses, firmness grades and pore (cell) counts; e.g., type 3-900 indicates a firmness of 3 (meaning that the material had been compressed by a factor of 3 from the original foam material) and that it had a pore count of 90 pores per lineal inch before compression.

Aerodynamic Considerations

General. — In general, high sound attenuation is achieved with a lined duct when the ratio of the cross dimension of the duct to the wavelength at the frequency for which maximum attenuation is desired (d/λ), is on the order of 1.0 or less. Using this general rule, it was determined that the flow lines of the fan-discharge duct might be acceptable as they were. However, for the JT3D inlet a typical duct diameter is about 50 inches and the d/λ ratio is about 11 (assuming that 3000 Hz is approximately the frequency at which maximum attenuation should be obtained). This large d/λ value indicated that very small attenuations could be expected by the addition of an acoustical lining to the cowl wall of the standard inlet, although a design of this type is installed in some airplanes (reference 33).

Therefore, it was decided that some kind of modification to the inlet shape would be required in order to achieve duct passageways for which the

d/λ ratio would be more favorable, which would offer large backward-facing areas to which acoustical treatment could be applied, and which would minimize aerodynamic performance losses. A study to determine the proper shape for the inlet was conducted using analytical aerodynamic techniques. The basic shape selected for the study was the so-called "lightbulb" inlet, because of the resemblance of the revised centerbody to an ordinary incandescent light bulb. This shape has the apparent advantages of simplicity, rigidity and ease of maintenance. In this type of configuration, the inlet centerbody (or bullet), and the cowl are enlarged and lengthened to increase the sound-absorbing surface area and to place as much of the sound-absorbent surface as possible in direct view of the compressor face.

Objective. — The objective of the aerodynamic studies was to develop a series of lightbulb inlets having different size centerbodies. For each centerbody, the inlets were to be as short as possible to eliminate excess weight and skin-friction drag penalties. The internal lines were to be shaped to prevent losses due to shock waves and to boundary-layer separations over the normal engine operating range. From an analytical study of several inlet geometries, three promising inlets were selected and tested.

Design procedures. — A critical operating point for the inlet of a subsonic transport is the static condition. At this condition, the highest internal surface Mach numbers are encountered, and the surface pressure gradients that cause boundary-layer separations are the most adverse. Therefore, the inlets were developed for and tested under static conditions.

The initial phase of the aerodynamic part of the program consisted of an analytical study with the objective of producing a set of inlet lines that minimized adverse pressure gradients and supersonic flows which might cause boundary-layer separation on the cowl and bullet. The analytical method determined the flow within the inlet using a potential-flow computer program (reference 34). A solution for incompressible flow was first obtained. The effects of Mach number were then estimated by assuming that local pressures would vary with Mach number according to the Goethert rule,

$$C_p = \frac{C_{p_o}}{\sqrt{1 - M_1^2}} \qquad (2)$$

All pressure coefficients have been referred to the conditions at the inlet throat. The reference throat was taken at the minimum radius of the inlet lip for all configurations.

In designing a specific configuration, the procedure was to draw a trial set of lines and compute the pressure distributions. These lines were then modified in order to improve the flow, and the pressure distributions were recomputed. This process was repeated until a satisfactory pressure distribution was obtained. Boundary-layer calculations were then made for the final configurations using a Truckenbrodt boundary-layer computer program. The calculations were made for Reynolds numbers corresponding to the following:

- Static operation with high-velocity airflow

- Static operation with low-velocity (incompressible) airflow
- Representative cruise operation
- Reduced power at high altitude.

All configurations were indicated by the boundary-layer calculations to be free from separations at Reynolds numbers corresponding to static operation. At the Reynolds number representing cruise operation, separations were predicted only for the two inlets having the largest centerbodies. All the lightbulb inlets had predicted separations at the Reynolds number representing reduced power at high altitude. For this flight condition, however, a loss in aircraft performance is unimportant, provided that engine compressor stalls do not occur.

The analytical procedure is limited in its ability to determine the effect of compressibility on the surface pressure distributions, to accurately predict separation, and to determine the total pressure loss caused by the separation. Consequently, the analytical program served to predict the flow behavior in the inlet, but the quantitative effects on performance had to be determined by wind-tunnel model testing.

EXPERIMENTAL WORK

Two separate and distinct experimental programs were conducted, aerodynamic and acoustical. The aerodynamic study consisted of wind-tunnel tests to evaluate the lightbulb inlet models developed by the analytical aerodynamic design analyses. The acoustical test programs included (1) measurement of the sound pressures on the walls of a fan-discharge inlet duct of a full-scale JT3D turbofan engine, (2) laboratory studies of fundamental acoustical properties of duct lining treatment concepts and (3) model duct transmission-loss tests to study the effects of treatment area and airflow velocity on attenuation. This section of the report describes the tests that were run and discusses the results that were obtained.

Aerodynamic Wind-Tunnel Tests

Description of models. — A scale model inlet representing the JT3D engine installation for the DC-8 airplane was selected for a reference inlet. The actual inlet is not a body of revolution as was the model (it has a thicker lip at the bottom), but the approximation was considered appropriate for a comparative investigation. For this study, the lightbulb inlets were derived from the reference shape by changing the internal cowl lines aft of the inlet station to accommodate the requirements for duct area imposed by the centerbodies. Although five lightbulb inlet models were designed, two were discarded because the small blockages (14 and 17 percent) provided insufficient area for acoustical treatment. Blockage is defined as the change of compressor-face area that can be seen from a position forward of the inlet relative to that of the standard inlet. The characteristics of the configurations tested are given in the following tabulation:

Test configuration number	Percent blockage	Nominal inlet duct length, inches
1	0	44.8
2	55	74.5
3	75	84.5
4	95	101.0

A comparison of the wind-tunnel model lines is given in figure 4. The inlet lips of the lightbulb inlets were blunted compared to the reference inlet by fairing them into a 2:1 ellipse to prevent any lip separations. This was permissible since only the pressure losses of the internal flow were desired. For an airplane it may be desirable to modify the shape of the inlet lip. The inlet lip of the basic inlet was left unchanged to compare model surface pressures with full-scale test data.

The models were made of aluminum. The model scale was 0.175 compared to the full-scale JT3D nacelle. Each model was instrumented with as many as 30 surface pressure taps. A complete model is shown in figure 5. A comparison of the four test-model centerbodies is shown in figure 6. The vortex generators shown on bullets 3 and 4 in figure 6 were added after the first tests with these models, to determine if total-pressure losses could be reduced. These vortex generators were 0.087-in. high, 0.175-in. long and were angled at 15° to the streamlines. However, the total-pressure losses were increased and the vortex generators were eliminated from further consideration. The total-pressure losses at the engine face were measured by a six-armed total-pressure rake having 15 probe tubes in each arm. The tubes were more closely spaced in the area of the duct periphery to better define the boundary layer.

Description of test facility and procedures. — Wind-tunnel tests of these lightbulb inlet models were performed at the Douglas Aerophysics Laboratory in a 4-foot blowdown tunnel. The tunnel was modified for static testing by blocking the end of the test section with a bulkhead. Figure 7 shows the model as installed in the test chamber. A schematic of the arrangement is shown in figure 8. Air supplied from the blowdown tank was brought through the diffusing section to the test chamber.

After the air passed through the model, the flow rate was measured by an 8.5-inch orifice in the 12-inch line. Flow control was provided by a remotely operated butterfly valve downstream of the orifice. The air was then vented to the atmosphere. The range of testing was generally as shown for configuration 2 in figure 9. A special run was made at a nominal total pressure of 26 psia for configuration 1 only.

Since it is very desirable to simulate full-scale Reynolds numbers during a test, any reduction of model size compared to full size should be compensated by increasing the air density, or the velocity, or by decreasing the viscosity. For these tests where inlet Mach number was also to be simulated and since flow viscosity cannot easily be changed, the solution was to increase

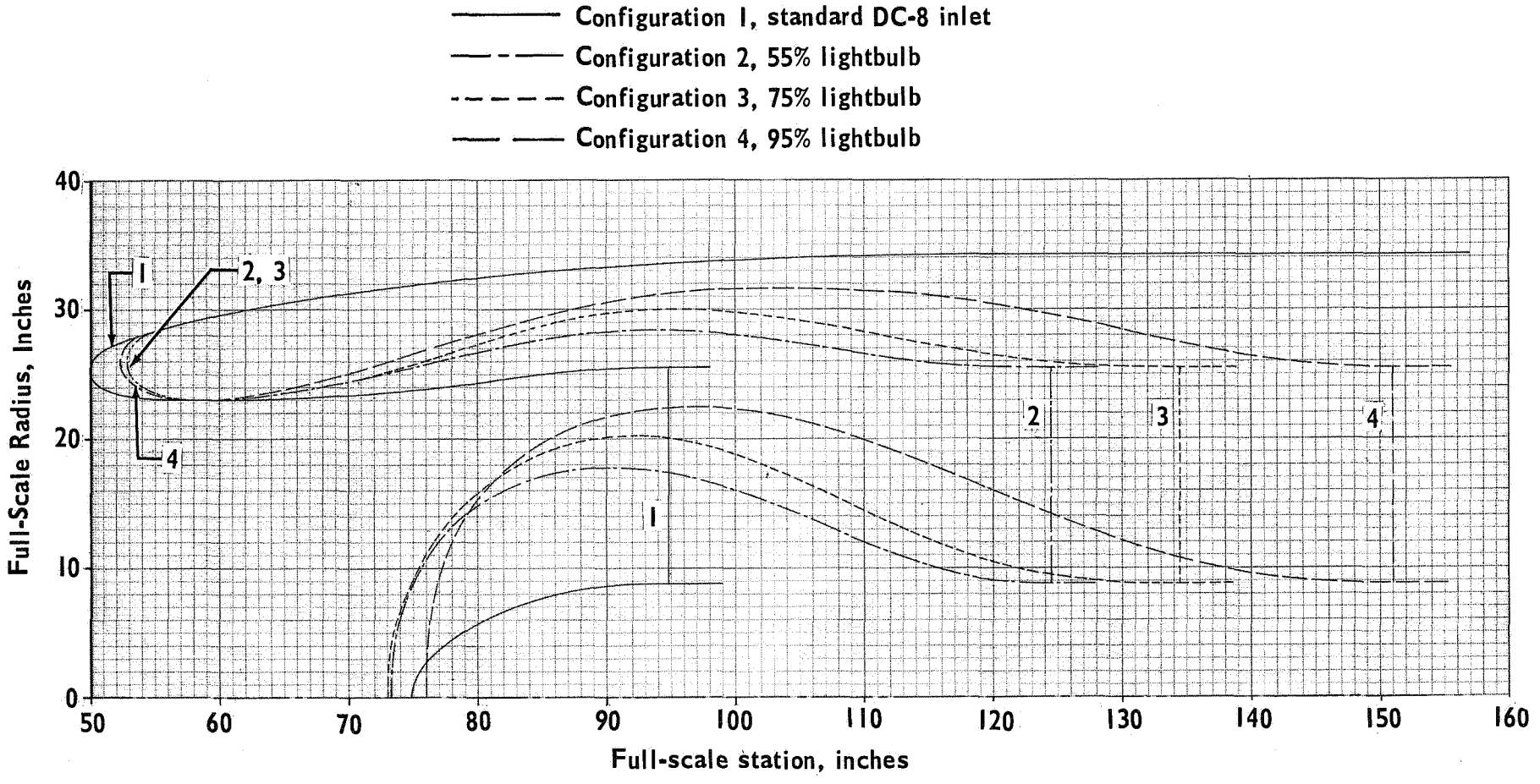

Figure 4.- Comparison of wind tunnel model configurations.

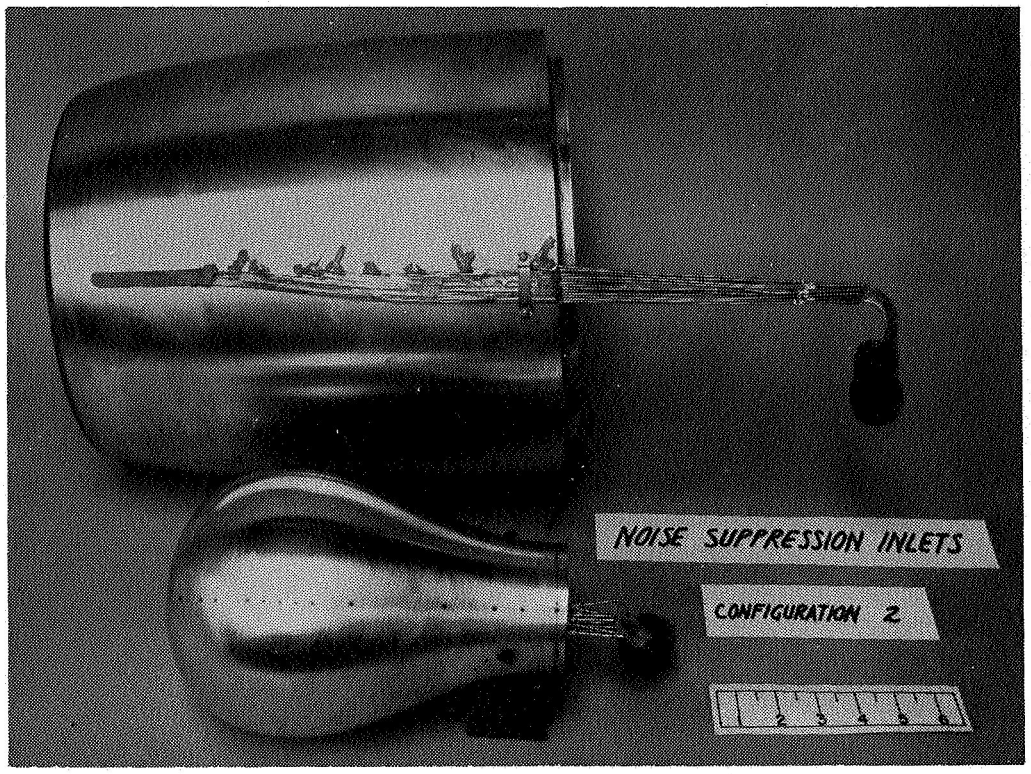

Figure 5.- Typical complete wind tunnel model (55% lightbulb inlet).

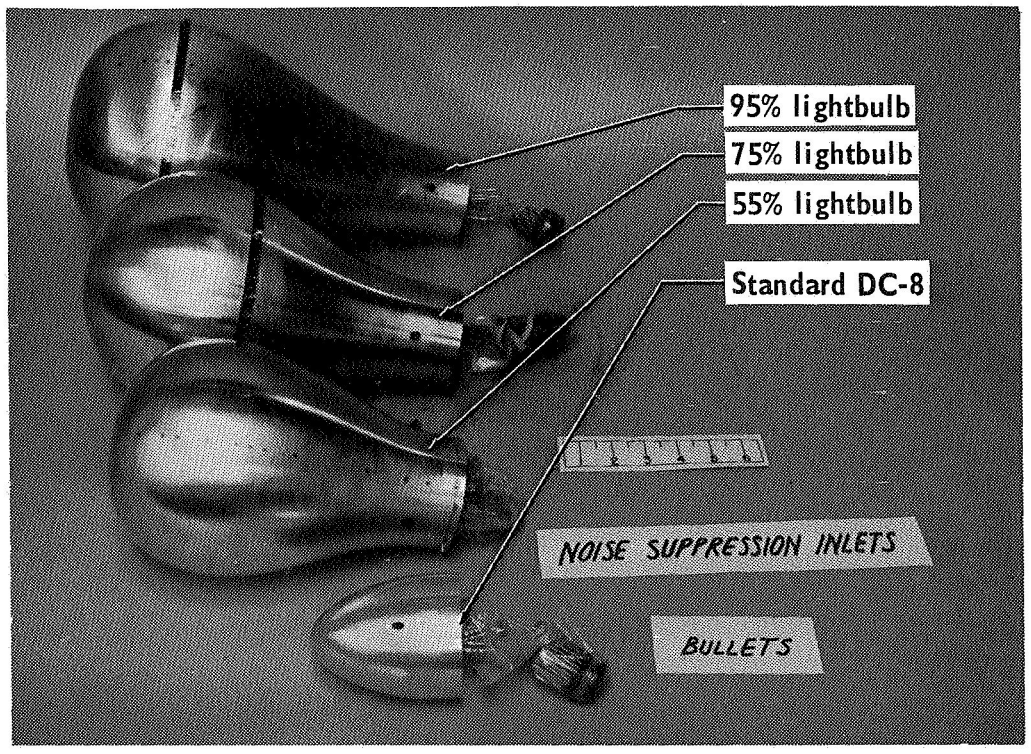

Figure 6.- Comparison of model bullets.

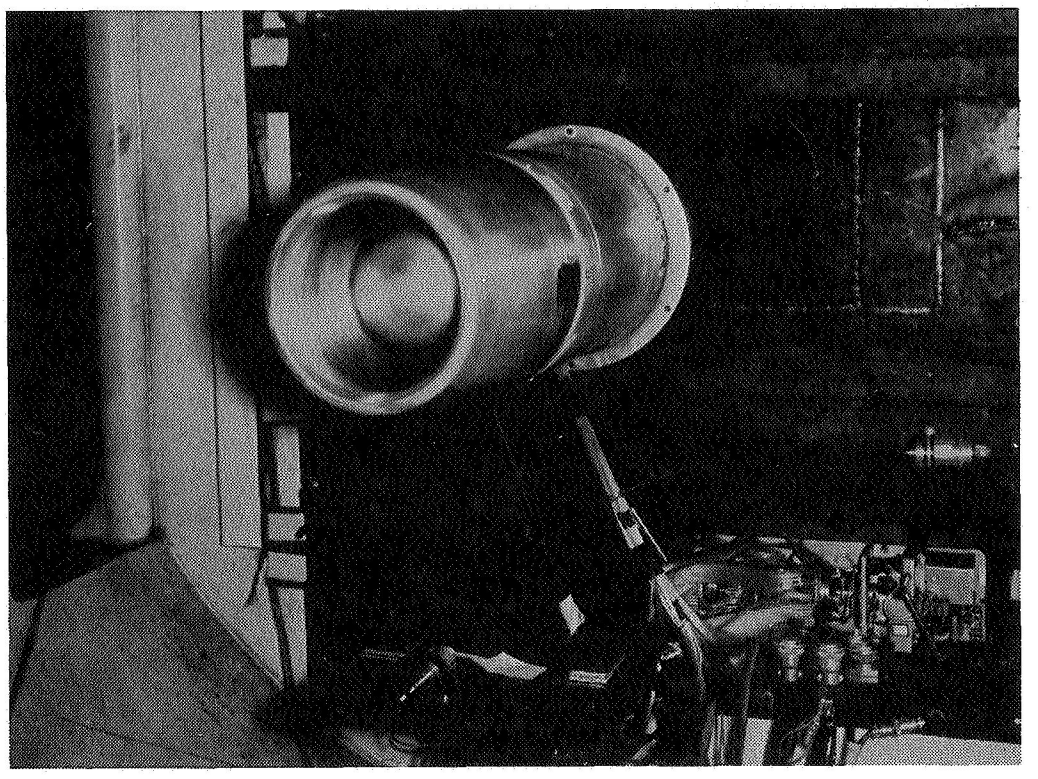

Figure 7. - Configuration 2 (55% lightbulb inlet) installed in tunnel.

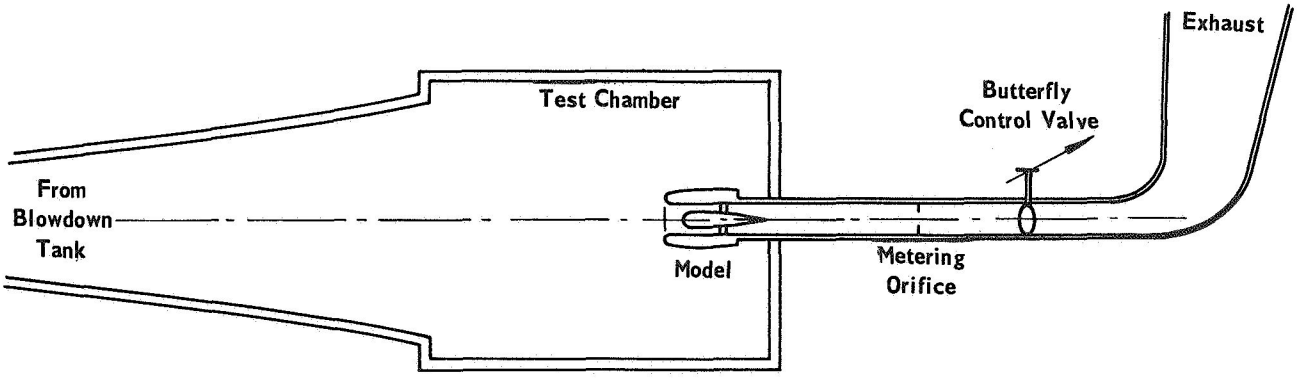

Figure 8. - Schematic arrangement of wind-tunnel test.

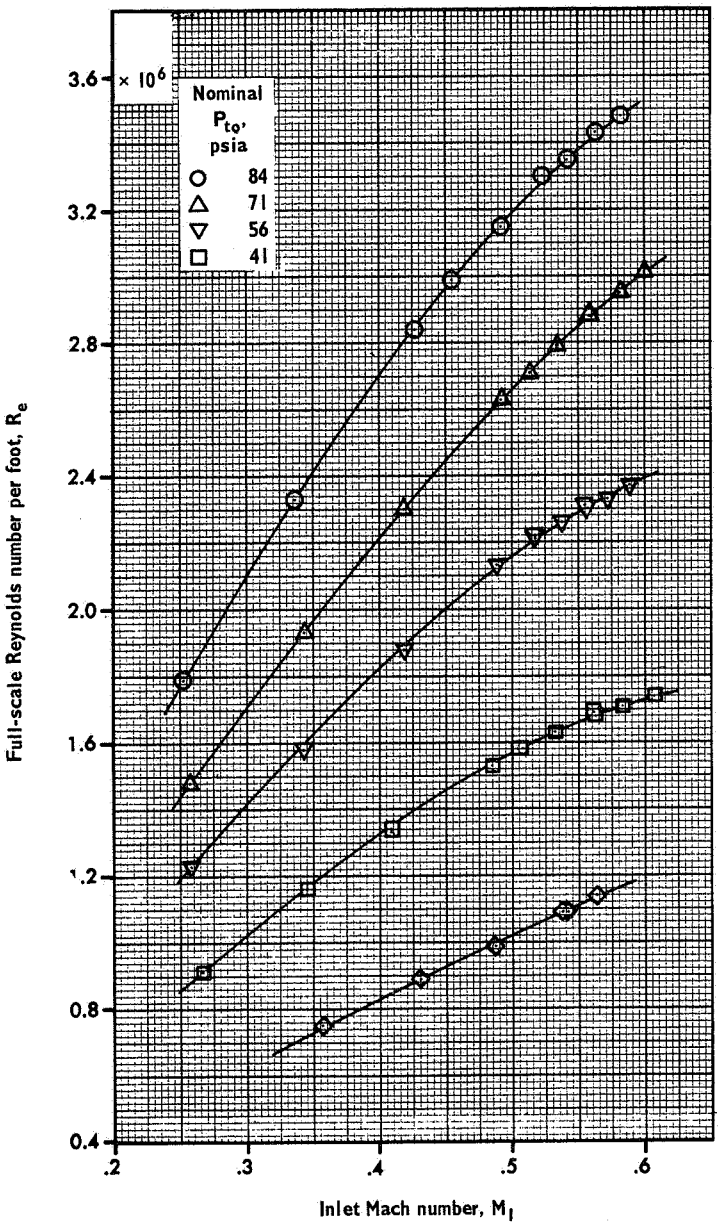

(a) Standard DC-8 inlet, configuration 1.

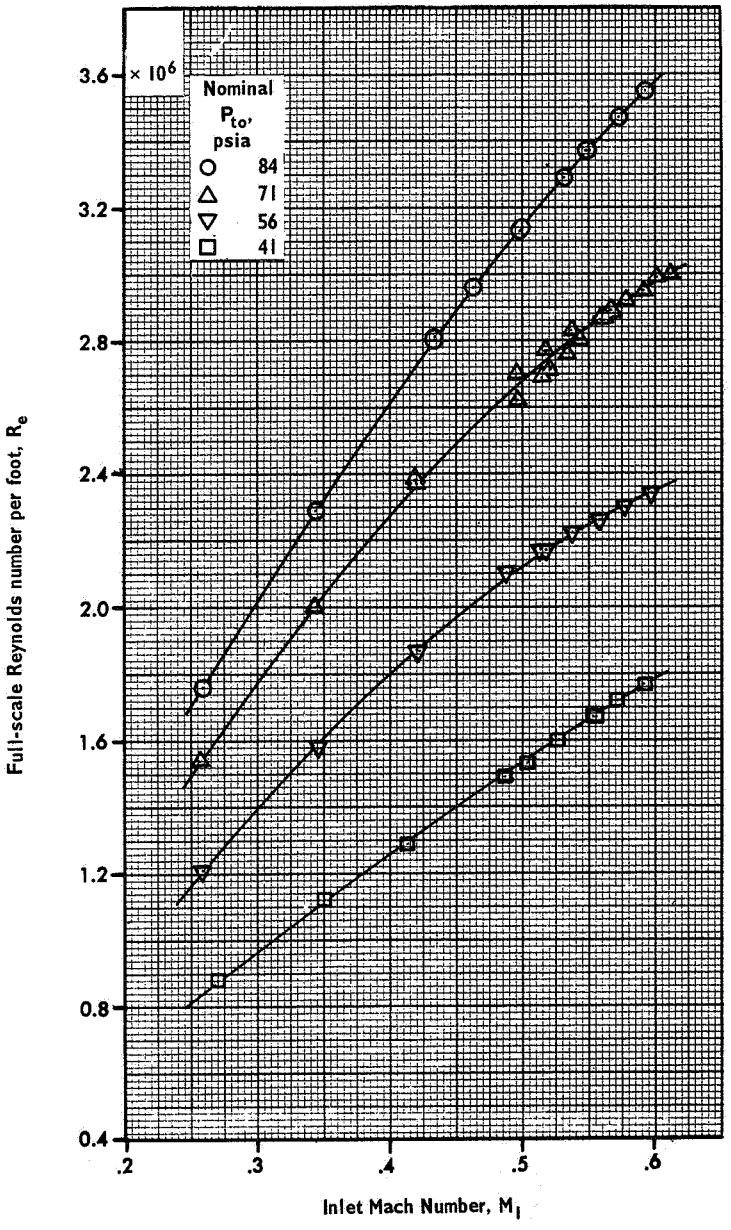

(b) 55% lightbulb inlet, configuration 2.

Figure 9. - Typical range of wind-tunnel testing conditions.

air density. The increase in density was made possible in the blowdown wind-tunnel at the Aerophysics Laboratory by increasing the stagnation pressure to 84 psia to produce a model Reynolds number, per foot, equal to the full-scale value, per foot. The nominal total pressure levels of the test were 84.4, 70.7, 56.3 and 41.1 psia. These correspond to full-scale Reynolds number, per foot, ratios of 1.0, 0.84, 0.66 and 0.49, respectively.

The model surface pressures, the total pressures at the engine face, and the upstream orifice pressure were all measured by transducers referenced to the test-chamber ambient pressure. The pressure drop across the flow rate orifice was measured by an electromanometer, and temperatures in the test chamber and upstream of the orifice were measured by thermocouples.

Data were taken at constant total (test-chamber ambient) pressure; the inlet Mach number for each data point was set by adjustment of the flow rate. The pressure at each tap was sampled 10 times, and the average of these samples was used as the effective value. At the conclusion of a run, the data were reduced by a digital computer. The flow rate was calculated, and from this and the reference inlet-lip throat area, the inlet-station velocity, Mach number, dynamic pressure, and equivalent full-scale Reynolds number per foot were computed. The rake total pressures were integrated over the compressor face area to find the area-weighted total-pressure loss of the inlet configuration. All reduced data were then tabulated for each data point.

Discussion of wind-tunnel test results. — Engine face pressure-recovery profiles are shown in figure 10 for the normal operating range of inlet Mach number and for a ratio of model to full-scale Reynolds number of 1. The pressures are the average of the six total head tubes at each radius location. The same information is presented in a different fashion in figure 11. In this figure, inlet-total-pressure losses are plotted against fractional engine face area.

The total-pressure loss of configuration 1 is almost entirely due to the skin friction on the cowl. There is a large increase in loss at Mach numbers greater than 0.50 due to a separation over the relatively sharp inlet lip. For configuration 2, the cowl loss is somewhat greater than the bullet loss, as is to be expected from the greater wetted area, but both losses are small. For configuration 3, the cowl and bullet losses are about equal at low Mach numbers, but a greater increase of loss with Mach number arises from the bullet. Configuration 4 indicates approximately equal low-speed cowl and bullet losses, but at higher Mach numbers there was probably a separation on the cowl.

The inlet total-pressure-loss coefficients at full-scale Reynolds number are summarized in figure 12 for the four configurations. The premature increase of inlet loss with Mach number for configuration 1 probably was due to a shock wave and separation on the cowl surface near the inlet throat. For the actual DC-8 inlet, this premature loss does not occur because of the thicker lip at the bottom of the inlet (cf., figure 2d). This is believed to give relief to the entire inlet. Actual DC-8 inlet performance was used to extrapolate the inlet performance of configuration 1 (dashed line on figure 12).

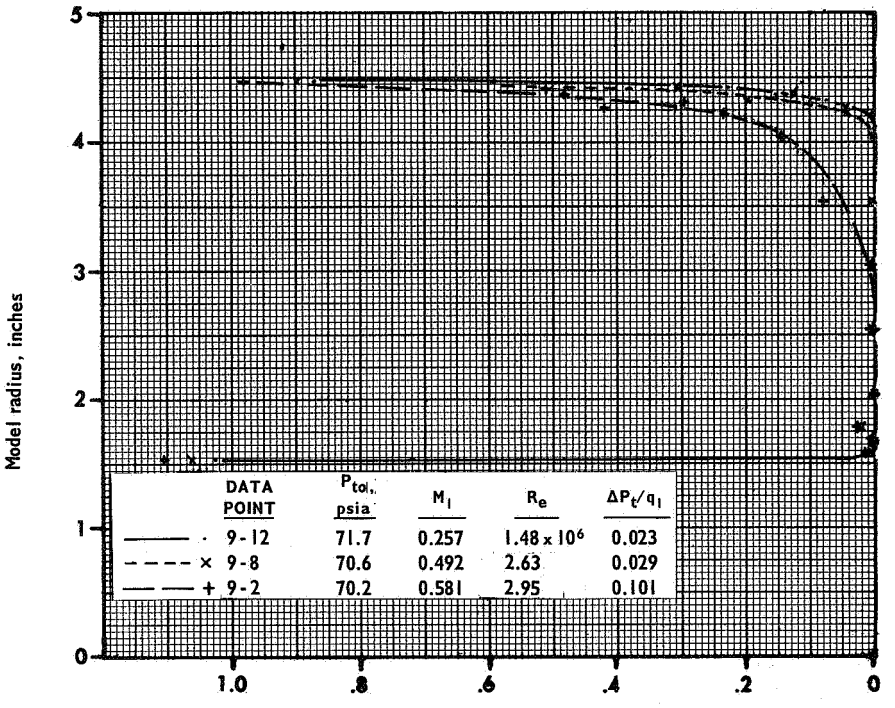

Local total pressure loss coefficient, $\Delta P_t/q_1$

(a) Standard DC-8 inlet, configuration 1.

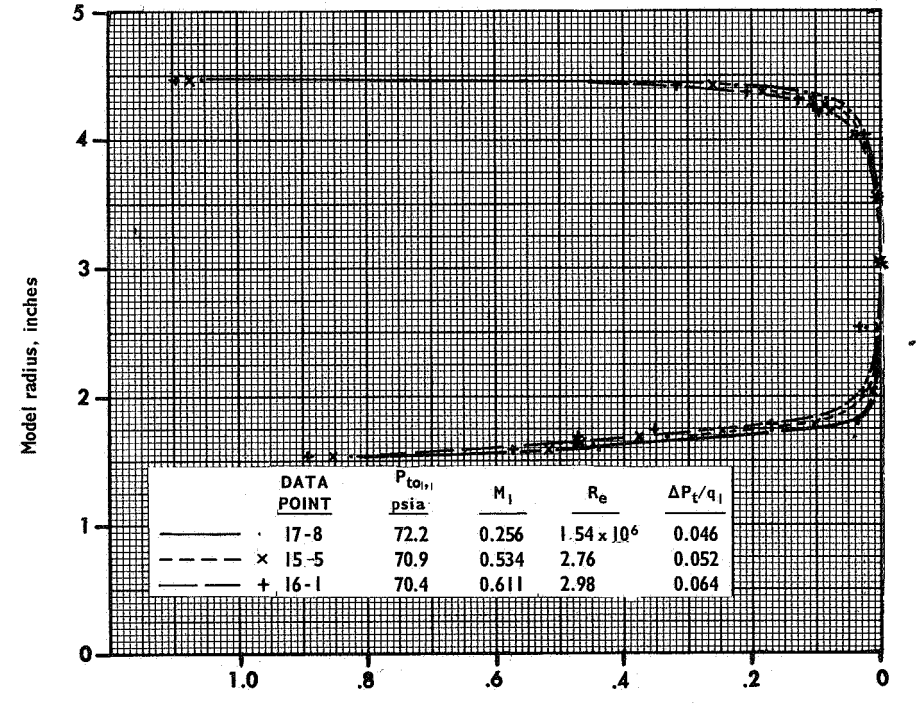

Local total pressure loss coefficient, $\Delta P_t/q_1$

(b) 55% lightbulb inlet, configuration 2.

Figure 10.- Effect of Mach number on engine face local total pressure loss coefficients – physical profiles.

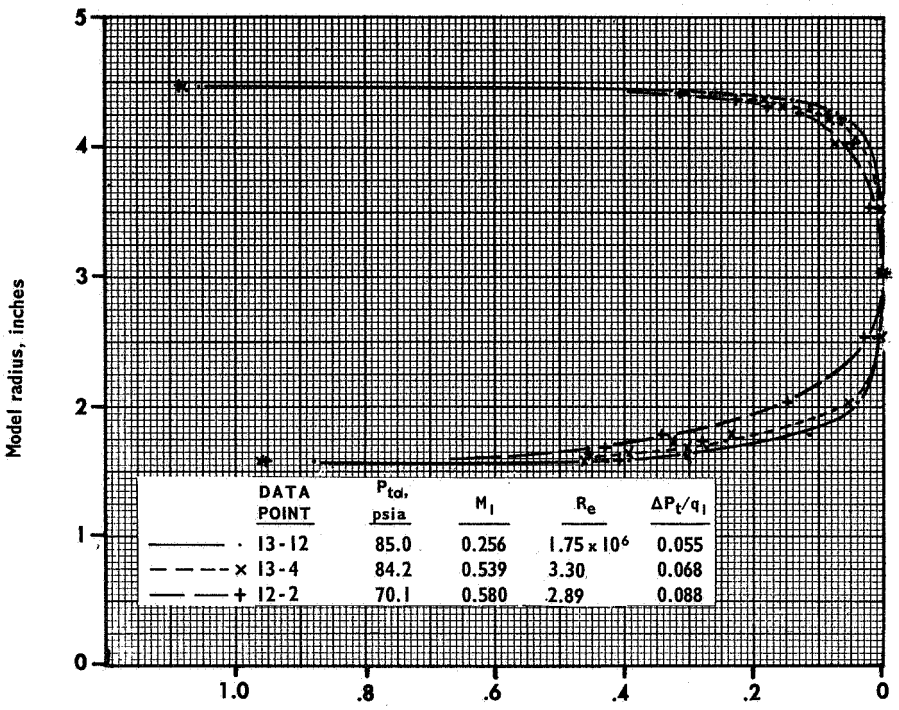

(c) 75% lightbulb inlet, configuration 3.

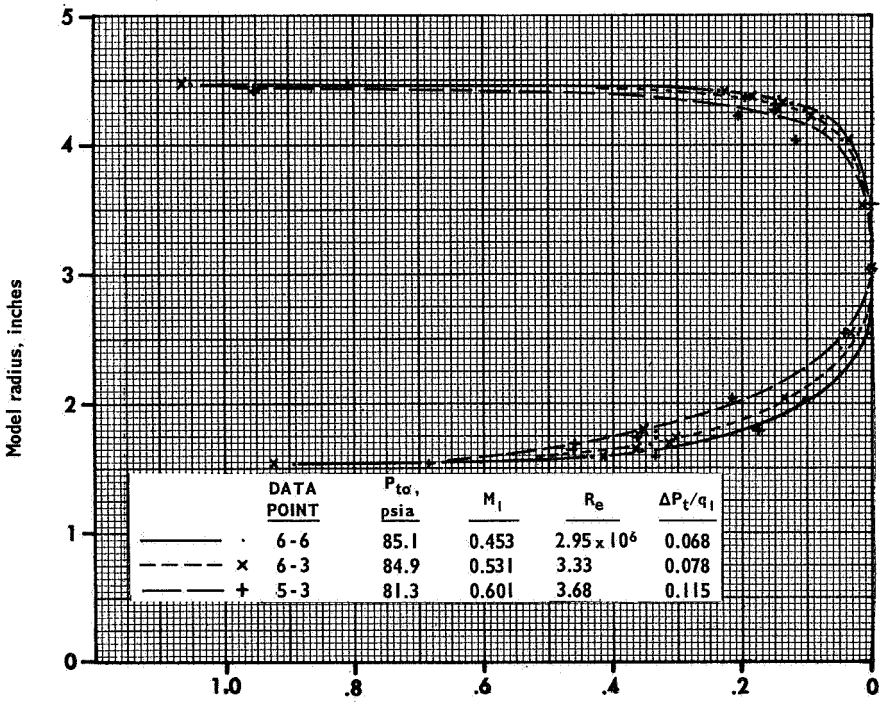

(d) 95% lightbulb inlet, configuration 4.

Figure 10. – Concluded.

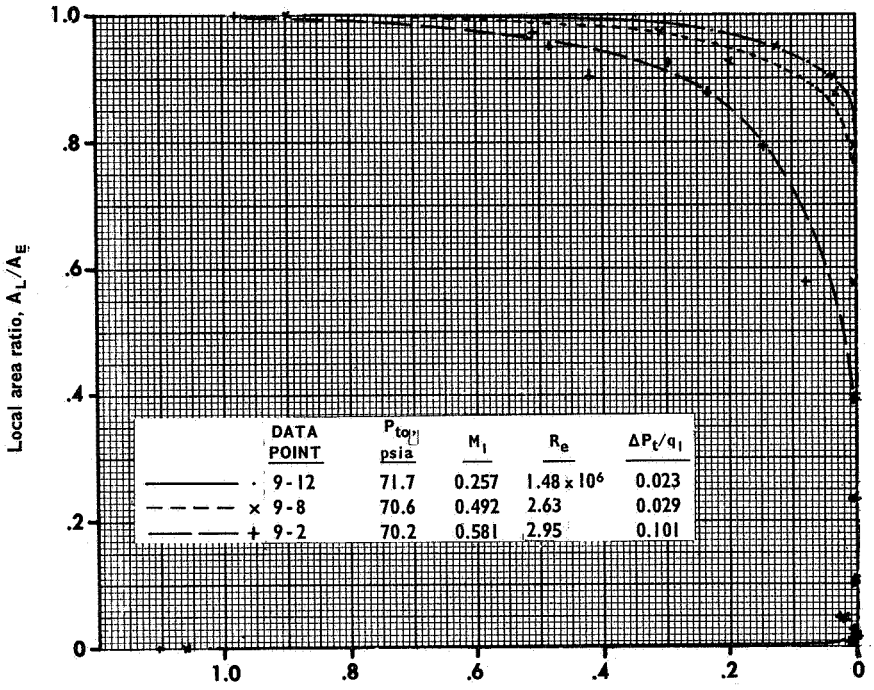

(a) Standard DC-8 inlet, configuration 1.

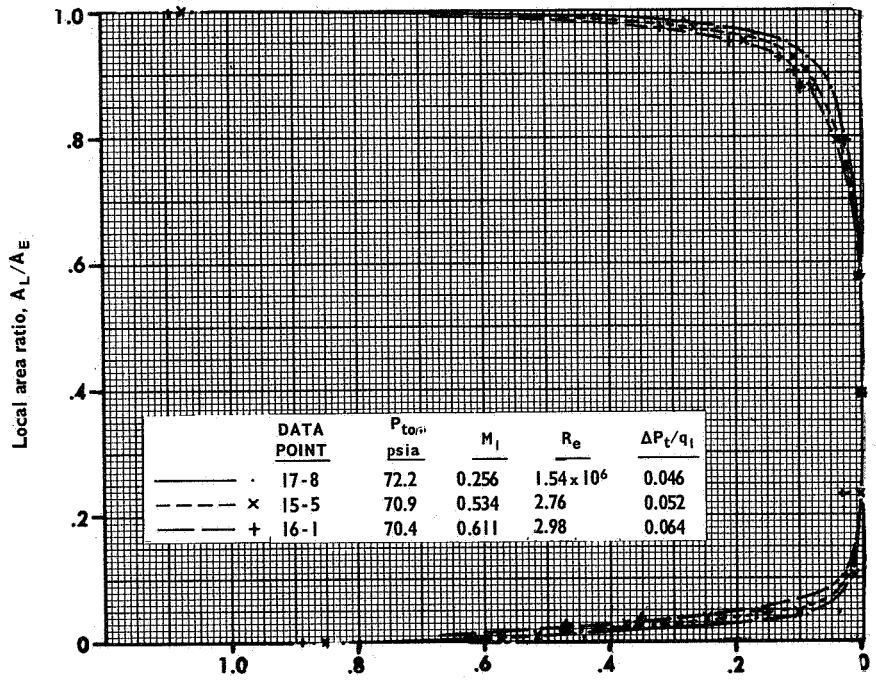

(b) 55% lightbulb inlet, configuration 2.

Figure 11.- Effect of Mach number on engine face local total pressure loss coefficients – area-weighted profiles.

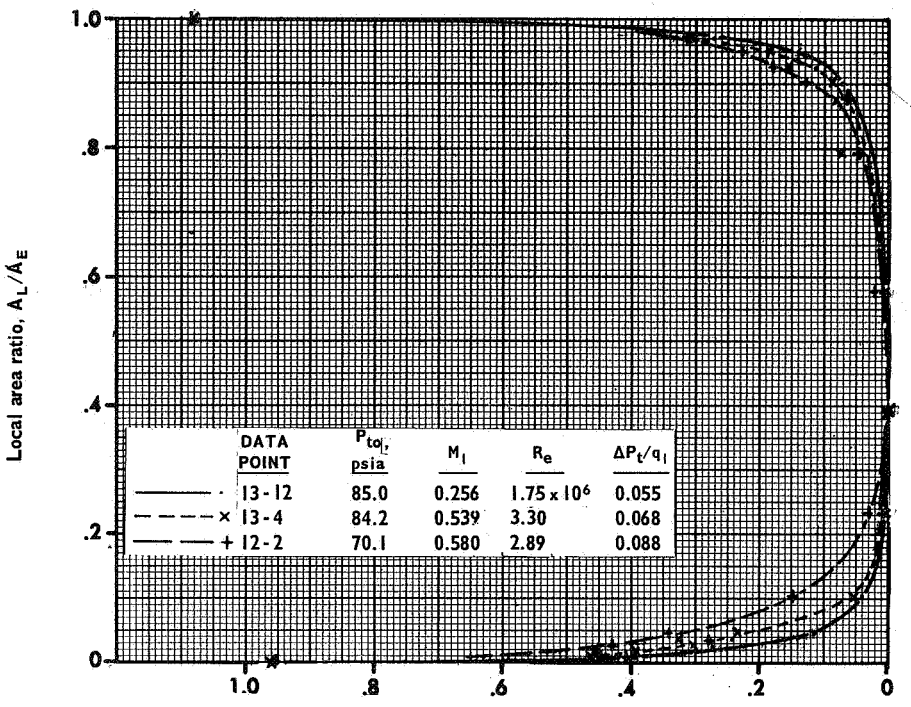

(c) 75% lightbulb inlet, configuration 3.

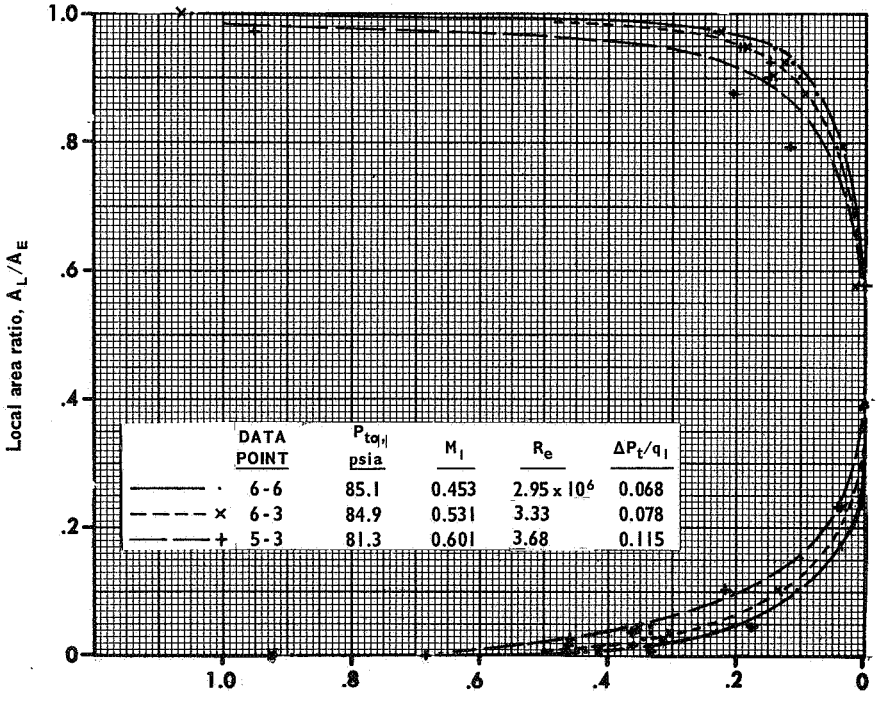

(d) 95% lightbulb inlet, configuration 4.

Figure 11. – Concluded.

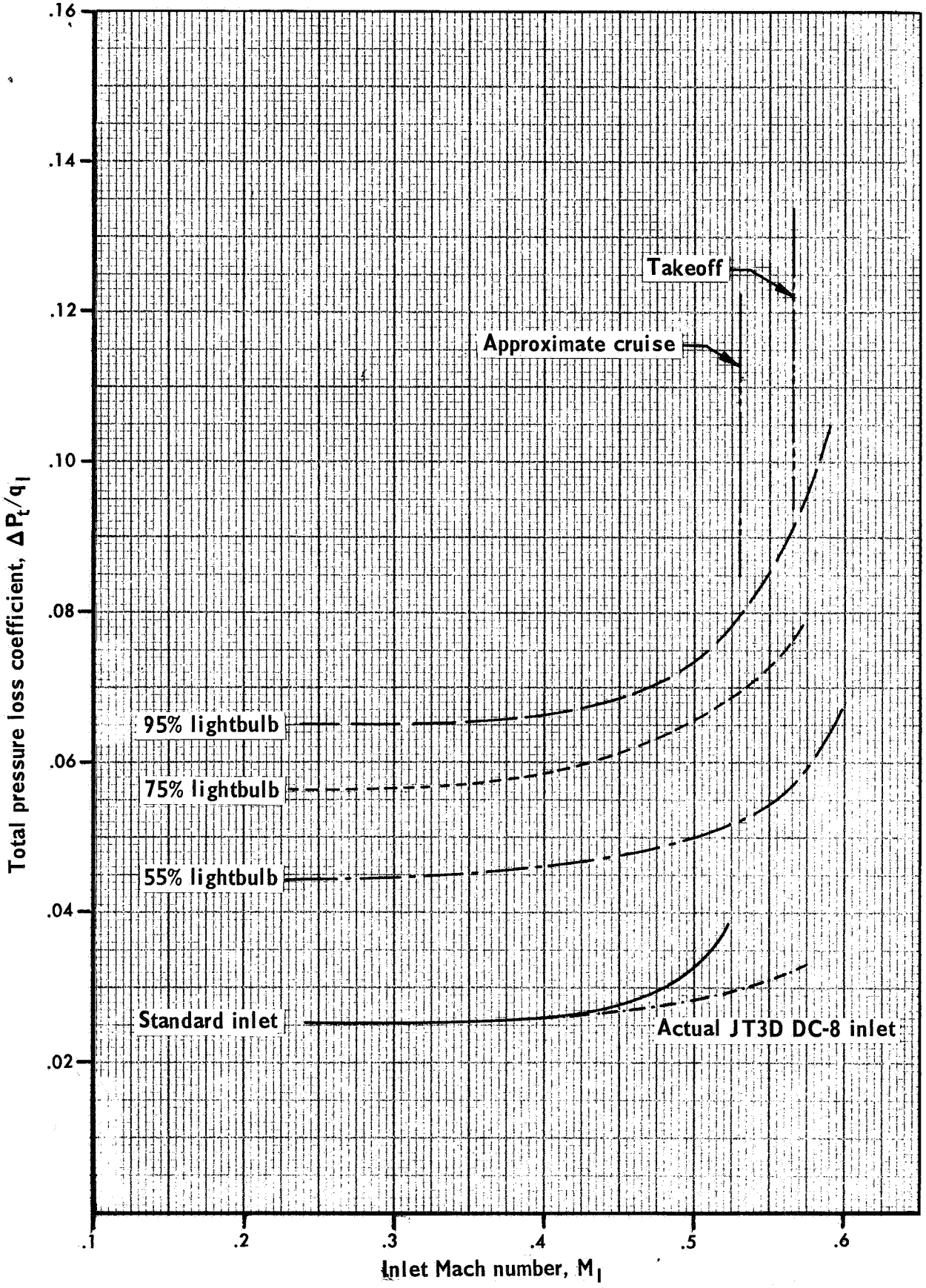

Figure 12.- Summary of total pressure loss coefficients at full scale Reynolds numbers.

At low speeds ($M_1 < 0.35$) the total-pressure losses were fairly proportional to the internal wetted area, as measured from the leading-edge of the inlet lip to the engine station. The comparison is summarized in figure 13. The deviations from the straight line are in part due to the different velocity distributions within the inlet.

Figure 14 shows typical surface pressure-coefficient distributions for all configurations. This figure demonstrates the applicability of the potential-flow calculations. The potential-flow solutions were made for the lip shape shown by the dashed lines on figure 14. The solid lines represent the shapes tested. At low velocities, the potential-flow solutions correlated well with the data. However, at high Mach numbers the peak pressures were greater than predicted.

It may be seen in figure 14 that supersonic velocities occurred on the bullet of configuration 3 and on configuration 2. As a consequence, these configurations must be considered marginal although the performance shown in figure 13 is good. Enlarging the duct area in the vicinity of the pressure peak is recommended for any additional tests with these configurations. The design of the enlargement may be accomplished effectively with the potential flow program.

Wind-tunnel tests were also made at reduced Reynolds numbers. Typical smoothed total-pressure-loss data for a range of stagnation pressures (Reynolds number) are shown in figure 15 for configurations 1 and 2. The influence of Reynolds number was slight, consisting essentially of an increased skin friction effect, providing that flow separations did not occur. However, configuration 1 with its sharp inlet lip showed evidence of flow separation. This inlet demonstrated a pronounced influence due to Reynolds number, showing how erroneous wind-tunnel data can be when tests are made at low Reynolds numbers.

Full-Scale JT3D Duct-Wall SPL Measurements

In order to determine the degree of nonlinearity in the acoustical resistance of the surface lining material that might need to be considered in the design of the duct linings for the JT3D engine and to obtain a better understanding of the actual acoustical environment, measurements were made of the sound pressure levels at the wall of an inlet duct and a fan-discharge duct. Data were obtained at two positions in the inlet at a station about 3 in. forward of the leading edges of the inlet-guide vanes — one location was about 18° clockwise of the top centerline (0°) and the other was about 108° clockwise of the top; a third location was on the wall of the left-hand fan-discharge duct. The tests were conducted during September 1965, on the Douglas DC-8 engine test stand located at Edwards Air Force Base, using a JT3D-3 turbofan engine equipped with prototype long fan-discharge ducts. These prototype ducts (which were built during the DC-8 long fan duct development program as prototypes for the current production articles) were the only fan-discharge ducts that could be obtained at the time.

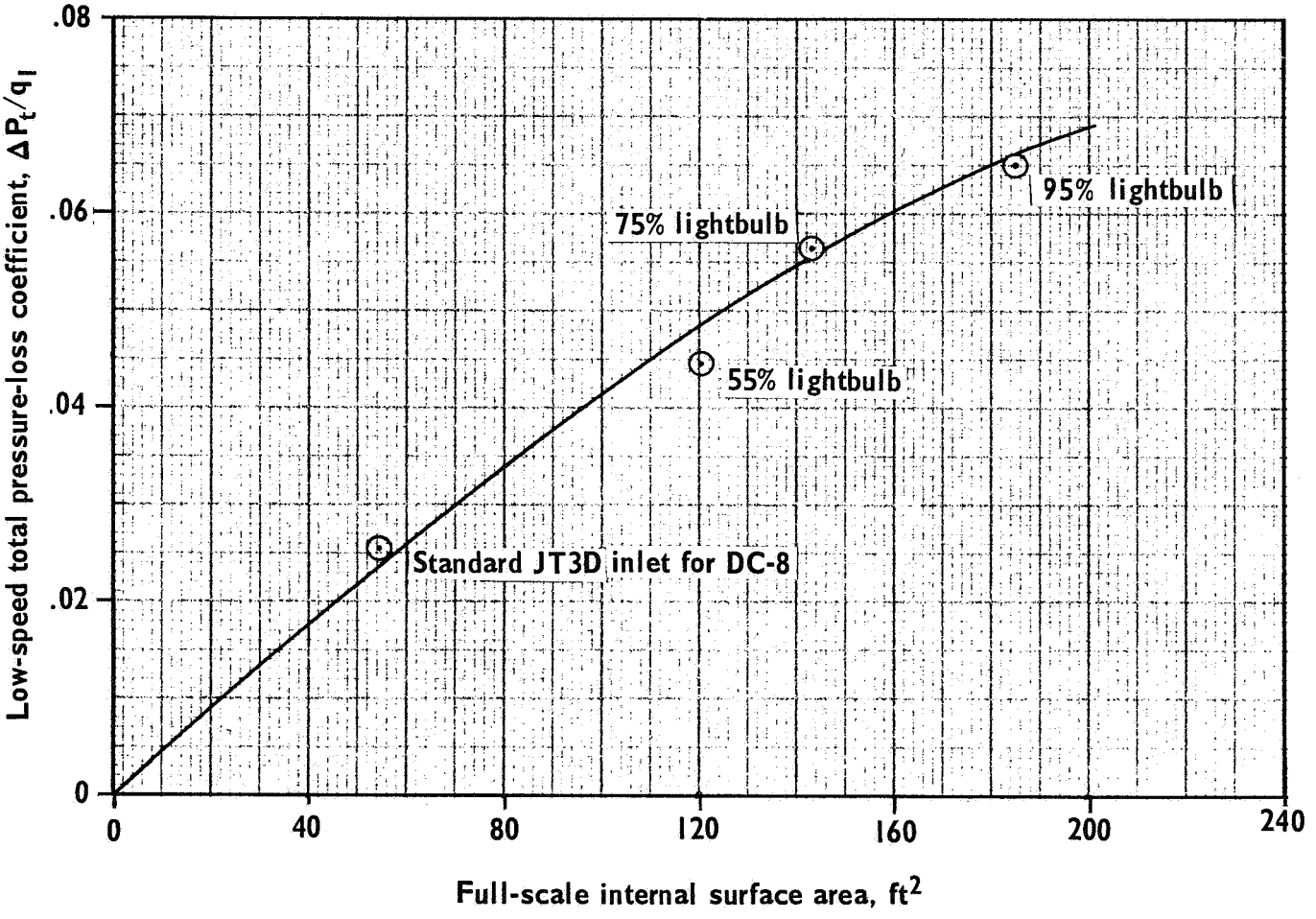

Figure 13.- Low-speed total pressure-loss coefficients of lightbulb inlets ($M_1 < 0.3$).

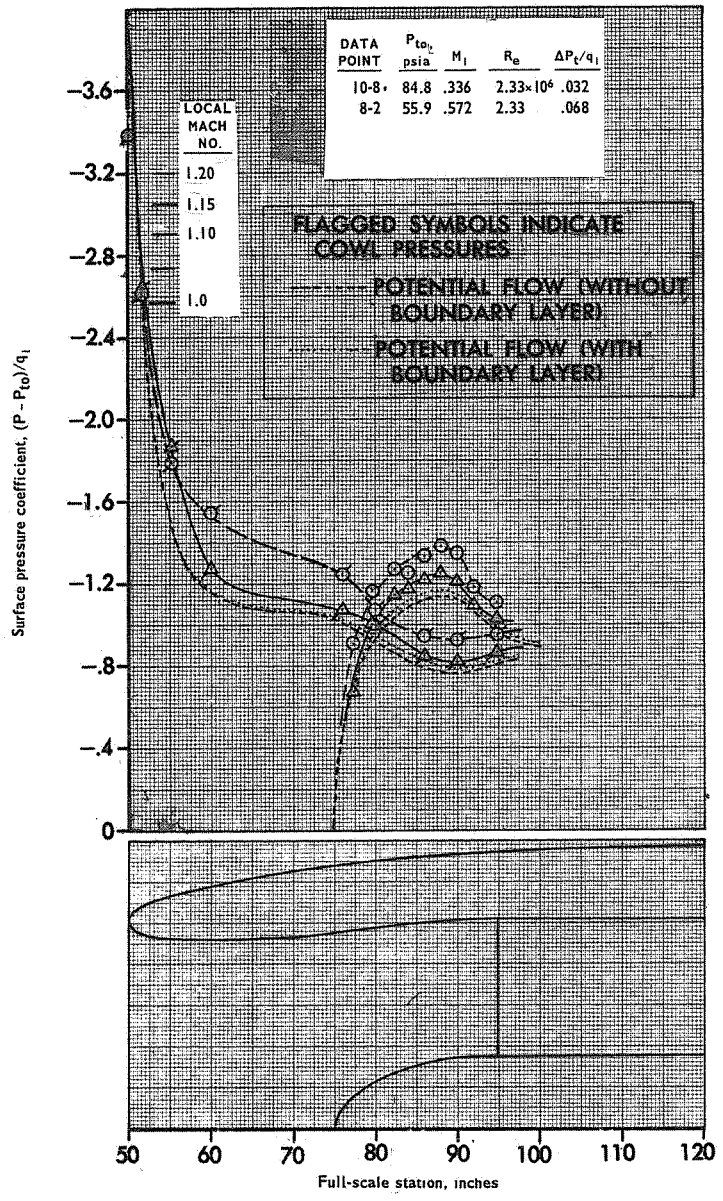

(a) Standard DC-8 inlet, configuration 1.

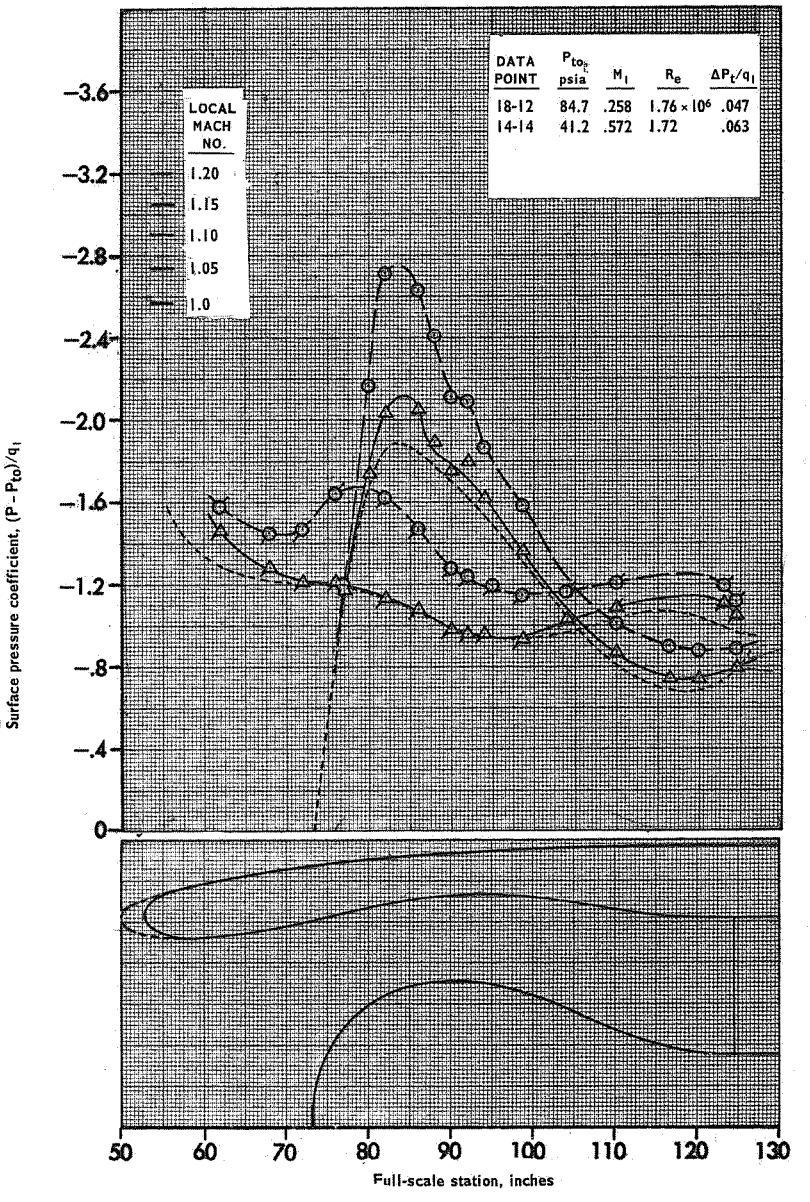

(b) 55% lightbulb inlet, configuration 2.

Figure 14.- Effect of inlet Mach number on surface pressure coefficients.

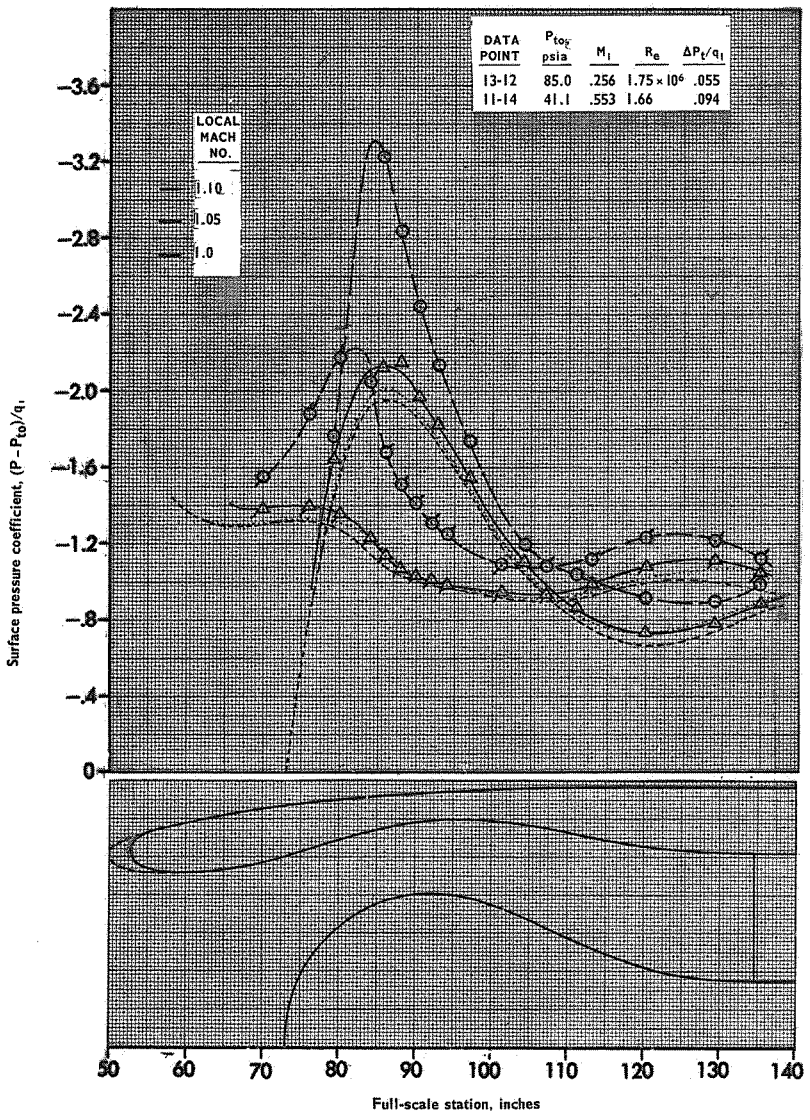

(c) 75% lightbulb inlet, configuration 3.

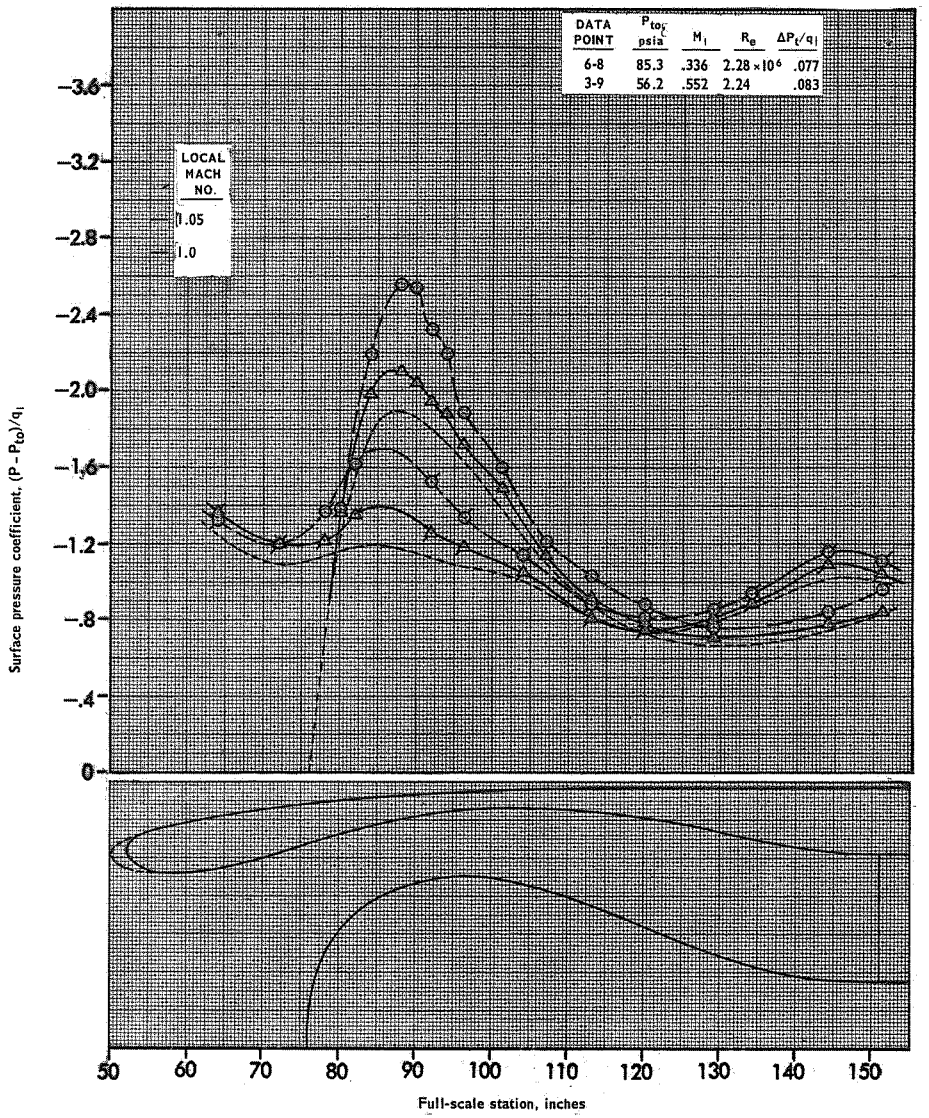

(d) 95% lightbulb inlet, configuration 4.

Figure 14.- Concluded.

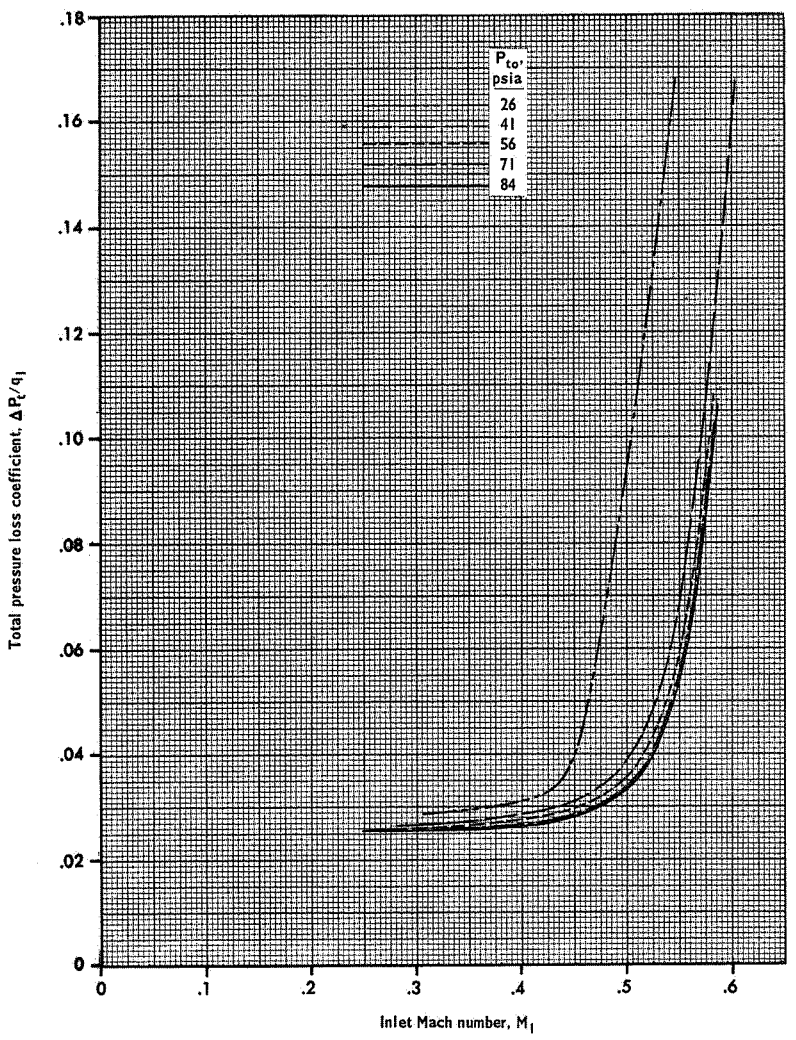

(a) Standard DC-8 inlet, configuration 1.

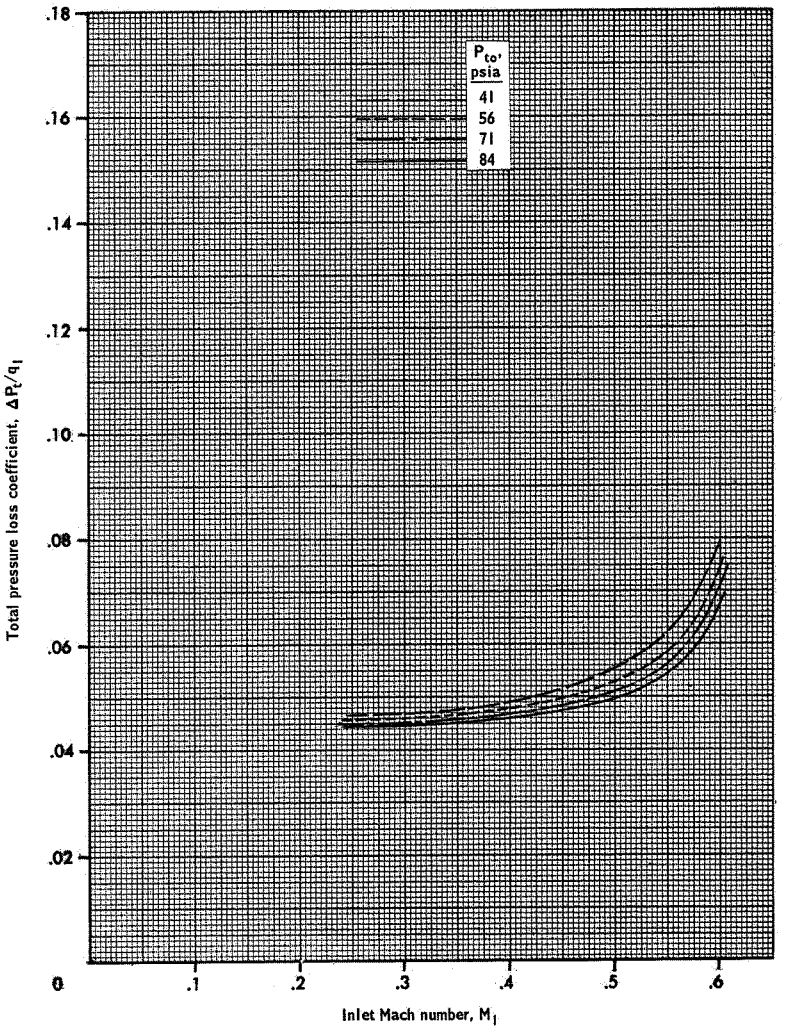

(b) 55% lightbulb inlet, configuration 2.

Figure 15.- Effect of stagnation pressure on total pressure-loss coefficients.

Measurements were made with a 0.25-in. diameter microphone (Bruel and Kjaer type 4136) mounted flush with the duct wall. The microphone located on the fan-discharge duct was installed on the bifurcated part of the duct about 20 in. downstream of the fan-air-exit attach flange and about 4 in. upstream of what would be the nozzle station on a short fan-discharge duct. It was located on the outboard duct wall about 5 in. below the horizontal centerline. Sound-pressure levels were recorded on magnetic tape at several engine power settings between idle and takeoff. The data were analyzed with a narrow-band filter (6 percent) to observe the discrete tones at blade-passage frequencies and their harmonics.

Representative inlet and fan-discharge duct data are shown in figure 16. The data have been reduced to pressure spectrum levels (representing the mean-square sound pressure per unit frequency) for the wide band random part of the spectrum. This presentation makes the line spectra from the pure tones very evident, the height of the line representing the amplitude of the pure tone. Several important features can be observed. At takeoff (EPR 1.82), the level of the discrete frequency tones is very high. However, the level is still higher at reduced engine power settings. The maximum level measured was in the fan-discharge duct for an EPR of 1.50 where a value of 161 dB at about 3000 Hz was observed, figure 16b. No data were obtained at higher engine powers in the fan duct due to an unsatisfactory microphone mounting which allowed the microphone cartridge to be damaged. The amplitude of the discrete frequency tones above the estimated random background noise level is shown to be between 30 and 50 dB.

In the inlet duct, the frequencies that were observed were all related to the number of blades (35) on the first rotor stage; no fundamental or harmonic frequencies related to the number of blades on the second rotor stage (32) were observed.

In the fan-discharge duct, frequencies related to the number of blades on both the first and second rotor stages were observed. At idle (EPR 1.04), the tones were multiples of 32 blades; at EPR 1.22 all the observed tones were multiples of 35 blades; at EPR 1.41 multiples of both 32 and 35 blades were noted, and at EPR 1.50, the tones were related only to 32 blades. Therefore, it appears that only the first rotor stage produces tones in both inlets and fan ducts at landing power settings (EPR about 1.2) and that at high engine power settings, the first rotor stage generates the inlet tones while the second rotor stage generates the tones in the fan-discharge ducts.

In addition to the SPL's at the fundamental frequencies, measurements were obtained at the second, third, and sometimes the fourth harmonic of the fundamental. A fifth harmonic was observed once at a frequency of about 13 000 Hz.

Figure 17 shows the variation of the SPL's at the frequency of the fundamental and the second harmonic as a function of EPR for the inlet duct location and the fan duct location. The maximum levels do not occur at takeoff RPM, but rather at a lower RPM corresponding roughly to an EPR of 1.45. On a standard day at sea level for static conditions, this EPR

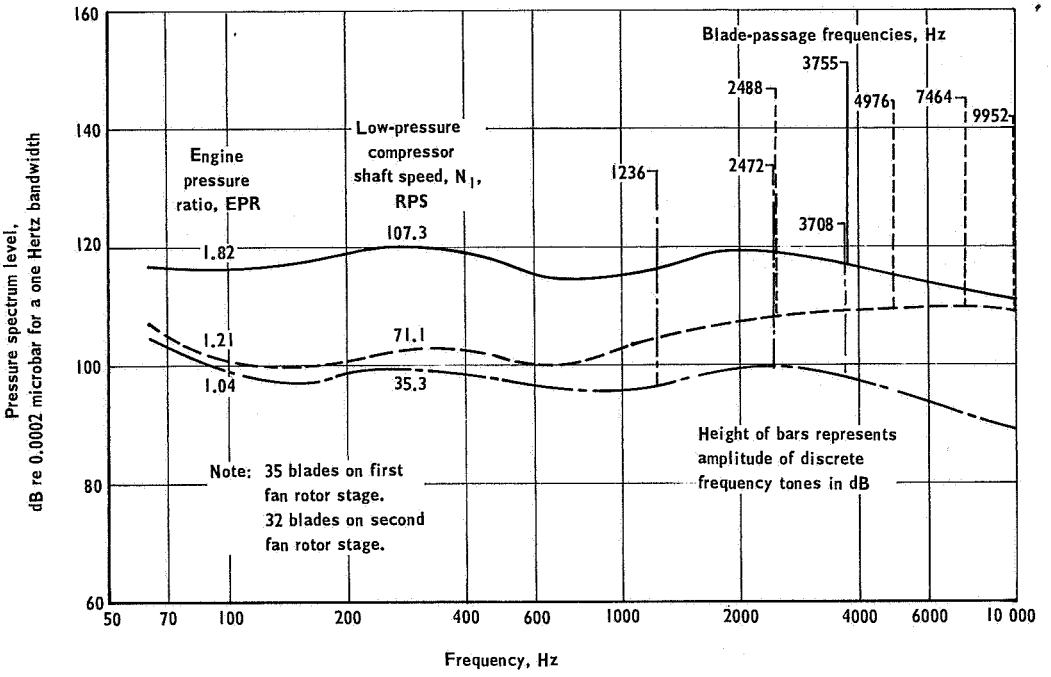

(a) Microphone located on inlet case about 3-inches forward of inlet-guide vanes.

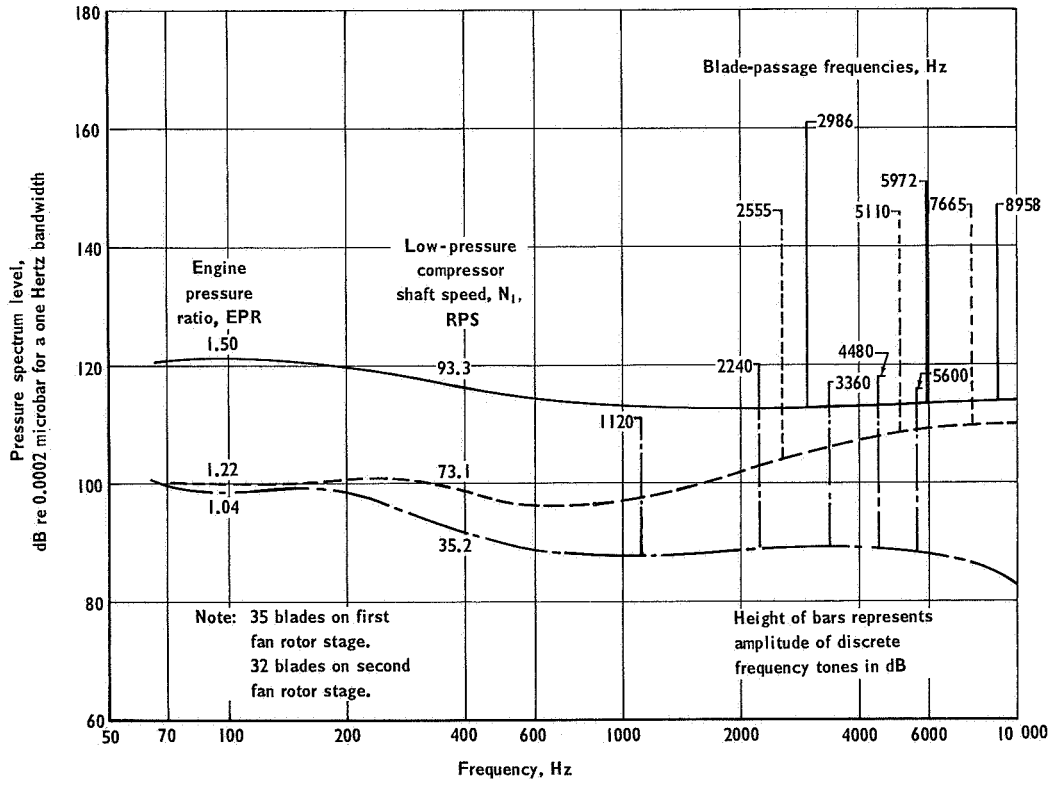

(b) Microphone located on left-hand fan-exhaust duct about 20-inches aft of fan-exhaust-duct-to-engine-case attachment flange.

Figure 16.- Spectra of acoustic excitation at the wall of the inlet and the fan-discharge ducts.

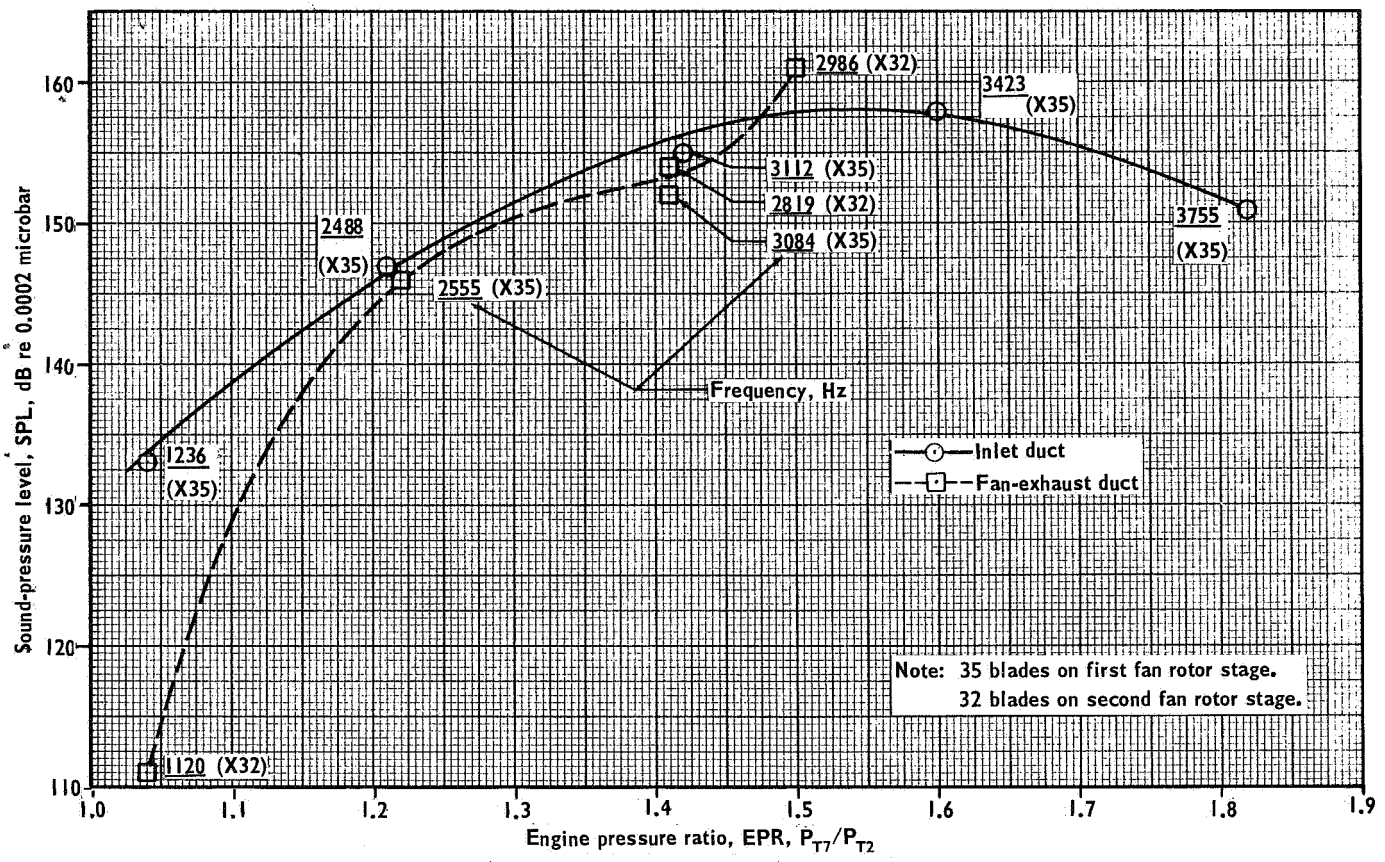

(a) SPL at the fundamental blade-passage frequency.

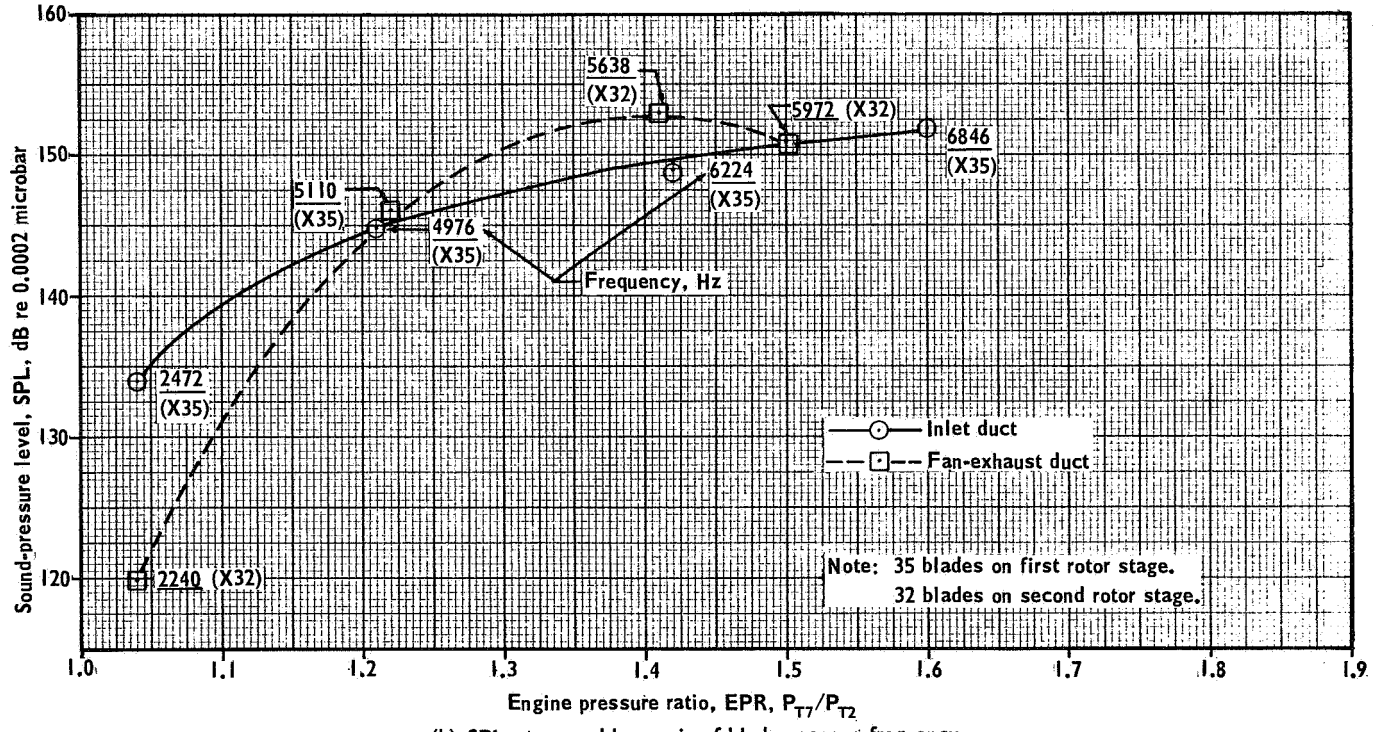

(b) SPL at second harmonic of blade-passage frequency.

Figure 17.- Variation of sound-pressure level in the inlet and fan-discharge ducts as a function of engine pressure ratio.

corresponds to a total net thrust which is about 67 percent of the maximum available thrust (18 000 lb). In studying these curves, it should be recalled that the EPR during takeoff is about 1.83 and during landing, it is usually between 1.1 and 1.2, depending on the landing weight. At a reduced throttle setting corresponding to that which might be used following takeoff (e.g., in a noise-abatement type of operation), the EPR might be between 1.3 and 1.4.

The tests described above have shown that the discrete-frequency sound-pressure levels to which the sound absorbent duct lining is likely to be exposed will be between 145 and 160 dB and that, if the treatment is to be effective during takeoff as well as landing, the frequency range in which absorption is required is between 1500 and 10 000 Hz. Furthermore, it was shown that the fan-discharge duct sees the pressure field of the first and second fan rotor stage while the inlet sees only the pressure field associated with the first fan rotor stage. This observation could be useful in future efforts by the engine manufacturers to control or reduce the noise at the source. Finally, the magnitude of the pure tones above the spectrum level of the random background was observed to be between 30 and 50 dB, depending on the frequency and the engine power setting.

Laboratory Acoustical Studies

Two kinds of laboratory tests were run to study the acoustical properties of the materials to be used for the transmission-loss tests; namely, airflow-resistance tests and normal-incidence acoustic-impedance tests. The results obtained from these tests along with the transmission-loss (TL) tests and certain engineering design information supplied by the vendors, serve as the basis for the recommended duct lining techniques for the nacelle acoustical treatment.

Airflow resistance tests. — Specific airflow resistance, one of the important basic properties of a porous acoustical material, reference 35, is defined as the airflow resistance per unit thickness of the material. The airflow resistance of a material sample is usually measured under steady airflow conditions and equals the ratio of the pressure drop across the sample, ΔP, to the velocity, u, of the linear airflow through the sample. The velocity u is most conveniently determined by measuring the volume rate of flow U and then dividing this quantity by the area of the sample S. Therefore, with the centimeter-gram-second system of units, the equation is

$$R_f = \frac{\Delta P}{u} = \frac{\Delta P}{U/S} \qquad \frac{\text{dynes/cm}^2}{\text{cm/sec}} \quad \text{or cgs rayls} \qquad (3)$$

The specific airflow resistance is then obtained by dividing by the average thickness of the sample, t, to obtain in a mixed system of units (for more ready comparison to results obtained by other investigators),

$$R_1 = \frac{R_f}{t} \qquad \text{cgs rayls/inch} \qquad (4)$$

Hereafter, the term cgs rayls will be abbreviated to rayls, a unit which will be recognized as having been named for Lord Rayleigh.

The apparatus used to determine the specific airflow resistance (or flow resistance for short) is shown in figure 18. A small vacuum pump was used to draw air from the atmosphere through the sample. Rotameter-type flow meters capable of measuring a flow range of 100 to 22 000 cm^3/min determined the volume rate of flow. The pressure drop across the sample was measured with a precision micromanometer which used a null indicator to permit very accurate determinations of the pressure drop. Pressure drops ranged from 0.005 to 0.1 inch of water (12.5 to 250 dynes/cm^2). The sample holder tube, shown in figure 18b, was specifically designed to avoid flow around the edge of the sample which can occur with a more conventional type flow resistance measuring tube. Samples undergoing test were tightly clamped between wide flanges covered with rubber gasketing to prevent flow through the inlet face of the tube flange and sample. Tests run with the edge perimeter completely sealed established that there was no edge flow contribution in these tests on thin samples (0.1-in. thick).

Results of flow resistance tests on two types of fibermetals are shown in figure 19. The flow resistance increases very rapidly as the density approaches that of a solid sheet, i.e., 100-percent dense stainless steel. For a given density and thickness, material made with finer fibers (C-28 with nominal 0.003-in. diameter fibers) has greater flow resistance than material made with coarser fibers (C-38 with nominal 0.004-in. diameter fibers). This is attributed to the fact that there are more wires per unit volume with the finer fibers and thus more and smaller void spaces, or pores, and hence more viscous resistance to the passage of airflow, i.e., greater flow resistance. Another factor accounting for the displacement between the two curves in figure 19 is that all of the 0.003-in. diameter fiber samples were without any screen reinforcing while all of the 0.004-in. diameter fiber samples had screen reinforcing. The screen reinforcing just acts to increase the strength and also the density without changing the flow resistance. Thus, if the C-38 samples had not been screen reinforced the resulting curve in figure 19 would have just shifted parallel to itself to the left. Typical results taken from references 25 and 36, for other porous acoustical absorbers, are also shown for comparison with the fiber metal. These materials are known to be excellent absorbers and were used in the TL tests as alternatives to air for cavity-filling materials behind a lining of fibermetal.

Since the flow resistance of porous materials can be a function of the flow velocity (or particle velocity of the air molecules), measurements were made over a range of flows. The result of a series of tests of this sort is given below for 10-cm diameter samples of type C-38 fibermetal with a nominal thickness of 0.040 inch, screen reinforced on both sides with 18-mesh, 0.009-in. box weave wire screen. From these results, it appears that, at least over this very limited range of particle velocities, the flow resistance is essentially constant. However, data supplied by the vendor indicate that nonlinear effects occur at higher particle velocities. These nonlinear effects are attributed to acoustic streaming phenomena and to the onset of turbulent airflow through the pores of the material. As the flow becomes turbulent the friction increases, over that which exists when the flow is laminar, and a greater pressure differential is required to push air at the same flow rate through a given thickness of sample.

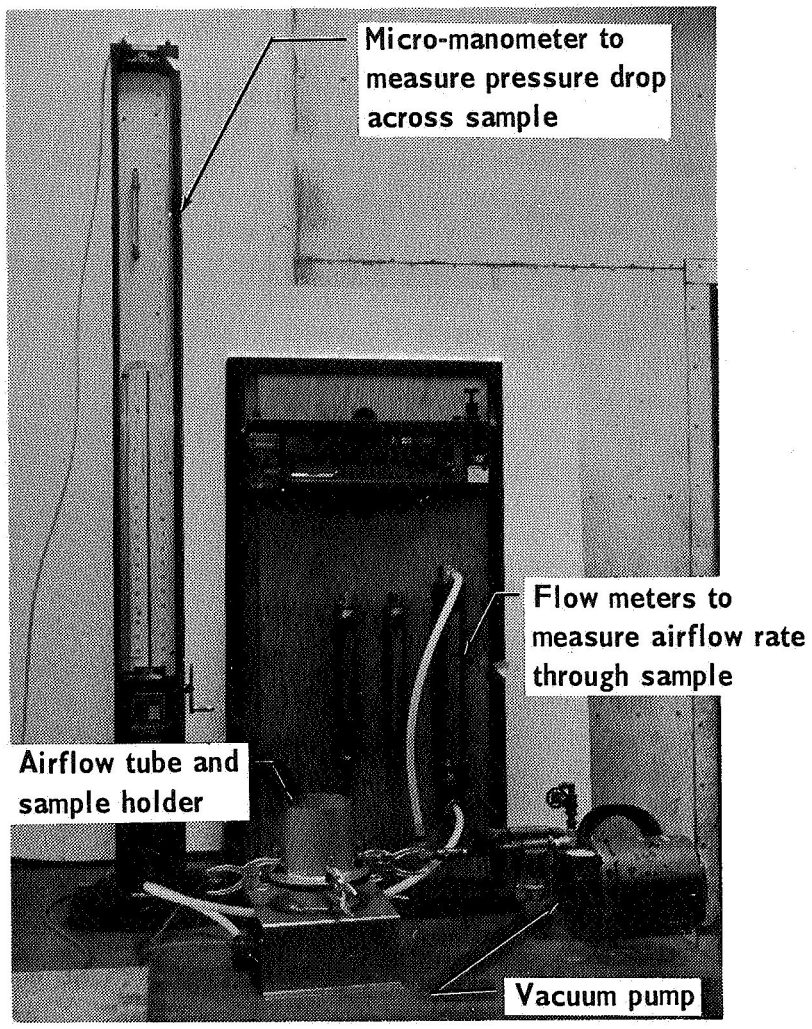

(a) Flow-resistance apparatus; four clamps on airflow tube shown for illustration, eight clamps used for tests.

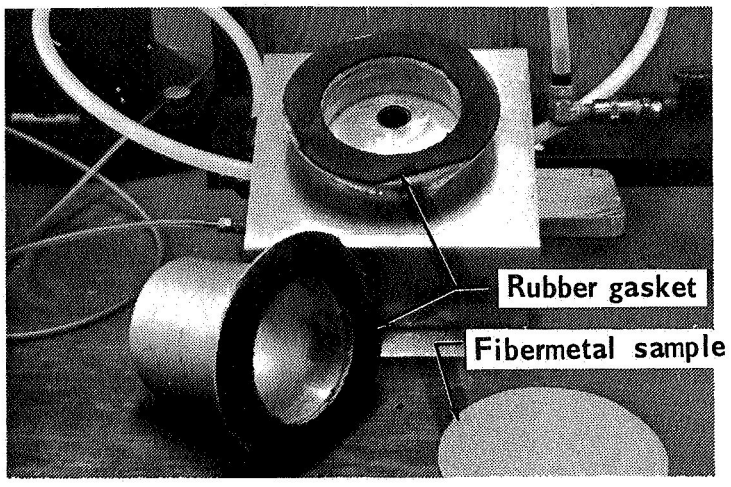

(b) Close-up of 10-cm airflow tube.

Figure 18.- Apparatus for laboratory determination of acoustical properties of materials.

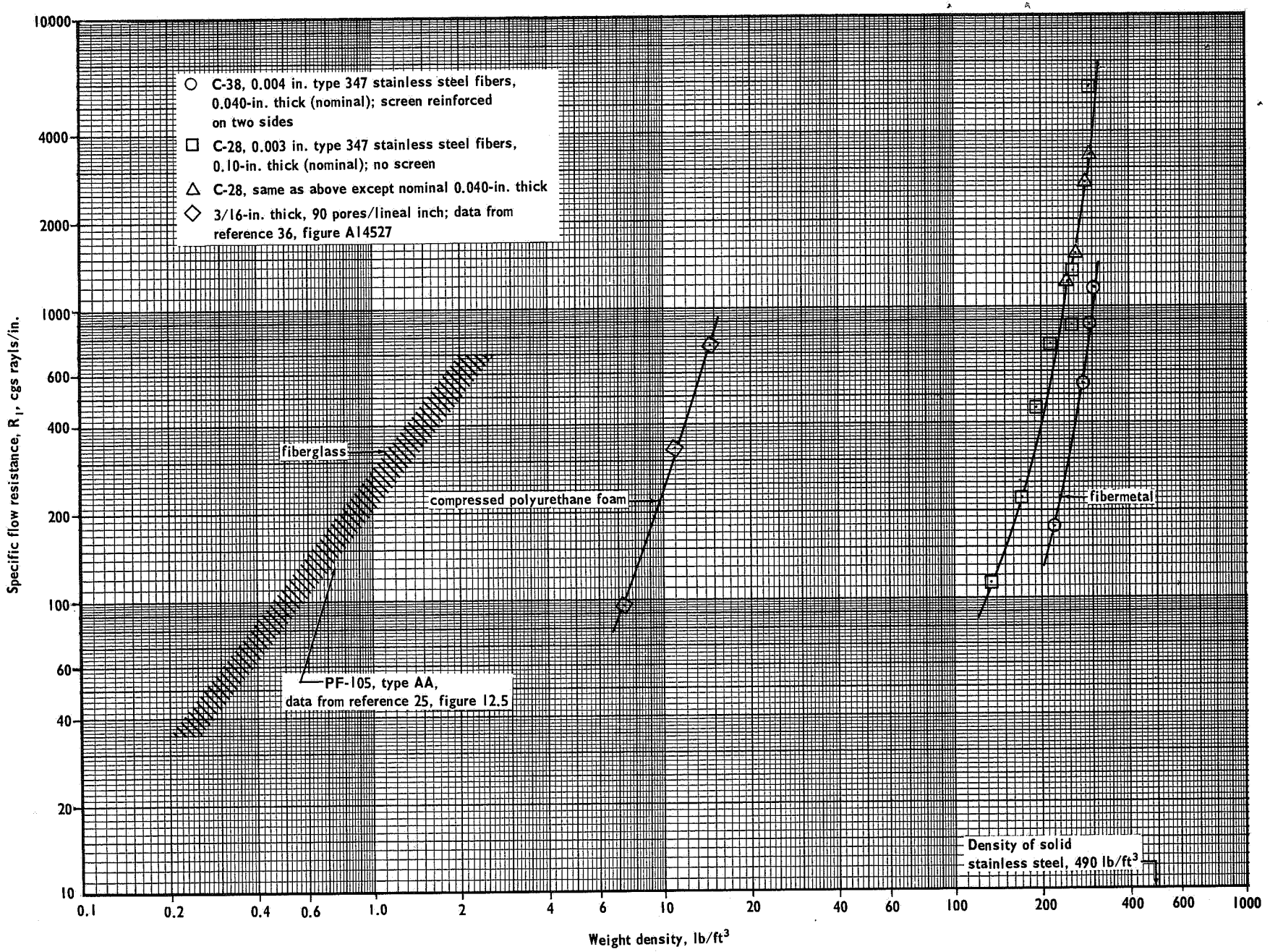

Figure 19.- Specific flow resistance of acoustical materials.

Particle velocity, cm/sec	Flow resistance, cgs rayls			
	Sample 23 Nom. 10 rayl	Sample 5 Nom. 25 rayl	Sample 19 Nom. 40 rayl	Sample 10A Nom. 60 rayl
1.70	8.8	23.5	38.2	55.7
2.54	7.8	24.4	39.1	58.7
3.40	7.3	25.7	40.3	60.2
4.24	8.8	24.1	40.5	60.5

Figure 20 illustrates the nonlinear behavior of fibermetal by a series of curves showing the flow resistance as a function of the sound pressure level of a plane acoustic wave having a particle velocity equal to that of the measured steady, linear airflow rate. The curves shown in figure 20 are the result of steady airflow-resistance tests over a wide range of flow velocities (9 to 600 cm/sec) for each of the five samples. Since it has been shown, references 22 and 35, that the airflow resistance, determined under dc steady-flow conditions, closely approximates the real part of the acoustic impedance, determined under ac alternating-flow conditions, the measured linear particle velocities are shown in figure 20 as being equivalent to an acoustic particle velocity or sound pressure level.

The calculation of the equivalent SPL proceeds as follows: consider a free, plane, progressive sound wave in which the rms sound pressure, p, and the rms particle velocity of the wave, u, are related by the characteristic impedance, Z_o, of the air.

Thus,

$$\frac{p}{u} = Z_o \tag{5}$$

and

$$SPL = 20 \log_{10} \frac{p}{p_{ref}} = 20 \log_{10} uZ_o + 74, \text{ in dB} \tag{6}$$

The impedance of the air is a resistance equal to the product of the density of the air and the speed of sound through the air. Thus, for standard conditions (15°C at sea level),

$$Z_o = \rho_o c = 41.6 \text{ rayls} \tag{7}$$

in the cgs system of units. Substituting equation (7) into equation (6) gives the following relation for the equivalent sound pressure level:

$$SPL_{eq} = 20 \log_{10} u + 106.4 \tag{8}$$

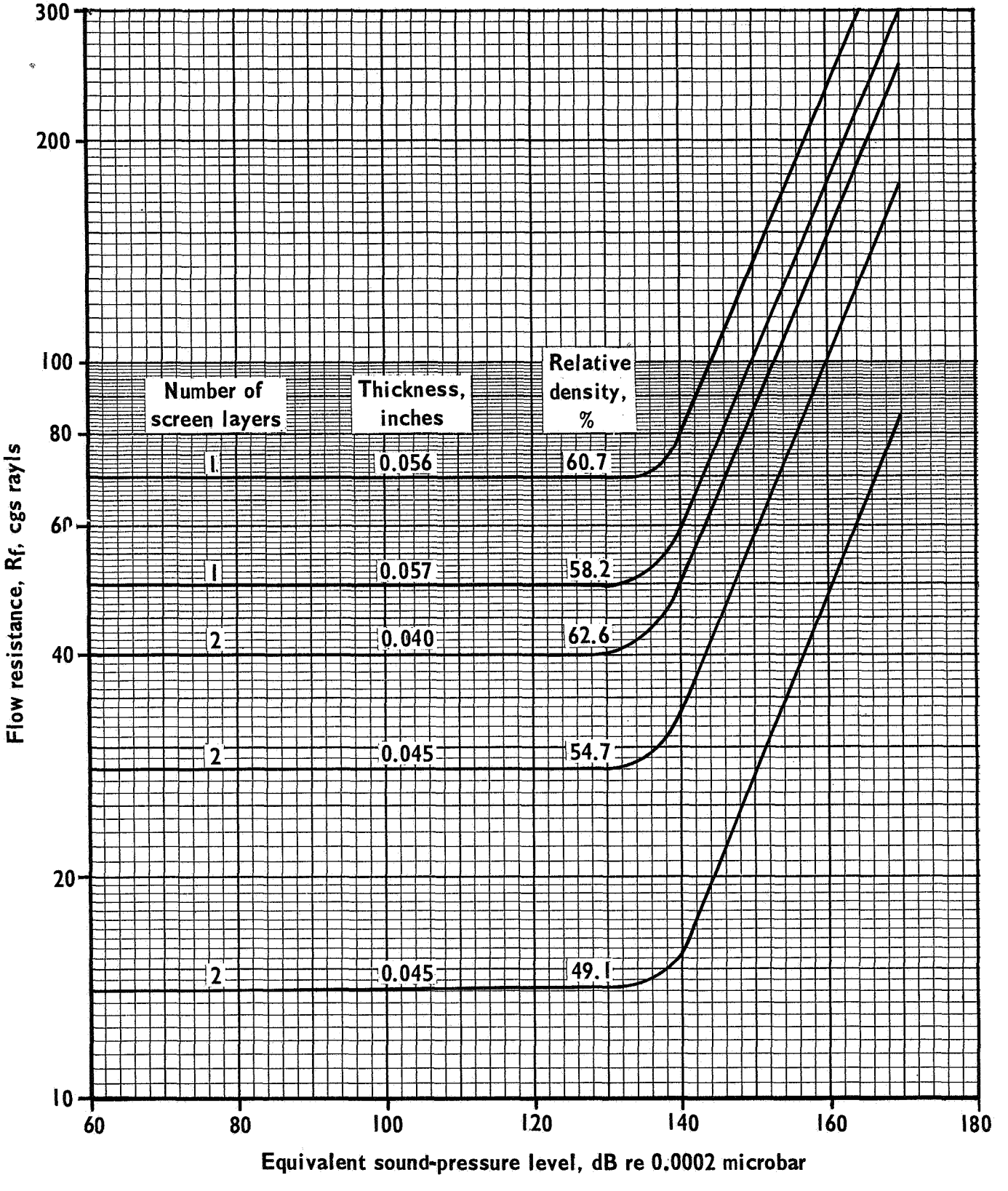

Figure 20.- Variation of flow resistance of type C-38 fibermetal with equivalent sound-pressure level. (Data courtesy of the Huyck Metals Company, Milford, Conn.).

In application of this equation the rms particle velocity u of the free, plane, progressive wave is assumed to be equivalent to the linear, dc airflow velocity through the tube of the flow resistance apparatus.

The indicated increases in the flow resistance in figure 20 are rather drastic. For example, a piece of fibermetal which behaves as 28-rayl material for SPL's less than 130 dB would have a flow resistance of 175 rayls at 170 dB. Conversely, if it is desired to have the flow resistance of the lining material be equal to 40 rayls at a level of 160 dB, then it would appear that approximately 13-rayl materials should be specified for the lining since the flow resistance is always specified in the linear region of the curve.

Acoustic impedance tests. — Various studies have indicated that the sound absorbing ability of a particular type of acoustical absorbent may be determined by first measuring the basic acoustic properties of the material, correcting for the differences in the method of mounting the material through consideration of the boundary conditions, and finally correcting for the effect of the environment by detailed consideration of the nature of the sound field to which the material is exposed. The basic acoustical properties that are required by the theory are the complex propagation constant and the characteristic impedance. The propagation constant is strictly a function of the material and can be characterized by certain physical properties of the material.

Beranek, reference 35, lists the following five factors as the ones required to determine the propagation constant of a porous material: specific airflow resistance, porosity, structure factor, volume coefficient of elasticity of the air in the interstices and the volume coefficient of elasticity of the skeleton of the material. The specific airflow resistance has been described above; the porosity is related to the density for material with solid fibers and no binder (i.e., fibermetal).

Thus, the porosity Y is

$$Y = 1 - \frac{\sigma_s}{\sigma_f} \tag{9}$$

where σ_s is the density, or weight density, of the sample and σ_f is the density of the fibers. Referring to figure 19 the porosity of C-38 fibermetal with screen on two sides is seen to vary from about 55 percent to about 35 percent. This range probably encompasses the range of values useful for acoustical applications. There was no simple, well-established method for determining the value for the last three factors mentioned above and hence the propagation constants could not be determined.

Although the propagation constant was not measured, the specific acoustic impedance was determined for various combinations of fibermetal and cavity backing treatments. The definition of the specific acoustic impedance is the complex ratio of the sound pressure to the component of particle velocity normal to the surface of the sample. In theory, the sample is considered as being semi-infinitely thick.

The specific acoustic impedance was determined with a B&K type 4002 standing-wave tube which had been modified to use a high-power high-frequency loudspeaker, figure 21. In this apparatus, the loudspeaker establishes a standing wave pattern in the tube which is probed by a small-diameter tube attached to a movable cart containing a microphone. A 3-cm diameter brass tube was used as a standing-wave tube. Sinusoidal signals with frequencies between 1250 and 6300 Hz were used to excite the tube. The SPL's at the points of the maximum and minimum pressures and the locations of these maxima and minima are used to calculate the specific acoustic impedance. The maximum SPL's were on the order of 100 to 115 dB. The specific acoustic impedance (or, for short, the acoustic impedance) was determined from the equations given in reference 35, pp. 318-321. An IBM model 7094 digital computer was used to perform the calculations.

The acoustic impedance in rayls has been normalized by the characteristic impedance of the air, i.e.,

$$Z = \frac{Z_A}{\rho_o c} = \frac{R_A}{\rho_o c} + j \frac{X_A}{\rho_o c} \qquad (10)$$

where $R_A/\rho_o c$ is the normalized real part and $X_A/\rho_o c$ is the normalized reactive part of the acoustic impedance. The acoustic impedance Z_A is a complex quantity because, in general, the pressure and the particle velocity are not in phase.

Figures 22 and 23 illustrate some of the typical results obtained from the impedance measurements and show the variation with frequency of the real and reactive parts of the specific impedance ratio of a 25-rayl fibermetal surface with various cavities. Figure 22 shows the effect of increasing the depth of an air-filled cavity behind the fibermetal. The real part is essentially independent of frequency, in this frequency range, and also of the backing depth, maintaining a value of about 0.7 $\rho_o c$ units (i.e., 0.7×41.6 or about 29 rayls). The reactive part shows a regular progression as the depth of the cavity is increased. In interpreting these curves, the real part is related to the energy losses due to viscosity and is similar to a radiation resistance since acoustic power is being transmitted across a surface. The dynamic resistance is slightly larger than the static resistance (29 rayls compared to 25 rayls) but it does not vary rapidly with frequency.

The acoustic reactance consists of two parts

$$X_A = \omega M_A - 1/\omega C_A \qquad (11)$$

where M_A is the acoustic mass and C_A is the acoustic compliance. Thus, when the reactance is positive it is dominated by a mass inertance term (because it is the inertia of the mass of air in the pores that has to be overcome by the kinetic energy of the applied pressure) and when the reactance is negative, it is dominated by the compliance term. The compliance is

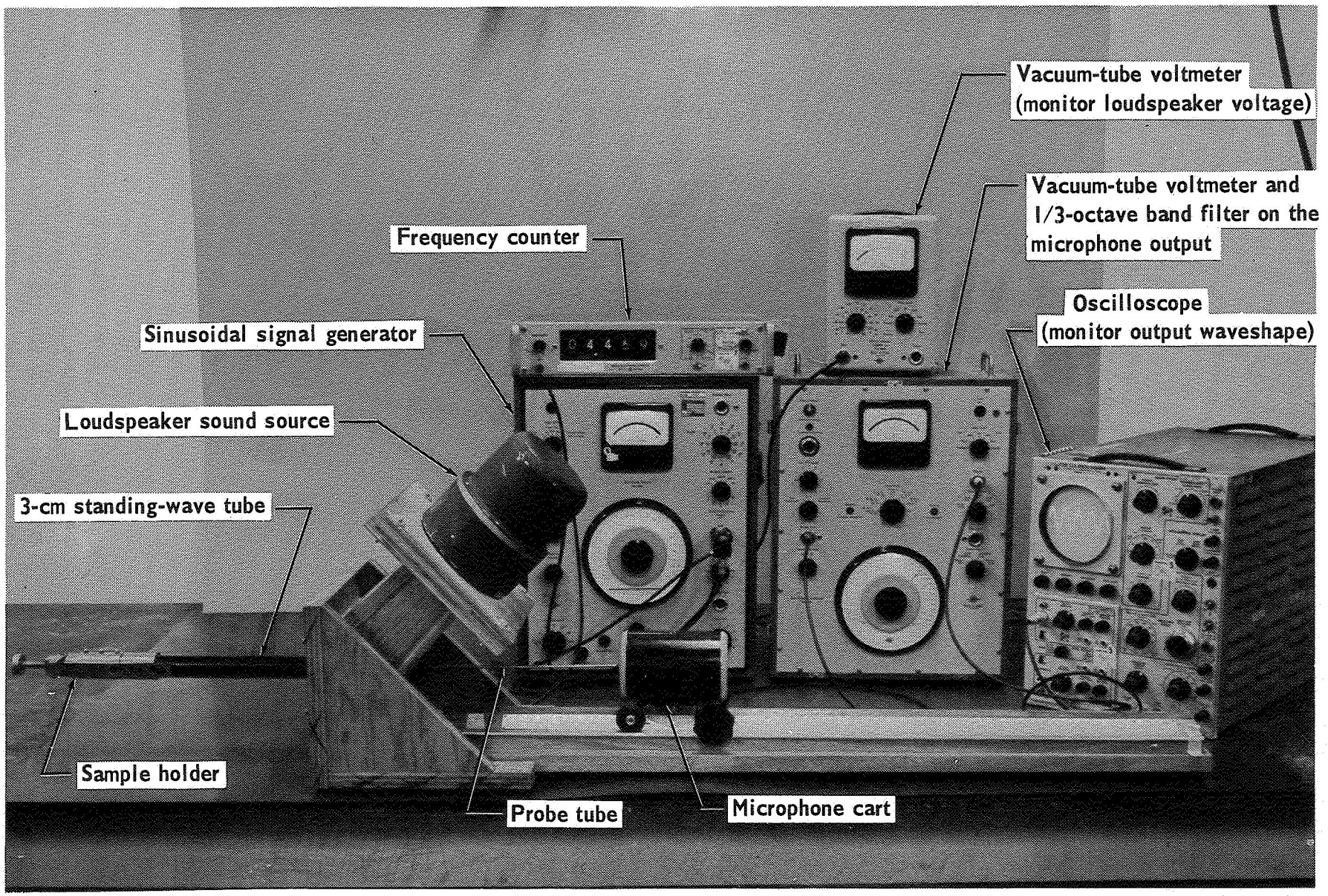

Figure 21.-Standing-wave tube apparatus for measuring acoustic impedance.

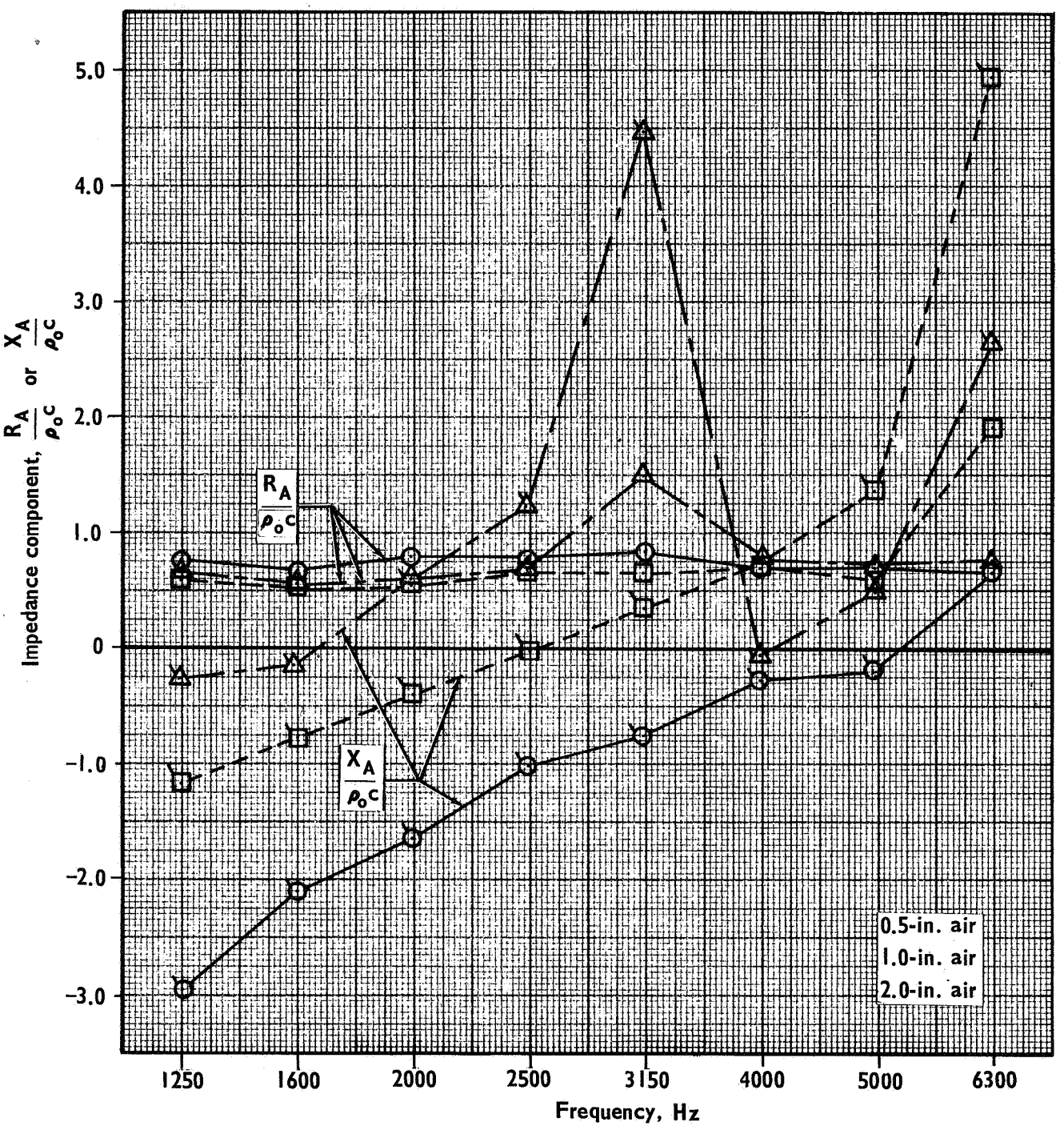

Figure 22.- Real and reactive parts of the acoustic impedance for 25-rayl fibermetal with various air-filled backing cavities.

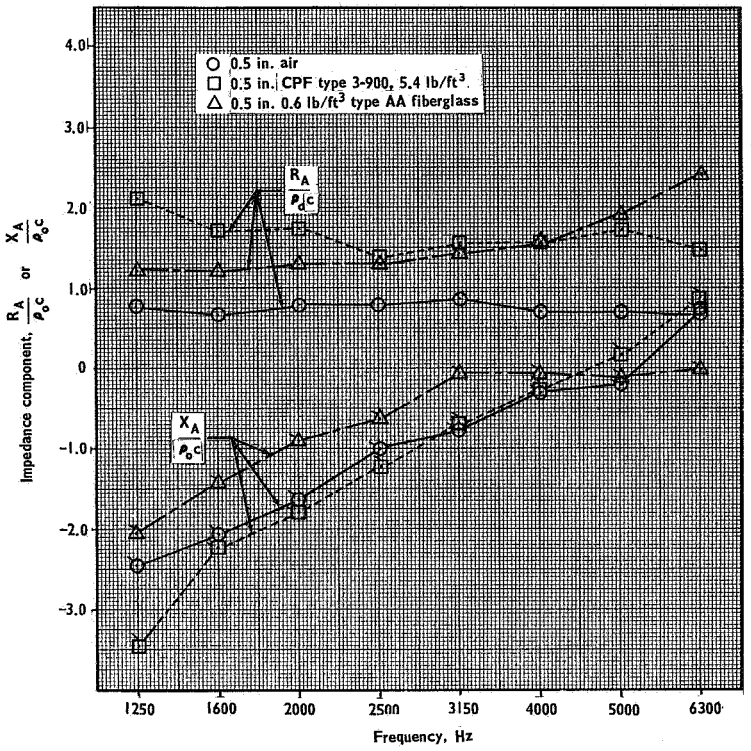

(a) 0.5-in. thick cavity.

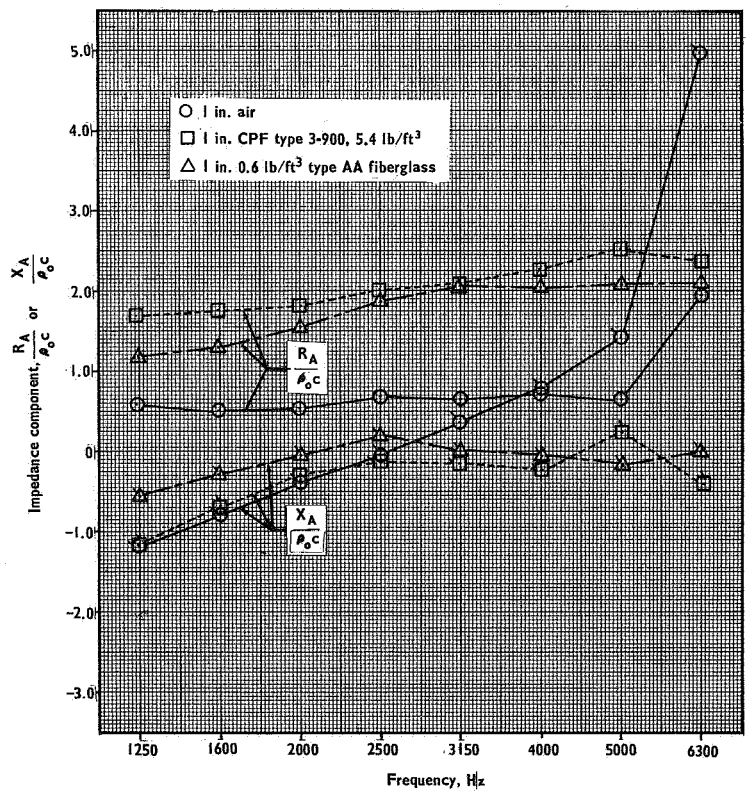

(b) 1.0-in. thick cavity.

Figure 23.- Real and reactive parts of the acoustic impedance for 25-rayl fibermetal with various cavity filling materials.

related to the stiffness of the air in the volumes of the pores. It is the potential energy stored in the spring-like stiffness of this volume that reacts with the kinetic energy of the mass inertance to produce the resonance phenomena at certain frequencies. At resonance, the mass reactance equals the compliance reactance and the total reactance is zero because these two components are 90° out-of-phase with each other. The frequency of resonance can be estimated then as the frequency where the reactance curve crosses the frequency axis.

For a 1-in.-deep cavity at 6300 Hz, the reactance and resistance have positive peak values, figure 22. At this frequency, there exists a standing wave structure in the cavity (the half-wavelength at 6300 Hz is about 1 in.) and the high pressures at the surface of the fibermetal create a large mass-like term, due to an increase in the effective density of the air in the pores. The total acoustic impedance is greatly increased when this occurs and the sound absorbing ability of the system is correspondingly reduced. For a 2-in.-deep cavity, a half-wavelength occurs at 3150 Hz and a full wavelength occurs at 6300 Hz. The reactance curve has corresponding peaks at 3150 and 6300 Hz. The 0.5-in.-deep cavity shows only a rising reactance curve because the half-wavelength occurs at 12 600 Hz.

Figure 23 shows the effect of filling 0.5-in.- and 1.0-in.-deep cavities behind 25-rayl fibermetal with two different types of porous absorbers. Stuffing the cavity increases the dynamic flow resistance ($R_A/\rho_o c$) and decreases the high-frequency reactance. From figure 19, we can estimate that the flow resistance of type 3-900 compressed polyurethane foam is about 23 rayls in a 0.5-in. thickness while type AA fiberglass (with a density of 1.2 lb/ft^3) has a flow resistance of about 160 rayls for the same thickness; for 1.0-in. thicknesses, the flow resistances are just doubled. Type AA fiberglass has a nominal fiber diameter of 0.00004 inch. Figure 24 shows the variation in the impedance for a 1-in.-deep air-filled cavity with fibermetal surfaces of various flow resistances. Although increasing the flow resistance from 10 to 40 rayls did not affect the reactance greatly, the real part of the impedance did increase in direct proportion to the increase in static flow resistance. Further study of the impedance data is required to determine possibilities for modifications to an absorbent structure to increase its absorptivity.

Figures 25 through 29 illustrate the trends in the normal-incidence absorption coefficients that were obtained for various absorptive structures. The normal-incidence acoustic absorption coefficient α_N was computed from the standing-wave ratios (SWR):

$$\alpha_N = 1 - \left[\frac{SWR - 1}{SWR + 1}\right]^2 \qquad (12)$$

Four samples of fibermetal with flow resistances of 10, 25, 40 and 60 rayls were used with four different backing materials of varying thicknesses: air, type 3-900 compressed polyurethane foam, and type AA fiberglass with densities of 0.6 and 1.2 lb/ft^3. Descriptions of the configurations and the calculated components of the acoustic impedance and the average absorption coefficients are given in table I.

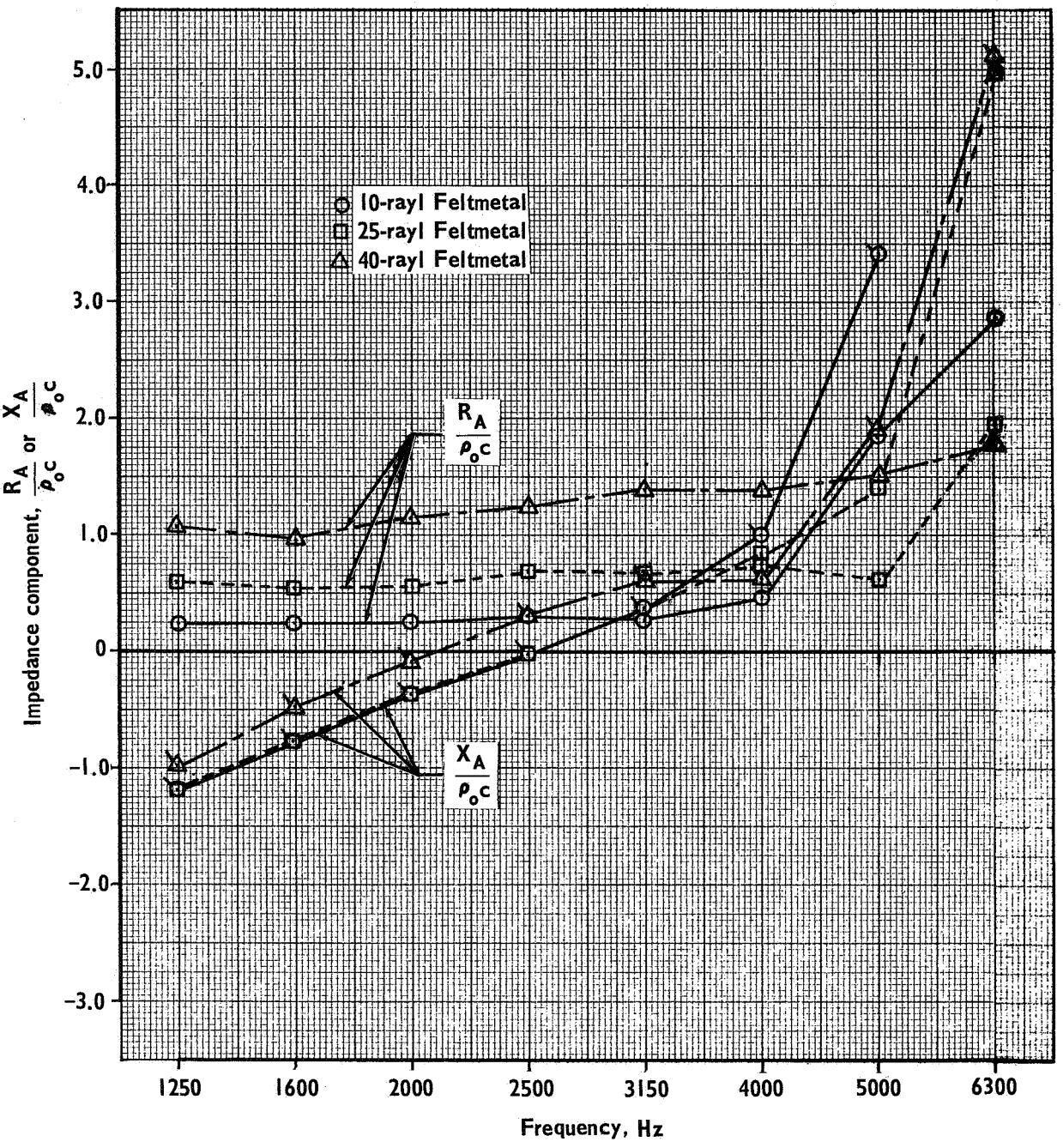

Figure 24.- Real and reactive parts of the acoustic impedance for a 1-in. deep air-filled cavity with fibermetal surfaces of various flow resistances.

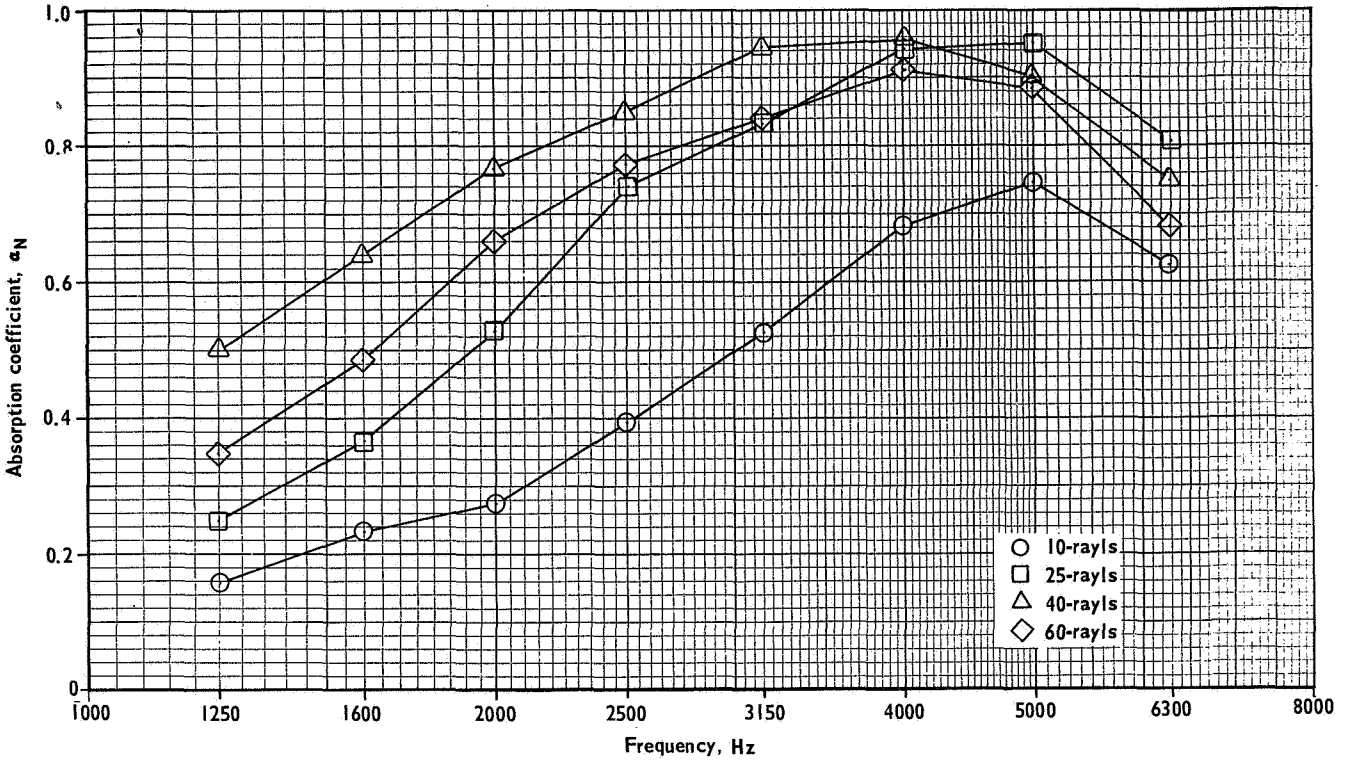

(a) 0.5-in. deep cavity.

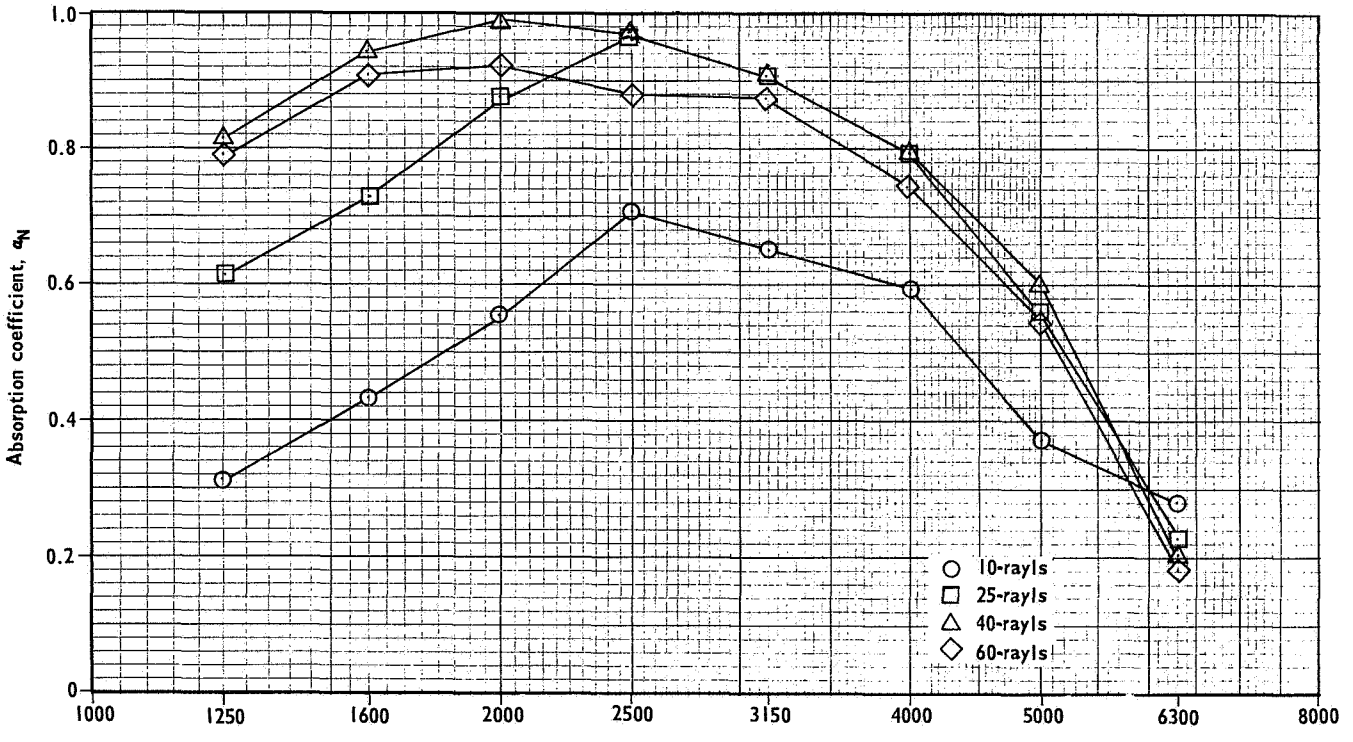

(b) 1.0-in. deep cavity.

Figure 25.- Normal-incidence absorption coefficients of fibermetal surfaces with various air-filled cavities.

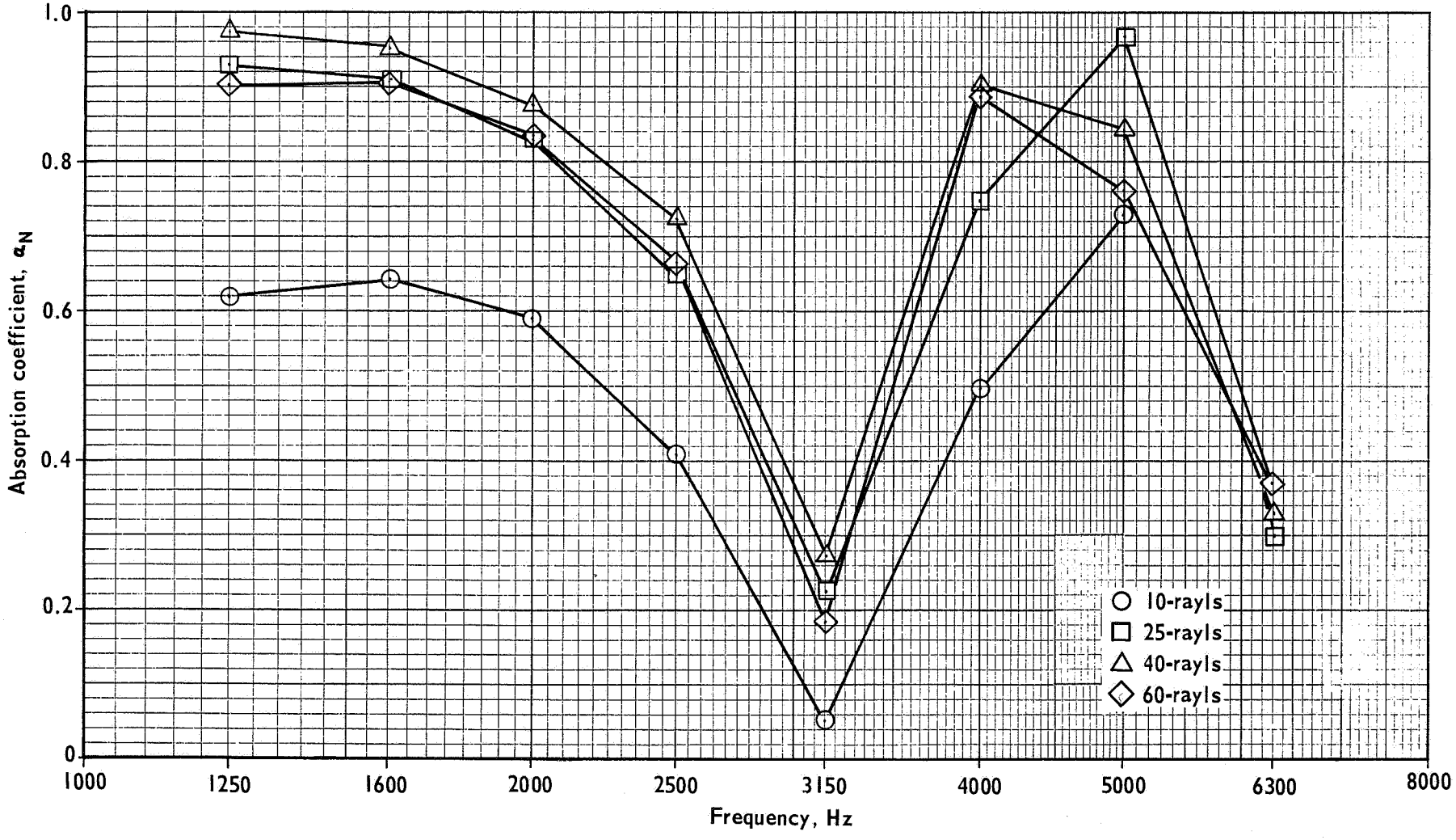

(c) 2.0-in. deep cavity.

Figure 25.- Concluded.

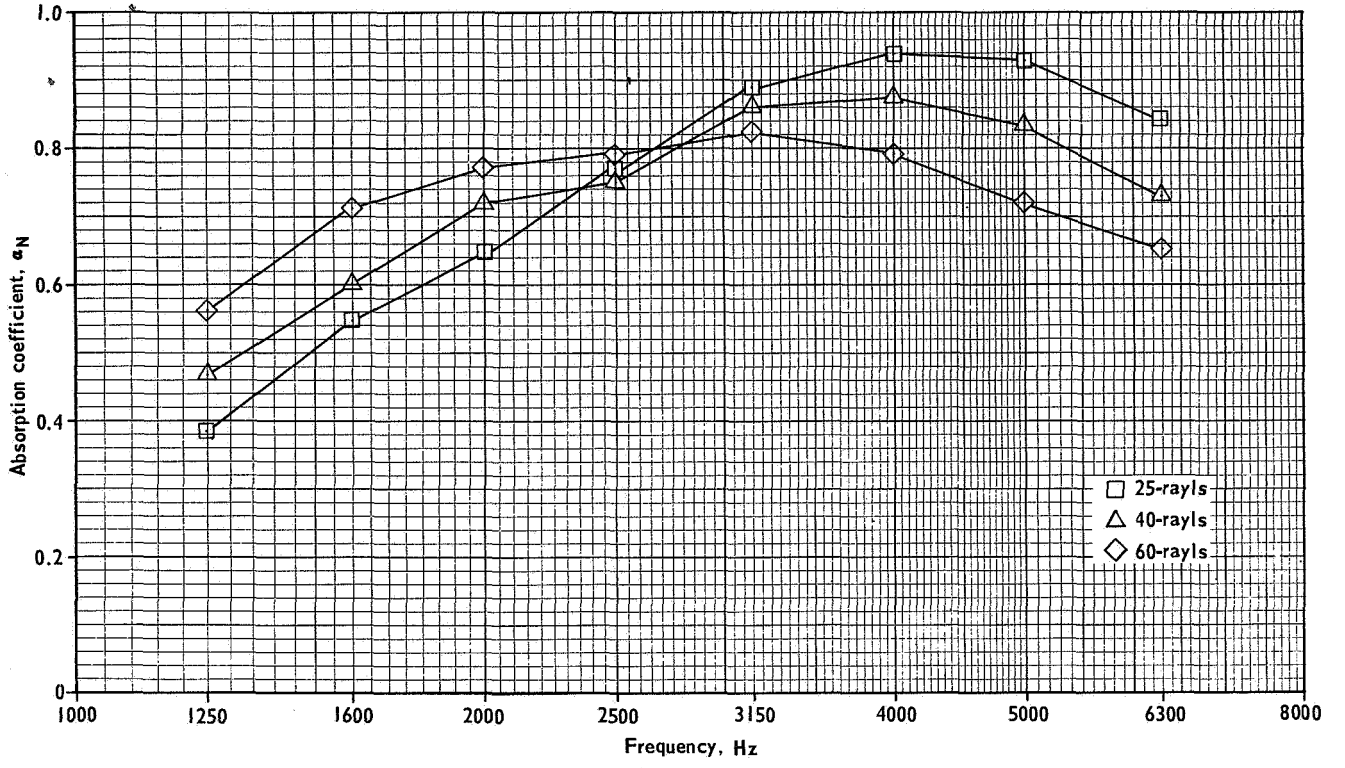

(a) 0.5-in. deep cavity.

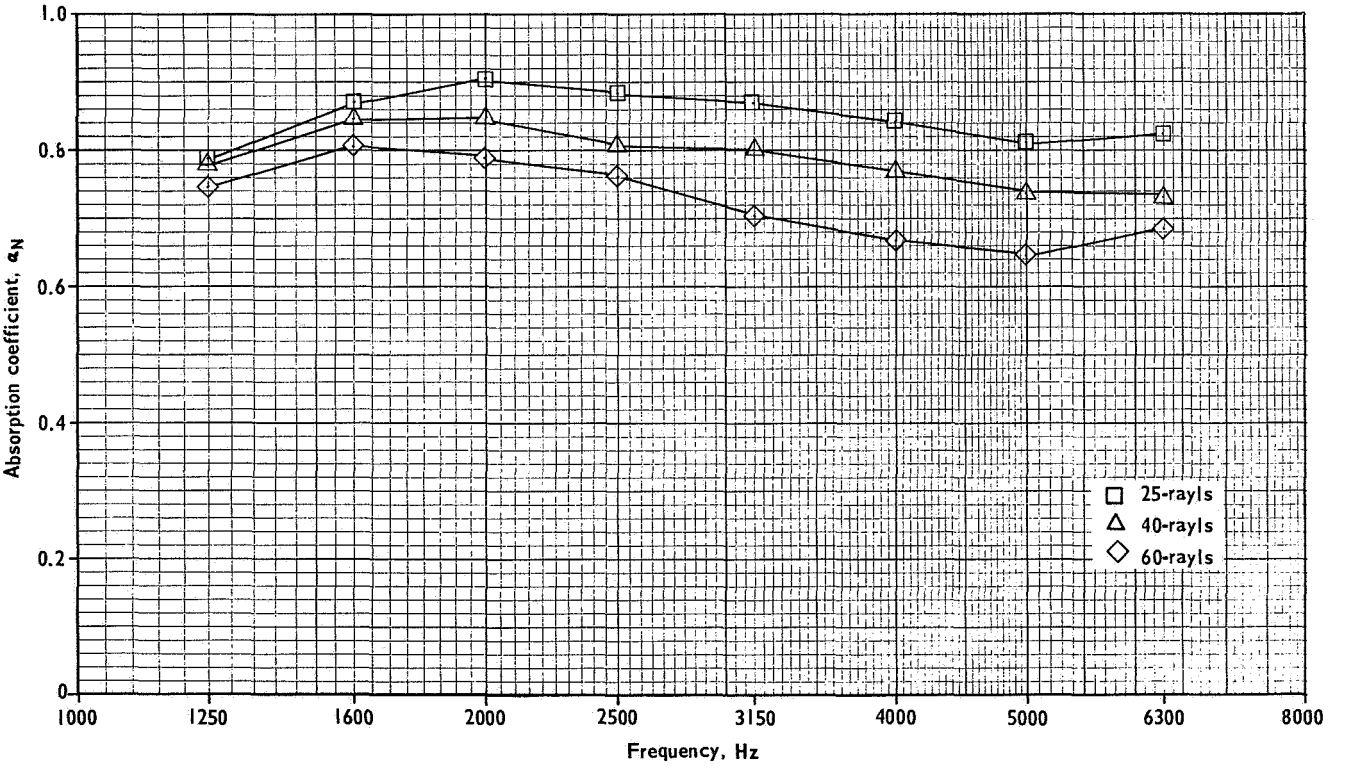

(b) 1.0-in. deep cavity.

Figure 26.- Normal-incidence absorption coefficients of fibermetal surfaces and cavities filled with type 3-900 compressed polyurethane foam.

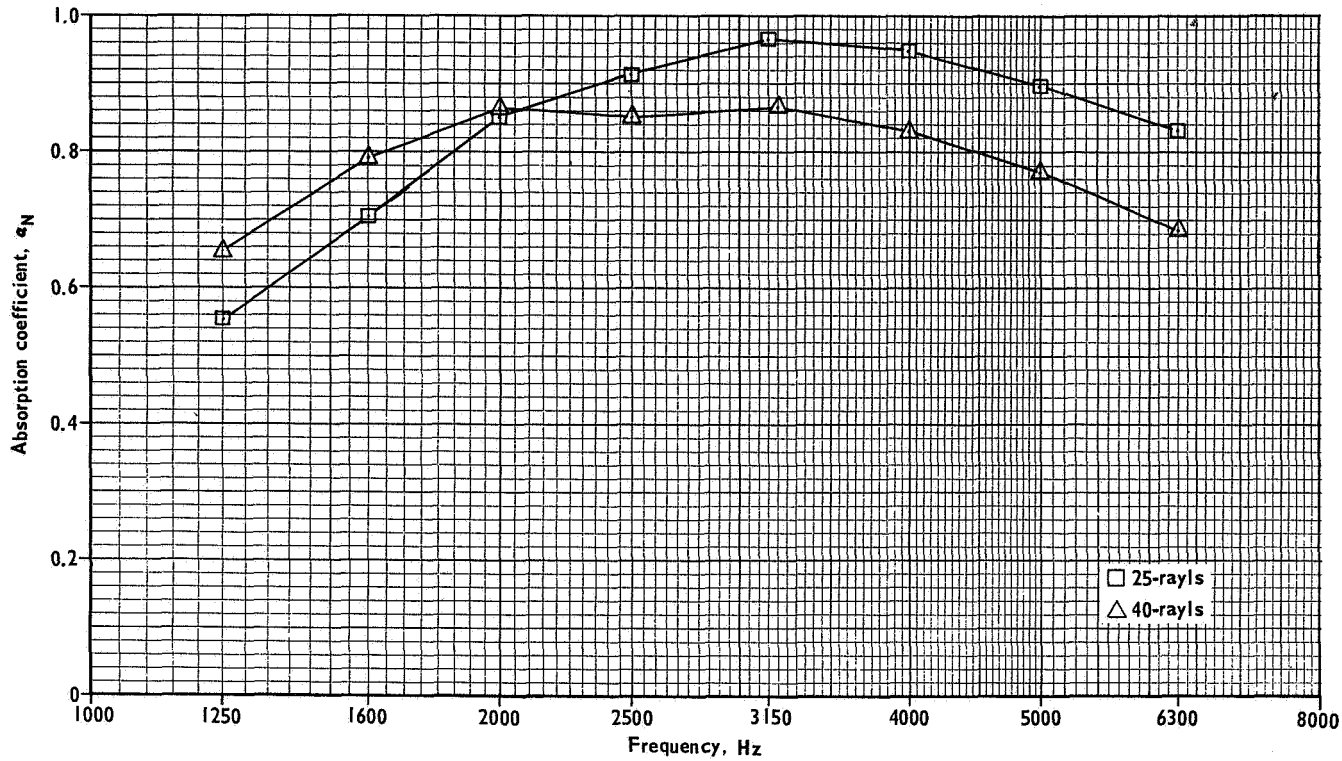

(a) Fiberglass density 0.6 lb/ft^3.

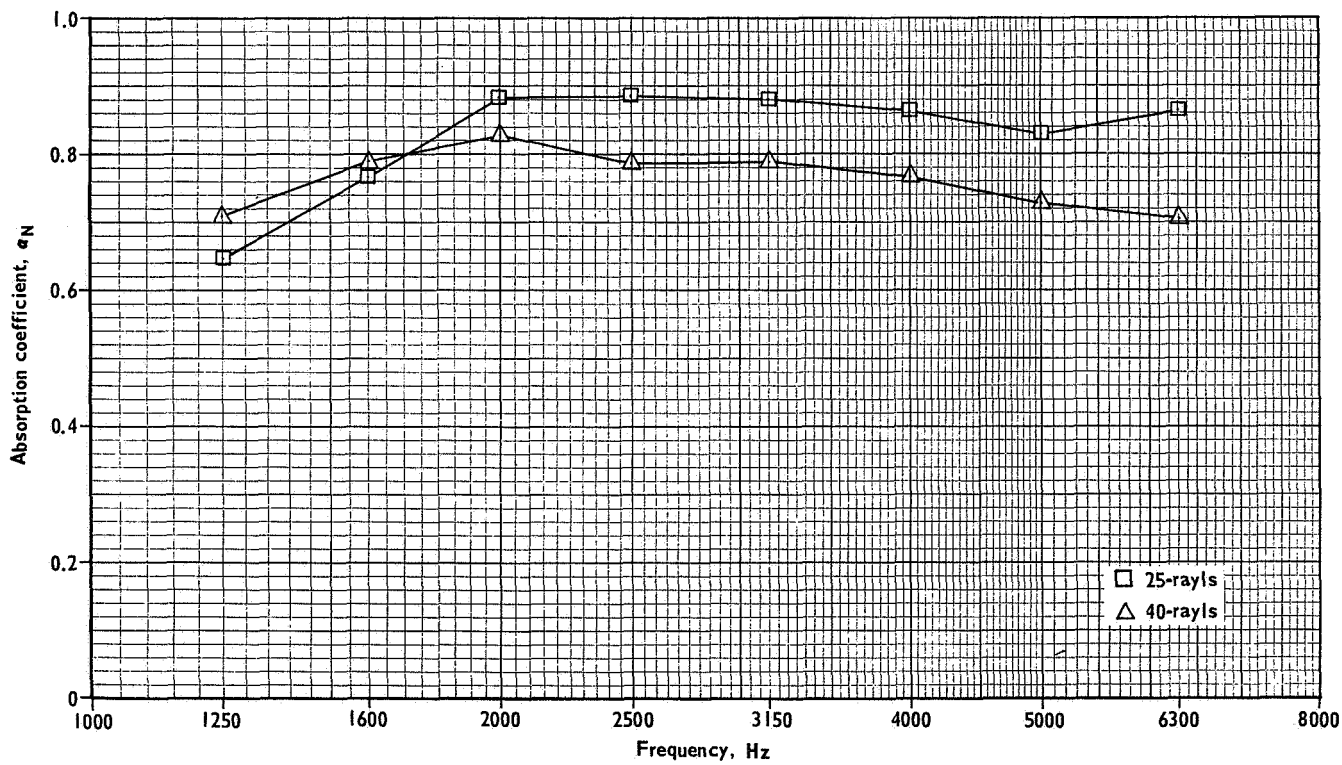

(b) Fiberglass density 1.2 lb/ft^3.

Figure 27.- Normal-incidence absorption coefficients of fibermetal surfaces and 0.5-in. deep cavities filled with type AA fiberglass.

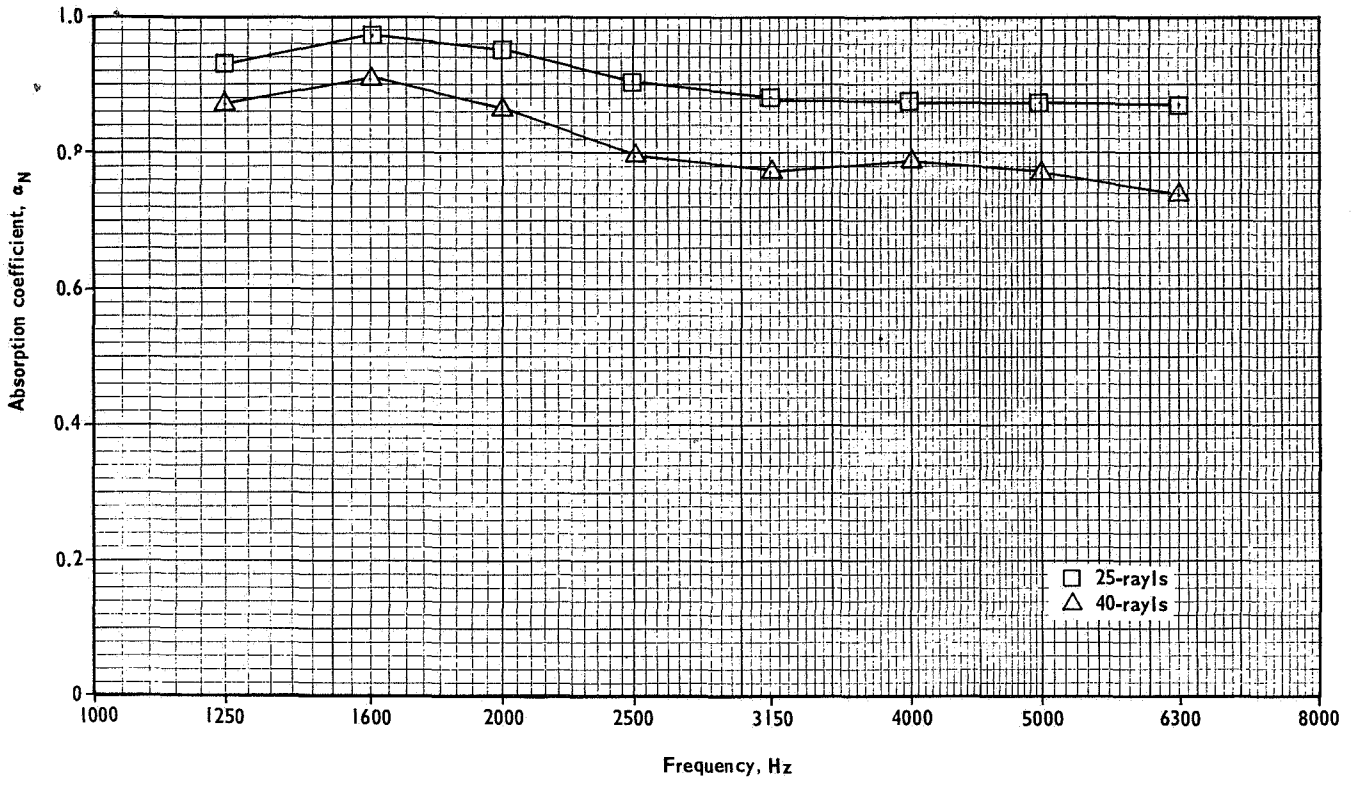

(a) Fiberglass density 0.6 lb/ft^3.

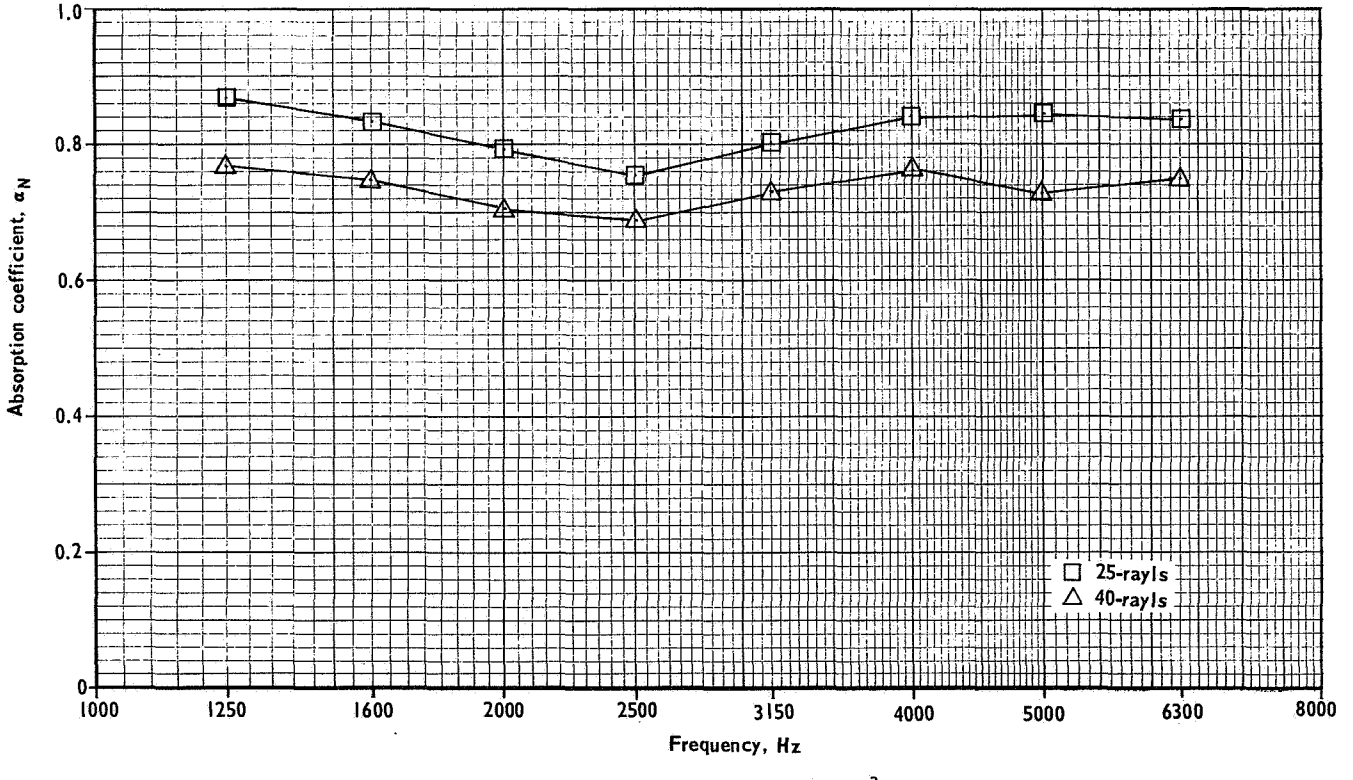

(b) Fiberglass density 1.2 lb/ft^3.

Figure 28. - Normal-incidence absorption coefficients of fibermetal surfaces and 1.0-in. deep cavities filled with type AA fiberglass.

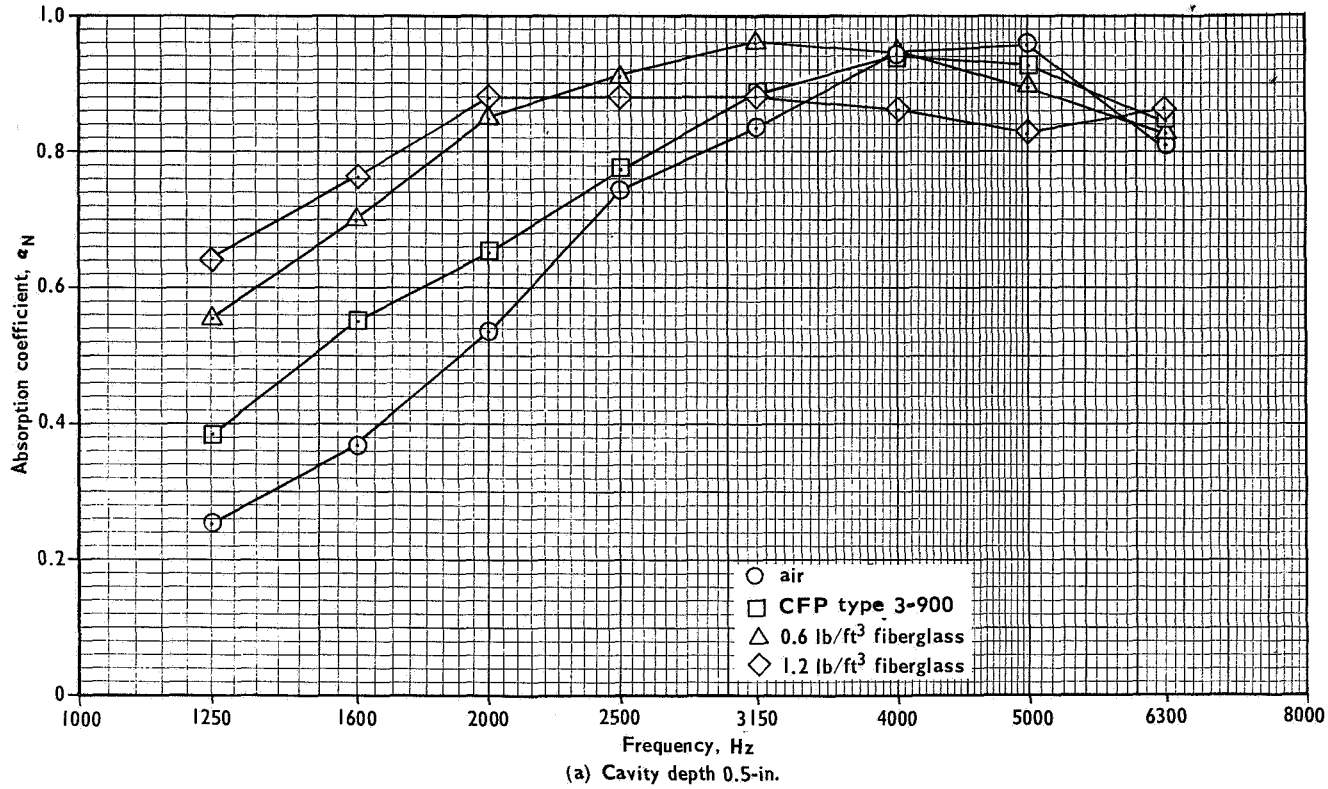

(a) Cavity depth 0.5-in.

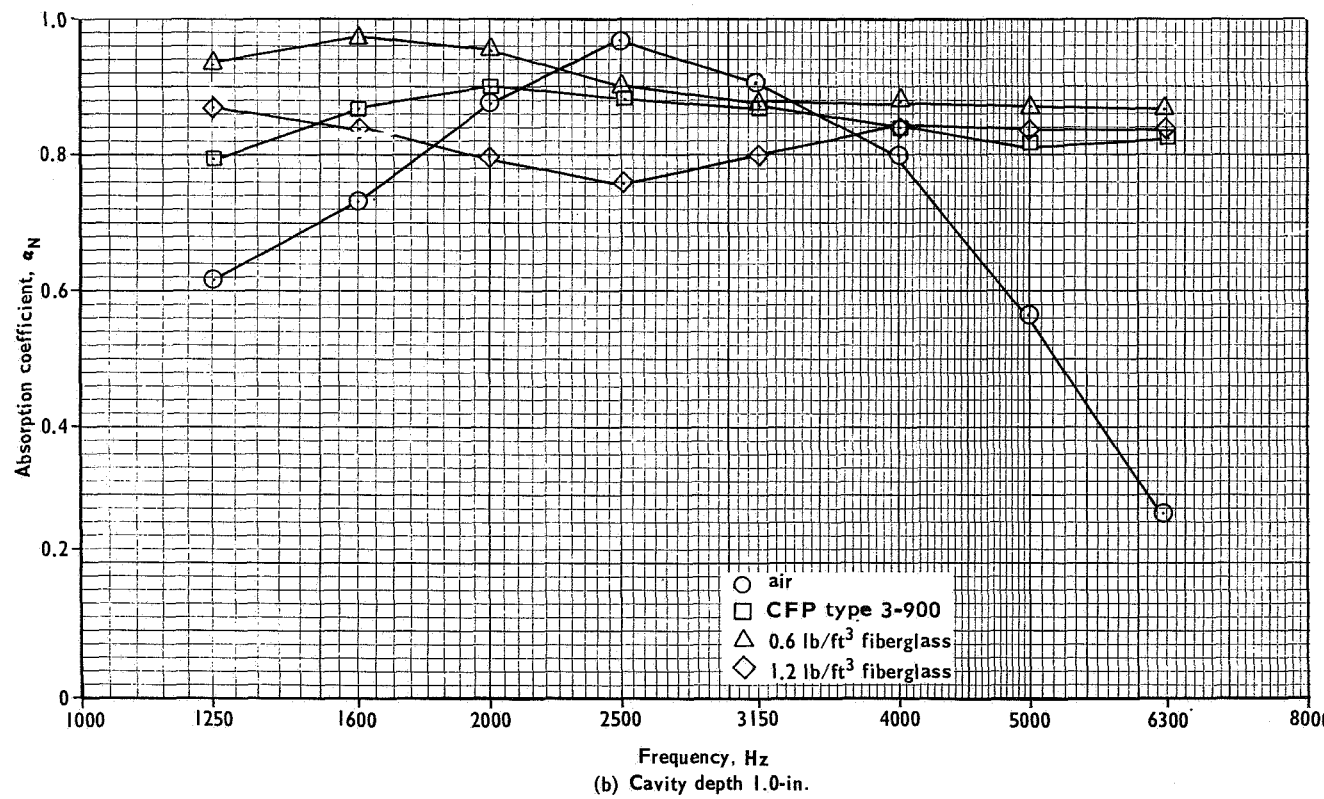

(b) Cavity depth 1.0-in.

Figure 29. - Normal-incidence absorption coefficients of a 25-rayl fibermetal surface with various depth cavities and with various filling materials in the cavities.

The following observations were made from a study of the data given in figures 25 through 29:

- With air backing, dips in the absorption spectra occur at frequencies whose wavelength and half-wavelength correspond to the depth of the cavity. At these frequencies the resistive and reactive components have large positive values (cf., figure 22) and the impedance is very high, causing most of the incident sound energy to be reflected back toward the source rather than to be absorbed.
- With air backing, the highest absorption coefficients were generally always obtained with the 40-rayl fibermetal. This may be related to the conclusion from theoretical considerations that maximum energy transfer for perpendicular incidence occurs when the impedance of the absorptive lining equals the characteristic impedance of the air, i.e., about 42 rayls.
- When the cavity behind the fibermetal surface was filled with a porous absorber, the highest absorption coefficients were always obtained with the lining material which had the lowest flow resistance. That is, 40-rayl material was better than 60-rayl and 25-rayl was better than 40-rayl. It is suspected that 10-rayl might have been better than 25-rayl but no tests were run with 10-rayl material except with air-filled cavities.
- The best of all the combinations tested was the 25-rayl material over a 1.0-in.-deep cavity filled with 0.6 lb/ft^3 type AA fiberglass. The normal-incidence absorption coefficient in this case was never less than 0.87 (i.e., absorbing 87 percent or more of the incident energy) in the frequency range from 1250 to 6300 Hz.
- Filling the cavity behind the lining material changes the absorptivity. Apparently, the stuffing material acts to prevent the formation of the standing waves within the cavity and modifies the impedance in such a way as to increase the absorptivity. The change in the behavior of the components of the impedance is shown in figure 23. For the 0.5-in cavity, and for frequencies between 1600 and 3150 Hz, it is the increased dynamic resistance alone in the case of compressed polyurethane foam that raises the impedance and the absorptivity; with fiberglass, the dynamic resistance is only slightly greater than that of the air-filled cavity, but the mass reactance of the fiberglass is higher than either that of compressed foam or air and this seems to be the factor that increases the low frequency absorption. The same trends were observed for the 1.0-in.-deep cavity, figure 23b, where the increase in apparent flow resistance of the structure is quite noticeable.

Figure 30 gives the results of a special test with 0.5-in. air and 0.5-in. CPF type 3-900 under 25-rayl fibermetal. In these tests, the location of the two materials behind the fibermetal was varied. Greater absorption, above 2000 Hz, was obtained by locating the layer of air between the fibermetal and the compressed polyurethane foam compared to locating the CPF next to the fibermetal with the air gap then behind the CPF. The attenuation with air first and CPF second provided more absorption than with the cavity filled with 1.0 in. of CPF and is almost as good as, and sometimes better than, the best of the previous configurations, namely, 1.0 in. of 0.6 lb/ft^3

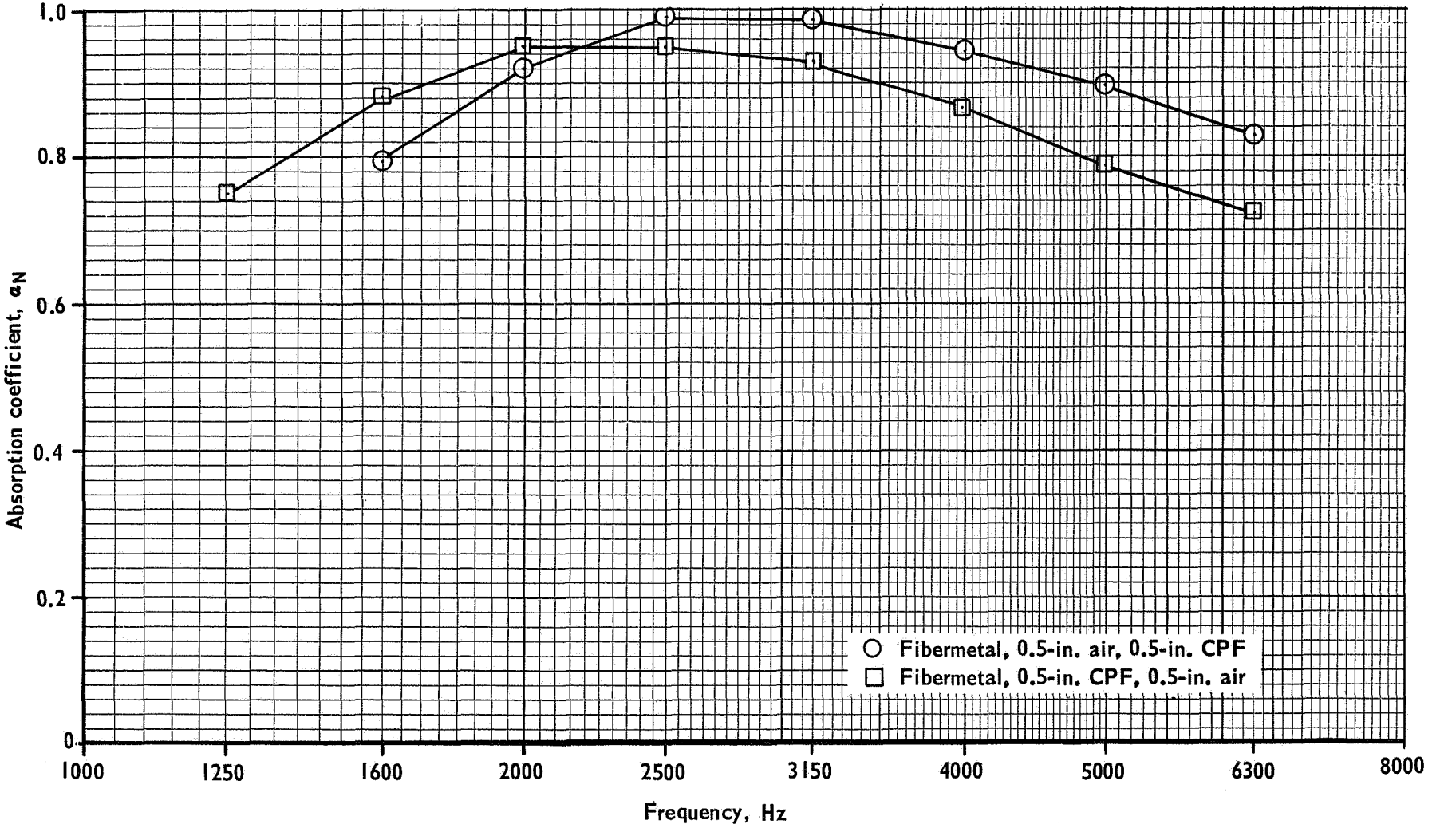

Figure 30.- Normal-incidence absorption coefficients of a 25-rayl fibermetal surface with a 1.0-inch deep cavity; the cavity is filled with air and CPF type 3-900 in two different arrangements.

type AA fiberglass. This last surprising result may be due to the fact that this construction may be similar to the series or double resonator discussed by Zwikker and Kosten, reference 22, page 158, wherein a second resistive layer is interposed with appropriate air gaps, between one flow-resistive layer and an impervious back wall. This technique raises the absorptivity and increases the bandwidth of high effective absorption.

The observations made above have all been for calculated values of the normal-incidence absorption coefficient. However, because the nature of the sound field in the inlet duct and in the fan-discharge duct is not well known, a few comparisons were made with a random-incidence absorption coefficient. This quantity, α_R, was computed from the calculated values of the normal-incidence absorption coefficient, α_N, suitably averaged over two or three different runs, using a method developed by London, reference 37. A curve relating α_R to α_N is shown in figure 31.

Study of figure 31 reveals that the effect of correcting α_N to α_R is to greatly increase low absorption values and to not significantly affect the high absorption values. Figure 32 shows comparisons of the random incidence absorption coefficients for 0.5- and 1.0-in.-deep cavities. The improvement in absorptivity due to filling the cavity with a porous absorber is not so dramatic when compared on the basis of α_R. Indeed, for the 1.0-in. cavity, there is very little difference between air, CPF, and fiberglass below 4000 Hz, the absorption coefficient being essentially limited to the maximum value of the α_R curve, figure 31. Since it is not known what incidence should be used for duct test comparisons, the normal incidence absorption coefficients are considered to be the best guide because they provide the most severe test, at least for α_N values less than 0.8.

P&WA Rig-Model Duct Transmission-Loss Tests

Background. — Although laboratory-type tests to determine the acoustical properties of various materials yield useful information which can be used in the design of actual duct liners, it was deemed mandatory to run additional tests to observe the behavior of various duct lining designs with air flowing over the treament. These tests were run at a P&WA facility in East Hartford, Connecticut. This facility, which had evolved after several years of experimentation, permitted the rapid determination of the transmission-loss of sound propagating through a duct with various rates of airflow; with the choice of having the sound propagate either with the airflow (fan-discharge) or against the flow (inlet). In actuality, only the quantity Noise Reduction or the difference between the SPL's at the input to the duct (source side) and at the outlet of the duct (receiver side) is determined. The transmission loss is the ratio, expressed in decibels, of the input acoustic power to the output acoustic power. Measurement of the TL is very difficult because there are no commercially available acoustic wattmeters and because it is very difficult to get a true measure of the input power because a certain amount of the input power is reflected back toward the source by the duct. This reflected power would

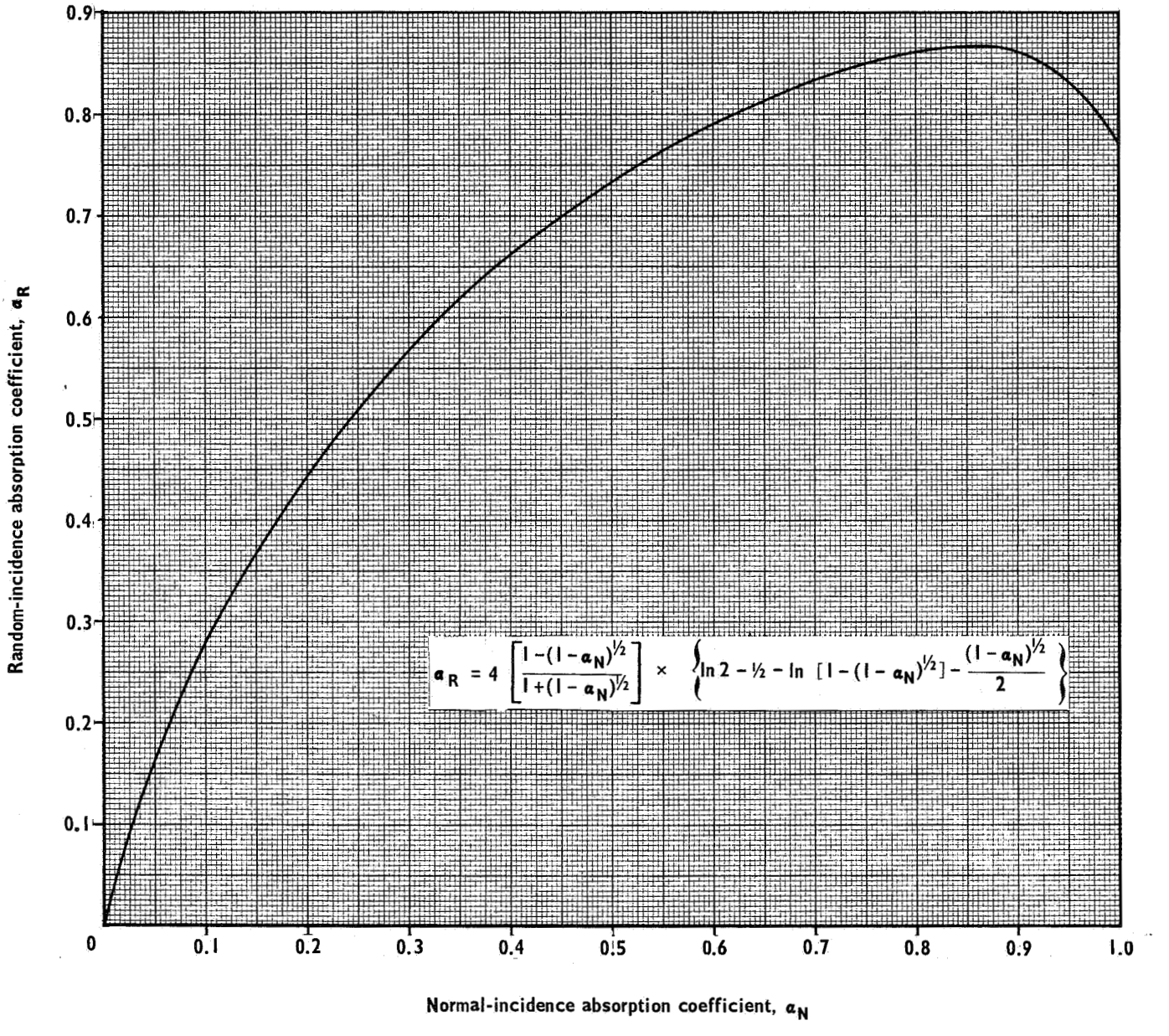

Figure 31.- Relationship between random and normal-incidence absorption coefficients, from equation 12 of London, reference 37.

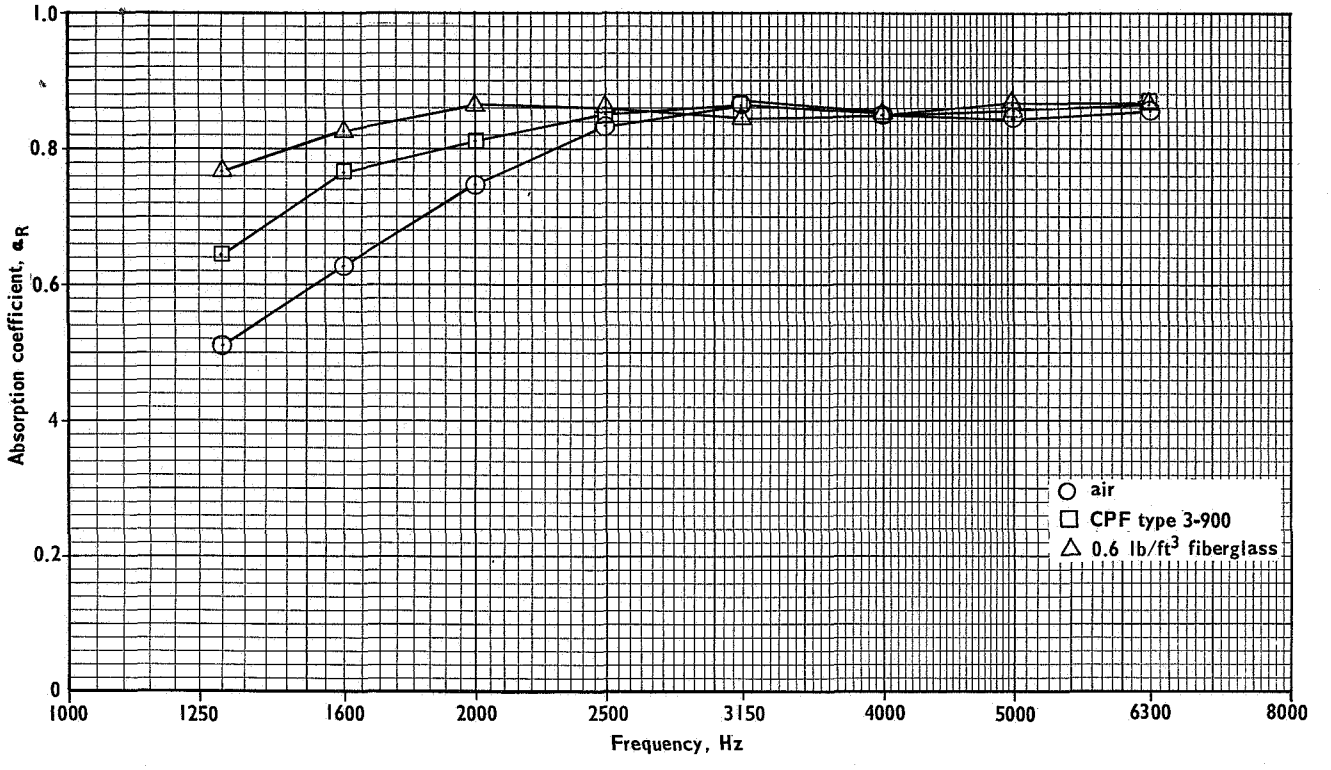

(a) Cavity depth 0.5-in.

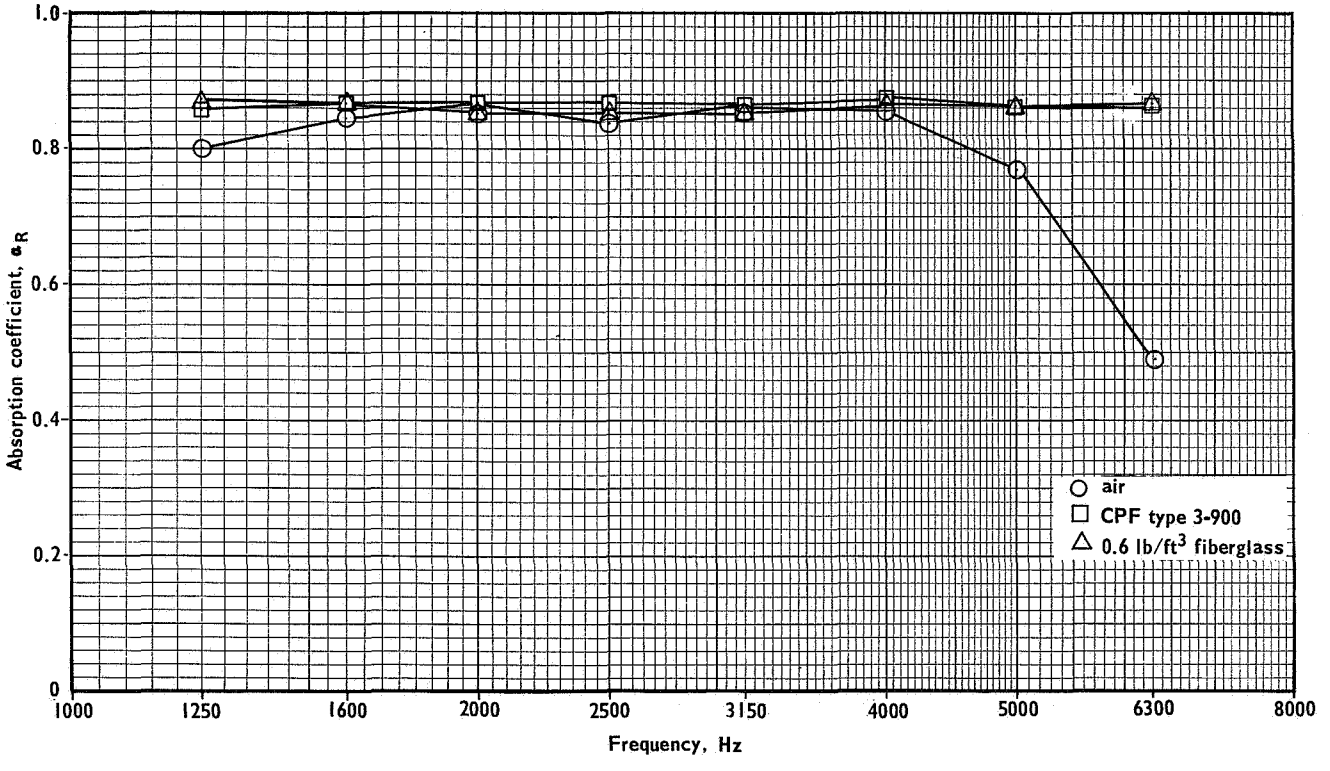

(b) Cavity depth 1.0 in.

Figure 32.- Random-incidence absorption coefficients of a 25-rayl fibermetal surface with various depth cavities and with various filling materials in the cavities.

have to be separated from the indicated input power reading to get the true input power. In this report, no distinction is made between the TL and the Noise Reduction and the term transmission loss will be used to refer to the SPL difference between the source room and the receiver room.

Single point SPL measurements in the source and receiver rooms are made under the assumption of uniform sound energy density in the two rooms. This procedure greatly simplifies testing, compared to duct-probing tests or to measurements of the radiated noise field from a duct exhausting into the atmosphere. However, it should be pointed out that these duct tests can be regarded only as a means for ranking various duct lining treatments. Actual performance of a given design must be determined from full-scale ground runup and flyover noise tests. Furthermore, it is not possible to make meaningful estimates for the full-scale performance from the duct transmission loss tests. No tests, as far as the authors can determine, have ever been run which adequately and carefully compare the TL of the same exact duct treatment at the same flow conditions from duct model tests and full-scale engine tests. Thus, the duct TL tests are to be used only as a guide in the choice of a duct lining treatment. The determination of the actual amount of noise reduction that can be produced by a given treatment must await the result of engine test-stand ground runup acoustical tests and airplane flyover noise measurements.

Description of test ducts. — Five duct models for transmission loss tests were constructed: three inlet models and two fan-discharge models. These ducts were not models in the sense of being scaled-down versions of complete full-size articles; rather, each was a complete section of the corresponding full-scale duct. Sub-scale modeling was avoided because of difficulties involved in attempting to scale the acoustical absorptivity of a lined duct when there is air flowing through the duct. Thus, the actual full-scale radial duct dimension was preserved in all the models.

Although it was desirable to make the duct models as large as possible in order to most closely simulate full-scale conditions, there was a limitation imposed on the maximum cross-sectional area of a duct. In November, when the transmission loss tests started, a criterion had been established by P&WA whereby a velocity of 300 ft/sec could be obtained in a duct whose minimum cross-sectional area (throat area) was no more than about 80 sq. in. Therefore, each duct was designed considering this area limitation. Conveniently, this limitation was compatible with the modeling practice described above.

Initial limitation on duct velocity. — Since an understanding of the method used to calculate the flow velocities and an appreciation for the accuracy of the values obtained from these calculations will be useful in a discussion of the results, the limitation of the facility will be explained a little further.

The weight density of the air is given by:

$$g\rho = 0.07651 \left(\frac{P}{P_t}\right)\left(\frac{T_t}{T}\right) \text{ lb/ft}^3 \qquad (13)$$

with the acceleration of gravity g in ft/sec^2, and the density ρ in slugs/ft^3. The pressure P is the static pressure of the air at the point or station of interest and the temperature T is the static temperature at the same point; both P and T are in absolute units. The pressure P_t and the temperature T_t represent local total (or stagnation) quantities. Convenient units are: pressure in inches of mercury (in. Hg absolute) and temperature in degrees Rankine (°R). Assuming P_t = 29.92 in. Hg, and T_t = 518.688°R, gives:

$$g\rho = 1.325 \left[\frac{P \text{ in in. Hg}}{T \text{ in } °R}\right] \quad \text{lb/ft}^3 \tag{14}$$

The incompressible Bernoulli equation for steady non-viscous flow is

$$P_t = P + 0.5\rho v^2 \quad \text{lb/ft}^2 \tag{15}$$

where v is the steady flow velocity in ft/sec. Rearranging equation (15) and substituting the relation for the density from equation (14) gives

$$P_t - P = \Delta P = \frac{0.5\left[1.325\ (P/T)\right]v^2}{g} \quad \text{lb/ft}^2 \tag{16}$$

where ΔP is the differential pressure between the local total and the static pressure in lb/ft^2. Solving for the velocity v from equation (16) and using g = 32.17 ft/sec^2 gives

$$v^2 = (48.5)(T)\left(\frac{\Delta P}{P}\right) \tag{17}$$

Since the differential pressure is usually a small quantity, it is customary to measure it in inches of water (or occasionally another fluid of appropriate density such as acetylene tetrabromide). Thus, by introducing a conversion factor of 5.204 to convert a ΔP value from in. H_2O to ft/lb^2, we obtain

$$v = 15.9\sqrt{T}\sqrt{\frac{\Delta P}{P}} \quad \text{ft/sec} \tag{18}$$

with T in °R, ΔP in in. H_2O, and P in in. Hg. (If a manometer fluid other than water were used to measure the ΔP, one would need to multiply the constant in equation (18) by the square root of the specific gravity of the fluid.)

At the beginning of the program, air was supplied by a blower system at a volume flow rate of 10 500 standard ft^3/min (SCFM). The system was limited to a maximum pressure rise across the blower of 30 in. of H_2O. Because of the line losses due to friction, etc., the maximum differential pressure delivered was only 20.5 in. H_2O in any test section. Assuming

that the static pressure and the static temperature equalled ambient values (a reasonable assumption at these low velocities) and using typical values of P = 30 in. Hg and T = 489°R, we obtain

$$v = (15.9)\left(\sqrt{489}\right)\left(\sqrt{\frac{20.5}{30}}\right)$$

$$= 290 \text{ ft/sec} \qquad (19)$$

To have increased the velocity above this value would have required either raising the static temperature or decreasing the static pressure or both, but none of these options was available at the time. The total pressure, and hence the ΔP, could not be raised because the blower was a pressure-limited device. An ejector or diffuser could have been used, had there been adequate time and funds, to reduce the static pressure. These techniques would, eventually, have been limited by the maximum mass flow output of the blower. The limitation on the maximum size of the throat area was determined empirically by P&WA, as mentioned earlier, as a reasonable compromise between a duct with a larger throat area and a lower maximum velocity and a duct with a smaller throat area and a higher maximum velocity but more difficult scaling problems. For a given mass flow rate, increasing the area raises the static pressure, reduces the differential pressure and reduces the velocity. On the other hand, reducing the area tends to decrease the static pressure (until the mass flow limit of the blower is reached, and increase the velocity.

Fan-discharge ducts. — With these thoughts in mind, the fan-discharge ducts were built to simulate the central and end portions of one full-scale duct. Referring to figure 2b, a full-scale duct can be seen to consist of a central portion extending either side of the horizontal centerline to a flow splitter. The end portion then extends from the first splitter, up or down from the horizontal centerline, to the top or bottom of the duct. These three parts, the central and the two end parts, are approximately equal in area and divide the duct into thirds. The two end portions are approximately mirror images of each other about the horizontal centerline so that only one end portion, or end duct as it was called, was required. The exit area of one full-scale fan-discharge duct is about 260 in.^{2} and dividing it into thirds approximately satisfied the criterion of an 80 in.^{2} throat area.

Inlet ducts. — The inlet models were built as 22° wedge-shaped segments of an actual full-size inlet. Three models were made; one corresponding to the internal flow lines of the standard DC-8 inlet and two to the lightbulb inlet flow lines (55 percent and 75 percent blockage) as determined from aerodynamic calculations, figure 4. A 22° segment of a standard DC-8 inlet for the JT3D engine installation has a throat area of about 80 in.^{2}. At the request of the contractor, P&WA ran a series of tests to evaluate the differences in TL produced by a lined wedge with acoustic treatment on its circumferential surface, and by a full round duct with the same acoustic treatment. Tests were run at zero airflow; the diameter of the cylinder used for the 360° duct was 25.5 inches. Wedges with included angles of 22°, 45°, 90°, and 180° were investigated. The 180° and the 360° ducts gave about the same attenuations; the 22°, 45° and 90° wedge results grouped together about 7.5 dB below the results of the 360° duct with the 22° wedge giving the least attenuation. It was concluded that results obtained from tests in the presence of airflow using 22°

segments would probably underestimate, or at worst equal, those that would be obtained with a 360° inlet and that useful comparison tests on inlet treatments could be run.

Models. – Using the guides described above, the duct models shown in figures 33 and 34 were designed and built. Figure 33 gives the significant duct dimensions and shows the panel treatment areas for the center fan-discharge duct, the 55-percent and 75-percent lightbulb inlets, and the standard DC-8 inlet. Cutaway views illustrating some of the design features for the center and end fan-discharge ducts, the 55-percent lightbulb inlet and the standard inlet are given in figure 34. Note that the end duct (which was by far the most difficult to build because of the helical flow path, the compound curvatures, and the area gradient from the duct inlet to the exit) was built without a central radial splitter although it has one in the actual installation. On the other hand, because of the simpler geometry, the center duct incorporated provisions for the addition of a central radial splitter as well as a combination of radial and circumferential splitters, even though the actual installation has no splitters. It was felt that the effect of dividing the flow path into smaller channels might be learned from the center duct and that the effect of the twisted flow lines (blockage) might be learned from the end duct tests. Note further that the cross-section of most of the ducts was made using straight lines for ease in construction, rather than curved lines as in the real duct, i.e., the arcs of the bounding curves on the inboard and outboard walls were approximated by chords. This was felt to be adequate since the radius of curvature was reasonably large for all ducts except the end duct. The lines of the end duct simulate those of the actual installation except for the circular end cap on the actual end duct. This curved end cap was approximated by a straight radial wall.

On each of the ducts, fibermetal panels replaced corresponding aluminum surfaces. Each duct also, in its treated area, had provisions for a 1-in.-deep cavity which could be filled either with air or with a porous acoustical absorber. The fan-discharge ducts had provisions for putting treatment on all four walls along the entire length. Details of the construction of the end duct are shown in figure 35; the center duct was built using similar techniques. The twisted flow path and the curvature of the panels is quite evident in figure 35. The fibermetal (or sheet aluminum hardwalls) was supported by Z-shaped frames and held in place with flathead screws which went into captive nuts attached under the frames. The end and the center ducts each had one removable side to allow access to the duct interior without removing the rest of the duct from the installation between the two reverberant chambers.

Figure 36 shows construction details of the 75-percent lightbulb inlet; the other two inlets were built in similar fashion. The trapezoidal shape of the duct exit, the triangular shape of the duct inlet and the location of the treated areas on the cowl and centerbody walls can be seen in the figure. Note that the walls which form the radial side walls are solid sheet aluminum; no treatment was applied to these walls.

Test facility. – The test facility was operated by the Sound Research Group at the Airport Laboratory of the Pratt & Whitney Aircraft Company in East Hartford, Connecticut. A duct transmission loss test consisted of installing a test duct between two reverberant rooms, in one of which was an intense sound source, and measuring the difference in the SPL's in the

Note: All dimensions in inches.

Panel number	(1)	(2)	(3)	(4)
Treated panel area, in.^{2}	408.9	187.6	432.7	187.6

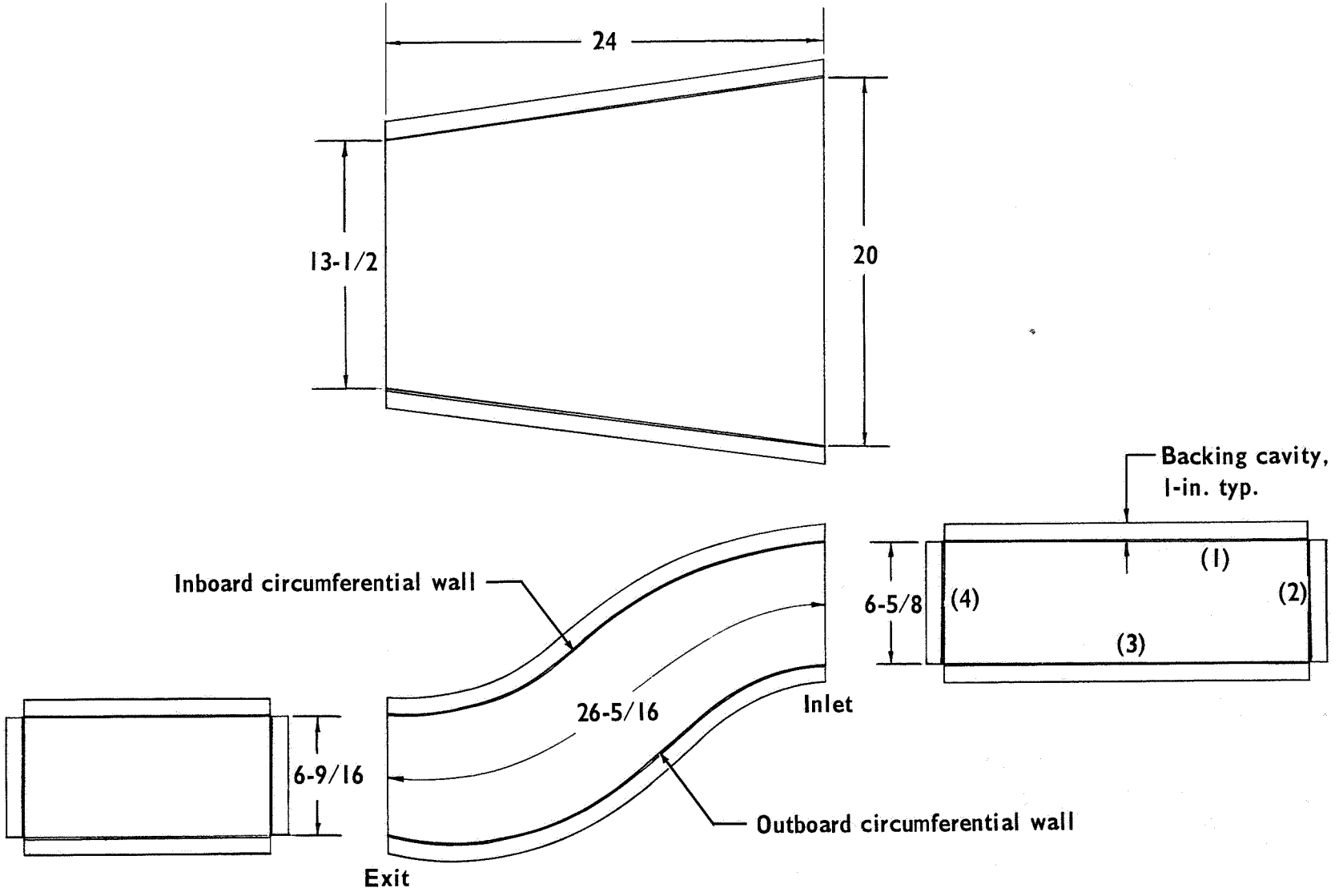

(a) Center fan-discharge duct.

Figure 33.- Significant duct dimensions and panel treatment areas.

Panel number	(1)	(2)	(3)	(4)	(5)
Panel length, in.	13.37	18.84	17.78	13.28	17.65
Average panel width, in.	12.68	11.31	11.52	8.08	6.17
Treated panel area, in.^{2}	169.7	213.0	204.8	107.2	108.9

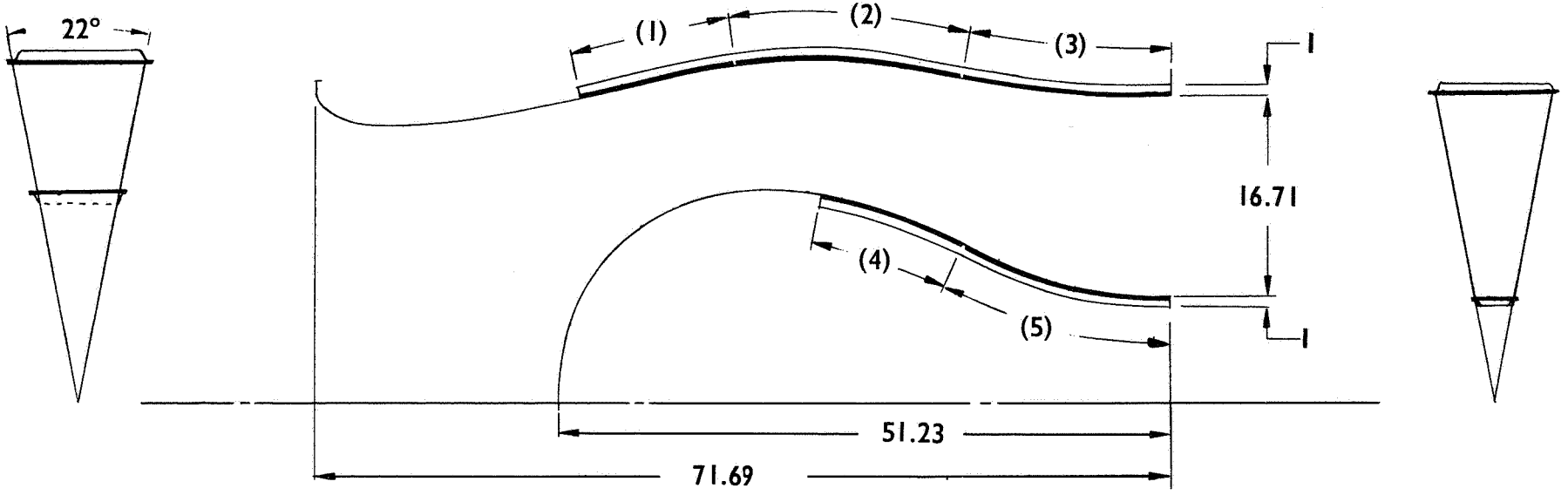

Note: All dimensions in inches

(b) 55% lightbulb inlet duct.

Figure 33.- Continued.

Panel number	(1)	(2)	(3)	(4)	(5)
Panel length, in.	19.48	22.0	17.23	18.72	18.02
Average panel width, in.	12.88	13.14	12.95	7.71	5.79
Treated panel area, in.^{2}	250.4	289.6	223.5	144.3	104.5

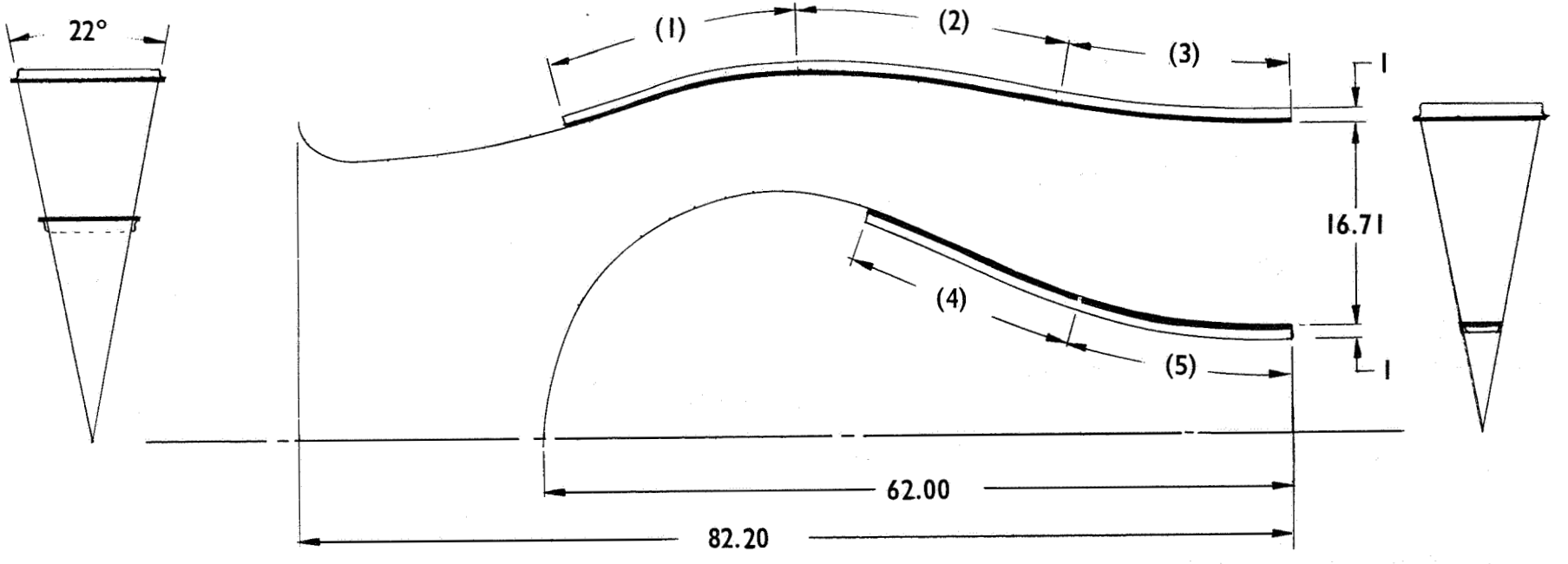

Note: All dimensions in inches

(c) 75% lightbulb inlet duct.

Figure 33.- Continued.

Panel number	(1)	(2)	(3)	(4)
Panel length, in.	9.94	9.94	9.75	8.82
Average panel width, in.	11.23	11.71	11.87	5.39
Treated panel area, in^2	111.6	116.3	115.8	47.6

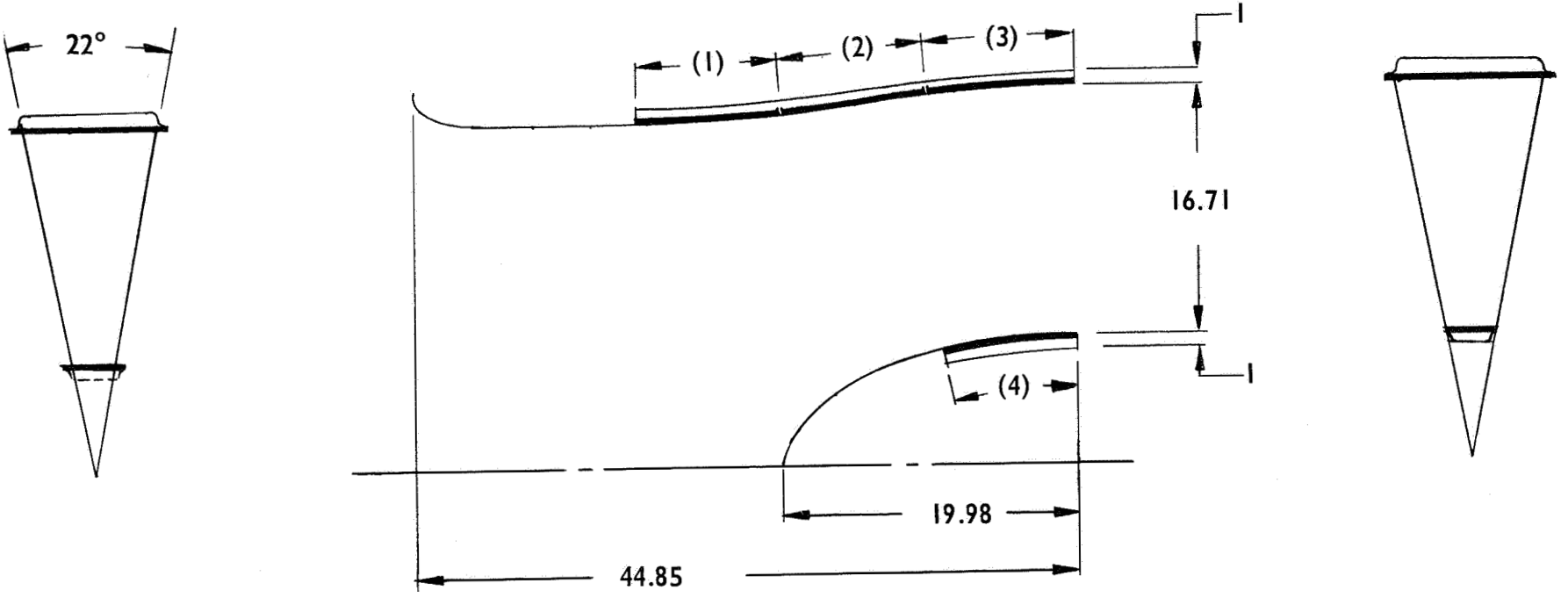

Note: All dimensions in inches

(d) Standard DC-8 inlet duct.

Figure 33.- Concluded.

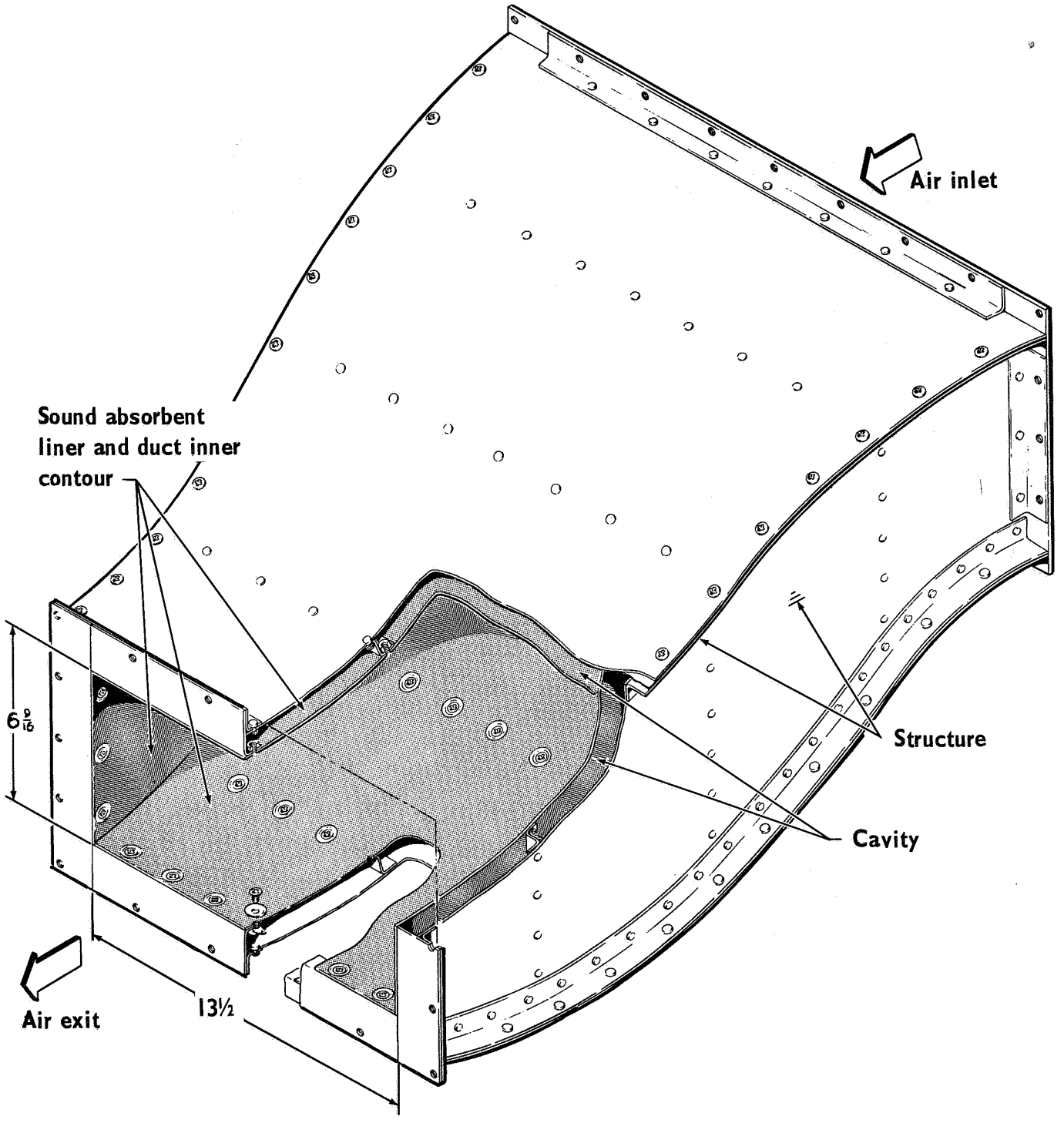

(a) Center fan-discharge duct.

Figure 34. - Cutaway views of acoustically-treated ducts used for transmission-loss tests.

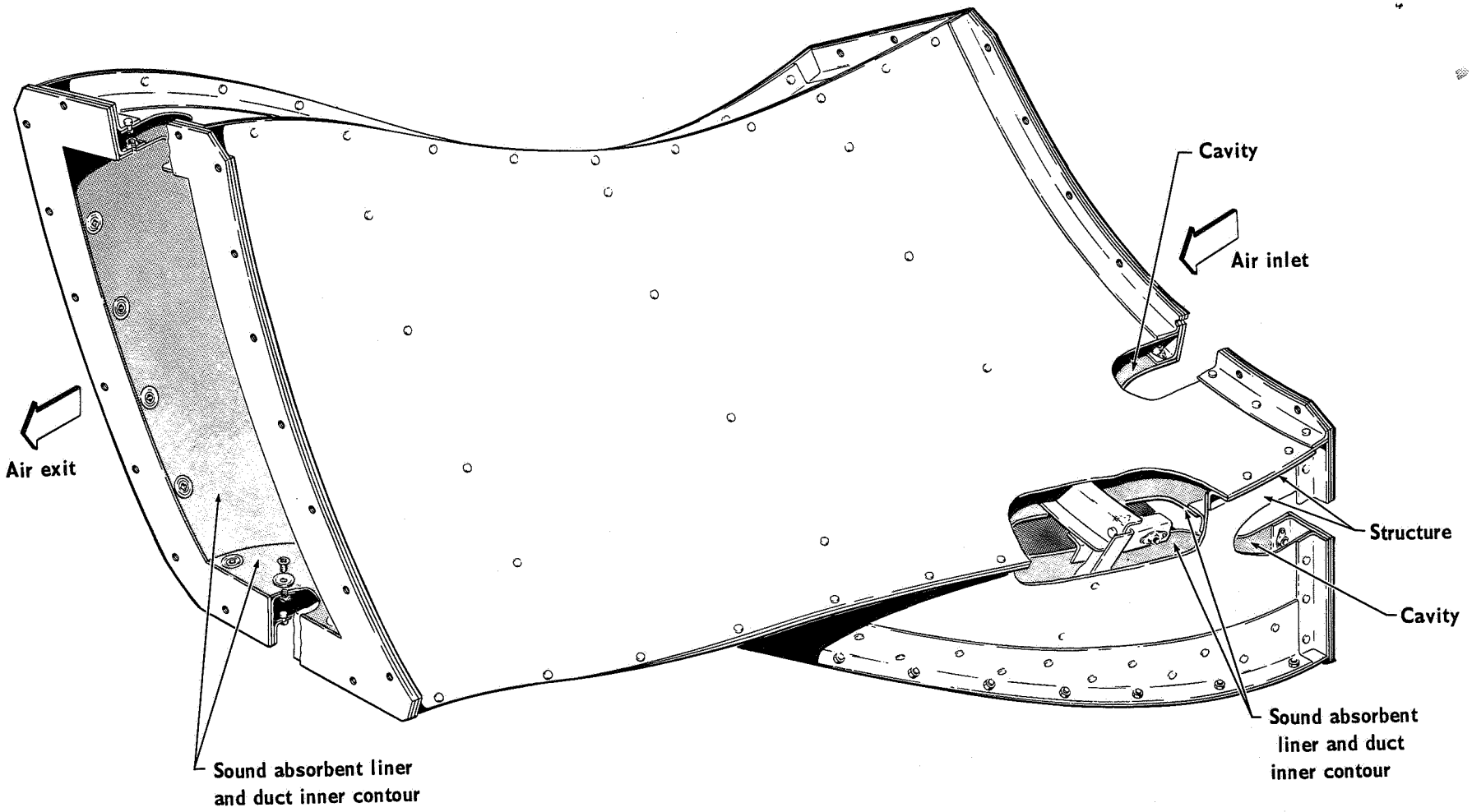

(b) End fan-discharge duct.

Figure 34.– Continued

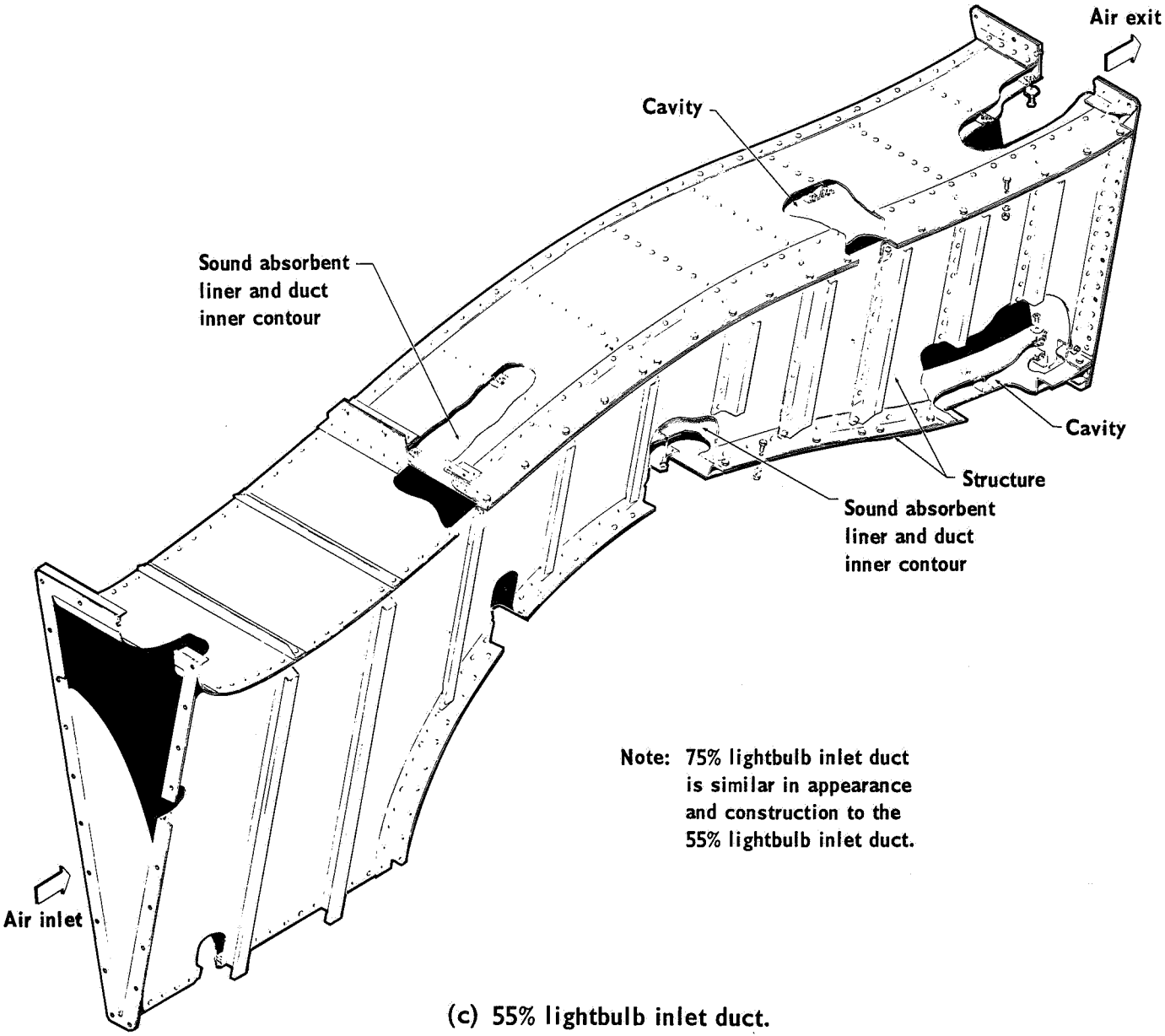

Note: 75% lightbulb inlet duct is similar in appearance and construction to the 55% lightbulb inlet duct.

(c) 55% lightbulb inlet duct.

Figure 34. - Continued.

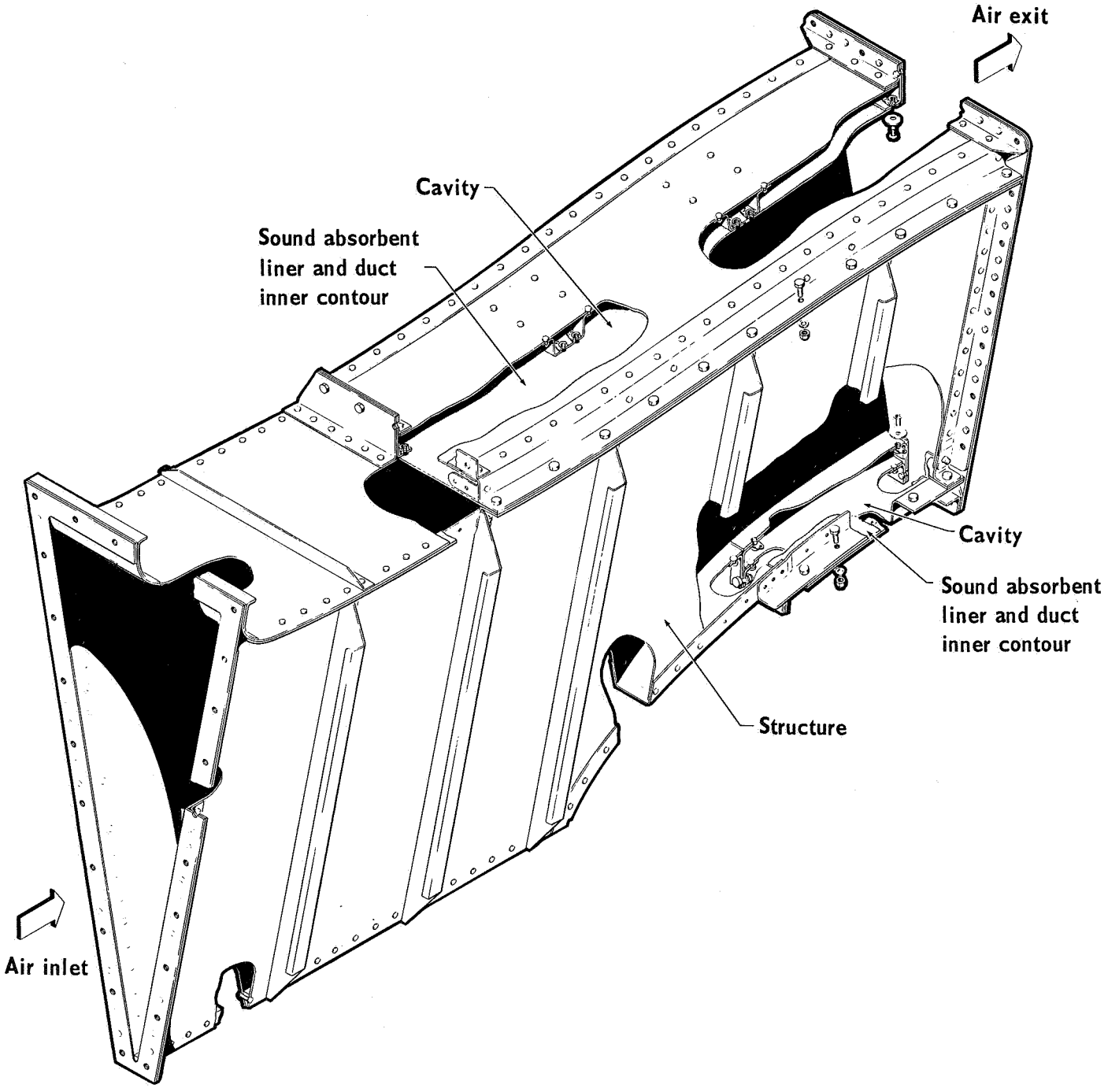

(d) Standard DC-8 inlet duct.

Figure 34. – Concluded.

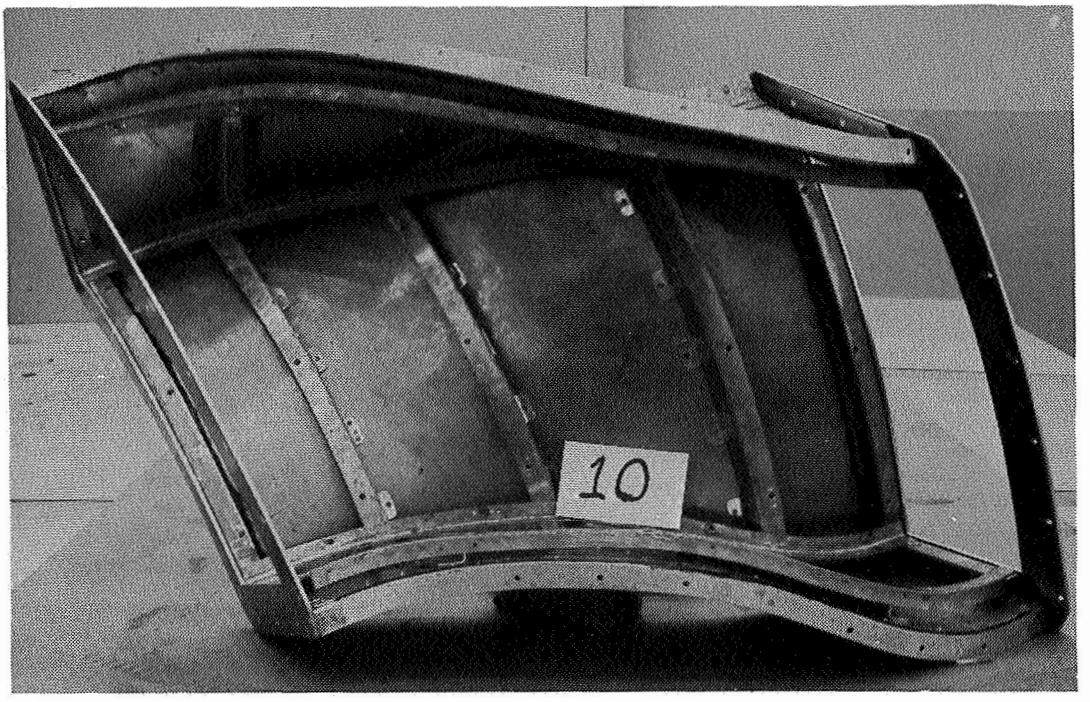

(a) View of duct interior, cover off, no linings on inner walls.

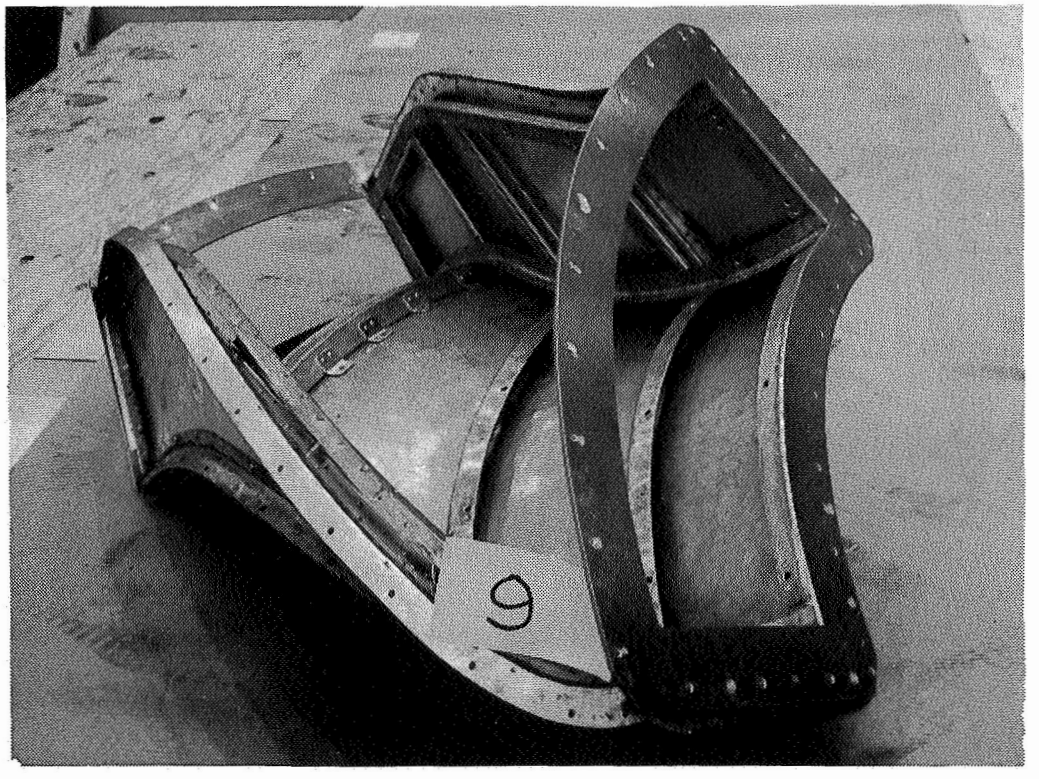

(b) 3/4-front view of duct looking at duct inlet, cover and linings removed.

Figure 35.- Construction details of end fan-discharge duct.

(c) Top cover – outboard circumferential wall.

(d) Edge-on view of top cover.

Figure 35. - Continued.

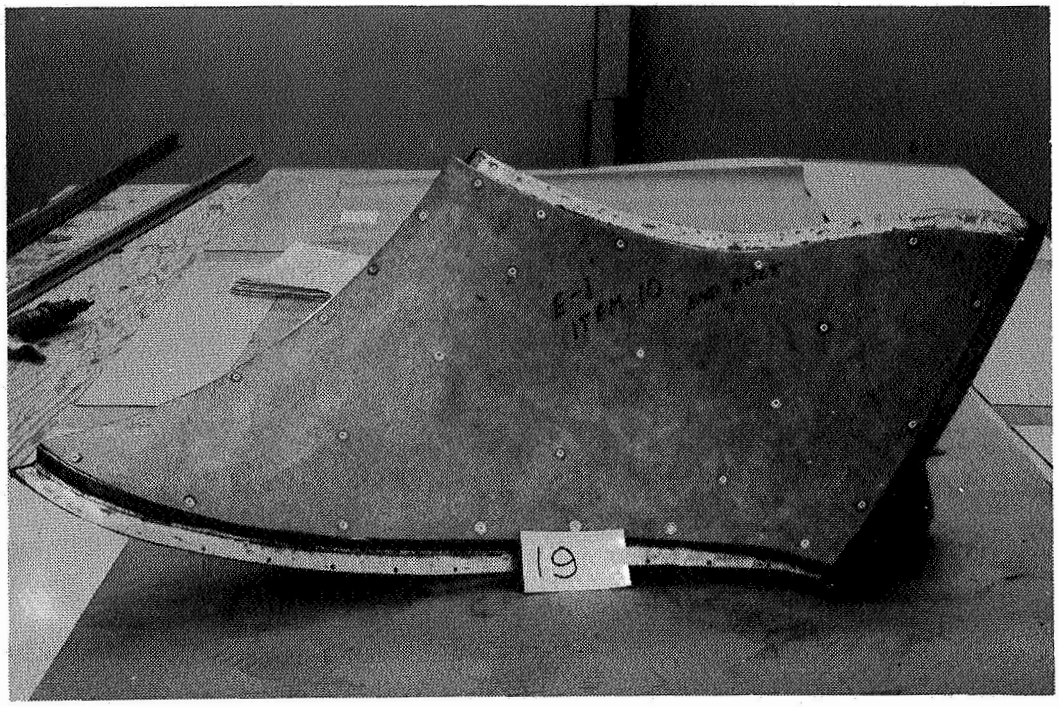

(e) Top cover with 25-rayl fibermetal in place.

(f) 3/4-front view from duct inlet with 25-rayl fibermetal in place on three walls.

Figure 35. - Continued.

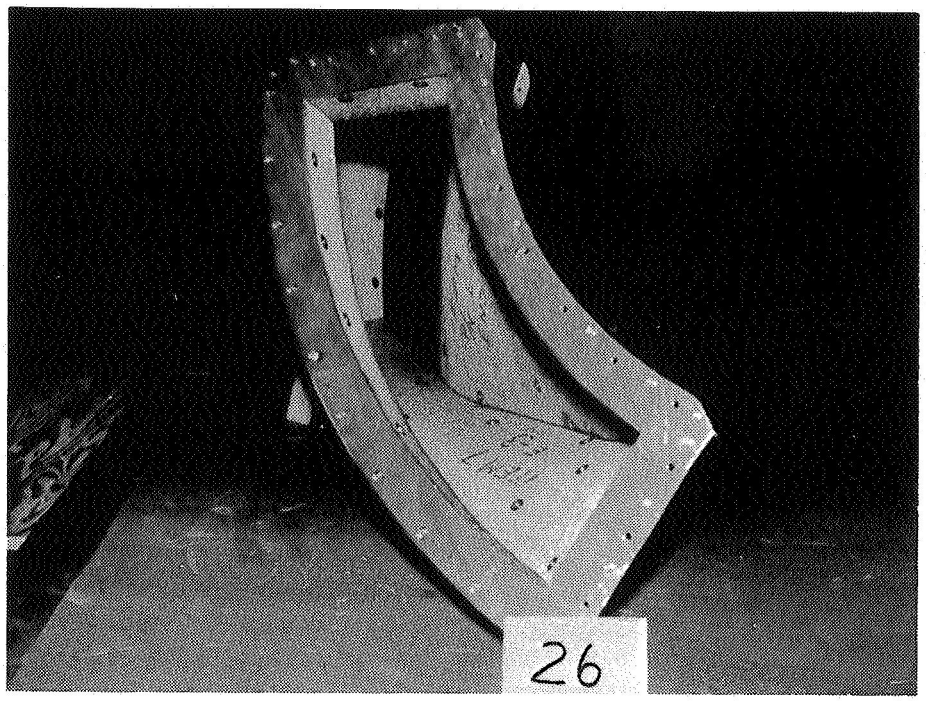

(g) View of complete duct from inlet, or fan-discharge, end; 25-rayl fibermetal on four walls.

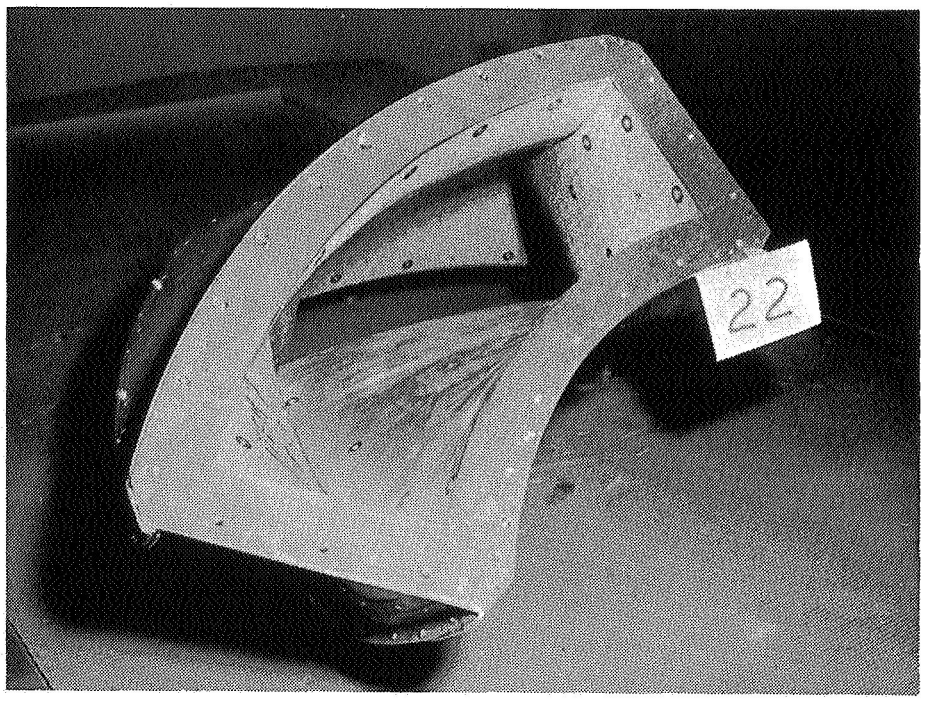

(h) View of complete duct from inlet, or fan-discharge, end; 25-rayl fibermetal on three walls, sheet aluminum on fourth wall, i.e., the inboard circumferential wall which is to the bottom right in the photograph.

Figure 35.- Concluded.

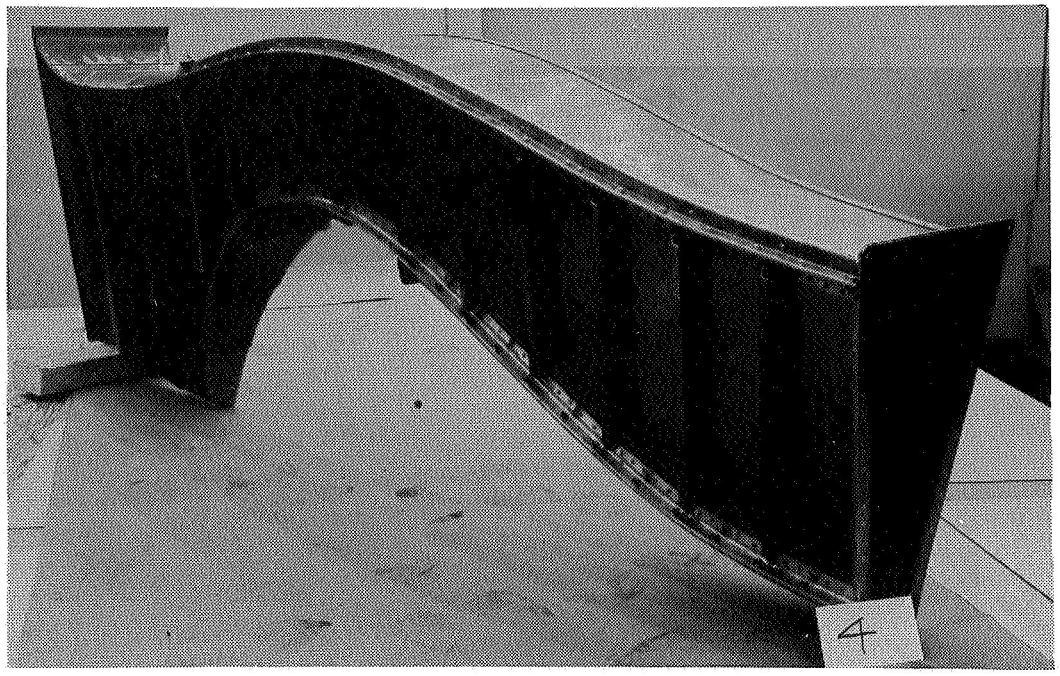

(a) 3/4-rear view showing removable cover on cowl over the acoustical-treatment area and trapezoidal duct exit.

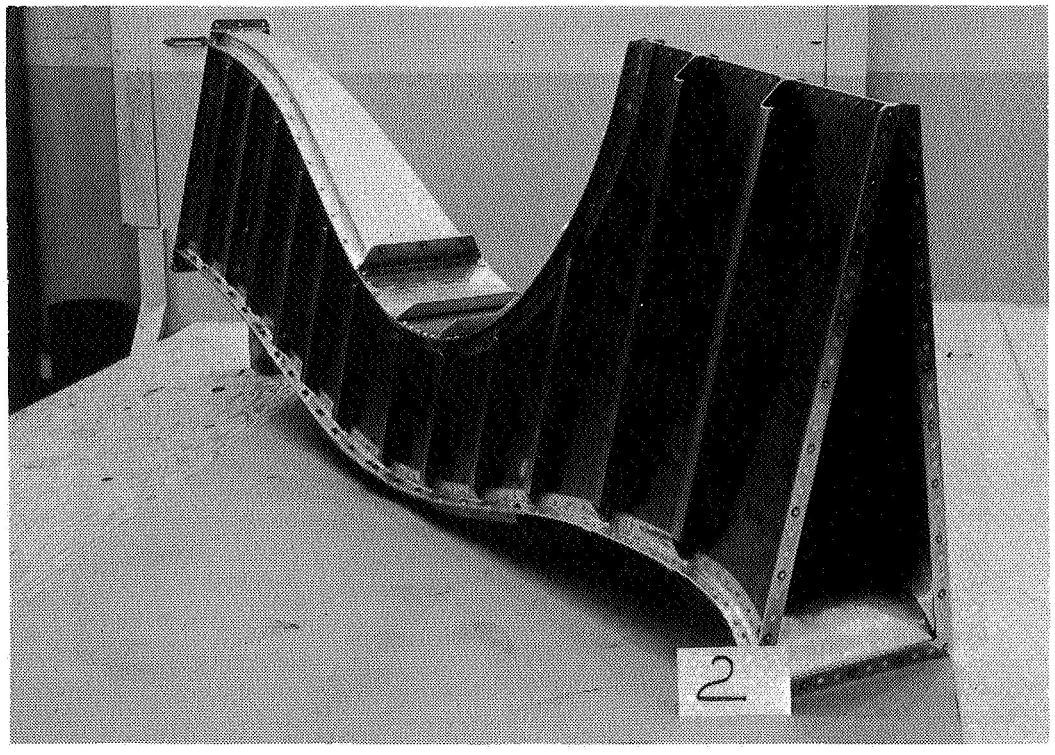

(b) 3/4-front view (upside down) showing removable cover on centerbody over the acoustical treatment area and triangular duct inlet.

Figure 36.- Construction details of 75% lightbulb inlet duct – typical of 55% and standard inlet ducts.

source and receiver rooms. Each test had air flowing through the ducts at some desired velocity. Three distinctly different systems were utilized in the course of the testing (December 1965 to February 1966). Each system had a unique set of conditions and intercomparisons of the data from one system with those from another is not advisable.

In the first system slightly compressed air was supplied to the test section by a blower-type air supply. A pulse jet, located in the upstream room, was used as the source of sound. In the second system, large-capacity vacuum pumps pulled air from the atmosphere through the test ducts. Two electropneumatic transducers were the source of sound and were attached to the downstream room. The third system used the vacuum pumps for the air supply with the pulse jet as the sound source in the upstream room.

Six different test series were run with the five ducts in these three systems; two series with the center duct and one each with the remaining four ducts. One of the center duct series and the end duct were conducted using the first system. All the inlets were run with the second system. The second series of center duct tests were run using the third system. The instrument and equipment used in the first and second systems are shown in figure 37. The third system used the pulse jet sound source of figure 37a and the vacuum pumps of figure 37b.

Reverberant chambers. — The two reverberant chambers were identical in internal volume and shape. The chambers were built with no parallel walls to discourage standing waves and to increase the diffusivity; the internal volume was 268 ft^3 and the internal surface area was 325 ft^2. The upstream chamber (chamber no. 1) was constructed of 0.25-in. steel plates welded together and covered on the outside with a 2-in. layer of a vibration damping material. Air from the blower was forced into the chamber through a large-diameter pipe welded to the roof of the chamber.

With the first system, the downstream chamber (chamber no. 2) was identical in construction to the upstream chamber. Air was exhausted to the atmosphere through a short, upward-bending stack. For the second and third systems, the downstream chamber was replaced by a chamber having the same internal geometry but considerably more rigid. This new chamber was constructed of 0.5-in.-thick steel plates welded together and then braced all over with steel I-beams. The I-beams had 8-in. flanges and 7-in. webs, were made out of 0.5-in.-thick steel, and were welded to each of the six sides of the chamber with 6-in. spacing between the flanges. A vacuum pumping system was used to evacuate the downstream chamber. A 30-in.-diameter pipe connected the chamber to the vacuum system. For this installation, the supply pipe from the blower was disconnected and the line capped off. Air was drawn into the upstream chamber through a bellmouth-shaped inlet attached to the access door. A conical plug was fitted in the bellmouth and was lined with a sound absorbing material behind a perforated panel to reduce the noise that might have entered the chamber due to the relatively high-velocity flow between the plug and the bellmouth. This was required during the inlet tests when the upstream chamber was used as the sound receiver room and problems in obtaining adequate signal-to-noise ratios existed at high duct velocities.

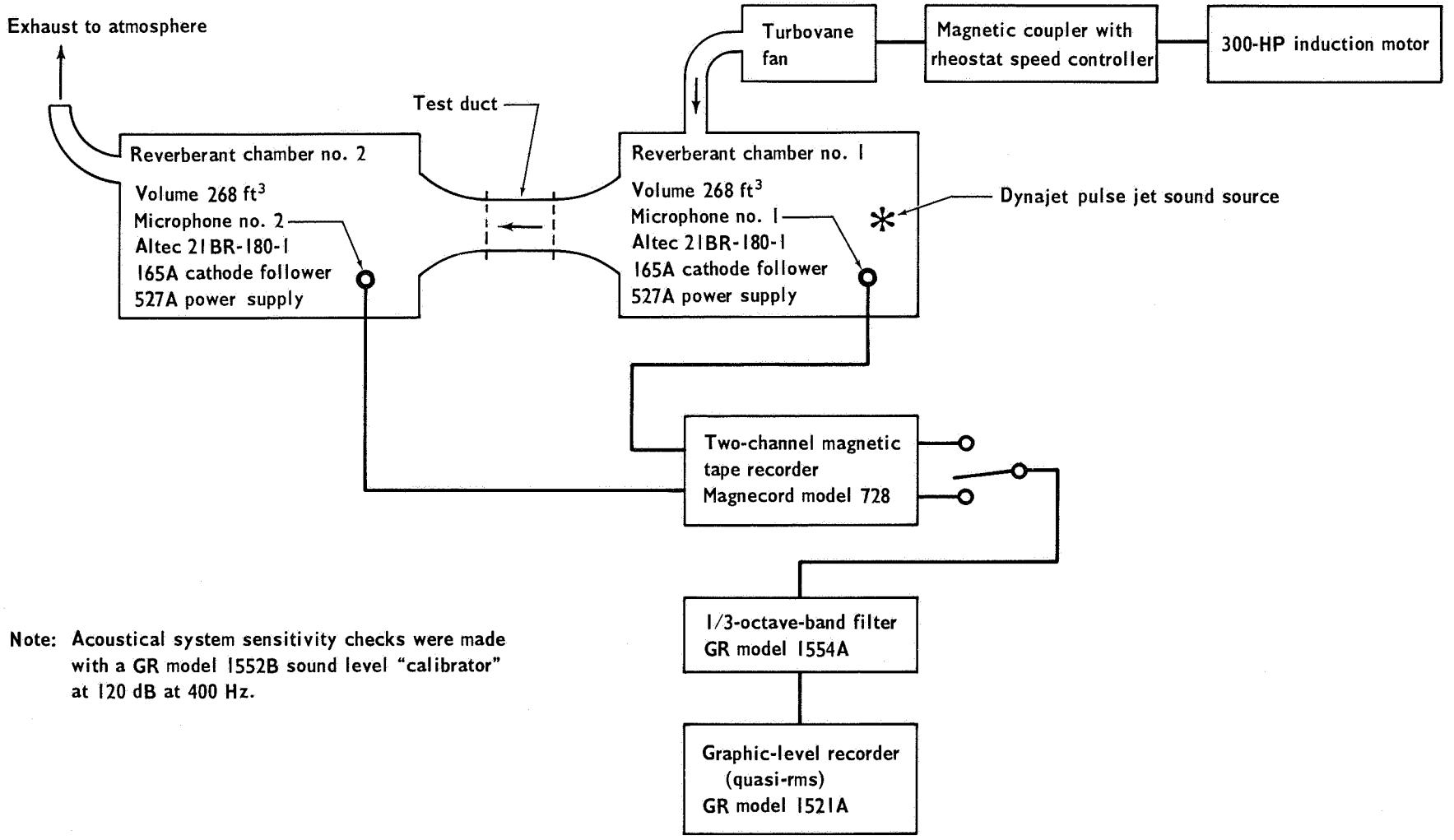

Note: Acoustical system sensitivity checks were made with a GR model 1552B sound level "calibrator" at 120 dB at 400 Hz.

(a) Blower system for the A and E-series fan-discharge duct runs; no inlet duct runs were made using the blower system.

Figure 37. – Schematic arrangement of instrumentation and equipment used for transmission-loss tests.

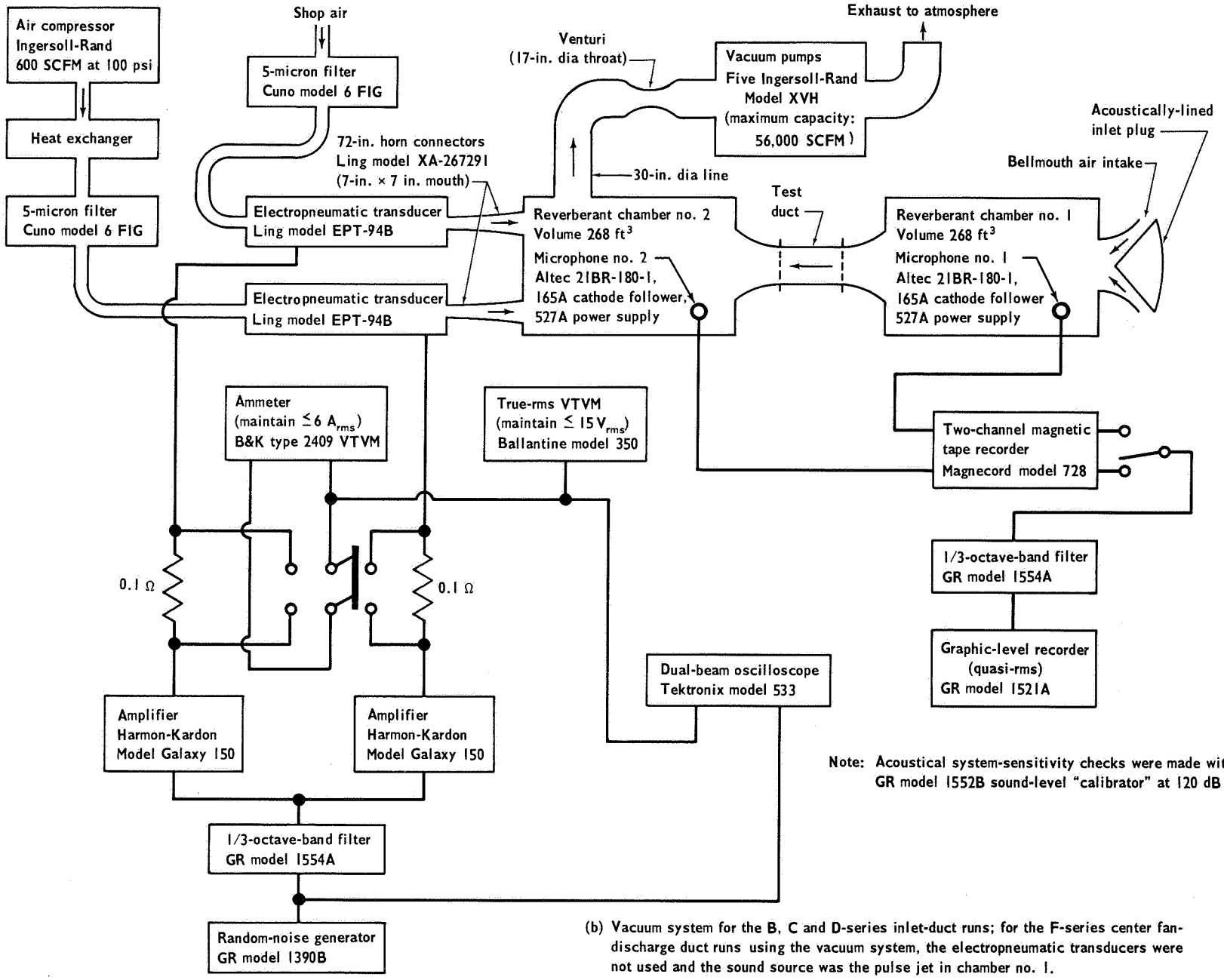

Note: Acoustical system-sensitivity checks were made with a GR model 1552B sound-level "calibrator" at 120 dB at 400 Hz.

(b) Vacuum system for the B, C and D-series inlet-duct runs; for the F-series center fan-discharge duct runs using the vacuum system, the electropneumatic transducers were not used and the sound source was the pulse jet in chamber no. 1.

Figure 37. - Concluded.

Sound sources. — Figure 38 shows the two types of sound sources that were used. The pulse jet (a modified pulse-jet engine made by the Dynajet Corp.) produced an intense sound which had a line spectrum with energy at the firing frequency (about 220 Hz) and harmonics thereof. Because of the reverberant nature of the room in which the source was installed, the number of room modes excited by the source was large and the modal density (per unit frequency) was such that above 2000 Hz the spectrum of the sound measured in the chamber was very similar to that from a random noise source with almost constant energy in 1/3-octave bands (average SPL of 133 dB). This type of noise source, rather than a sinusoidal one, was favored since the excitation of a great many duct modes at once was thought to give the best simulation of the behavior of a duct lining treatment in an actual installation (where the rotating pressure field can excite radial and circumferential modes).

The electropneumatic transducers (Ling model EPT 94-B), figure 38b, were used for the inlet duct tests (where the sound was propagating upstream against the air flow) because it was felt that the pulse jet would not produce an intense enough sound to give adequate signal-to-background noise ratios in the receiver chamber, especially with the duct walls lined with acoustically absorbent material. The transducers were coupled to the downstream chamber with 6-foot-long exponential horns having a cut-off frequency of 50 Hz. The transducers were excited with 1/3-octave bands of random noise (1600 to 6300 Hz) and the voice coil current was maintained at the maximum value of 6 amperes rms. The voice coil current and voltage were monitored as shown in figure 37b. Unfortunately, it was learned after the tests were complete that this was an incorrect procedure at these frequencies because a 6A current does not provide enough force to open the valves far enough to produce any significant modulation of the static pressure of the air flowing through the ports. It was not possible to increase the current because of voice coil heating problems. According to the vendor, maximum high-frequency output is obtained by exciting the transducers with lower frequency energy only, e.g., 1/3-octave energy in the 500 or 630 Hz bands, and then relying on distortion and air noise to produce a wide-band random signal above 1000 Hz with a decreasing, though more intense, spectrum level. Use of the 6-foot-long exponential horns caused an additional loss in high-frequency signal strength. A much shorter horn would have been desirable.

Although these techniques to increase the source signal strength were not followed, it was possible to obtain adequate signal-to-noise ratios (at least 6 dB at the maximum throat velocity) in the receiver room even though the SPL in the 6300-Hz band was 10 to 15 dB lower in the source room with the electropneumatic transducers than with the pulse jet. This was only due to the fact that the transmission losses produced by the inlet duct linings were rather small at 6300 Hz. When the center duct was installed again for the F-series runs, the transmission losses were much greater and the corresponding receiver room SPL's were much lower. Thus, it was impossible to use the electropneumatic transducers for these runs. This was the reason for the return to the pulse-jet sound source in the third system.

Airflow velocity. — As discussed above, equation (19), the maximum duct throat velocity possible with the blower system was only about 300 ft/sec. The actual standard JT3D inlet or fan discharge average duct throat velocities as installed on the DC-8 airplanes are considerably higher as indicated in the table below.

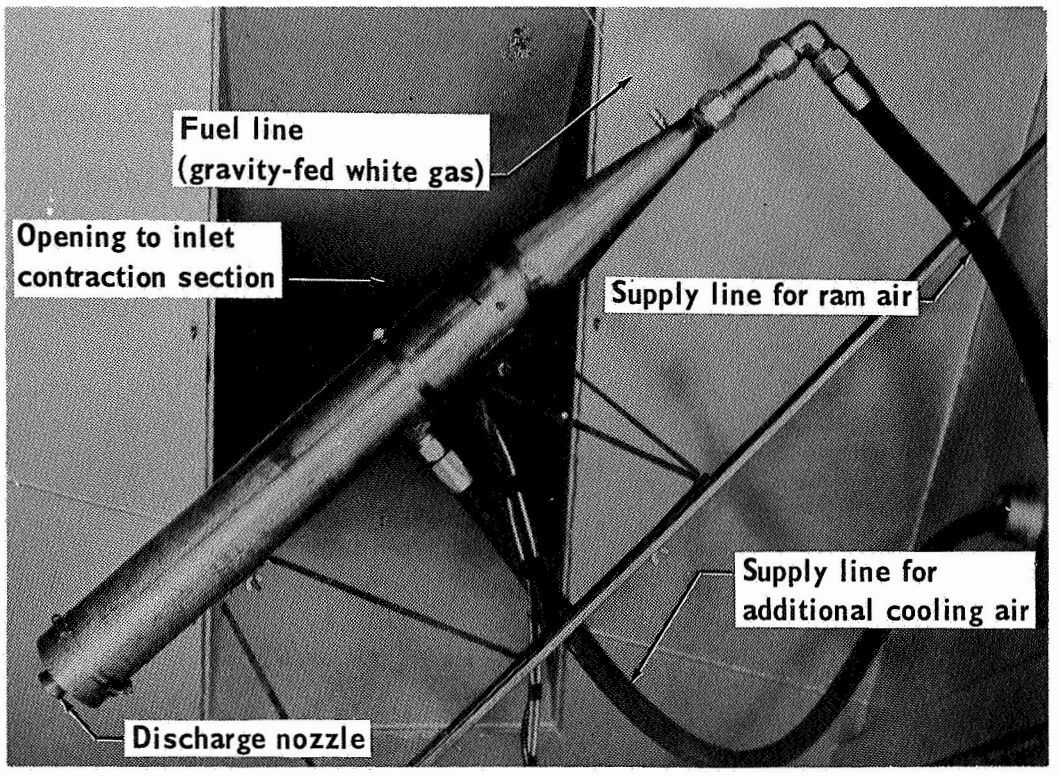

(a) Pulse jet installed in chamber number 1.

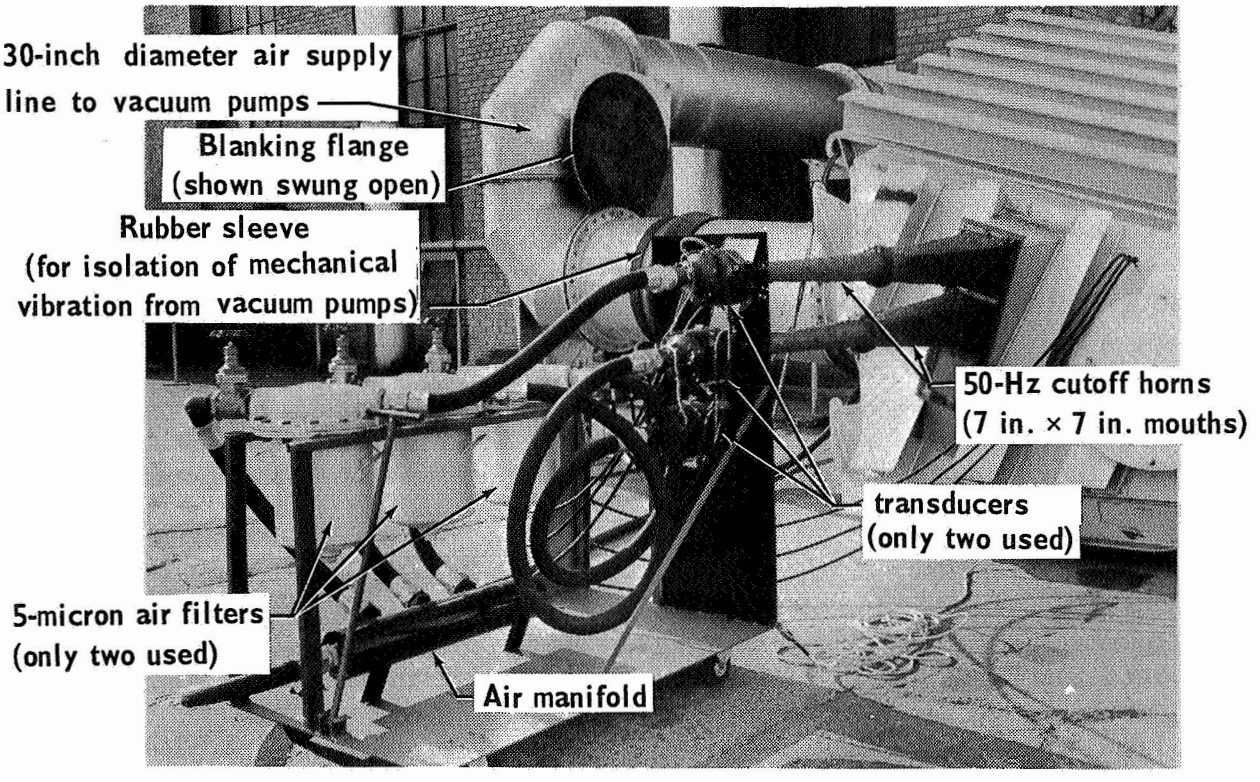

(b) Electro-pneumatic transducers coupled to chamber number 2.

Figure 38. - Sound sources used for dual-reverberant chamber transmission-loss tests.

Condition (M = 0.25)	Duct throat velocity, ft/sec	
	Inlet	Fan duct
Takeoff, altitude 1000 ft	600	1050
Landing, altitude 500 ft	375	750

The actual duct velocities during landing will vary somewhat from these values due to variations in the landing gross weights and flap settings, but not more than about ±10 percent of the indicated value. With the lightbulb inlets the inlet velocities would be just slightly greater and since it was felt to be quite desirable to examine the acoustical behavior of the lining under actual conditions, the facility was modified as described above to make use of the capability of the vacuum system to induce a greater mass flow through the ducts. The vacuum system could induce a maximum volume flow of 56 000 ft^3/min, under standard pressure and temperature (56 000 SCFM) compared to 44 000 SCFM with the blower system.

However, for the inlet ducts, the determination of an accurate mean value to use for the duct throat velocity proved to be a difficult chore, principally because it was not feasible to probe the flow in the area of the throat. For the 55-percent and 75-percent lightbulb inlets, the throat was located in the acoustically treated area and for the standard inlet the throat was located at a duct station where the cross-section was changing from triangular to trapezoidal and the flow was far from uniform. The simplified formula, equation (18), used for the blower system runs could not be used because average value for ΔP, static pressure, and temperature at the throat could not be determined.

The procedure that was finally used was an indirect one that proceeded as follows. First, values for the weight flow of air through the system, were determined with a calibrated venturi meter. Then, from the continuity equation, the throat velocity was calculated using an approximate value for the average density of the air in the throat. A more detailed explanation of the procedure used is given in the appendix. The accuracy of any of the average throat velocity values given with the SPL measurements is estimated to be only about ±20 percent, except for the F-series with the center duct where the accuracy is estimated as ±5 percent.

Test procedures. — During the test program two different kinds of acoustical tests were run. These were: signal-to-background noise ratio tests and transmission-loss tests. This section describes the objectives of these tests and the procedures used to accomplish the tests.

Signal-to-background noise ratio tests: Aside from the electrical system noise, the background noise in the transmission loss tests was the noise created by turbulence as the air flowed through the test ducts and transition sections. The possibility of inadequate signal-to-noise (S/N) ratio existed in the receiver chamber because of inadequate signal strength and high

background noise levels. There was, of course, never a S/N ratio problem in the source chamber. It was necessary therefore to conduct tests to determine the limitations of the facility for measuring transmission loss as a function of frequency and duct airflow velocity.

The S/N ratio in the receiver chamber with the air flowing through the system is the difference in the SPL with the sound source on and the sound source off. This ratio, in decibels, was determined for all the runs made using the vacuum system for various duct flow velocities and, in 1/3-octave bands, over the frequency range from 1600 to 6300 Hz. The ratio is defined only for hardwall tests because this is the reference or baseline case. Minimum S/N ratios always occurred at the highest frequencies, when the sound signal was weakest, and at the highest velocities, when the flow noise was greatest.

The maximum transmission loss and the maximum attenuation that could be measured were determined from the receiver chamber S/N ratio measurements by an analogy to panel sound-transmission-loss tests. The maximum TL for the hardwall ducts is found from

$$(\text{Maximum TL})_{\text{hardwall}} = (\text{TL})_{\text{hardwall}} + (\text{S/N})_{\text{hardwall}} \quad (20)$$

at any frequency and duct velocity This quantity is a direct measure of the limitation of the facility for TL measurements. It is impossible to determine the TL of a duct lining treatment if that TL exceeds the maximum hardwall TL for the indicated duct velocity and frequency band; conversely, the maximum hardwall TL limits the maximum duct velocity at which tests can be run unless the S/N ratio can be raised either by increasing the signal strength, reducing the flow noise, or both.

The measure of the ability of a duct lining treatment to reduce the intensity of the sound propagating down a duct is defined in this report as the attenuation. Attenuation is determined by comparing the TL obtained with a treated duct to that obtained with a hardwall, untreated duct. The TL from a treated duct cannot exceed the maximum hardwall TL and should be smaller by at least 3 dB than the maximum value in order to have less than a 2-dB error. (Two sound sources differing in level by 3 dB produce a total level 1.8 dB greater than the higher single source level.)

Thus we have, as a limit,

$$(\text{Maximum TL})_{\text{treatment}} = (\text{Maximum TL})_{\text{hardwall}} - 3 \text{ dB} \quad (21)$$

or, from the definition of the maximum hardwall TL, equation (20),

$$(\text{TL})_{\text{hardwall}} + (\text{S/N})_{\text{hardwall}} - (\text{Maximum TL})_{\text{treatment}} = 3 \text{ dB} \quad (22)$$

Attenuation is defined as

$$\text{Attenuation} = (TL)_{\text{treatment}} - (TL)_{\text{hardwall}} \quad (23)$$

Combining (22) and (23) gives

$$\text{Maximum attenuation} = (S/N)_{\text{hardwall}} - 3\text{dB} \quad (24)$$

Figure 39 illustrates typical values of the maximum hardwall TL and the maximum attenuation* for an inlet duct and a fan-discharge duct. With the fan-discharge ducts, a given treatment configuration produced greater transmission losses in the high frequencies than an approximately equal area of the same configuration in the inlet ducts. This fact is most likely due to (1) the difference in the shapes of the ducts, and (2) the difference between the relative directions of the airflow and the sound propagation. Therefore, even though the high-frequency strength of the pulse-jet sound source was much greater than that of the electropneumatic transducers (resulting in higher S/N ratios), the attenuations produced by the various treatments (due to the larger treated area in the center fan-discharge duct than in any of the inlet ducts) were often close to the maximum attenuation limitation and therefore the maximum duct throat velocity had to be limited to only 400 ft/sec. In the inlet duct tests it was possible to go to a slightly higher throat velocity (465 ft/sec) even with the lower strength electropneumatic transducers, but only because of the low transmission losses produced by the various treatments. For the configurations that were tested and with the test facility as it was used, the limitations were always only in the 5000 and 6300 Hz bands.

It should be pointed out that these limitations are not immutable and that they could have been overcome if time and funds had been available. However, these were the limitations of the facility that existed during this test program.

Transmission-loss tests: The test procedure for the TL tests was similar to that described above for the S/N ratio tests. Figures 40 and 41 show how an inlet duct and a fan-discharge duct were installed in the dual-reverberant chamber facility for the transmission-loss tests. This is an outdoor facility and the tests were conducted during the winter season. With a test duct and the desired duct lining configuration installed, the desired average duct throat velocity was set (either by the speed of the turbovane fan for the blower system tests or by the flow-control butterfly valve for the vacuum system tests), the sound source was turned on and the steady-state SPL's in the two chambers were recorded on a two-channel tape recorder, figure 37. A 90-second sample of the signal was recorded in order to have

*Study of the tabulated results will indicate that there are some inlet duct configurations for which the attenuation is indicated to be more than the maximum values shown in figure 39b. Obviously, for these cases, the 3-dB criterion has been relaxed (to 1 or even 0 dB) and these results are not to be considered as reliable as those which do satisfy the criterion.

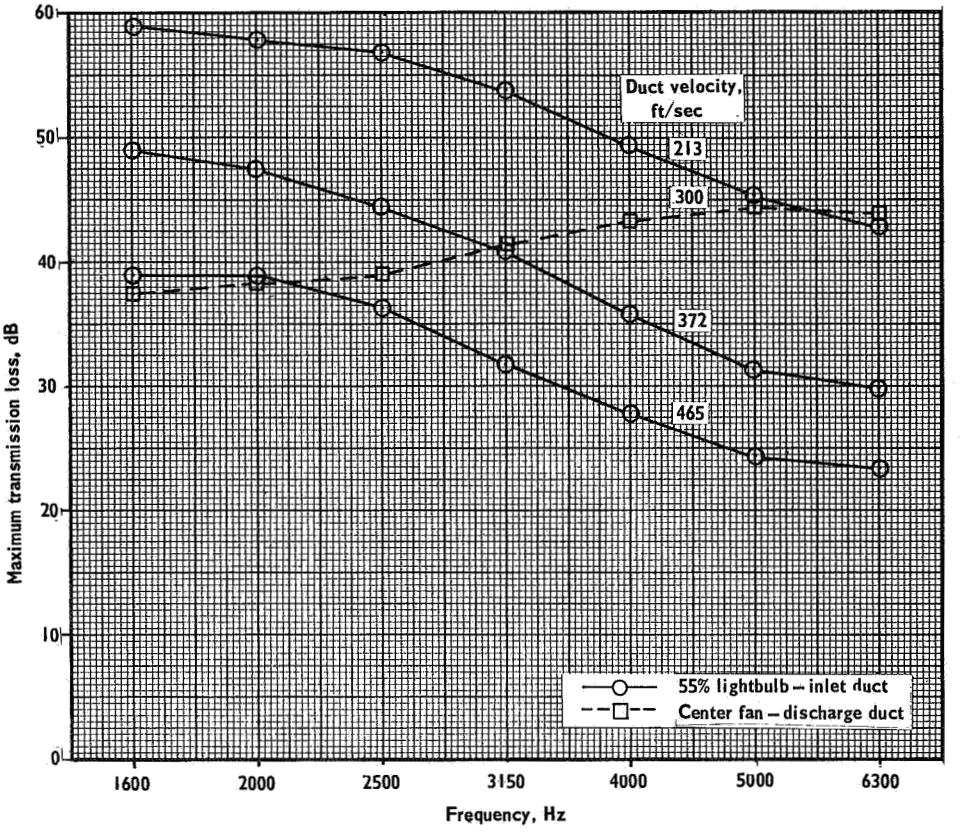

(a) Maximum transmission loss = $(TL)_{hardwall} + (S/N)_{hardwall}$

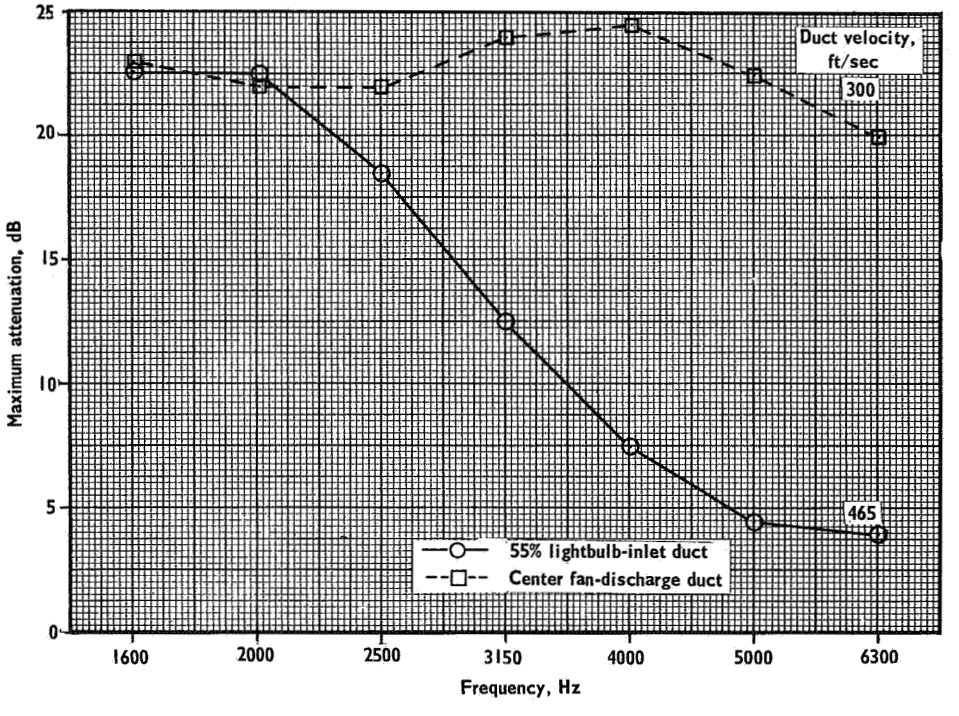

(b) Maximum attenuation = $(S/N)_{hardwall} - 3$ dB

Figure 39.- Acoustical limitations of transmission-loss test facility.

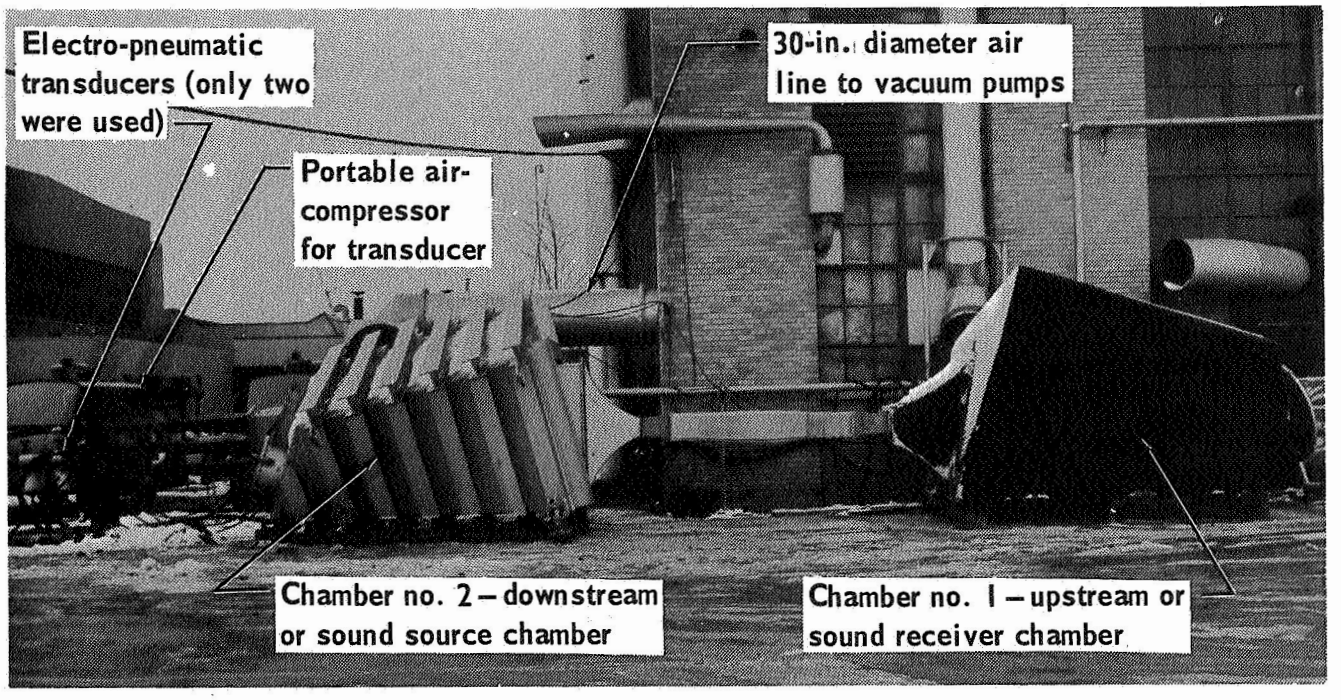

(a) Side view

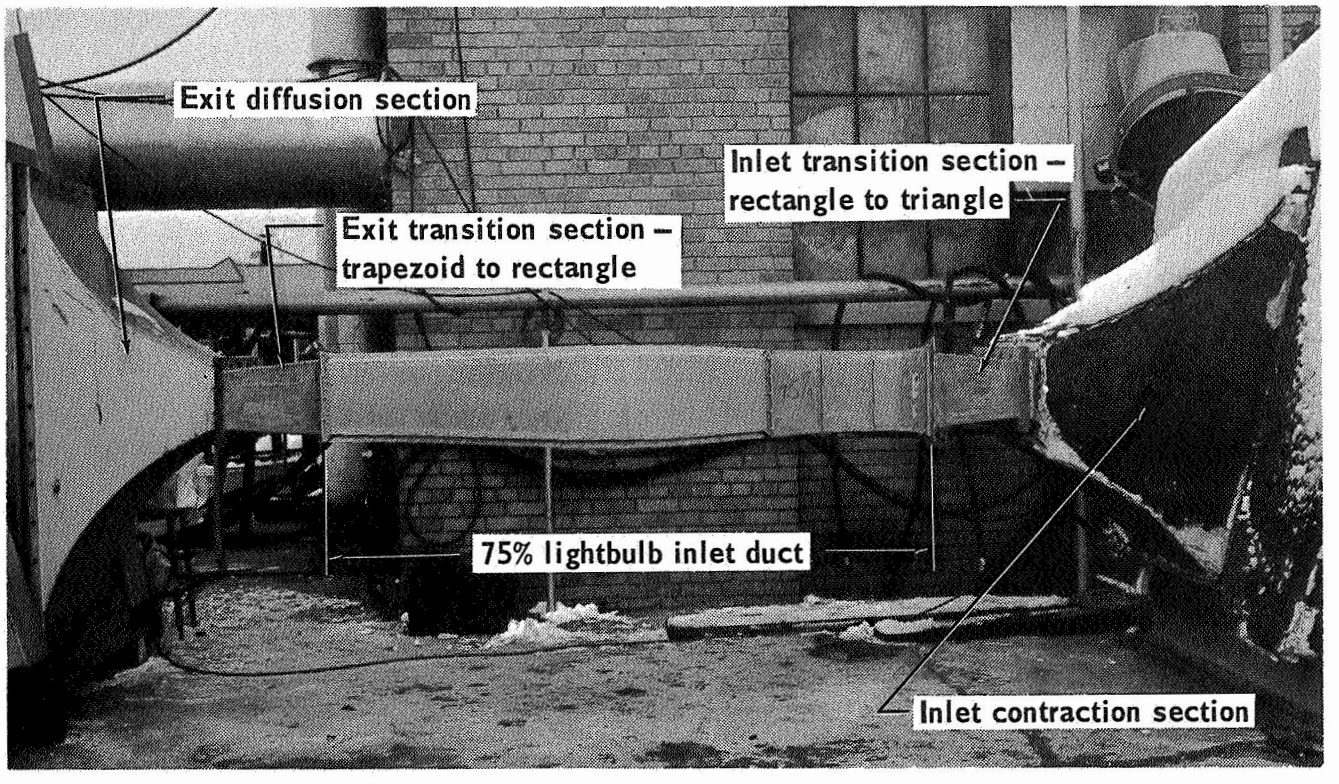

(b) Closer up view showing inlet and exit transition sections.

Figure 40.- Dual-reverberant chamber installation of lightbulb-inlet ducts, vacuum system runs.

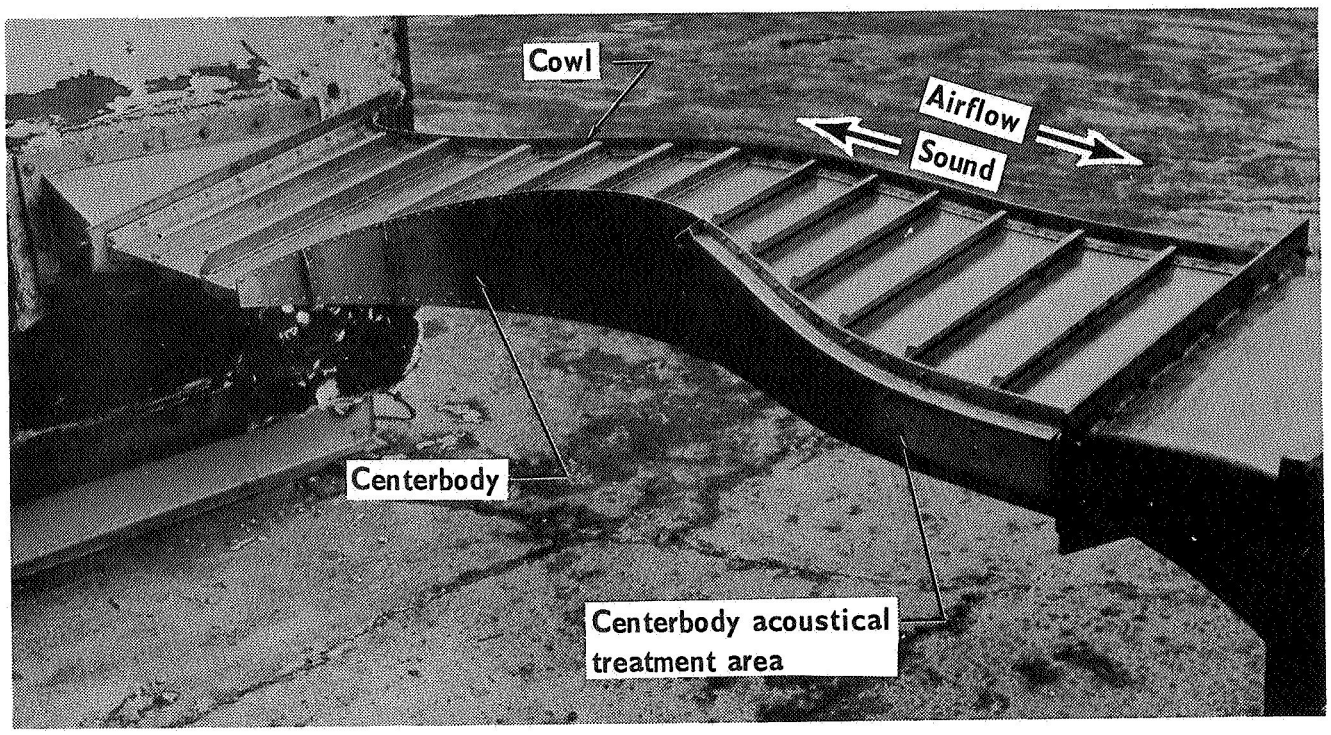

(c) 75% lightbulb-inlet duct.

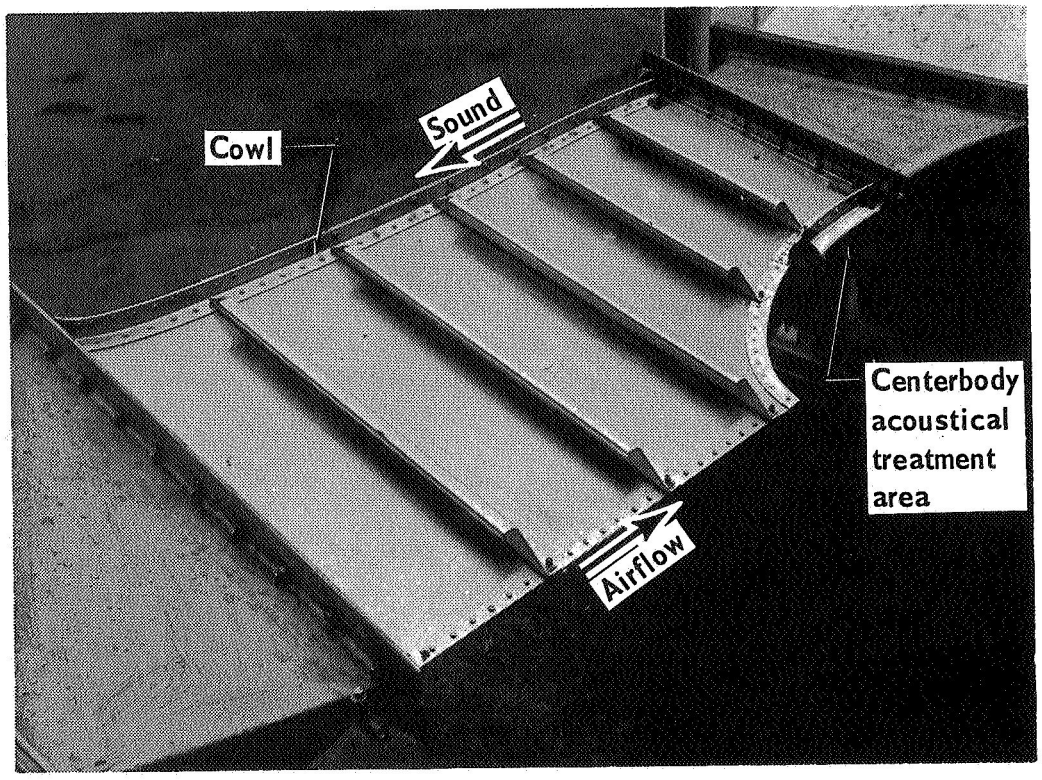

(d) Standard DC-8 inlet duct.

Figure 40. - Concluded.

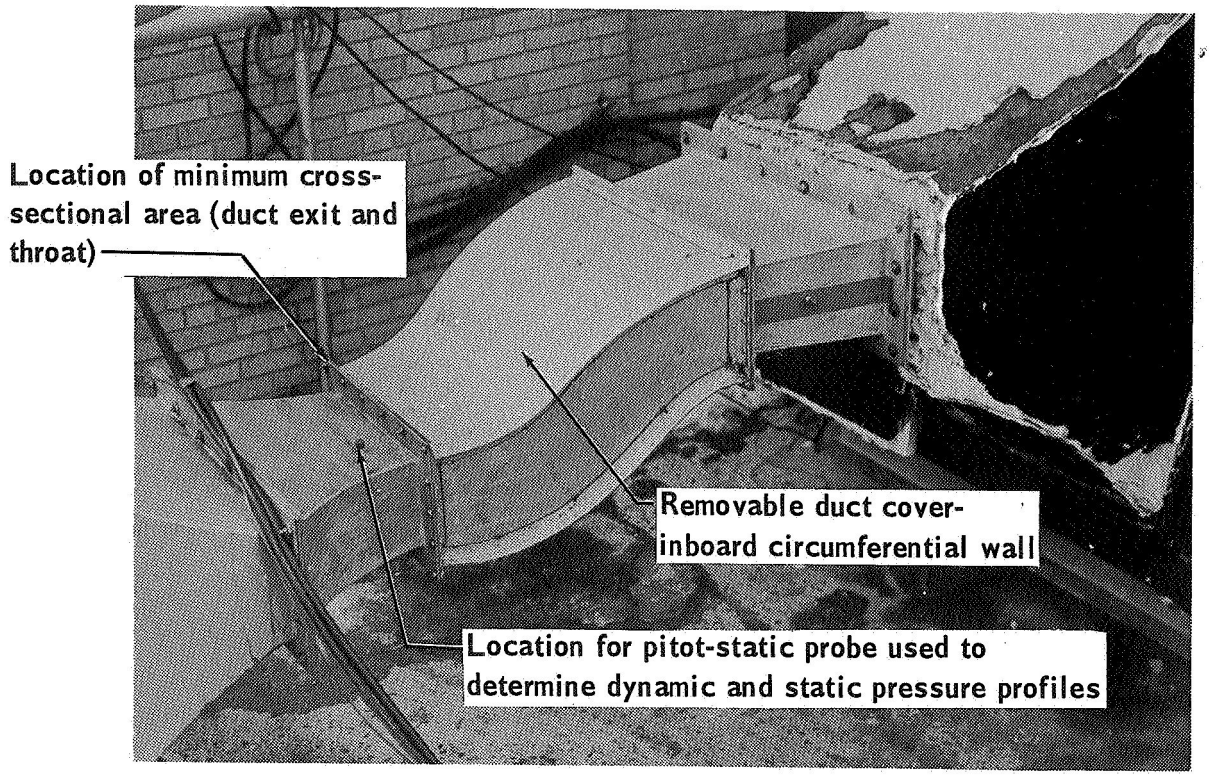

(a) 3/4 view

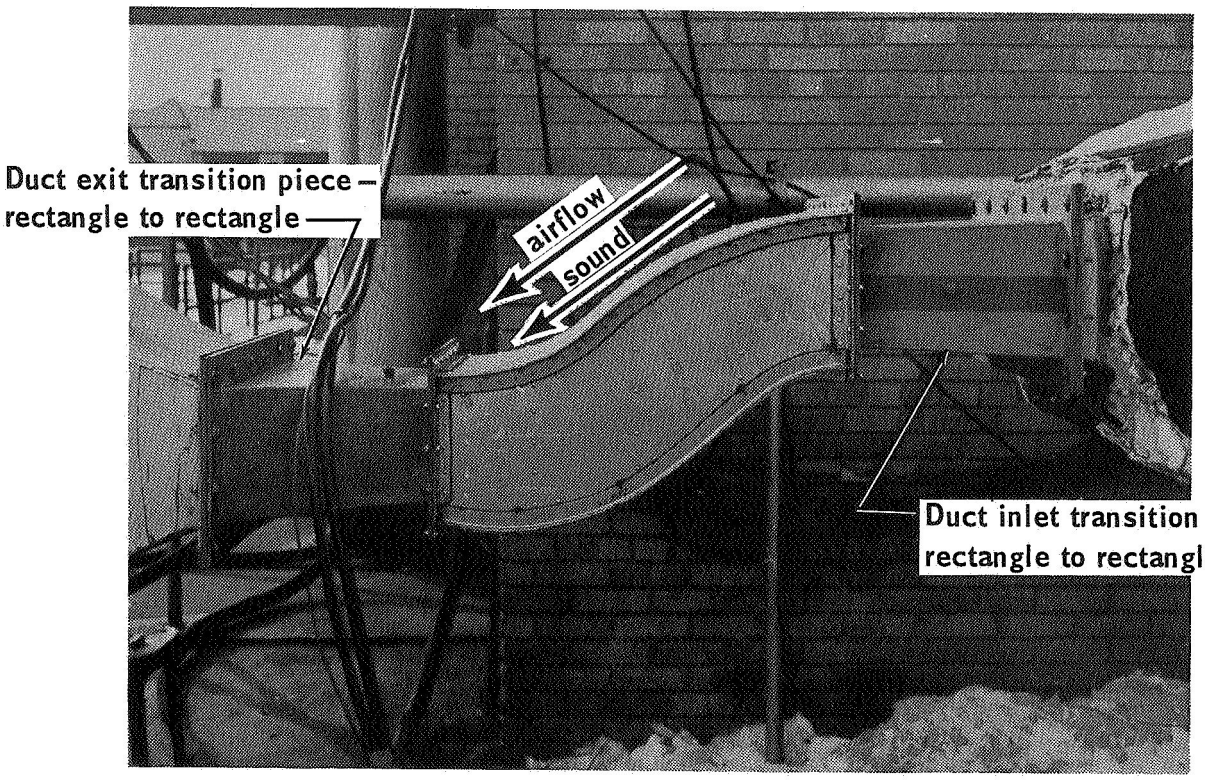

(b) Side view

Figure 41. - Dual-reverberant chamber installation of center fan-discharge duct.

a recording that was long enough to analyze automatically with the 1/3-octave band filter and graphic level recorder without having to make any tape loops or to re-wind the tape.

The filter used for the analysis had a continuously variable center frequency tuned by a chain-drive mechanism on the level recorder in synchronism with preprinted paper. The bandwidth of the filter was a constant percentage (here 23 percent or 1/3-octave bands). (The end duct runs data were reduced with an 8-percent narrow band filter instead of the 1/3-octave band filter.) The paper records (traces) were read at the standard 1/3-octave band center frequencies from 1600 to 6300 Hz. No attempt was made to obtain an optimum value of the pen writing speed or to do any kind of averaging of the varying lines on the traces; whatever value for the SPL that was indicated on the trace at the desired center frequency was the value given. Above 2000 Hz there were so many room modes per unit frequency, with none being very strong, that the variation in the observed SPL was about ±0.5 dB with either sound source. Below 2000 Hz the modal structure of the sound field in the chambers was such that, with the pulse-jet sound source, in the 1600-Hz band a change of 100 Hz in the center frequency could cause a change of 2 to 3 dB.

Taking the above factors into account, the accuracy of the SPL readings is estimated to be ±1 dB for the 1600 and 2000 Hz bands and ±0.5 dB for the remaining bands, as long as the comfortable 3-dB margin with respect to the S/N ratio and the maximum TL is maintained. The accuracy of the corresponding TL values is therefore estimated to be ±1.4 dB for the 1600- and 2000-Hz bands and ±0.7 dB for the 2500- to 6300-Hz bands; the accuracy of the corresponding attenuation values is ±2 dB and ±1 dB, respectively. The precision of the results (i.e., the reproducibility of any given test) was good providing the duct velocities could be set to the same values. Repeat runs showed that the transmission losses could, in general, be duplicated within ±1 dB.

Test configurations and test variables. — With all of the flexibility that was designed into the test program the number of possible test configurations and test variables was very large. It was decided to concentrate the effort on determining the effects of as many of the following seven variables as possible for both the fan-discharge and the inlet ducts:

- Backing treatment (cavity-filling material)
- Backing or cavity depth
- Flow resistance of the fibermetal lining material
- Area of treatment
- Duct velocity
- Reduction in the length and width of the duct by the addition of radial and circumferential splitters (center fan duct only)
- Type of fibermetal, aluminum vs stainless steel (55-percent lightbulb inlet duct only).

Configuration codes (or run number codes) were assigned to each test run in a logical pattern in an attempt to organize the mass of data that had been accumulated and to aid in analyzing the effects of the variables presented above. The five ducts were assigned letter codes as follows: A = center duct - blower system, B = 55-percent lightbulb, C = standard DC-8 JT3D inlet, D = 75-percent lightbulb inlet, E = end duct, F = center duct - vacuum system. The general pattern for all of the configuration codes was as follows: first a letter, indicating the duct; then a number, indicating the run number; finally, a dash number to indicate the average throat duct velocity. The general pattern for assignment of code numbers to a given test and for explanation of the particular test configuration is shown in Table II. The The pattern follows an outline format which is repeated over and over again for each basically different configuration. Detailed test outlines and configuration code listings are given in Tables III and XVI for the fan-discharge ducts and the inlet ducts, respectively. Detailed explanations of the configuration codes along with detailed descriptions of the physical arrangement for each test are given in Tables IV, V, VI, XVII, XVIII, and XIX for configurations A, F, E, B, D, and C, respectively. These tables are not numbered in sequence because it was felt important to keep the explanation of the configuration codes together with the tabulated data for each to assist in discussing the results and for subsequent use of the results by others.

Discussion of TL Test Results. — A total of 217 tests with the five duct models (counting each configuration and each duct velocity for which data were obtained as a test) were conducted in which 101 different treatment configurations were evaluated. In general, efforts were made to explore the effect of just one of the seven test variables at a time. In view of the great number of possible combinations of acoustic treatment, duct geometries and duct velocities, it was not feasible to conduct a completely exhaustive study. Therefore, evaluation of the results, during the course of testing, guided the selection of the variables to be considered.

The data and the results discussed in this section are all presented in a collection of tables (tables II through XXVIII) at the end of this report. The sound-pressure levels, transmission-loss values and attenuation values are tabulated along with the detailed explanations of configuration codes and test outlines as described in the preceding section. The curves presented are all identified with the configuration codes for aid in collating the plots with the tabulated results. Most of the tests were conducted with two duct models: the center fan-discharge duct (configurations A and F) and the 55-percent lightbulb inlet (configuration B). Additional tests with the other duct models were made using the most promising configurations from the initial tests.

In the discussion that follow, the effects of all of the test variables, mentioned above except one (duct velocity) will be discussed for each of the five test ducts. Due to S/N ratio limitations, data over a wide enough range of duct velocities could not be obtained to adequately document velocity effects. There are, however, some limited results (which are tabulated but not plotted) which show the following trends: (1) there is a reduction in attenuation in the fan-discharge ducts as the velocity is increased from 100 to 400 ft/sec, and (2) the effect on the attenuation produced by increasing the average duct airflow velocity over an inlet treatment is negligible for duct velocities ranging from 75 to 465 ft/sec. These two results tend to

corroborate the work of Mechel and Schilz, reference 26, but additional work is needed to define the effect of velocity on attenuation.

Results obtained from the tests on each of the five duct models are presented below. The analyses for the inlet ducts are for the maximum throat velocity in each duct, i.e., 465 ft/sec in the 55-percent and 75-percent lightbulb inlets and 358 ft/sec in the standard inlet. The analyses for the fan-discharge ducts are for the one throat velocity for which comparative data exist for the three fan-discharge duct series, i.e., for 300 ft/sec.

Center fan-discharge duct: A total of 41 treatment configurations was tested with the center duct, 26 in the A-series and 15 in the F-series (see table III). The test results for these series are given in tables VII, VIII, X, XI, XIII, and XIV. Figure 42 compares various backing treatments behind 25-rayl fibermetal; for these comparisons the four walls of the duct were all completely treated and an untreated, hardwalled radial splitter was installed. The radial splitter bisected the two circumferential walls.

A comparison of 1-inch-deep cavity-filling materials is given in figure 42a. For frequencies greater than 2500 Hz, the air-filled cavity provided the greatest attenuation (defined by comparison of the TL with treatment to the corresponding hardwall TL, equation (23)); below 2500 Hz, the CPF type 4-900 was the best. The smallest attenuation was that produced by the ceramic fiber type CF-600 with a density of 6 lb/ft^3.

When the cavity depth was reduced to 0.5 inch, figure 42b, the air-filled cavity produced the least attenuation. Filling the cavity with porous material increased the attenuation by substantial amounts. The best results were achieved with CPF 4-900. The effect of reducing the cavity depth to 0.25 inch is shown in figure 42c for backing materials of air and CPF type 3-900. The 0.25-in. CPF type 3-900 was markedly superior to the 0.25-in. air.

From this series of tests, it would seem that, for maximum attenuation, cavity depths of 0.5 in. or less should be filled with a porous material such as CPF types 3-900 or 4-900. For depths of 1 inch, the best material would appear to be air, a fortunate result because of the low weight density of air compared to any other cavity filling materials. Increasing the depth of the air-filled cavities (0.25 to 0.5 to 1 inch) gives progressively greater attenuations. The suggestion is that even greater depths might be better, although (judging from the impedance tube studies) at some loss in attenuation above 4000 Hz.

The effect of varying the rayl number of the fibermetal is given in figure 43 where the results of tests with 25- and 60-rayl material are shown with various backing treatments and two different external duct geometries. For the first case, figure 43a, acoustical treatment was applied to the four duct walls and an untreated radial splitter was installed. In the second arrangement, only the two circumferential walls (the larger walls) were treated; the radial walls and the radial splitter were hardwall. In both cases, the results indicate that when the treatment was more effective (i.e., produced fairly large attenuations), the 25-rayl material was superior to the 60-rayl material. Compare, for example, cavities filled with 1 inch of air or 0.5 inch of CPF type 3-900, figures 42a and 42b. When the treatment was

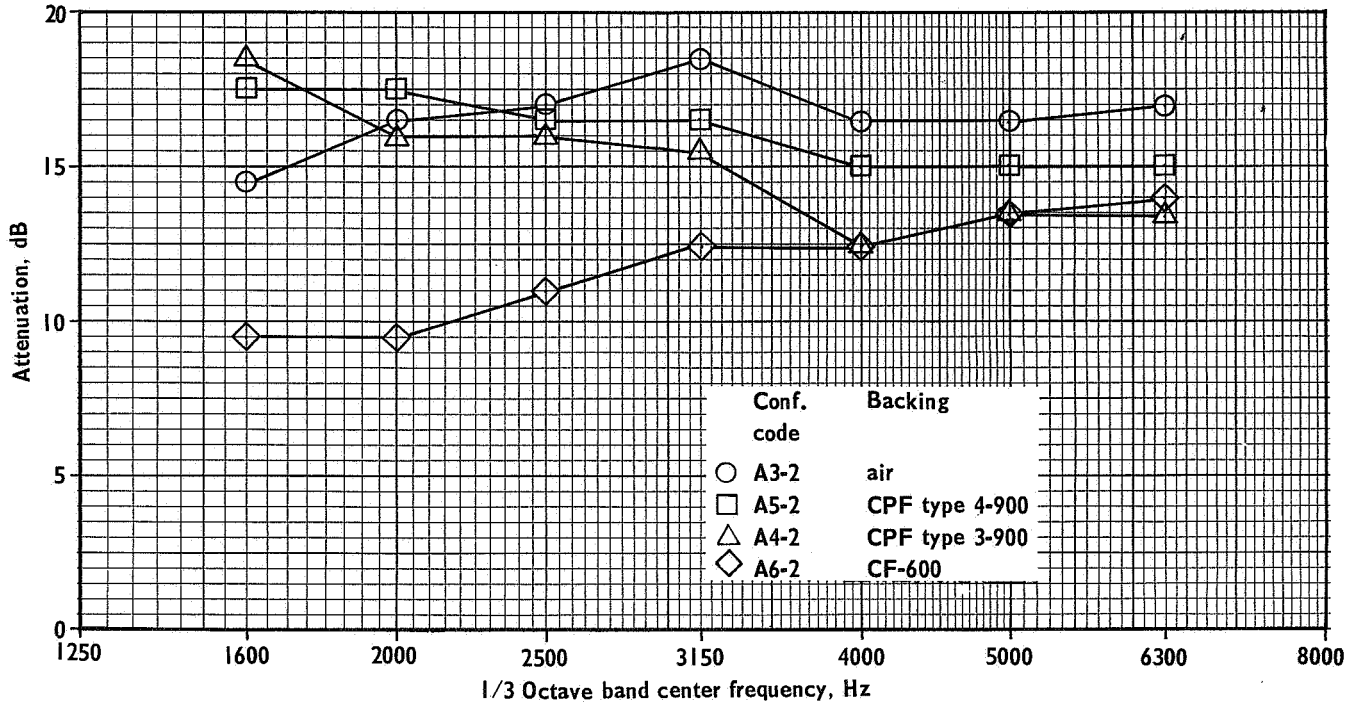

(a) One-inch backing depth.

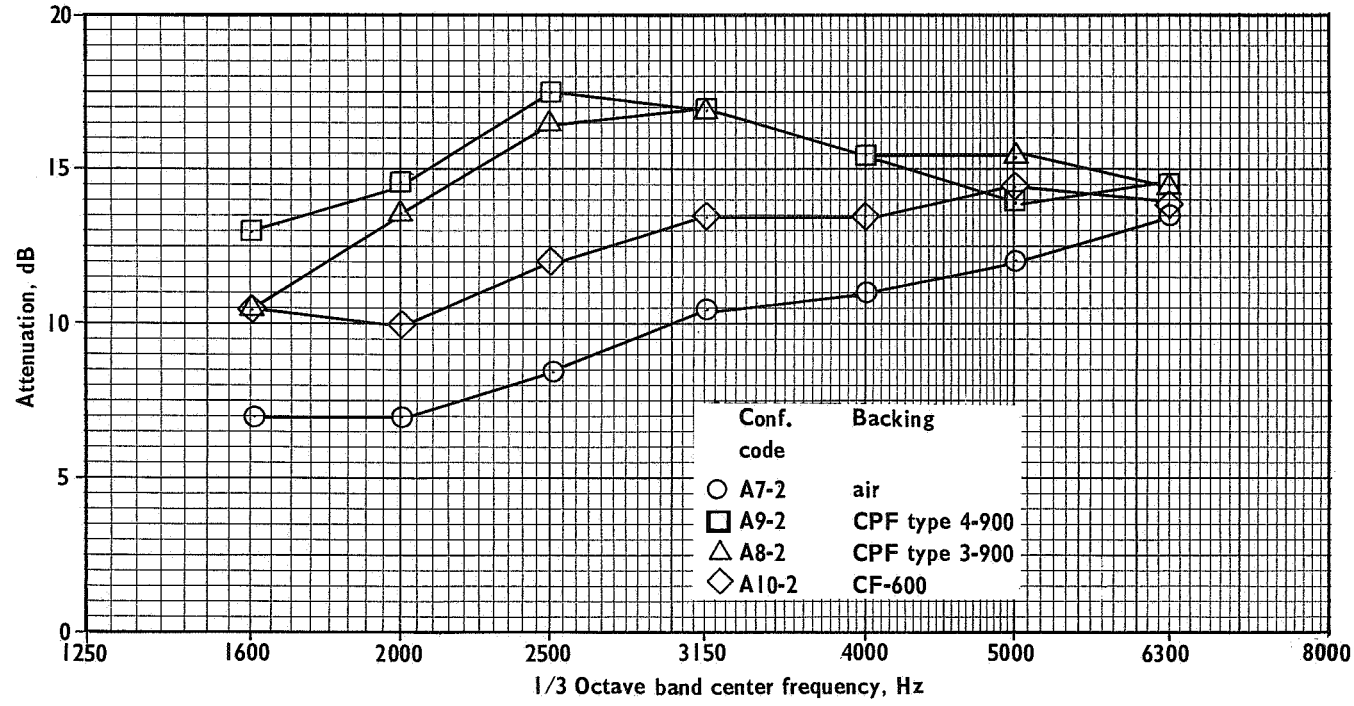

(b) One-half inch backing depth.

Figure 42.- Center fan-discharge duct: Effect of varying backing treatments under 25-rayl fibermetal.

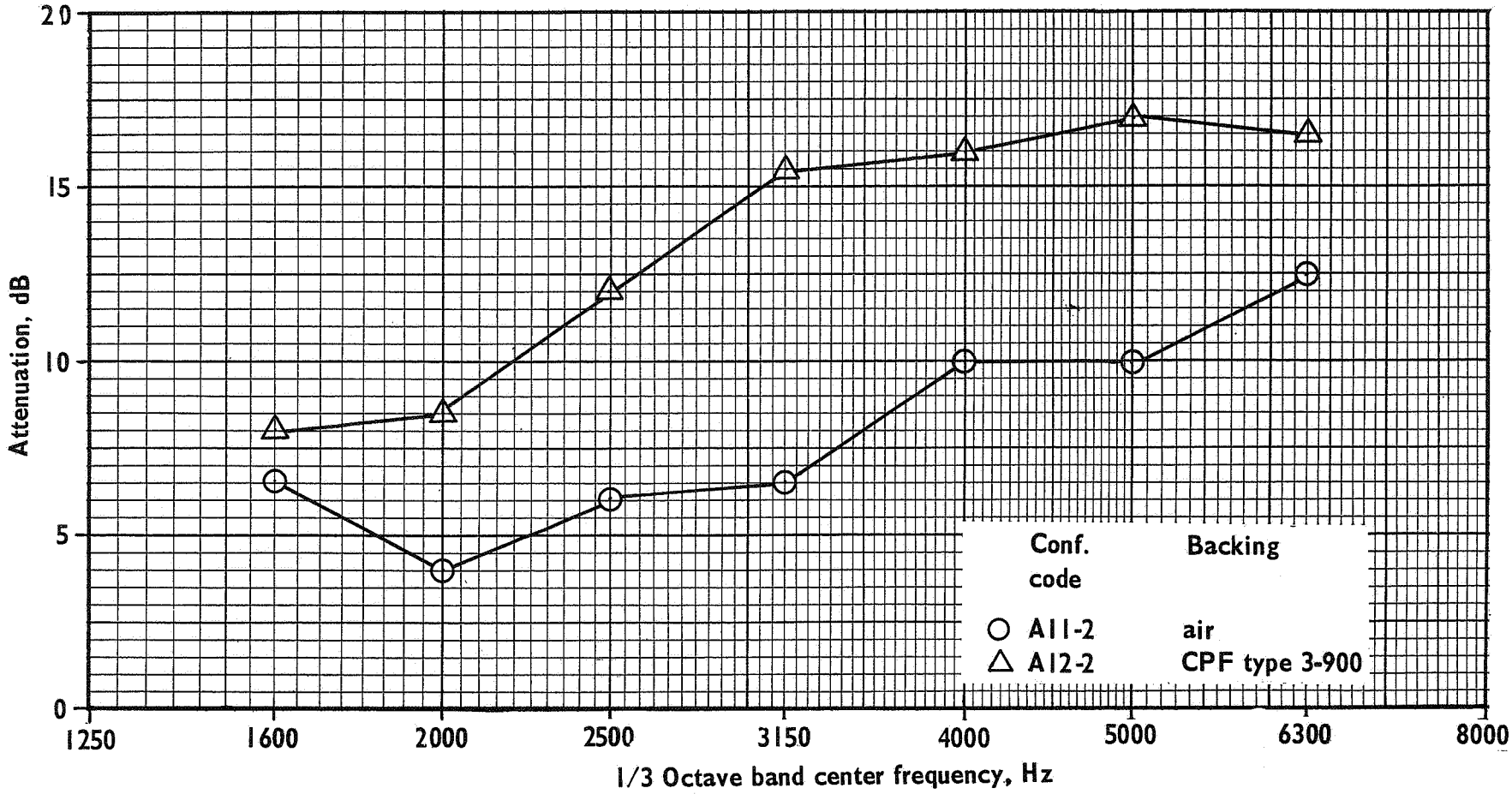

(c) One-quarter inch backing depth.

Figure 42. - Concluded.

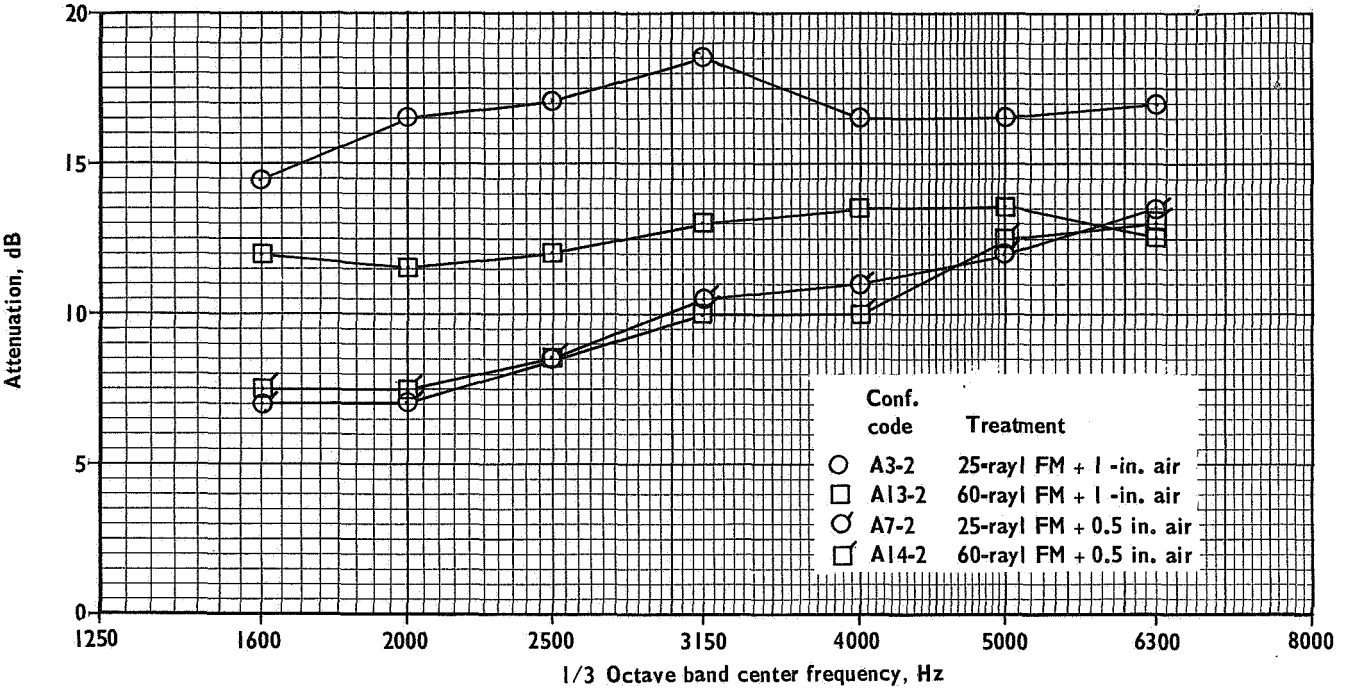

(a) Four walls treated; hardwall radial splitter installed.

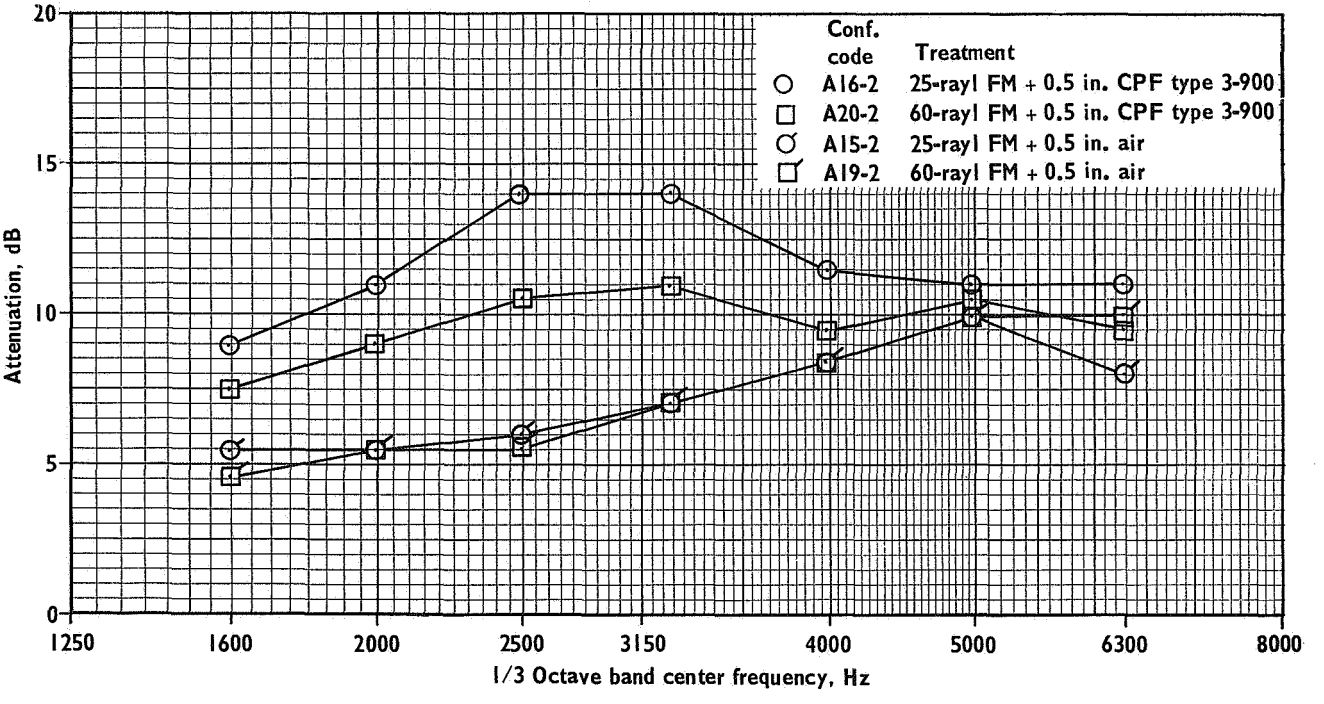

(b) Two circumferential walls treated; two radial walls, hardwall; hardwall radial splitter.

Figure 43. - Center fan-discharge duct; Effect of varying the flow resistance of fibermetal lining.

not as effective, there was a negligible difference between 25- and 60-rayl material, e.g., as with 0.5-inch air-filled cavities. These results are in general agreement with the results of the impedance tube tests which indicated the desirability of the lower values of flow resistance for the fibermetal. When selecting a duct lining design, it appears that the acoustical impedance of the total duct lining configuration (under the conditions of the actual full-scale environment) must be considered and not just the flow resistance of the surface material.

The effect of treating only the two circumferential walls compared to treating all four walls is shown in figure 44. Two cases are shown: one case from the A-series of runs with 0.5 inch of CPF type 3-900 behind 25-rayl fibermetal and the other case from the F-series of runs with a 1.0-inch air-filled cavity behind 25-rayl fibermetal. In the first case, figure 44a, there was an untreated radial splitter installed; no splitter was installed for the second case, figure 44b.

The attenuation produced with the four-wall treatment was always greater than that produced with the two-wall treatment by 2 to 5 dB, depending on frequency and configuration. It is felt that this is primarily an area-of-treatment effect and the conclusion is that the maximum attenuation will always be produced by the configuration that has the greatest amount of treated area.

Figure 45 shows the results of another test to determine the effect of varying the amount of treated area. In these tests the treated area varied from 25 percent to 100 percent of the area of the two circumferential walls; the radial walls were untreated and there were no splitters installed. The data indicate that there is almost a linear relationship between the percentage of the treated area and the attenuation, at least for frequencies around 2500 Hz.

The effect of revising the internal duct dimensions by the addition of splitters is shown in figure 46. When all of the internal surfaces were hardwall, figure 46a, installation of a radial splitter increased the transmission loss by about 5 dB. Installation of a circumferential splitter along with the radial splitter did not significantly change the transmission loss above that produced when the radial splitter alone was installed. Since all of the internal surfaces were hardwall, the amount of acoustical power absorbed by the duct walls was negligible. The power radiated out through the side walls of the duct should have been the same in the three cases. Therefore, the increase in transmission loss produced when the splitters were installed is attributed to an increase in the amount of acoustic power reflected back toward the source when the longer duct cross-dimension was reduced by the installation of a radial splitter. Installation of the radial splitter transformed the inlet to the duct from one 6-5/8 × 20-inch opening to two 6-5/8 × 9-3/4-inch openings. The conclusion drawn from the data presented in figure 46a is that, with hardwalled ducts, it is worthwhile to consider adding an untreated splitter parallel to the short side of a rectangular duct (making two approximately square ducts out of the rectangular one). However, installation of an untreated splitter parallel to the long side of the duct, in addition to one parallel to the short side, produces no change in the transmission loss.

Figure 46b gives the results obtained when the four duct walls were treated with 0.5-in. CPF type 3-900 behind 25-rayl fibermetal. In contrast to the results obtained when the four duct walls were hardwall, figure 46a,

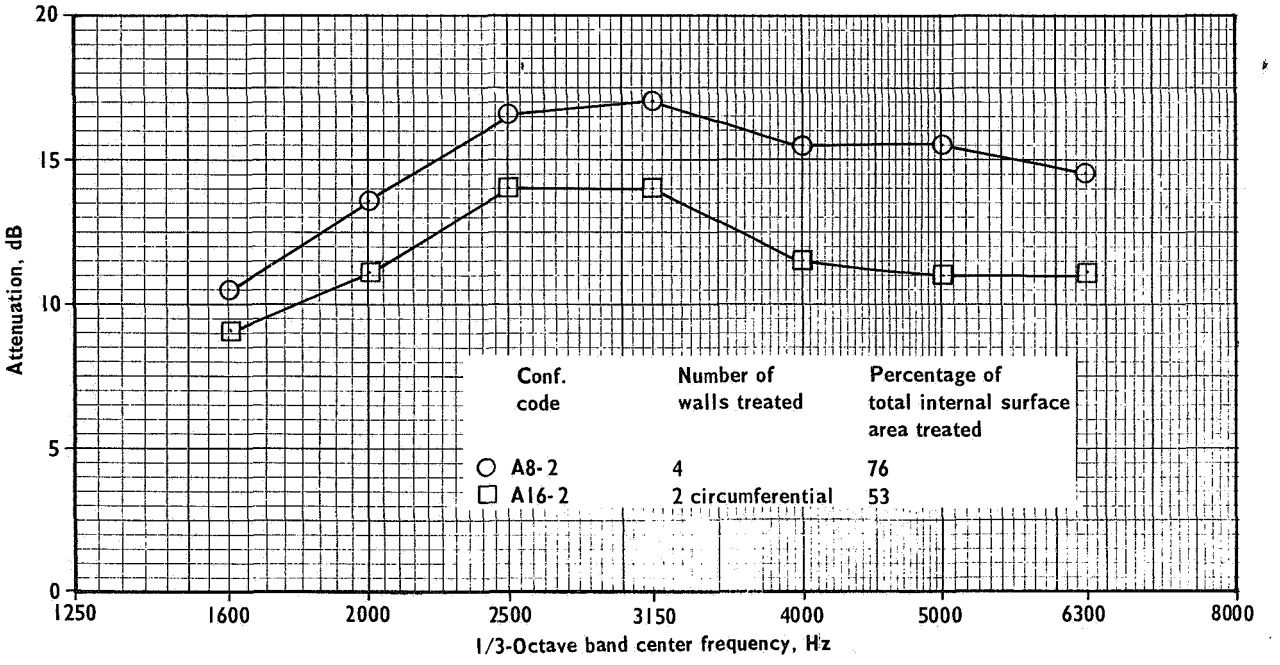

(a) One-half inch CPF type 3-900 backing material; hardwall radial splitter.

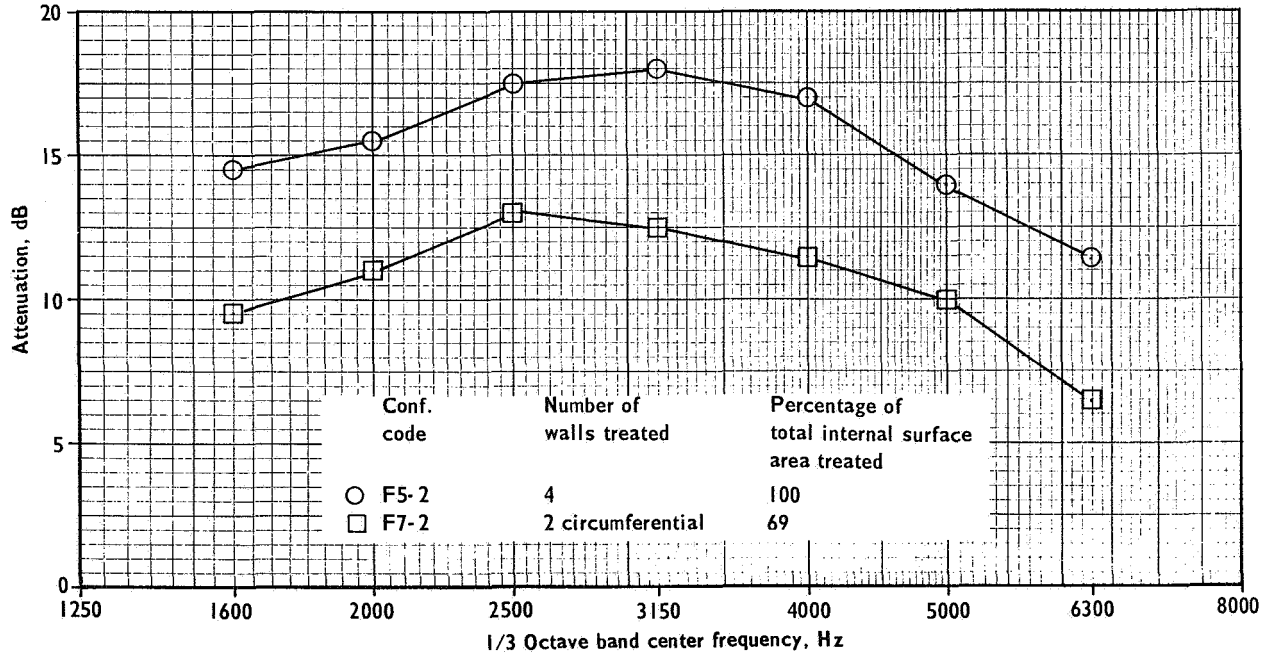

(b) One inch air backing material; no internal splitter.

Figure 44.- Center fan-discharge duct: Comparison of two wall treatment and four wall treatment under 25-rayl fibermetal.

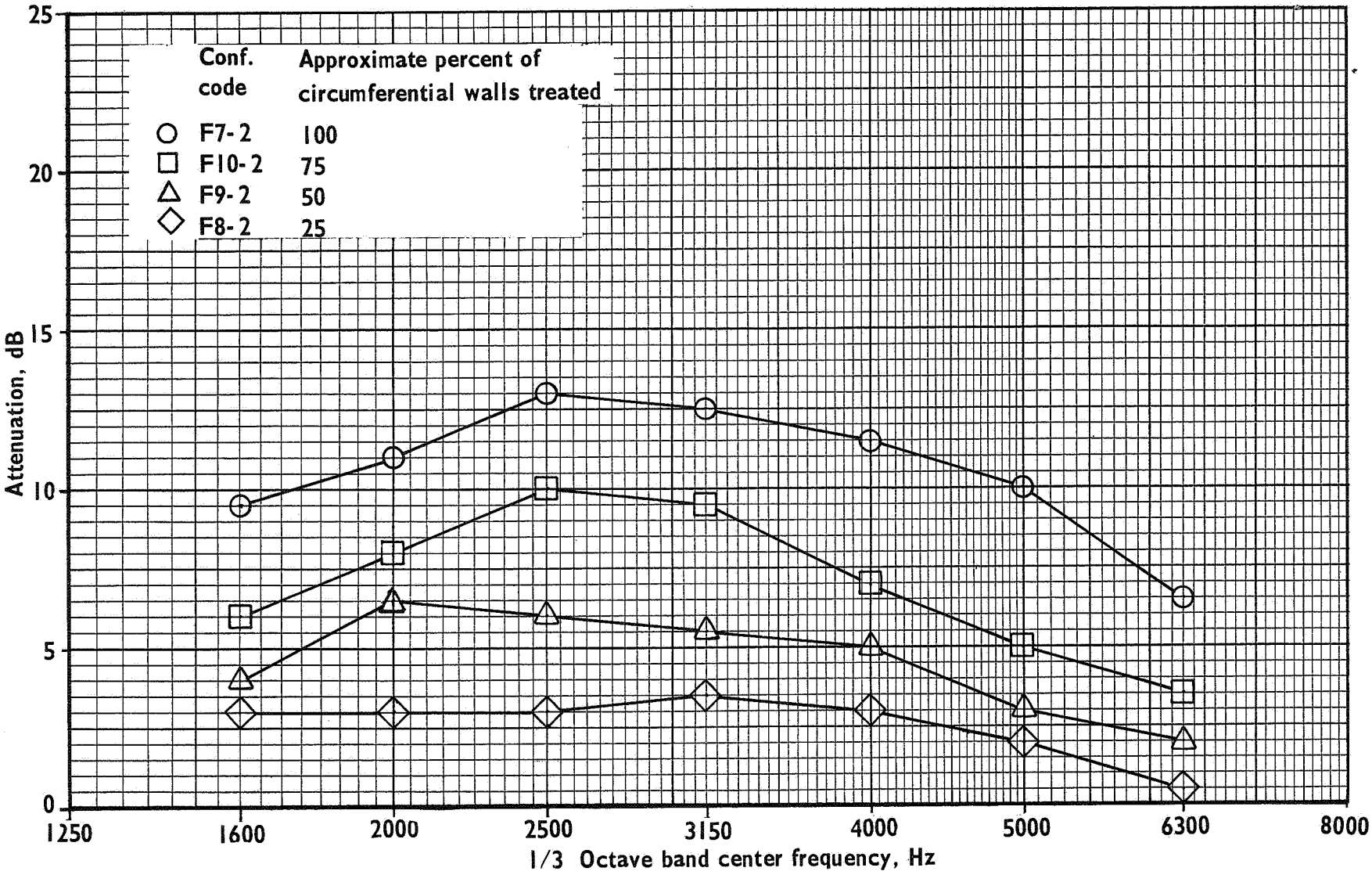

Figure 45. - Center fan-discharge duct: Effect of varying the amount of treated area: treatment was 25-rayl fibermetal over 1-in. air-filled cavity on the two circumferential walls, radials walls hardwall, no splitters.

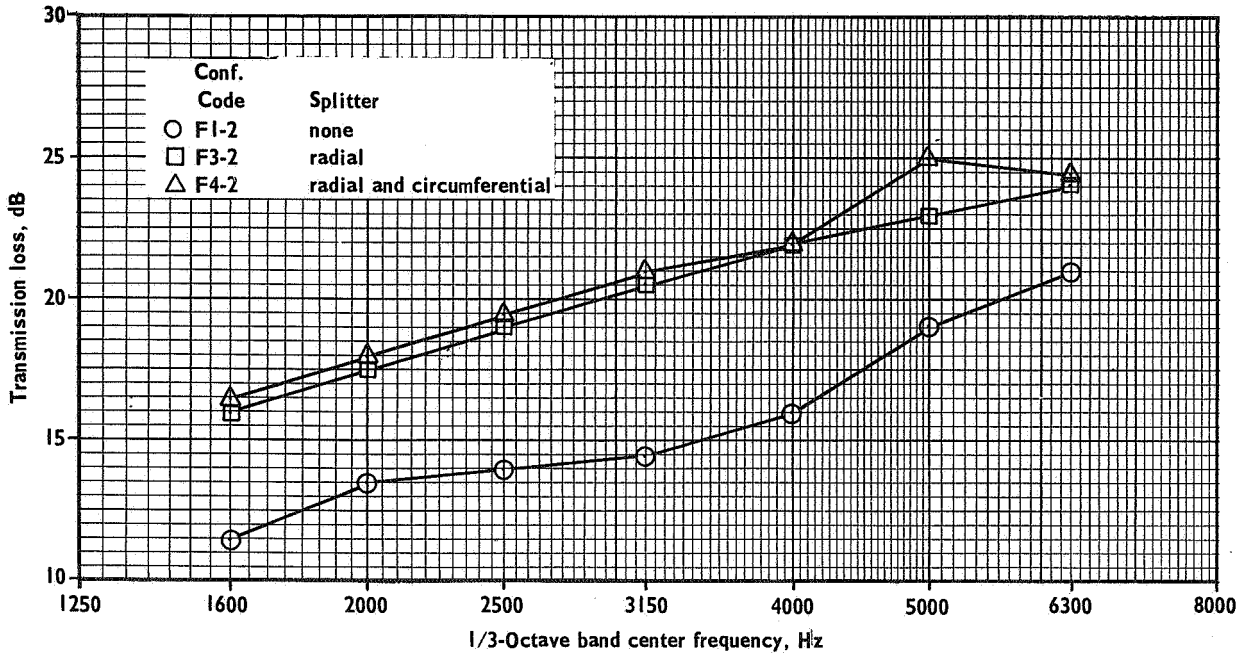

(a) All internal surfaces hardwall.

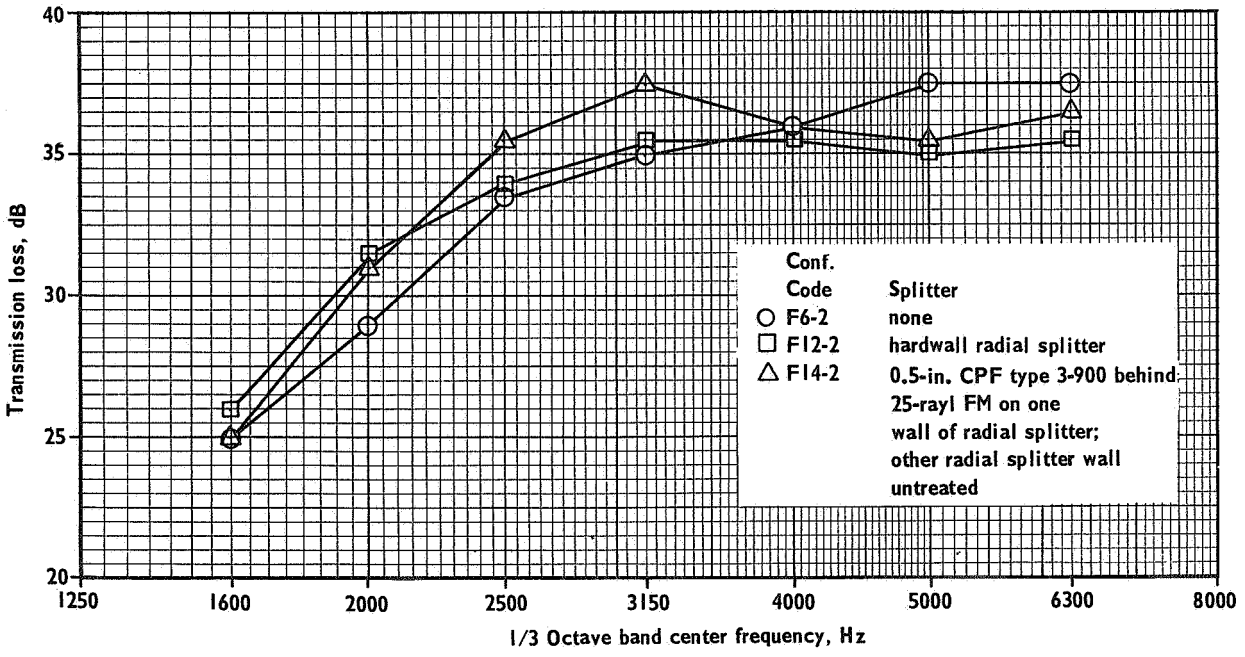

(b) Four boundary duct walls treated with 0.5-in. CPF type 3-900 behind 25-rayl fibermetal.

Figure 46. - Center fan-discharge duct: Effect of installing splitters.

addition of a hardwall radial splitter produced essentially no change in the TL. Installing acoustical treatment on the radial splitter resulted in a modest improvement in the transmission loss at some frequencies.

The conclusion here is that, if the boundary walls of a duct are treated with an efficient acoustically absorbent material, installation of untreated splitters makes no change in the transmission loss. On the other hand, adding acoustical treatment to splitters which are already installed does increase the TL. This generalization may apply only to ducts with dimensions similar to those of the center duct and in the frequency range between 1600 and 6300 Hz, and also on the amount of treated area that can be added.

End fan-discharge duct: Tests with the end fan-discharge duct were conducted to complete the study of the full-scale JT3D fan duct and to determine the effects of adding acoustical treatment to a fan-discharge duct model whose flow path was quite unlike that of the center fan-discharge duct model. Ten treatment configurations were tested with the end duct. Values for the SPL's, TL's and attenuations for these E-series runs are given in tables IX, XII, and XV, respectively. The results for these tests are given in terms of analyses based on the use of an 8-percent bandwidth filter. There should be no difference in the transmission losses or attenuation values calculated from these SPL readings as compared to those that would have been calculated from 1/3-octave band SPL's, as long as the noise is random.

Figure 47 shows the effect on the attenuation achieved by the end duct with various backing treatments under 25-rayl fibermetal. Maximum attenuation (16 to 20 dB) was produced with the 0.5-in.-thick CPF type 3-900 backing material on all four walls, figure 47a. The attenuation produced by a 1.0-in. air-filled cavity was about 3 dB less, a result opposite to that obtained with the center duct tests. The results from a similar group of tests in which the treatment was applied only to the two circumferential walls is shown in figure 47b. Here again, maximum attenuation was achieved by the 0.5-in. CPF type 3-900. In both cases treatment with 0.5 in. of air gave the least attenuation and CPF type 4-900 was somewhat poorer than CPF type 3-900.

Comparison of the data shown in figure 47 indicates that, for the same type of treatment, from 3.5 to 6 dB greater attenuation can be produced by treating the two radial side walls in addition to the two circumferential walls. The same conclusion was noted from the results of the center duct tests where the backing treatments considered were also 0.5-in. CPF type 3-900 and 1.0-in. air.

Additional comparisons between the end duct and the center duct can be made by examining the transmission losses for the three cases which had the same acoustical treatment and the same duct velocities. These cases were: (1) all hardwall surfaces, E1-2 and F1-2; (2) 1.0-in. air behind 25-rayl fibermetal on four walls, E2-2 and F5-2; and (3) 0.5-in. CPF type 3-900 behind 25-rayl fibermetal on four walls, E4-2 and F6-2. Examination of these results, tables XI and XII, shows that the end duct produces 2 to 3 dB more transmission loss than the center duct for the same configuration. This increase in TL is felt to be due to the helical flow path and the compound curvature of the end duct. The curvature results in more of the input acoustic power being reflected back toward the source room (i.e., increased blockage) with a consequent increase in indicated transmission loss.

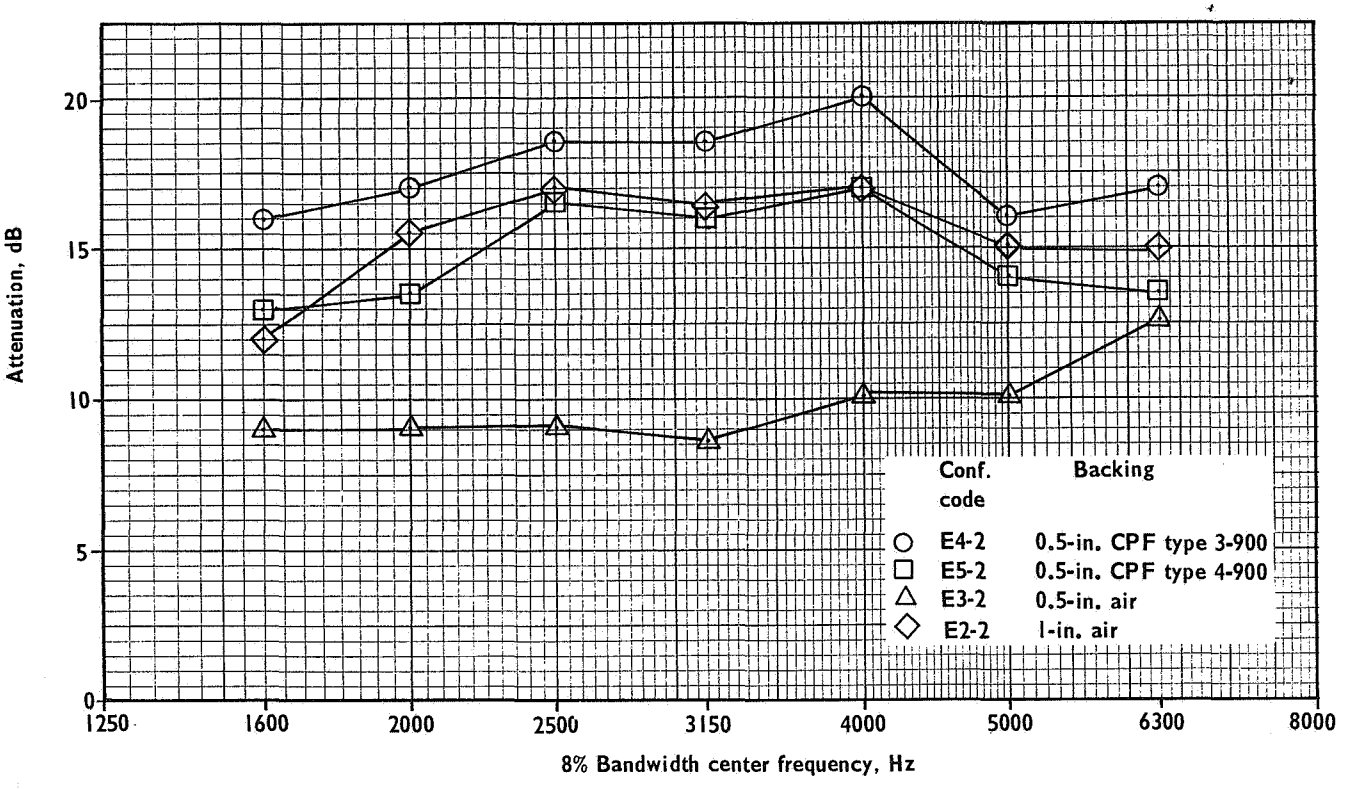

(a) Four walls treated.

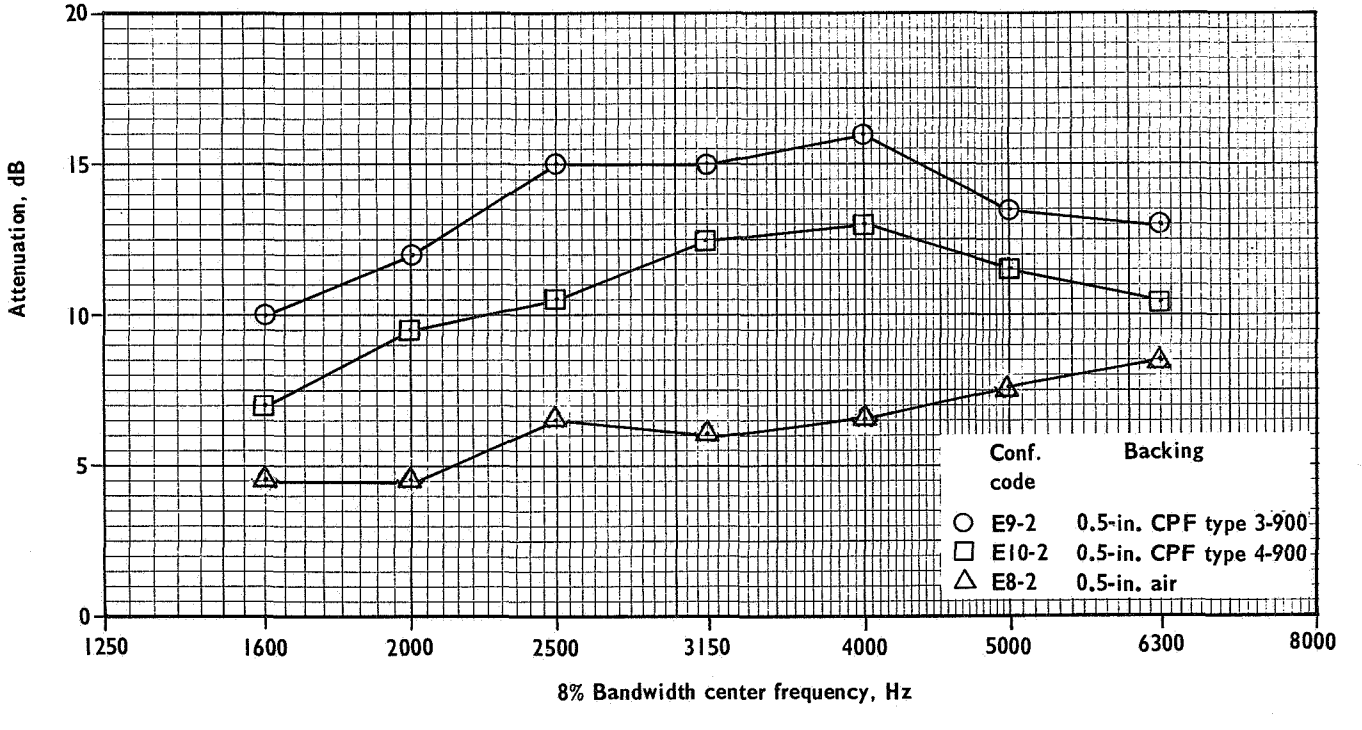

(b) Two circumferential walls treated; two radial walls, hardwall.

Figure 47. - End fan-discharge duct: Effect of varying backing treatments under 25-rayl fibermetal.

Fifty-five-percent lightbulb inlet duct: A total of 32 treatment configurations were examined using the 22° wedge model of the 55-percent lightbulb inlet duct, tables XVI and XVII. The values for the SPL's, TL's, and attenuations are given in tables XX, XXIII, and XXVI, respectively. The test variables were: backing material, backing depth, percentage of treated surface area, and the flow resistance of the fibermetal surface. The duct design, figure 33b, provided for five removable panels, three on the cowl and two on the centerbody.

Figure 48 compares the attenuation produced by four different backing treatments behind 25-rayl fibermetal. In these tests, only the panels on the cowl have acoustical treatment. Maximum attenuation was produced using 0.5-in.-thick CPF type 4-900, a result in agreement with the one obtained from the center fan-discharge duct tests. The poorest results were obtained with a 0.5-in. air-filled cavity, as also noted in the fan-discharge duct tests. The attenuation with the 1.0-in. air-filled cavity was better than that with the 0.5-in. air-filled cavity but not as good as that with the 0.5-in. cavity filled with porous material.

A series of tests was run with the optimum backing material behind 25-rayl fibermetal, i.e., 0.5-in. CPF type 4-900. The purpose of these tests was to study the effect of varying the percentage of treated area. The results of the tests are shown in figure 49 where the percentage treated area was varied from 27 to 100 percent. (Note that 100 percent means that all five panels are treated and not that all the internal surface area was treated.) A uniform and steady increase in attenuation is noted with increasing percentage treated area similar to the trend noted for the center duct tests, figure 45.

Heretofore, the backing treatment used behind the fibermetal surface in the 55-percent inlet duct tests has been either air, CPF type 3-900 or type 4-900. The ceramic fiber product was not used because of its poor performance in the center duct tests. However, fiberglass is another well-known material with high acoustical absorptivity and a series of tests was run to evaluate various thicknesses and densities of PF-105, type AA fiberglass behind 25-rayl fibermetal. This type of fiberglass is used widely for aircraft soundproofing insulation because of its good sound absorbing quality, high transmission loss, and low weight density.

Figure 50 gives the results of a series of tests with this material; all five panels of the duct were treated in these tests. Maximum attenuation occurred with a 0.5-in. thickness of 1.2 lb/ft^3 material. Increasing the density to 2.4 lb/ft^3, for the same thickness, reduced the attenuation by 1 to 3 dB, but only in the frequency range below 3150 Hz. This trend is physically reasonable and agrees with the results of fuselage panel sound transmission-loss tests with this material. However, maintaining the same density and increasing the thickness from 0.5 to 1.0 inch produced a curious decrease in attenuation instead of an anticipated increase. This result suggests once again the necessity for careful consideration of the total wall impedance.

Figure 51 compares the best of the attenuations achieved with 0.5-in. thickness compressed polyurethane foam and with fiberglass. The treatment configurations consisted of all five panels treated with 25-rayl fibermetal.

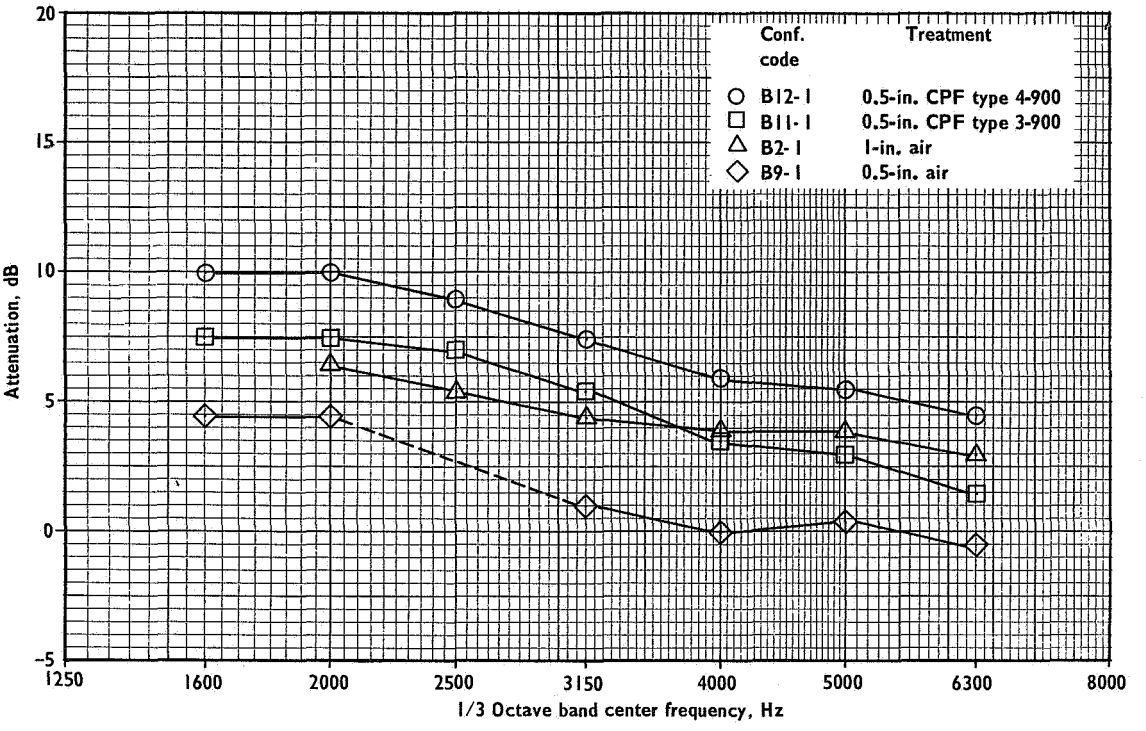

Figure 48.-55% lightbulb inlet duct: Effect of various backing treatments behind 25-rayl fibermetal; cowl only treated, centerbody hardwall.

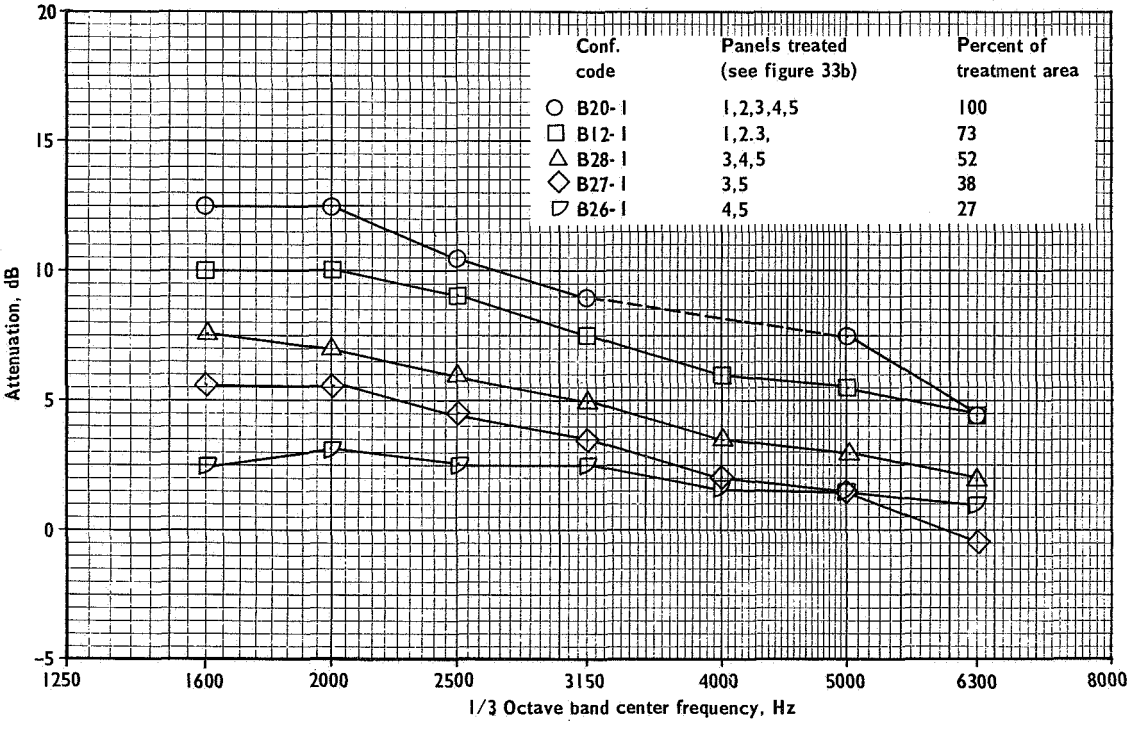

Figure 49.-55% lightbulb inlet duct: Effect of varying percentage treated area; cowl and centerbody treated with 0.5-in. CPF 4-900 under 25-rayl fibermetal.

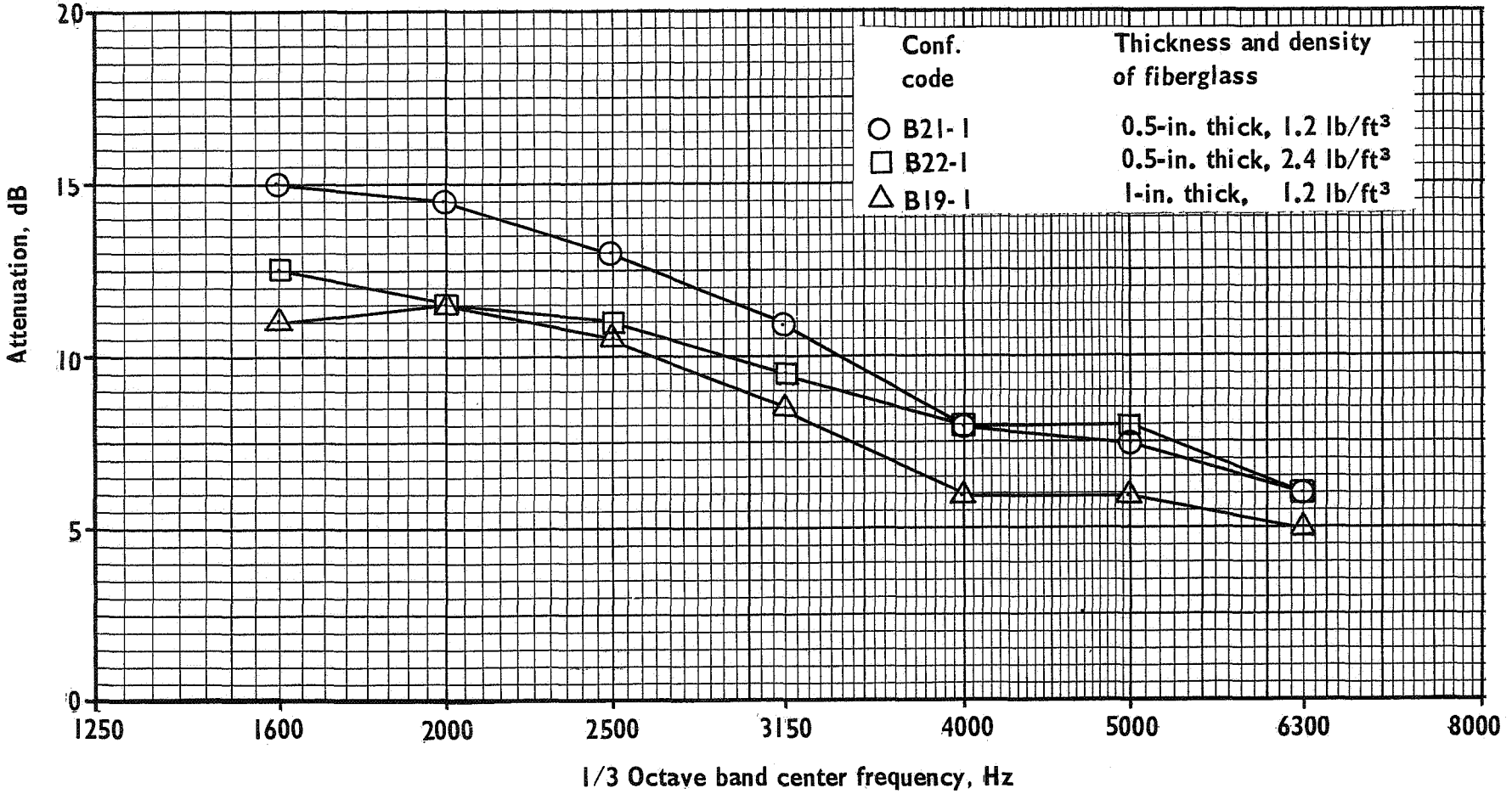

Figure 50.-55% lightbulb inlet duct: Effect of varying thickness and density of type AA fiberglass under 25-rayl fibermetal; all five panels treated.

It is seen that with the fiberglass backing, approximately 2 dB greater attenuations are achieved for frequencies below 3150 Hz than with the CPF type 4-900.

Figure 52 gives a comparison between 25-rayl and 60-rayl fibermetal surfaces backed by 0.5-in.-thick CPF type 4-900. In both tests, the maximum treatment area on the cowl and centerbody was used. It appears that there is very little difference between the two flow resistance values.

The fibermetal panels which had been used in the tests discussed thus far were all made from type 347 stainless steel wires. One of the undesirable features of this material is its relatively high surface weight density. Therefore, efforts are being conducted by the manufacturer to develop an aluminum product having the same acoustical properties as the stainless steel product along with desirable structural qualities, at substantial weight savings.

Three aluminum fibermetal panels were provided by the manufacturer for evaluation in the duct transmission loss tests. This product was fabricated from aluminum fibers of irregular cross-section in contrast to the stainless steel product which consisted of constant-diameter drawn wire fibers. The fibers were felted and bonded together to form a matrix by a process similar to that used for the stainless steel fibermetal. The panels had a flow resistance of 25 rayls and were of a size just large enough to be installed on the cowl of the 55-percent lightbulb inlet duct. The nominal thickness of the aluminum panels was 0.038 in. The weight density for this thickness was 0.33 lb/ft^2 in contrast to a weight density of 1.1 lb/ft^2 for the 0.040-in.-thick stainless steel panels, for the same rayl number. Tests were run with a number of different backing materials, including air, compressed polyurethane foam and fiberglass. The tests conducted have the configuration code numbers B3, B6, B8, B10, and B13. A study of the results (table XXVI) showed that, acoustically, the aluminum product was equal to the stainless steel product for each of the four configurations for which comparisons could be made. Future applications should consider the use of aluminum fibermetal when it becomes available in quantity.

Seventy-five-percent lightbulb inlet duct: The prime objective of the tests with the 75-percent inlet duct was to evaluate the effect of the increased surface area for acoustical treatment. Two basic configurations were tested; one in which the cowl only was treated and the other in which both the cowl and the centerbody were treated. A description of the six different treatment configurations that were tested is listed in tables XVI and XVIII. Values of the sound pressure levels, transmission losses and attenuations are given in tables XXI, XXIV, and XXVII, respectively.

Figure 53 compares the attenuations achieved for three different backing materials (1.0-in. air, 0.5-in. CPF type 3-900, and 0.5-in. CPF type 4-900) behind 25-rayl fibermetal surfaces. For these tests, all five panels of the duct were treated. Maximum attenuations occurred with the 0.5-in.-thick CPF type 4-900, as also observed in the tests with the 55-percent inlet duct. On the other hand, attenuations with the 1.0-in. air-filled cavity were considerably lower relative to the 0.5-in. CPF type 4-900, with this duct model than with the 55-percent lightbulb inlet duct.

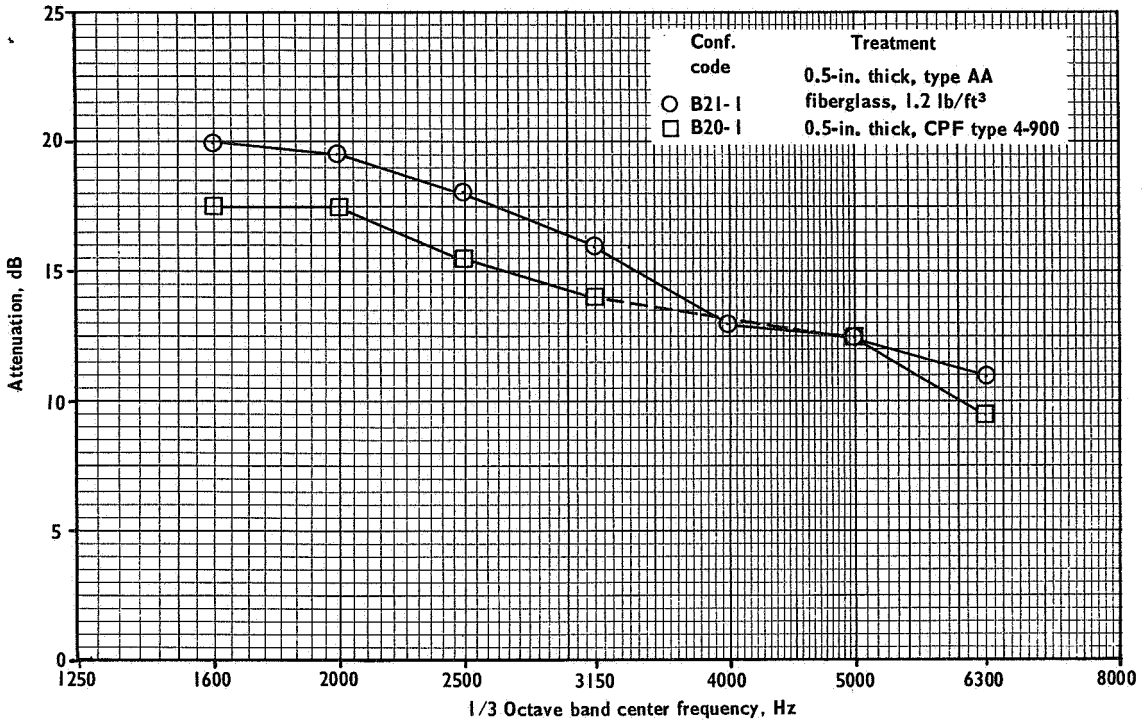

Figure 51.-55% lightbulb inlet duct: Comparison of fiberglass and compressed polyurethane foam behind 25-rayl fibermetal.

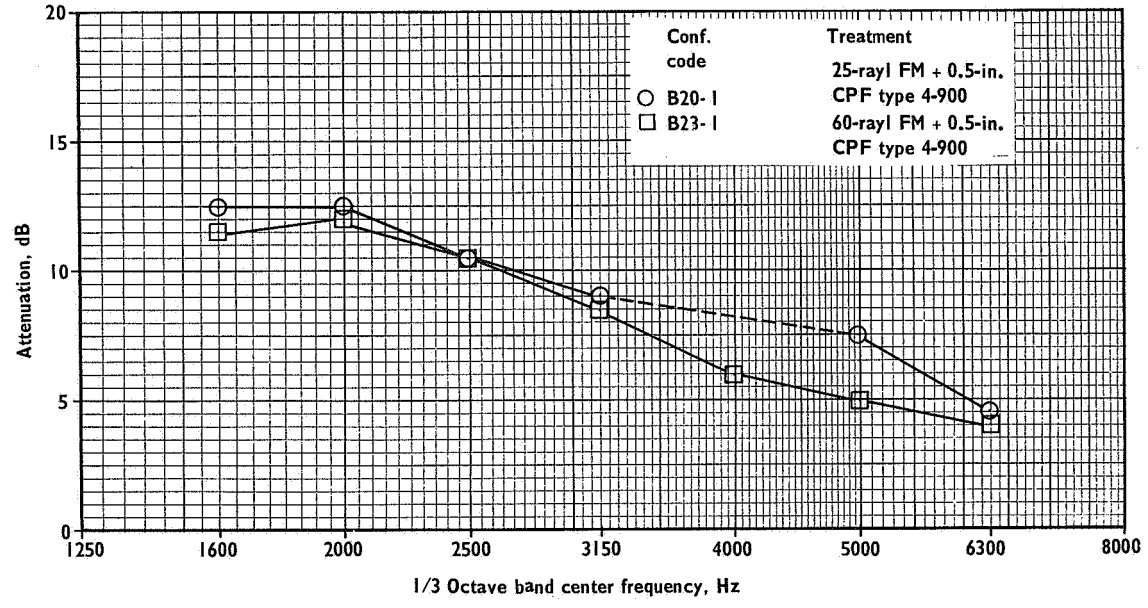

Figure 52.-55% lightbulb inlet duct: Comparison of 25-rayl and 60-rayl fibermetal; maximum treatment area on cowl and centerbody.

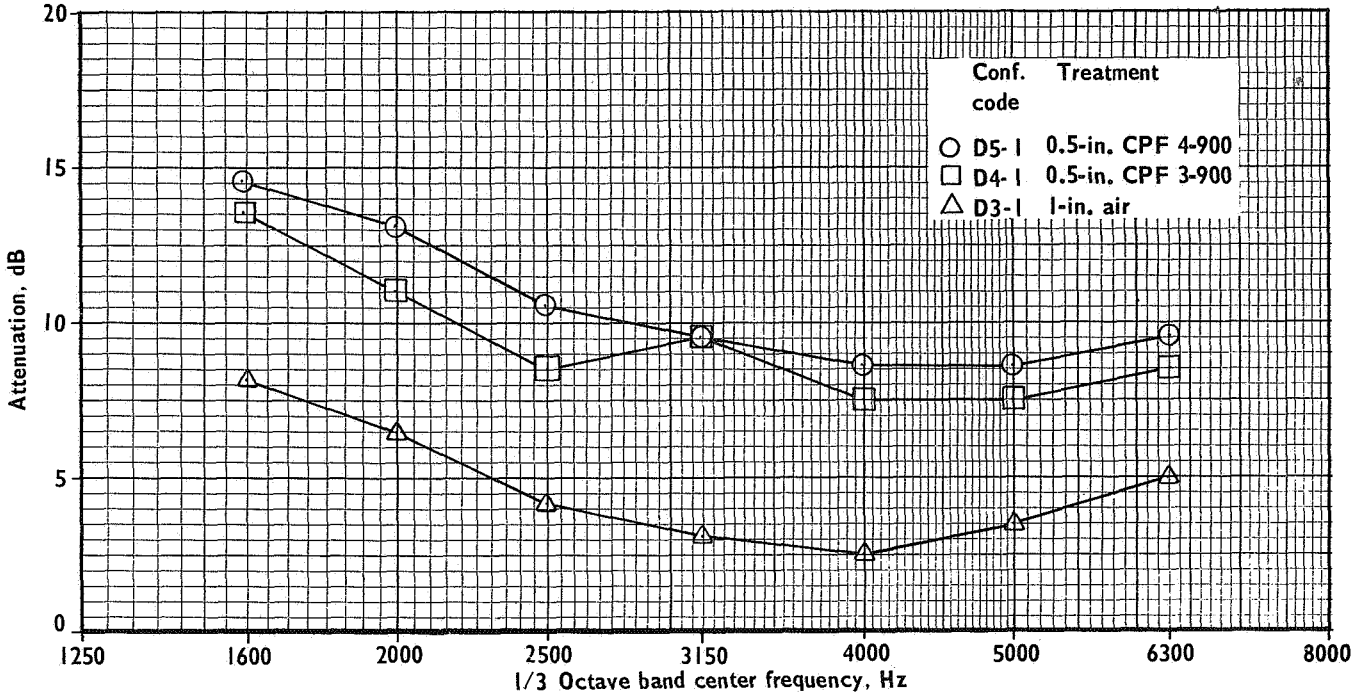

Figure 53.-75% lightbulb inlet duct: Effect of various backing treatments behind 25-rayl fibermetal; maximum area of treatment on cowl and centerbody.

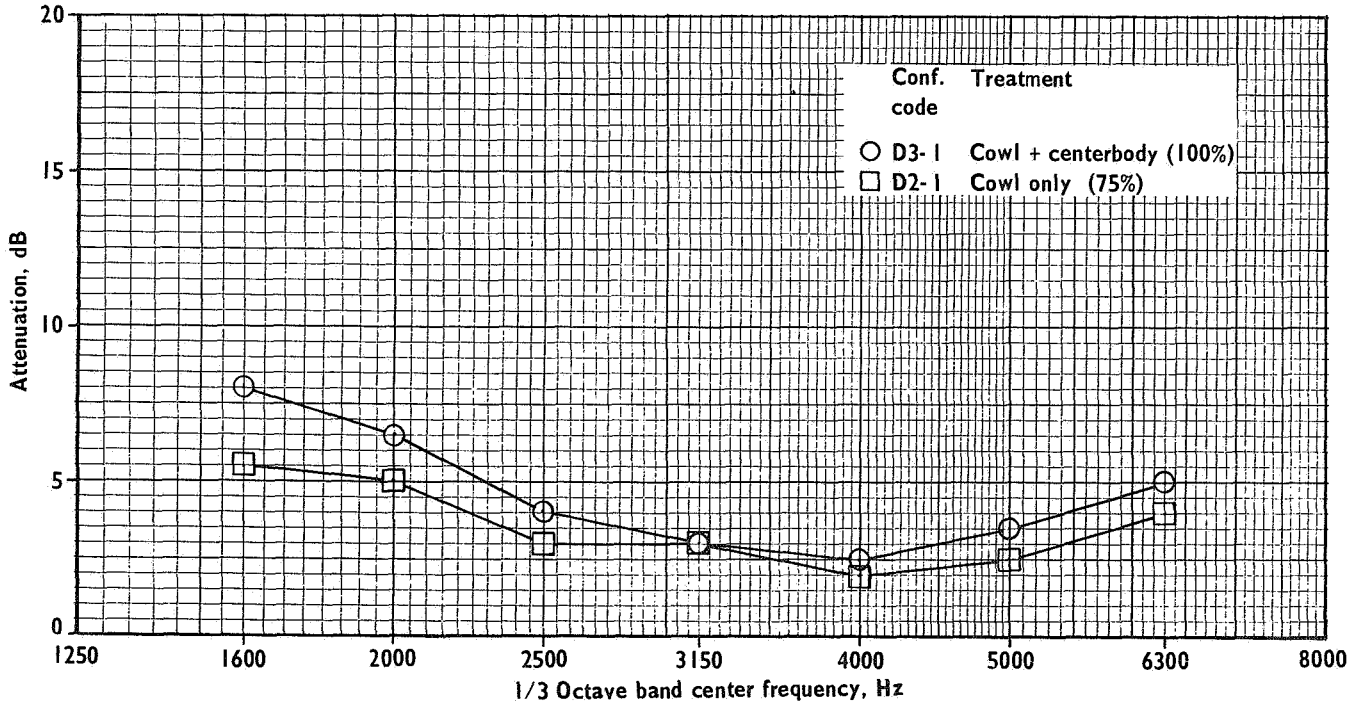

Figure 54.-75% lightbulb inlet duct: Effect of treatment area; 25-rayl fibermetal over 1-in. air.

Figure 54 compares the attenuations produced by treating both the cowl and the centerbody versus treating the cowl alone. The latter configuration represented 75 percent of the total area available for treatment. The treatment for both configurations consisted of 25-rayl fibermetal backed by a 1.0-in.-deep air-filled cavity. The results show that from 1 to 2 dB additional attenuation can be achieved by treating the centerbody. It is interesting to note that essentially similar results were obtained with the 55-percent inlet, figure 49, comparing the results with panels 1, 2, 3, 4, and 5 to those with panels 1, 2, and 3.

Standard DC-8 inlet duct: A total of 12 configurations was tested with the duct model representing a wedge section of a standard JT3D inlet duct. The design of this model provided for three acoustical treatment panels on the cowl and one on the centerbody. The treatment area on the cowl and on the centerbody (for each of the three inlet duct models) always represented the maximum area considered aerodynamically tolerable in a full-scale round inlet. The location for the panels on the cowl and on the centerbody was also chosen so that it might be representative of acceptable locations (avoiding adverse pressure gradients) in a full-scale inlet. The purpose of conducting tests with the treated standard inlet was to evaluate the performance of various treatment configurations in a duct with larger cross-dimensions and a reduced treatment area. Tables XVI and XIX describe the configurations tested; tables XXII, XXV, and XXVIII list the SPL's, TL's and attenuations, respectively.

Figure 55 compares the attenuations produced by three different backing treatments behind 25-rayl fibermetal with all four panels installed. Maximum attenuation was achieved, as with the other inlet ducts, with 0.5-in.-thick CPF type 4-900, while the least attenuation was produced by 1.0-in. air, again as with the other inlet ducts. The magnitude of the attenuation, in general, was considerably lower than that achieved with the 55-percent or 75-percent lightbulb inlet ducts. This was not unexpected since the total treated area was only 49 percent that of the 55-percent lightbulb and 39 percent that of the 75-percent lightbulb.

Results from tests in which the treated surface area was varied maintaining a constant acoustic treatment (0.5-in.-thick CPF type 4-900 behind 25-rayl fibermetal) are shown in figure 56. In general, an increase in the surface area was accompanied by an increase in attenuation, in accordance with the results obtained with the other inlet ducts.

Finally, figure 57 gives a comparison of the difference in attenuation produced by 25-rayl and 60-rayl fibermetal installed over 1.0-in. air-filled cavities on all cowl and centerbody panels. There was no significant difference between these two rayl numbers in this application, in agreement with the result obtained from the 55-percent lightbulb inlet duct tests.

Comparison of three inlet duct models: Comparisons of the transmission loss produced by the three inlet duct models are given in figure 58. The duct velocities are within 4 percent of each other. The effects just due to geometrical differences are shown in figure 58a, for the case when all

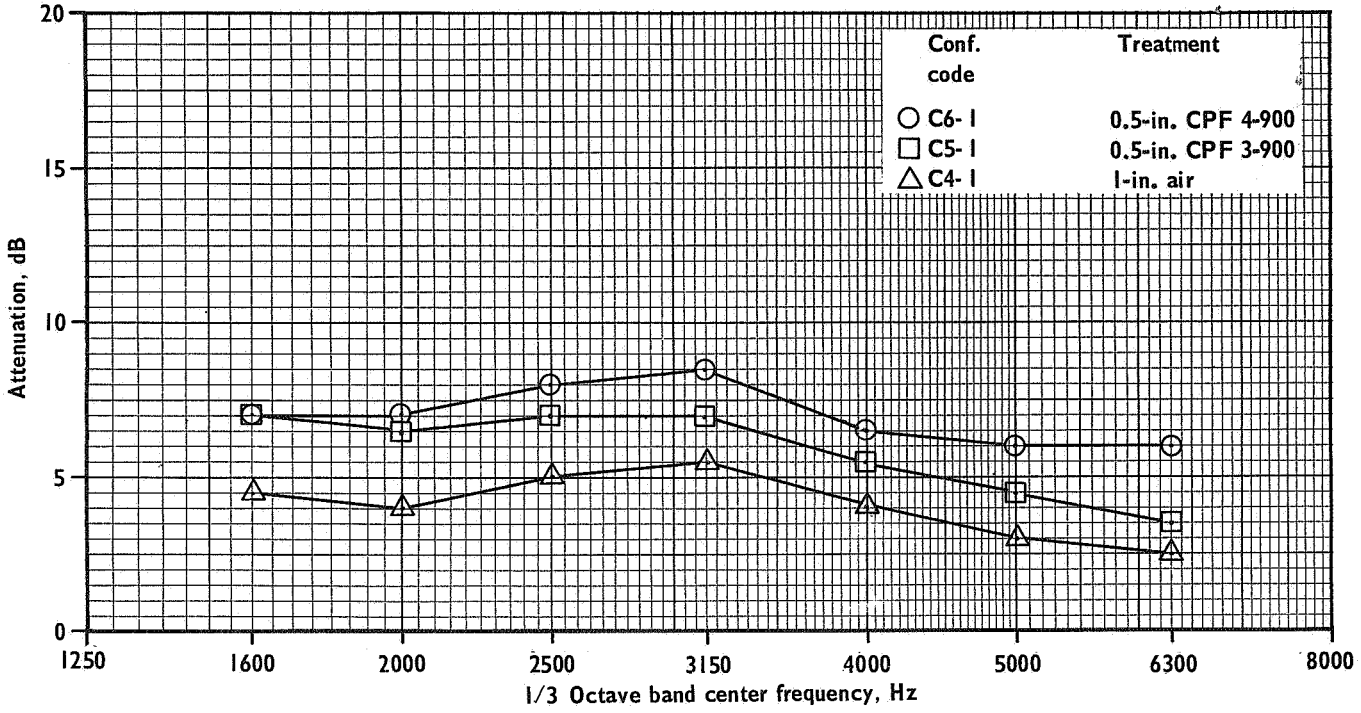

Figure 55. - Standard DC-8 inlet duct: Effect of various backing treatments behind 25-rayl fibermetal; maximum area of treatment on cowl and centerbody.

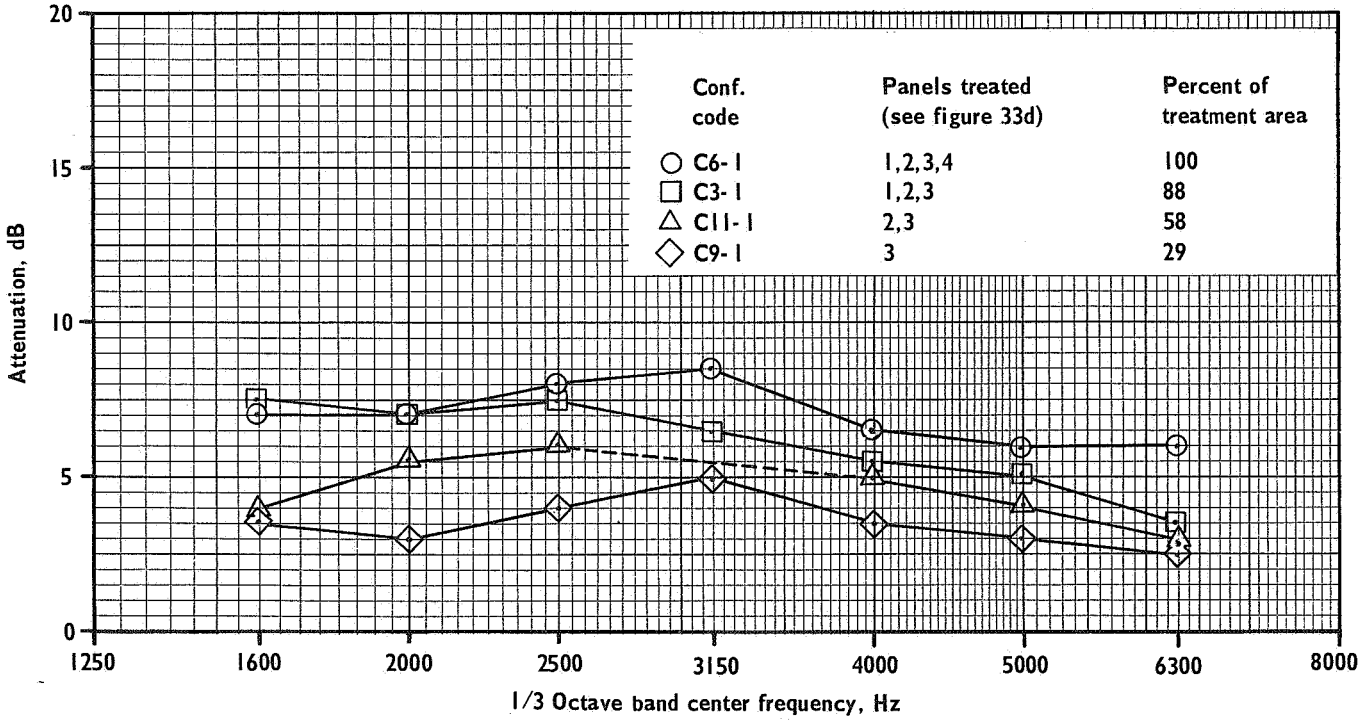

Figure 56. - Standard DC-8 inlet duct: Effect of varying percentage treated area; cowl and centerbody treated with 0.5-in. CPF type 4-900 under 25-rayl fibermetal.

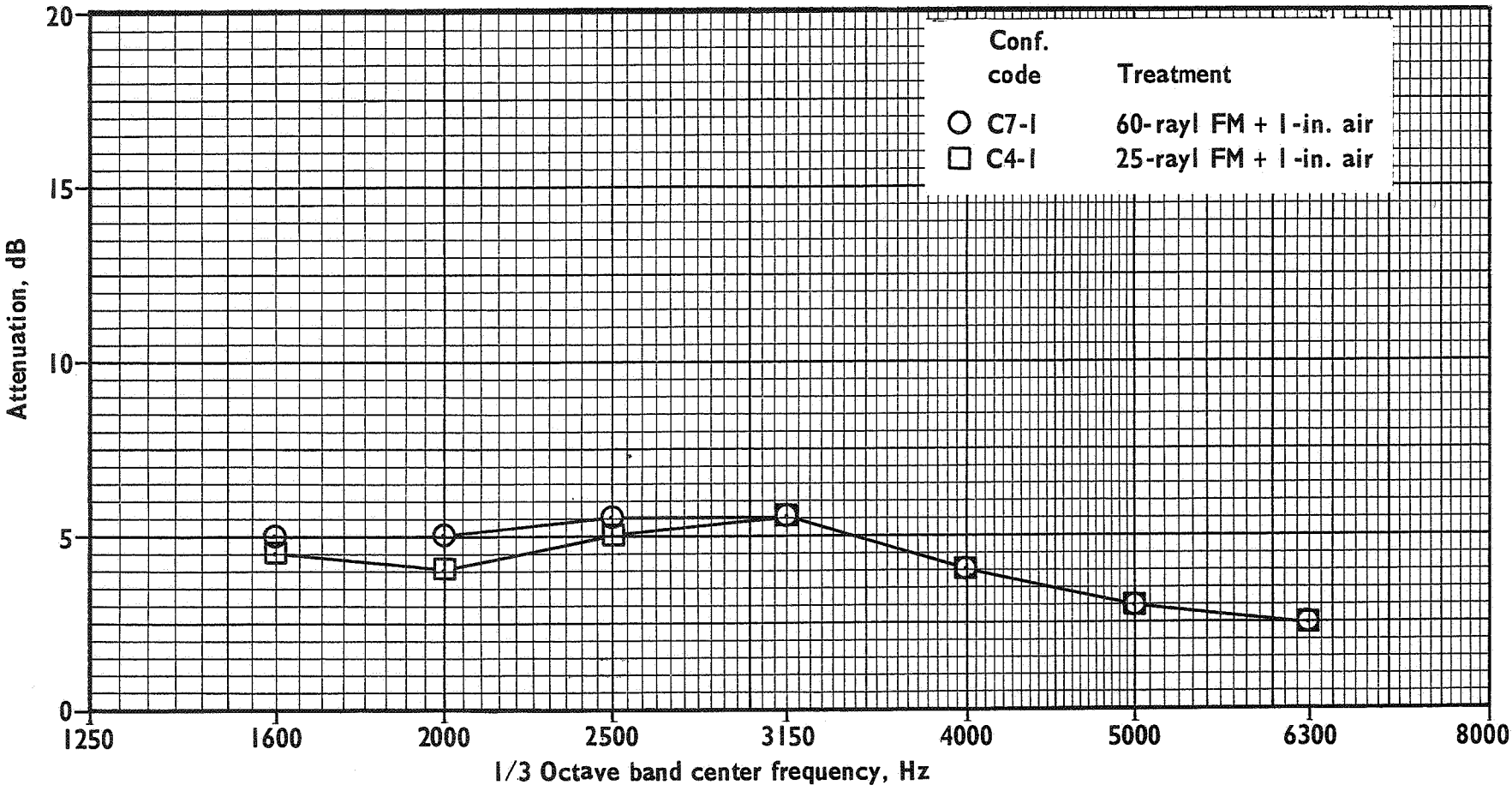

Figure 57. - Standard DC-8 inlet duct: Comparison of 25-rayl and 60-rayl fibermetal; maximum treatment area on cowl and centerbody.

internal surfaces were hardwalled surfaces. The 55-percent lightbulb inlet produced about 1.5 dB more TL than the standard inlet; the 75-percent lightbulb inlet produced about 2.5 dB more TL than the 55-percent lightbulb inlet. Since there was no acoustical treatment in the ducts, the differences in the TL must be due to the changes in the internal geometry which either cause increasingly larger portions of the incident acoustical energy to be reflected back into the source room or which permit increasingly larger amounts of the acoustical energy propagating through the ducts to be absorbed somehow by the duct walls, perhaps by acoustical radiation from the larger flat sidewalls of the 55-percent and 75-percent lightbulb inlet ducts compared to the standard inlet. No conclusive tests were ever run to define the separate effects of the geometrical differences (internal surface area, duct length, d/λ ratio, blockage, etc.); only the gross effects of the combination are known.

However, the results shown in figure 58b, for the case where the maximum available surface area on the cowl and centerbody were treated with 0.5-in. CPF type 4-900 behind 25-rayl fibermetal, tend to support one of the main observations from each of the five series of duct model tests. This observation was that the amount of treated area is one of the major factors determining the degree of noise reduction achieved by a given treatment. The data presented in figure 58b show that the treated 75-percent lightbulb inlet produced 3 to 5 dB more TL than the treated 55-percent lightbulb inlet, and that the treated 55-percent lightbulb inlet produced 7 to 9 dB more TL than the treated standard inlet. Calling the difference between the TL produced by the hardwalled inlets a blockage effect and subtracting a correction for blockage from the results in figure 58b gives the generalized result of about 6.5 dB for the increase in TL due to the increase in treated area of the 55-percent lightbulb inlet over that of the standard inlet and 1.5 dB for the increase of the area of 75-percent over the 55-percent lightbulb inlets.

These changes, interestingly enough, were noted to correlate with the ratio of the areas. Thus, with 391.3 $in.^2$ for the standard inlet, 803.6 $in.^2$ for the 55-percent lightbulb and 1012.3 $in.^2$ for the 75-percent lightbulb inlet (from table XVI), an estimate for the magnitude of the changes in transmission loss due to the change in treated surface area between the standard to the 55-percent lightbulb inlet is:

$$\Delta TL = 20 \log \frac{803.6}{391.3} = 6.2 \text{ dB}$$

and for the 55-percent to the 75-percent lightbulb inlet, it is:

$$\Delta TL = 20 \log \frac{1012.3}{803.6} = 2.0 \text{ dB}$$

The significance of this result is not known at this time and further work is needed to verify the validity and substantiate its general applicability. However, inspection of the results for an inlet duct where the geometry was

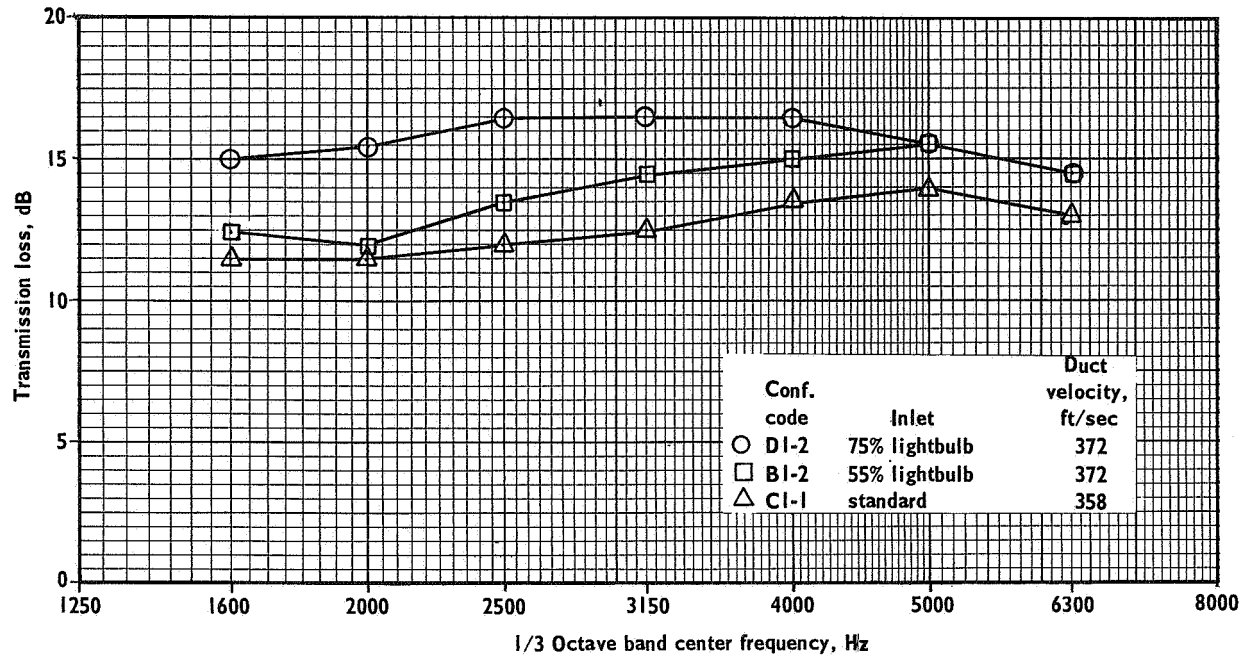

(a) All internal surfaces hardwall.

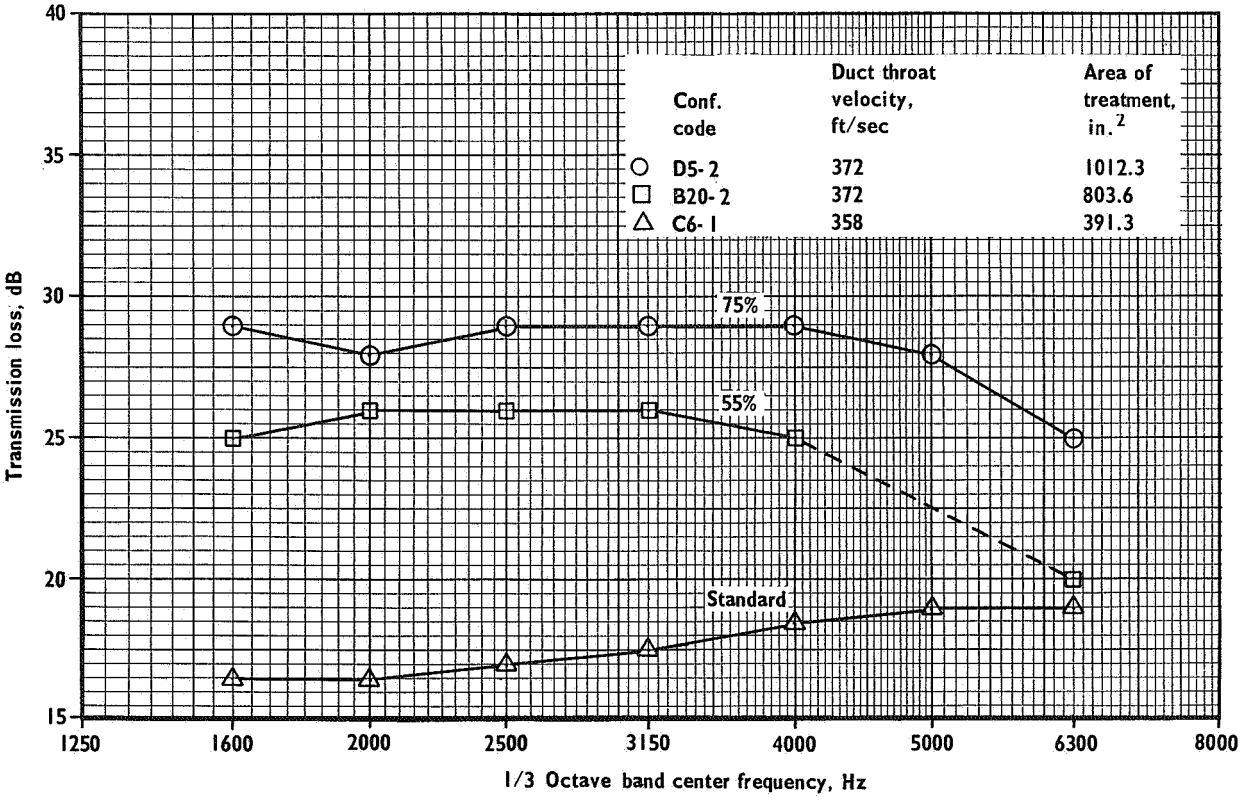

(b) 0.5-in. CPF type 4-900 behind 25-rayl fibermetal on the maximum area for treatment on the cowl and centerbody.

Figure 58.- Comparison of three inlet duct models.

fixed and only the area of treatment was varied (55-percent lightbulb inlet in figure 49) indicates that the rule works rather well for areas greater than 400 $in.^2$ but overestimates the changes when the areas were less than 400 $in.^2$. In addition, the rule seems to apply to the fan-discharge ducts, although the TL changes in these tests (e.g., figures 44 and 45) were always somewhat greater than predicted.

DISCUSSION OF NOISE-SUPPRESSION RATING TECHNIQUES

Although the prediction of the reduction in flyover noise annoyance and resultant change in community response is clearly outside the scope of work described in this report, it is felt worthwhile to discuss the topic of noise-suppression rating techniques. An estimate of the amount of noise suppression (measured in physical sound pressure level units of decibels) required to obtain a given amount of reduction in the noise levels perceived on the ground as the airplane flies overhead (as measured in psychoacoustical perceived noise level units of PNdB) will also be given.

Perceived Noise Levels and Correction Factors

The perceived noise level (in perceived-noise decibels or PNdB) came into use in 1959 as a means for measuring the degree of annoyance of aircraft flyover noise, reference 5, and has been generally accepted throughout the world as a valid technique. The perceived noise level (PNL) is computed from octave or 1/3-octave band SPL values (usually the peak values observed during a flyover) by determining an equivalent annoyance value, in noy units, for the SPL readings, converting the annoyance values to a total annoyance value and, finally, converting the total annoyance to PNL. The procedure is analogous to the computation of the loudness of a sound. The method used to determine the equivalent annoyance of a band of noise was based on the results of various psychoacoustical tests which used broadband random sounds as the disturbing noise.

Although the PNL is widely used today for determining the annoyance of the external noise of aircraft and also for monitoring aircraft flyover noise in order to enforce various noise-abatement regulations, it is generally agreed that it is inadequate for rating today's commercial jet transports because most of these aircraft are powered by turbofan-type engines which produce considerable discrete frequency noise. There is, as yet, no generally accepted procedure for correcting the PNdB values, calculated using the noy tables based on experiments with wideband sounds, for the more annoying effect of the presence of strong, high-frequency, pure-tone components in a background of wideband noise. In addition to these pure-tone corrections, a correction for the duration of the sound is needed to determine an "effective" perceived noise level. If the effective perceived noise level could be readily determined, other techniques (such as the composite noise rating or the noise and number index, references 38 and 39) could be used to obtain a measure of the resultant community response to the sound of a turbofan-powered aircraft flying overhead.

Until these improved methods can be developed into acceptable and easily applied techniques, aircraft and noise suppressor designs will be rated only by means of the flyover PNL. Use of the perceived noise level as a means of rating, however, may mean that a suppression device which reduces the amplitude of the discrete frequency components, may well produce a greater subjective response change than would be indicated by the change in the PNL alone.

Estimated Effect of Nacelle Acoustical Treatment on Flyover Noise Levels

While it is probably impossible to determine directly the change that any given type of duct-lining acoustical treatment will produce in community annoyance or response (based on the results of the work discussed in this report), it is possible to make estimates of changes to the peak flyover perceived noise levels produced by making various arbitrary amounts of reduction in the noise radiated out the fan-discharge ducts. Acoustical treatment is considered to be added to the fan-discharge ducts as a first step because the noise radiated from these ducts controls the peak PNL.

Estimates of the kind described above were made by the Pratt & Whitney Aircraft Company using sound pressure levels measured around a short-duct JT3D-1 turbofan engine on a static ground runup test stand. The acoustic power level and the directivity of the compressor noise radiated from the inlet and from the fan-discharge duct were computed separately as functions of engine power setting. Narrow-band filters separated pure-tone components and closely spaced microphones on a 150-ft arc were used to obtain the directivity patterns. The low-frequency jet exhaust noise was handled in a similar fashion using notch or comb filters to reject the discrete frequencies from the recorded signals.

These 150-ft measurements were then projected from each source separately to various sideline distances using inverse-square loss propagation plus an excess air-attenuation correction, reference 40. In addition, corrections were made for the forward motion of the airplane and for the presence of four engines rather than one. The peak PNL was then determined by scanning along the sideline to obtain peak SPL readings in octave bands and converting these SPL readings to a peak PNL. The relative contributions of the fan-discharge noise, the inlet noise and the jet exhaust noise were evaluated by noting the peak PNL that each source produced. The calculations were then repeated with the fan-discharge noise reduced by various arbitrary amounts (holding the inlet noise and the jet exhaust noise constant) to determine the effect of adding acoustical treatment to the fan-discharge ducts. Figure 59 shows the results of these calculations for a sideline distance, or altitude, of 1000 ft and for a takeoff thrust setting and a landing approach thrust setting.

In figure 59 the solid lines indicate the amount of reduction in peak flyover PNL that can be achieved by adding various amounts of acoustical treatment to the fan-discharge ducts. The dashed lines indicate the contributions of the noise radiated out the inlet (considered to be untreated) and the jet exhaust noise. For the takeoff thrust case, figure 59a, the curve indicates that a noise suppressing treatment producing a 5-dB reduction in fan

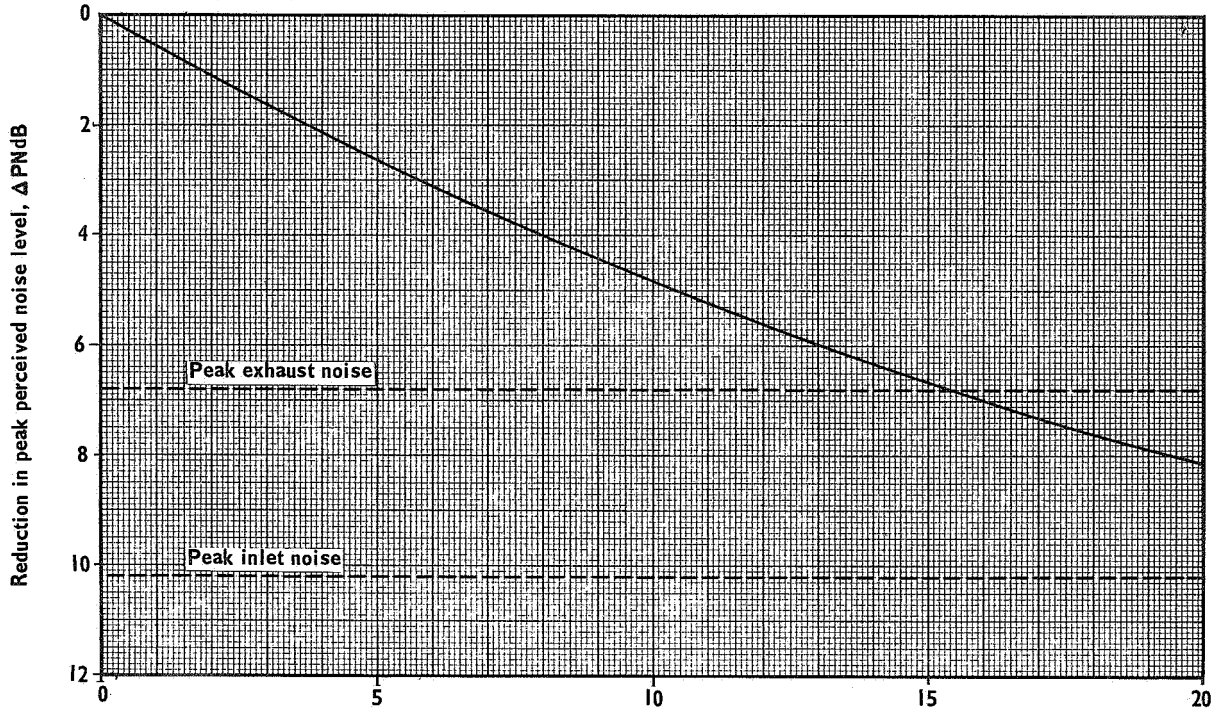

(a) Takeoff, Mach number 0.25, net thrust 14 574 lb/engine.

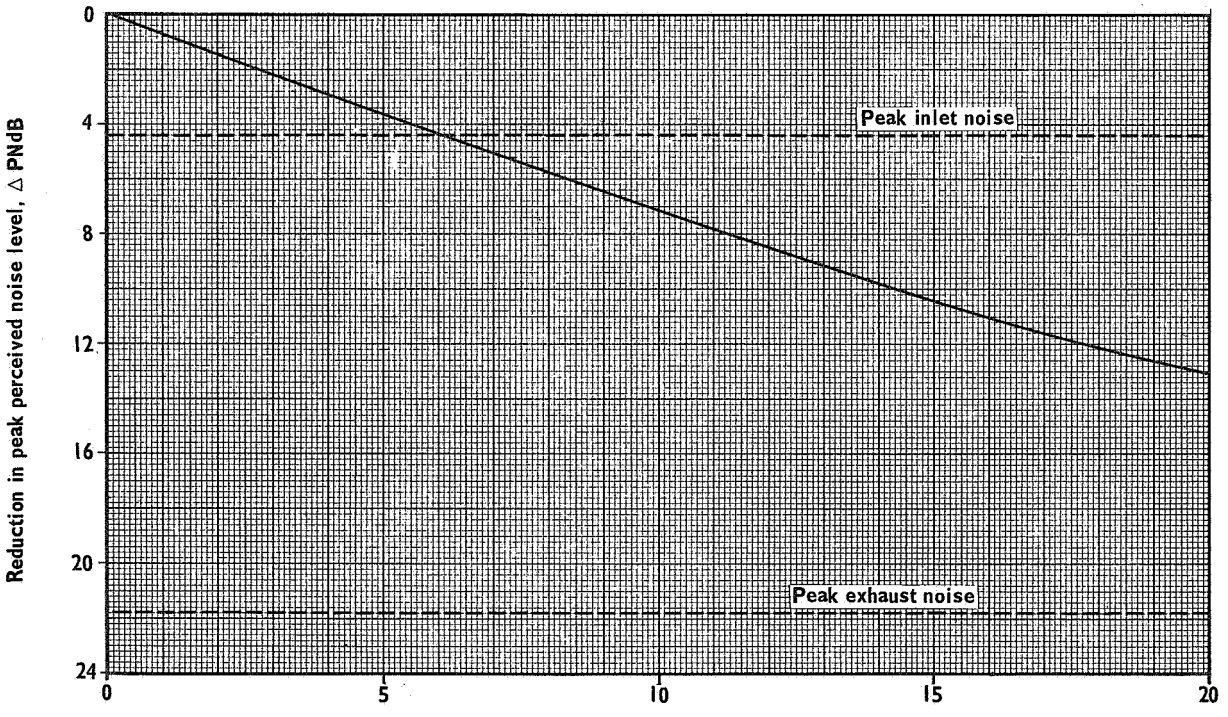

(b) Landing, Mach number 0.25, net thrust 3228 lb/engine.

Figure 59. - Estimated reduction in peak flyover perceived noise levels – short duct JT3D-3B engines – altitude 1000 feet. Acoustical treatment added to fan-discharge ducts only, no inlet treatment (Data courtesy of the Pratt & Whitney Aircraft Company, East Hartford, Conn.).

discharge noise will produce a reduction of about 2.5 PNdB in the peak flyover PNL; 15-dB suppression will mean about a 6.5 PNdB change. Larger changes than 6.5 PNdB are not possible at this engine power setting and altitude because of the contribution of the jet exhaust noise which is shown to be about 7 PNdB below the untreated fan-discharge noise, i.e., further reductions of the fan-discharge noise beyond 15 dB could not be detected unless something were done to reduce the jet exhaust noise. If the jet exhaust noise were reduced, then further reductions could be obtained up to the point where the inlet noise was controlling at about 10 PNdB down. (It may be possible to get below the limit presented by the jet exhaust noise by utilizing thrust reduction techniques after takeoff. Reducing the throttle setting does reduce the low-frequency sound considerably, although it has little effect on the compressor noise unless impractically large engine power reductions are made, figure 17.)

During landing, figure 59b, the contribution from inlet noise is much greater; the jet exhaust noise is much less. The maximum reduction, without adding treatment to the inlet, is only about 4 PNdB, requiring about 6 dB of suppression. If an effective inlet treatment could be installed, it might be possible to obtain 8 to 12 PNdB reduction by achieving 11 to 18 dB suppression of the fan-discharge noise. This degree of suppression will not be easily accomplished.

Comparison to contract goal and "elimination" of pure tones. — The objective of the program described in this report was to develop a preliminary engineering design of a nacelle configuration for a turbofan engine of current design such that its discrete frequency compressor noise would be markedly reduced in level. The goal, and the definition of "markedly reduced," was to "obtain, by means of the best combination of acoustic treatments, a reduction of the radiated discrete frequency noise components from the nacelle such that each of these discrete frequency components does not exceed in level a value of 5 dB below the 1/3-octave band noise level of the appropriate 1/3-octave band containing the discrete frequency."

If this goal were met it would mean that the discrete frequency components would be inaudible, which would be a very large change indeed. Any conceivable acoustical treatment that is to be added to an engine nacelle would reduce the broad-band vortex noise and flow noise as well as the pure-tone noise in the 1/3-octave bands containing the pure tones. Thus, by adding treatment, the masking level of the random noise surrounding the pure tones will be reduced along with the pure tones until the pure tones are reduced to the level of the broad-band noise from the jet exhaust. Judging from the results shown in figure 16, compliance with the goal as stated will require a suppression device that produces 40 to 50 dB of suppression. This amount of noise reduction is probably impossible to accomplish with any physically realizable device and, as shown by the estimates in figure 59, may be unnecessary because of the contribution of the jet exhaust noise to the flyover perceived noise level.

Since the change produced in the flyover perceived noise level will probably be the final criterion by which a nacelle acoustical treatment is to be judged, it is probably more realistic (although undoubtedly more risky) to assess the benefit produced by a given design technique in terms of an estimated ΔPNdB. The results of the duct model transmission-loss tests

indicate that, if an adequate area of treatment is provided and velocity effects are not severe, 12 to 15 dB of suppression of the noise radiated out the fan-discharge ducts might be realized. This amount of treatment might produce a 5 to 6 PNdB change in the peak flyover PNL during takeoff; greater reductions might be obtained by reducing the throttle setting after takeoff. If, in addition, a good inlet duct design can be produced, this amount of treatment in the fan ducts might result in about a 10-PNdB reduction during the landing approach; without inlet treatment, a 3- to 4-PNdB reduction may be attainable during landing.

It must be pointed out again that these rather small estimated changes to the calculated PNL would, in fact, result in much larger reductions in the subjective response because of the large reduction to the pure-tone level, i. e., the pure tones are more annoying to humans than the calculated PNL would indicate. Any device that produced 10-PNdB suppression for the JT3D turbofan engines during landing operations would represent a gain which would exceed by far any other aircraft noise reduction accomplishments made to date, including the costly jet exhaust noise suppressors developed for the turbojet engines and even the development of the turbofan engine itself.

Furthermore, it must be strongly emphasized that all of the estimates presented here of the changes in the flyover perceived noise level, that might be produced by a noise-suppression device, are based entirely on projections from static ground runup noise measurements. Since methods for predicting flyover noise levels from static measurements are not well established, it is recommended that considerable caution be exercised in the application of these estimates to any projected installation of a given nacelle acoustical treatment. Moreover, the estimates are based on projections from JT3D ground runup noise measurements and are not valid for any other engine because of the differences in the directivity patterns and strengths of the various sources. Separate estimates must be made in each particular case to account for these differences.

Effect on Airplane Performance

The noise reductions discussed above will not be achieved without some effect on airplane performance. Any effects that tend to degrade airplane performance must be minimal. The penalty will vary with the type of airline operation, the weight, the friction drag, the inlet total pressure losses at takeoff and cruise, and depreciation and maintenance allowances.

Airplane performance losses were estimated for the 55-percent, 75-percent, and 95-percent lightbulb inlets, and for the addition of sound absorbent lining to a standard DC-8 inlet. The estimates were made for a typical large commercial jet transport at the following three conditions:

1. Increase in direct operating cost when the airplane is not takeoff-field-length or gross-weight limited. This condition is typical of domestic operation.

2. Equivalent loss of payload when the airplane is takeoff-field-length limited.

3. Equivalent loss of payload when payload must be reduced in order not to exceed the maximum gross weight limit of the airplane for the case of maximum range at the maximum gross takeoff weight, assuming that the airplane is not takeoff-field-length limited. This condition is typical of some cargo operations from long runways.

For each case, the aircraft range was held constant. The results are summarized in the following table. Note that these are inlet losses only; no losses are included for treatment added to the fan-discharge ducts.

Inlet	Direct operating cost increase, percent	Takeoff-field-length limited equivalent payload loss, percent	Maximum-gross-weight-limited equivalent payload loss, percent
Standard	0.15	0.8	0.8
55% Lightbulb	0.85	7.8	5.6
75% Lightbulb	1.20	12.1	8.2
95% Lightbulb	1.54	15.7	10.6

Penalties are moderate when only additional fuel and fixed costs are considered, i.e., domestic operations; however, when payload must be reduced, the penalty can be quite large.

The penalty produced by adding treatment to the fan-discharge ducts is due to the additional weight required and to the increase in skin friction, assuming that recirculation, if any, of the air into and out of the porous duct surface can be controlled by proper design. Performance estimates were made for the effect of adding acoustical treatment to a short fan-discharge duct type of installation, with the same ground rules as used for the inlet treatment comparisons. Where the airplane is not takeoff-limited, the increase in direct operating cost was 0.18 percent. For the takeoff-limited case, the equivalent loss of payload was 1.6 percent; for the maximum-gross-weight condition, the equivalent payload loss was 1.2 percent. Losses due to the circulation of air through the fibermetal and into and out of the cavity are unknown at the present. The effects of such losses would have to be evaluated in another phase of the noise-suppression development program.

CONCLUSIONS

This report has presented the results of a study to develop a preliminary engineering design for an acoustical treatment that could be applied to the nacelle of current turbofan engines of the 15 000-lb maximum-thrust class and be effective in reducing the amplitude of the discrete-frequency tones produced by the fan. The study concentrated on the application of nacelle acoustical treatment to the P&WA JT3D front-fan turbofan engines. The recommended acoustical treatment consists of a sound-absorbing lining on the wall of the fan-discharge and the fan-inlet ducts.

Aerodynamic Tests

The present shape of the existing short fan-discharge ducts was considered adequate for effective application of an acoustical lining. However, the diameter of the standard JT3D inlet was too large for effective use of acoustical treatment on the walls (for any practical inlet length) and revised inlet shapes were needed to provide smaller cross dimensions. Analytical aerodynamic design studies were conducted to define various inlet shapes meeting this requirement. Inlets with various lightbulb-shaped centerbodies, producing various amounts of blockage of the compressor face area, were designed based on potential-flow calculations. Scale models of these lightbulb inlets were tested under static conditions in a specially modified wind tunnel. The performance of the inlets was determined at full-scale Reynolds numbers for the normal operating range of inlet Mach numbers. The inlet designs with 55-percent and 75-percent compressor-face blockage (relative to the area seen with the standard DC-8 inlet for the short fan-duct version of the JT3D engine) were noted to require small modifications to reduce some negative pressure peaks (supersonic velocities) on the centerbodies.

JT3D Duct SPL Measurements

The sound pressures at the wall of the inlet and fan-discharge ducts were measured on a JT3D engine mounted on an engine test stand. The results showed that the fan-discharge duct looks at the rotating pressure field associated with the first (35 blades) and the second (32 blades) fan rotor stages while only the pressure field from the first rotor stage was apparent in the inlet. At landing thrust, the fundamental blade passage frequency was about 2200 Hz; at the takeoff thrust setting, the fundamental frequency was about 3700 Hz. Harmonics of these fundamentals as high as the fourth were measured. The sound pressure level of the pure tones varied from 140 to 160 dB, depending on the engine power setting. The levels of the pure tones in the inlet and the fan-discharge ducts were comparable at the same engine power setting.

Nacelle Acoustical Treatment Designs

The acoustical design for the nacelle treatment considered the use of choked inlets and duct lining materials. Narrow-band resonators as well as wide-band acoustical absorbers were considered. It was decided that:

- Although a completely choked inlet would probably be effective in controlling noise radiated out the engine inlet, design of a choked inlet for current subsonic commercial jet transports would involve serious fluid dynamic and control problems, solutions of which were outside the scope of the program.

- Resonators consisting of perforated panels spaced out from a rigid back wall could not be used because of (1) the need for high absorptivity over a wide range of frequencies and (2) the great difficulty in adjusting the

acoustical resistance of the perforations to the proper value required under the actual environmental conditions. In an engine the perforated duct lining materials would be exposed simultaneously to a flow with a high mean velocity and high acoustical pressures accompanied by high particle velocities through the perforations. The resistance of the perforations under these conditions increases nonlinearly above the theoretical value for no-flow and low particle velocity conditions. Thus, considerable experimental investigation under actual full-scale conditions is required to obtain an adequate design.

- The use of conventional acoustical absorbing material alone for duct linings was not feasible, principally because of the erosion of the material by the high velocity air in the ducts and because of problems with fluid retention.

- A broadband resonator was required since both narrow-band, perforated-panel resonators and wide-band conventional acoustical absorbers could not be used.

The broadband resonator developed consists of a surface lining material made from a thin, porous fiber metal product with a cavity behind the porous material. The product used for most of the studies was made from stainless steel fibers. The cavity behind the porous surface material can be either air filled or filled with some type of acoustical absorber. The acoustical absorbers that were examined were: An open-cell compressed polyurethane foam product with 90 pores per lineal inch (uncompressed), a ceramic fiber product, and PF-105 type AA fiberglass with a nominal fiber diameter of 0.00004 inch.

Acoustical Property Evaluation Tests

Laboratory tests were conducted to examine the acoustical properties of various surface lining materials with various combinations of cavities and backing materials. Transmission-loss tests using two fan-discharge and three engine inlet duct models were also conducted to determine the effectiveness of various duct liner designs under conditions of varying velocity air flows in the duct. Results from these tests indicated that:

- Normal-incidence acoustical absorption coefficients greater than 0.85 over a frequency range from 1600 to 6300 Hz can be produced by the broadband resonator technique.

- Some of the trends observed from the duct model transmission-loss tests, when the acoustical treatment was installed adjacent to a convected medium, were different from those observed in the laboratory acoustical property evaluation tests. The reason for the disagreement is not evident at this time, although it is most likely connected with the fact that the laboratory tests were conducted with small samples under no flow conditions using sinusoidal signals while the transmission-loss tests were conducted with a much larger sample of acoustical treatment, with air flowing over the sample, and with wide-band random noise signals.

Generalized conclusions, which are common to results obtained from each of the five duct model transmission-loss tests, are:

- The extent of the treated area was the controlling parameter in the attenuations achieved by a given treatment configuration. Maximum attenuations were always produced by the treatment that was applied to the largest area. The effect of increasing the area of acoustical treatment can be estimated by the relation $\Delta TL = 20 \log (A_1/A_2)$.

- Changing the flow resistance (rayl number) of the lining surface produces only a small effect over the range of flow resistances tested (25 to 60 rayls). The inlet duct TL tests showed essentially no difference between 25- and 60-rayl material; the fan-discharge duct tests indicated that 25-rayl material was slightly better than 60-rayl material; the laboratory tests indicated that the absorption with 25-rayl material was somewhat greater than with 60-rayl material. When the duct lining is exposed to SPL's greater than those used in the TL tests (i.e., greater than 130 to 140 dB), it is anticipated that maximum attenuation will be produced by a lining material with somewhat lower flow resistance (10 to 15 rayls, as measured in the linear range of flow resistance values).

- The acoustical impedance of the total treatment and not just the flow resistance of the surface lining material must be carefully chosen, in order to select a duct lining design that will produce maximum noise reduction.

- Considering compressed polyurethane foam (CPF) types 3-900 and 4-900, ceramic fiber type CF-600, and air for backing materials in 0.5-in.-deep cavities, maximum attenuation was produced by the CPF type 4-900. The one exception to this result was in the end duct where CPF type 3-900 was slightly better on the average than the type 4-900. Conversely, air was universally found to give the least attenuation of any of the 0.5-in. backing materials, and cavities 0.5-in. deep, or less, must be filled with an absorbing material to produce significant attenuations.

- Type AA fiberglass was the only backing material superior to CPF type 4-900 for 0.5-in.-deep cavities. Maximum attenuation was achieved with a fiberglass density of 1.2 lb/ft^3. Although this backing material was tested only in the 55-percent lightbulb inlet duct, it is felt that the same trend would have been observed in the other four ducts.

The principal results unique to the fan-discharge duct transmission-loss tests are:

- Maximum attenuation, in the center duct, was produced by 25-rayl material over a 1.0-in. air-filled cavity. Attenuations ranging between 14.5 to 18.5 dB in the frequency range from 1600 to 6300 Hz were obtained with this configuration.

- The largest attenuations in the end fan-discharge duct were achieved with a 0.5-in. CPF type 3-900 behind 25-rayl

fibermetal. Attenuations ranging from 16 to 20 dB were measured.

- A trend toward decreasing attenuation with increasing velocity was noted in the range of velocities tested; i.e., 100 to 400 ft/sec. This trend corresponds to the reported results in the literature for the case of ducts in which the direction of airflow and sound propagation is the same.
- Addition of an untreated radial splitter to the center duct when all the internal surfaces were hardwall increased the transmission loss. Addition of the combination of untreated radial and circumferential splitters did not increase the TL above that produced when the radial splitter alone was installed.
- When the four boundary walls of the center duct had acoustical treatment installed, addition of an untreated radial splitter or untreated radial and circumferential splitters produced essentially no change in the observed TL. Adding treatment to the splitters increased the TL approximately in proportion to the logarithm of the ratio of the square of treated areas.
- The best overall duct lining treatment was 1.0-in. air behind 25-rayl fibermetal. This judgment is based on the results from both the center and the end fan-discharge duct tests, since these two types of ducts together form the JT3D fan-discharge duct.

The principal results unique to the inlet duct transmission-loss tests are:

- Aluminum fibermetal produced the same amount of attenuation as stainless steel fibermetal of the same thickness and flow resistance. Future applications should definitely consider use of aluminum fibermetal.
- Maximum attenuation in the 55-percent lightbulb inlet duct was produced by 25-rayl fibermetal over a 0.5-in.-deep cavity filled with 1.2 lb/ft^3 fiberglass. Attenuation ranged from 6 to 15 dB between 1600 to 6300 Hz.
- The best treatment tested on each of the three inlet ducts was 25-rayl fibermetal over a 0.5-in.-deep cavity filled with CPF type 4-900.
- Air-filled cavities, 1.0-in. deep, produced 3 to 6 dB less attenuation than 0.5-in.-deep cavities filled with CPF type 4-900.
- The effect of increased blockage of the line-of-sight to the rotor blades by the lightbulb inlets is small in comparison to the effect of adding acoustical treatment to a much larger surface area in a duct with smaller cross dimensions. However, there definitely was an effect whose magnitude, estimated from comparison of the TL produced by the hardwall ducts, was 1.5 dB between the 55-percent lightbulb and the standard inlet and 2.5 dB between the 75-percent and the 55-percent lightbulb inlet ducts.
- No clear-cut dependence of the attenuation on duct velocity could be determined in the range of velocities used in the tests, i.e., 75 to

465 ft/sec. This result corresponds to that reported in the literature for the case of ducts in which air and sound propagation are in opposite directions.

JT3D Nacelle Acoustical Treatment

The following recommendations are made from the studies conducted in this program for the design of JT3D turbofan-engine nacelle acoustical treatments to be applied to ducts whose cross dimensions are on the order of four to six inches:

- Install an absorptive treatment of the broadband resonator type over as large an area as possible using a thin, porous fibermetal surface with a laminar flow resistance between 10 and 25 rayls.
- For fan-discharge ducts, if not space-limited, use a 1.0-inch or slightly deeper air-filled cavity behind the porous surface. If a cavity depth of only 0.5-inch or less can be provided, fill the cavity with an absorbing material, such as 1.2 lb/ft^3 type AA fiberglass or type 4-900 compressed polyurethane foam, and treat a larger area than chosen for the airfilled cavity in order to get the same noise reduction.
- For inlet ducts, use 0.5-inch-deep cavities behind the porous surface. Fill the cavity with an absorbing material such as 1.2 lb/ft^3 type AA fiberglass or type 4-900 compressed polyurethane foam. If this design produces too severe a weight penalty or is unacceptable for some other reason, then use an air-filled cavity having a depth greater than 0.5 inch. The shape of the inlet must be carefully chosen to minimize adverse effects on noise reduction and airplane performance.

Appendix B gives recommended acoustical and mechanical design requirements and verification tests for the porous surface materials to be used in the nacelle treatments. These specification requirements apply only to research and development testing of the recommended design concepts for a broadband resonator; the specifications are not applicable, directly, for use in any operational commercial jet transport because of the many unknown and unpredictable factors that may be encountered.

RECOMMENDATIONS

It is recommended that the acoustical design principles and techniques discussed in this report be tested on a full-scale JT3D turbofan engine. Fan-discharge duct designs for both short and long duct installations should be considered. The inlet design might consider the 55-percent lightbulb as well as other designs incorporating the same principles but with smaller performance penalties. To minimize the cost of a full-scale development program, two types of acoustical tests are required to determine the best nacelle treatment: (1) ground runup noise measurements around an engine on a test stand and (2) flyover noise measurement of a large commercial jet transport with acoustical treatment applied to all four engines.

To support the design of these full-scale test articles, it is also recommended that additional laboratory studies be conducted to study the flow resistance and the acoustical impedance of the total duct lining treatment at higher particle velocities than those used in these preliminary tests. These measurements would then provide valuable correlation with the full-scale test results for use in selecting the best design.

APPENDIX A

PROCEDURE FOR DETERMINING AVERAGE DUCT THROAT VELOCITY FOR VACUUM SYSTEM RUNS

The duct models tested with the vacuum-system air supply consisted of the three inlet ducts and the center fan-discharge duct. The 55-percent lightbulb inlet duct, configuration B, was the first of these four ducts to be installed and a procedure to set the desired average velocity in the throat was established with this duct.

The 55-percent lightbulb inlet duct was installed as indicated in the sketch below.

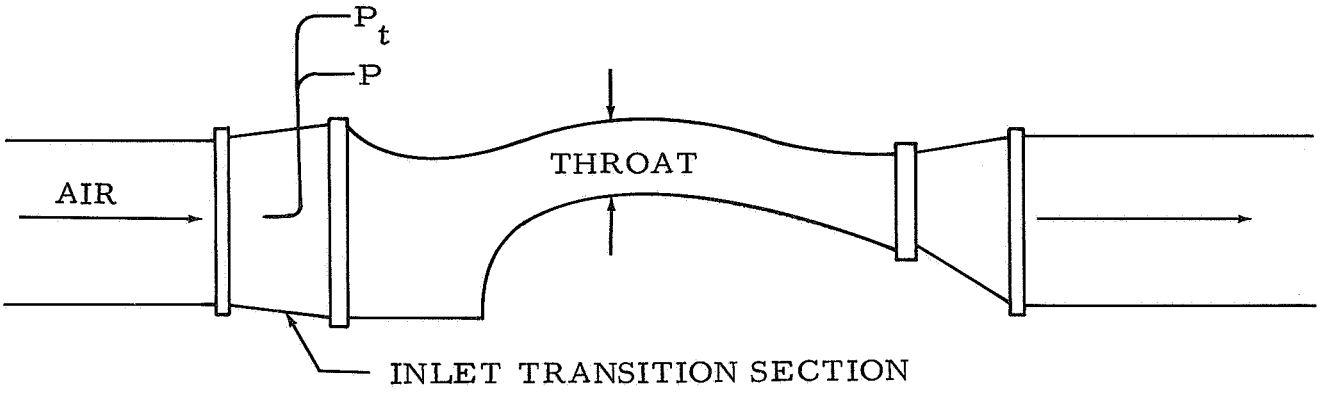

A pitot-static probe was installed in the inlet transition section and profiles of the inlet differential pressure ($\Delta P_{in} = P_t - 0$) across the duct were obtained. Approximate values for the average differential pressure in the duct were then obtained from the profile plots. The velocity in the inlet transition section in the plane of the probe measurements was determined with the aid of equation (15), assuming that the density of the air was the ambient standard value.

Thus,

$$v_{in} = \sqrt{\frac{2\Delta P_{in}}{\rho_o}} \text{ ft/sec} \qquad (25)$$

where

$$\rho_o = 0.00238 \text{ slugs/ft}^3$$

The throat velocity v_{th} was determined from the continuity equation. That is,

$$v_{th} = \frac{A_{in} v_{in}}{A_{th}} = \frac{A_{in}}{A_{th}} \sqrt{\frac{2}{\rho_o}} \sqrt{\Delta P_{in}} \text{ ft/sec} \qquad (26)$$

All of the 55-percent lightbulb inlet duct tests were run using 183.1 in.^{2} for the area of the inlet transition section, A_{in}, and 74.7 in.^{2} for the throat area, A_{th}. The flow rate was adjusted to give differential pressures

corresponding to velocities of 600, 500, 400, 300, 200, and 100 ft/sec. The 600 ft/sec velocity was the desired maximum value in order to simulate typical inlet conditions during takeoff; it also corresponded to the maximum velocity that could be attained and still preserve an adequate S/N ratio.

The flow rate in all cases was adjusted by changing the position of a butterfly valve in the 30-in. supply line to the five vacuum pumps. A calibrated venturi meter was installed in this line and the drop in the static pressure across the venturi, ΔP_{vent}, was correlated with the differential pressure in the inlet transition section, ΔP_{in}.

Since the velocity of the flow in the 30-in. line was always quite low, the static pressure was essentially constant and the mass flow of the air through the system depended primarily on the value of the differential pressure across the venturi. For the 55-percent lightbulb inlet duct, therefore, a value for ΔP_{vent} fixed a certain mass flow at each of the desired velocities. It was decided to conduct the standard inlet and the 75-percent lightbulb inlet duct tests at the same mass flow rates as used for the 55-percent lightbulb inlet duct tests. Maintaining the same mass flow meant that the throat velocity in the 55-percent and 75-percent lightbulb inlets should be equal, since the throat areas were the same, but that the throat velocity in the standard inlet would be lower, since the throat area here was larger.

When the 55-percent lightbulb inlet and standard inlet duct tests were complete, it was discovered that the throat area of the 55-percent lightbulb inlet ducts had been computed incorrectly and that the actual throat area was 90.6 $in.^2$ instead of 74.7 $in.^2$ The indicated velocities for the 55-percent lightbulb inlet tests were then reduced by the ratio of 74.7/90.6; the velocity that had been calculated to be 600 ft/sec was now 495 ft/sec, etc.

At this stage the applicability of the method for probing the inlet transition section to obtain an average value for ΔP at this station was questioned. It was realized that steady, uniform flow did not exist in the oddly shaped transition section (rectangular to triangular) and that the ΔP readings from the probe measurements, that had been used to set the flow, were unreliable. Since the tests could not be repeated, revised duct velocities were computed from calculated weight flow values.

The weight flow, W, of the air through the system was determined by means of a calibrated venturi meter installed in the 30-in. supply line. The meter was installed as indicated in the sketch below.

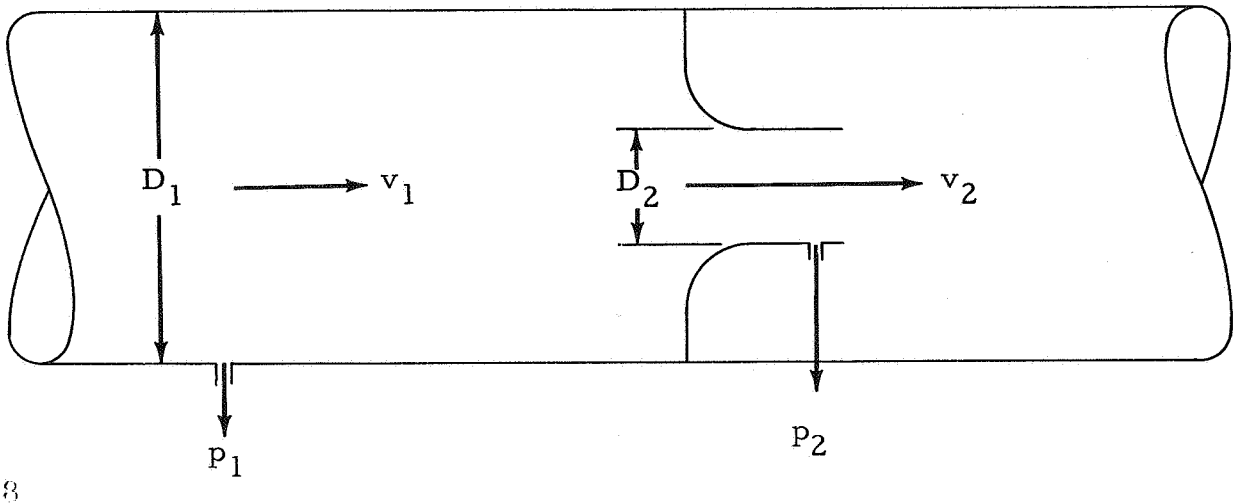

APPENDIX A

Assuming that the flow through the venturi is incompressible and frictionless with no loss in total pressure in going from station 1 to station 2, and that turbulence and expansion effects can be neglected, the weight flow through the venturi can be shown, from first principles, to be related to the pressures, temperatures and dimensions of the meter by,

$$W = \frac{A_2}{\sqrt{1-\beta^4}} \sqrt{\frac{2g}{R}} \sqrt{\frac{P_1 \Delta P}{T_1}} \quad \text{lb/sec} \qquad (27)$$

where

g = acceleration of gravity = 32.17 ft/sec^2

A_2 = venturi throat area = $\frac{\pi D_2^2}{4}$ = 1.6475 ft^2

β = ratio of venturi throat diameter to upstream pipe diameter = $\frac{D_2}{D_1}$ = 17.38/30.00 = 0.5793

R = gas constant for air = 53.35 ft-lb/lb-°R

P_1 = upstream static pressure, lb/ft^2

P_2 = static pressure at throat of venturi, lb/ft^2

ΔP = difference in static pressures between stations 1 and 2 = $P_1 - P_2$, lb/ft^2

T_1 = upstream static temperature, °R

In developing this equation, the density was assumed to be the upstream value because it is more easily determined at this station than at the throat of the venturi. Evaluating the dimensional constants and inserting conversion factors (to convert from practical measurement units for P_1 in inches of Hg and for ΔP in inches of H_2O to lb/ft^2) yields

$$W = 36.842 \sqrt{\frac{P_1 \Delta P}{T_1}} \quad \text{lb/sec} \qquad (28)$$

The actual compressibility of the flow is taken into account by introduction of a term called the adiabatic expansion factor, Y_a. This factor can be derived from compressible flow theory by assuming that the density decreases from station 1 to station 2 adiabatically. The expansion factor is a complicated function of the ratio of specific heats of the fluid, γ, the contraction ratio, β, and the pressure ratio $\Delta P/P_1$. It is tabulated in various handbooks.* In addition to the compressibility correction (or expansion factor), another term

*See, for example, SAE Aero-Space Applied Thermodynamics Manual, rev. January 1962, figure 3G-30.

called the velocity coefficient, C_V, is used to account for the difference between the physical throat area, A_2, and the actual flow area which is smaller due to a boundary layer along the walls of the venturi tube. This last correction term depends on the pipe Reynolds number and the contraction ratio and is usually determined by calibration. With these terms the weight flow becomes

$$W = 36.842\, C_V\, Y_a \sqrt{\frac{P_1\, \Delta P}{T_1}} \quad \text{lb/sec} \tag{29}$$

A calibration supplied with the venturi meter indicated that the actual expression should be

$$W = 35.2903 \left(1 - 0.04696 \frac{\Delta P}{P_1}\right) \sqrt{\frac{P_1\, \Delta P}{T_1}} \quad \text{lb/sec} \tag{30}$$

where the discharge coefficient, C_V, is apparently about 0.96 and the relation for Y_a is given by the term inside the parentheses.

This last equation was used to calculate the weight flows. Since T_1 was not measured, the upstream static temperature was assumed to be equal to the ambient standard value, i.e., $T_1 = T_{std} = 518.7°R$. The weight flows through the throat of a duct model were slightly greater than the calculated values through the venturi meter because the duct throat static temperature, which was assumed to equal the actual ambient temperature, was usually less than the standard ambient value. Thus,

$$W_{th} = W_{venturi} \sqrt{\frac{T_{std}}{T_{th}}} \tag{31}$$

This correction amounted to about a 5-percent change in the calculated weight flows.

Throat velocities were then calculated from the continuity relation

$$\frac{W_{th}}{g} = \rho_{th}\, A_{th}\, v_{th} \tag{32}$$

or, assuming that the static throat density was the ambient standard value, ρ_o,

$$v_{th} = \frac{W_{th}}{g \rho_o\, A_{th}} \quad \text{ft/sec} \tag{33}$$

Using the calculated value of 20.2 lb/sec as the maximum value of throat weight flow, 0.0765 lb/ft^3 for $g\rho_o$, 90.65 $in.^2$ for the throat area of the light-bulb inlets and 112.5 $in.^2$ for the standard inlet, gave the following maximum average throat velocities:

v_{th} = 423 ft/sec for the lightbulb inlets

and

v_{th} = 340 ft/sec for the standard inlet.

The first value compares to 495 ft/sec determined by the method of probing the inlet transition section with the 55-percent lightbulb inlet duct.

The F-series center-duct tests were run after the inlet tests were complete. For these tests, the throat velocities were determined by measuring static and differential pressure profiles at the throat since the throat was accessible for probing. Suitable "average" values were determined from the profiles. These average values were used with equations (18) and (32) with (14) to determine a comparison between the two approaches. Thus,

$$v_{th} = 15.9 \sqrt{T_{th}} \sqrt{\frac{(\Delta P)_{th}}{P_{th}}} \quad \text{ft/sec} \tag{34}$$

and

$$v_{th} = \frac{W_{th} T_{th}}{1.325\, P_{th}\, A_{th}} \quad \text{ft/sec} \tag{35}$$

For these calculations T_{th} was assumed to be equal to the ambient standard value, 518.7°R.

Velocities calculated from the two approaches were within 5 percent, or less, of each other, giving some credence to the probe tube data. The second method, equation (35), was used to set the velocities for the F-series tests, i.e., 100, 300 and 400 ft/sec.

When the center duct tests were completed, it was recognized that the assumption used in equation (33) to determine the throat velocities in the inlet ducts (namely, that the average density of the air in the throat of the lightbulb inlets was equal to the ambient standard density) was in error since the ambient standard pressure must have differed from whatever average static pressure had existed in the ducts during the tests. There would also have been a density change due to the change in the temperature of the air, but this effect could not be accounted for since no temperature measurements were ever made in the ducts. (The effect would have been minor in any case because the correction only enters as the ratio of the absolute temperatures and typical ambient temperatures during the tests ranged from 10°F to 40°F or 469°R to 499°R.)

Thus, with

$$g\rho_{th} = g\rho_o \frac{P_{th}}{P_{std}} \frac{T_{std}}{T_{th}} \quad \text{lb/ft}^3 \tag{36}$$

and with

$$T_{th} = T_{std} \tag{37}$$

we have,

$$v_{th_2} = \frac{W_{th}}{g\rho_{th} A_{th}} = \frac{W_{th}}{(g\rho_o)(P_{th})(P_{std}) A_{th}} \tag{38}$$

or,

$$v_{th_2} = v_{th_1} \times \frac{P_{std}}{P_{th}} \quad \text{ft/sec} \tag{39}$$

where v_{th_1} is the throat velocity calculated with assumption of standard ambient pressure and v_{th_2} is the throat velocity after correction for the decrease in static pressure.

Since the throat area of the center duct was approximately equal to that of the 55-percent and 75-percent lightbulb inlets (88.6 in.^{2} compared to 90.6 in.^{2}), and since reliable values for the average throat static pressure and for the venturi upstream static pressure were available from the center duct runs, it was decided to approximate the ratio P_{std}/P_{th} for the two lightbulb inlets by the ratio of $P_{venturi}/P_{throat}$ from the center duct runs. This ratio of static pressures was determined from a special series of tests in which the weight flows were set equal to those used in the inlet duct tests. A comparison of the throat velocities calculated by the two methods is given in the table below.

Weight flow, lb/sec	55% and 75%		Standard	
	Throat velocity, v_{th_1}, ft/sec	Throat velocity, v_{th_2}, ft/sec	Throat velocity, v_{th_1}, ft/sec	Throat velocity, v_{th_2}, ft/sec
20.2	423	465	340	358
16.9	344	372	278	290
13.3	270	286	218	225
10.3	205	213	165	169
6.8	134	137	108	110
3.9	75	75	61	61

The percentage increases in average throat velocity for the standard inlet were arbitrarily set equal to half the percentage increases in throat velocity for the 55-percent and 75-percent lightbulb inlets to allow for the greater throat area and hence lower velocity and higher static pressure in the standard inlet as compared to the lightbulb inlets.

Note that the maximum values shown in the table above could not have been increased above the values shown (even though the system was physically capable of doing so) because of the limit of adequate S/N ratio.

APPENDIX B

SPECIFICATIONS FOR POROUS SURFACE MATERIALS FOR NACELLE ACOUSTICAL TREATMENT

This specification describes the requirements for acoustical materials to be installed in the nacelles of jet engines for the purpose of reducing the discrete-frequency fan (or compressor) noise radiated from the fan-inlet and fan-discharge ducts.

The acoustical treatment for which these materials is required is described, in general terms, as a broadband resonator. The broadband resonator concept for duct linings consists of a porous metal surface material with a cavity behind it. The cavity is filled either with air or with an acoustically absorptive material. This specification describes the acoustical and mechanical requirements which must be met by the porous surface materials as they would be installed in an engine.

The complete nacelle duct lining treatment, as installed, shall have a normal-incidence acoustical absorption coefficient of not less than 0.80 over the frequency range of 1250 to 8000 Hz. The absorption coefficient of a sample of the complete treatment shall be determined from measurements of the maximum and minimum sound pressures and their locations along the central axis of a standing-wave-tube apparatus whose dimensions are appropriate for the frequency range. The value of the maximum SPL's in the tube shall be between 110 and 130 dB, re 0.0002 dynes/cm^2. It is noted that it is desirable to study the behavior of duct lining treatments at higher SPL's, if possible.

This specification applies only for research and development testing of the broadband resonator concept. It is not intended for application to operational commercial jet transports. Specifications for such use would be developed after development tests are completed.

REQUIREMENTS

Airflow Resistance of Surface Metal

The airflow resistance (in rayls) of the surface material at any test point on the sheet shall not deviate more than ±25 percent from the specified nominal flow resistance.

Mechanical Properties

The porous sheet surface material shall have the mechanical properties listed below. The ultimate tensile strength, elongation, and interlaminar shear strength requirements are specified in terms of two classes of materials, A and B. Materials that meet all requirements for Class A materials shall be known as Class A materials. A material that fails to meet any of the requirements for Class A materials shall be known as Class B material.

Minimum Effective Ultimate Tensile Strength. —

Class A material	10 000 psi
Class B material	1 000 psi

Elongation. — The material shall have the following minimum values for allowable elongation at the ultimate tensile strength:

Class A material	6 percent
Class B material	2 percent

Minimum Interlaminar Shear Strength. —

Class A material	250 psi
Class B material	75 psi

Surface Roughness. — The surface roughness of the material shall not exceed 1500 microinches, rms.

Bending. — Both classes of material shall be capable of being bent at room temperatures through a 90° angle with a minimum bend radius of 1.0 inch.

Corrosion Resistance. — The material shall have corrosion resistance at least equal to that of 2024 clad aluminum alloy.

Thickness. — The thickness of the surface material at any test point on the sheet shall not deviate more than ±15 percent from the specified nominal thickness.

Contaminated air erosion resistance. — The surface material shall withstand, without change in airflow resistance or mechanical properties, the erosive effects of sand and dust-laden air flowing over the material with a mean velocity of 1000 ft/sec.

Exposure to fluids. — The surface material shall withstand, without change in airflow resistance or mechanical properties, exposure to the many fluids typical of turbine-engine installations. These fluids include: lubricants, fuels, solvents, and cleaning materials.

Thermal Environment

Materials for use in fan-discharge ducts shall withstand exposure to air temperatures in the range between -65°F and +300°F. Materials for use in engine inlet ducts shall withstand exposure to air temperature in the range between -65°F and +200°F. No change in airflow resistance or mechanical properties shall be evident.

Icing

The surface material shall withstand repeated freezing and thawing of any water trapped or retained in its pores without change in airflow resistance or mechanical properties.

APPENDIX B

Surface Weight Density

The surface weight density of the material shall have the minimum practical value.

VERIFICATION TESTS

The tests specified below represent the best judgment of the contractor, at the date of this report, as to the types of tests needed to verify that the materials to be used for nacelle acoustical treatments will satisfy the design requirements stated above.

Airflow Resistance

The airflow resistance, in rayls, of the surface material shall be determined under steady flow conditions in an airflow resistance apparatus. The linear airflow rate shall be chosen so as to measure the laminar flow resistance of the material. The recommended flow rate is 10 cm/sec through a sample with a 10-cm diameter. The value for the flow resistance shall be reported as the ratio of the pressure drop across the material, in dynes/cm^2, to the linear airflow velocity through the sample, in cm/sec, i.e., in cgs rayls. For test purposes, a sheet of material shall be divided into an imaginary grid with 6-inch squares and the flow resistance shall be determined at the center of each square over the entire sheet. No two adjacent flow resistance readings shall differ by more than 40 percent of the specified nominal flow resistance.

Mechanical Properties

Minimum effective ultimate tensile. — Coupons shall be tested to determine the minimum effective ultimate tensile strength. The test shall be conducted per Federal Test Method Standard 406, method 1031 except that all specimens shall conform to the specifications of a specimen which has a thickness of 0.5-inch. A minimum of two tests shall be made on coupons which are representative of each discrete batch of material.

Elongation. — Obtain elongation data during ultimate tensile strength tests using the procedure of FTMS 406, method 1031.

Minimum effective interlaminar shear strength. — Coupons shall be tested per Federal Test Method Standard 406, method 1042.

Surface roughness. — Use a surface roughness gage such as a "Profilometer" or a "Surfindicator" over the surface of representative sheets of the material. The gage shall be capable of indicating a roughness of at least 2000 microinches, rms. Determine the roughness in several directions.

Bending. — Use a standard bending test and examine for cracks or other failures. A minimum of two tests shall be made on samples representative of each discrete batch of material.

Corrosion resistance. Material shall be tested for 48 hours of exposure in accordance with Federal Standard 151A, method 811.1. A sample of the material shall also be tested for resistance to exposure to salt spray as described in MIL-E-5009C, Military Specification, Engines, Aircraft, Turbojet and Turbofan, Tests for; paragraph 4.3.9, Corrosion Susceptibility Test. Following exposure to these corrosion tests, the sample of the material shall be tested to determine the effect on tensile strength, minimum bend radius, surface roughness, and airflow resistance. No change in any of these quantities shall be evident.

Thickness. — Thickness shall be measured with a micrometer having 0.25-inch (and, preferably, 0.50-inch) diameter anvils. As a minimum, measurements shall be made at the same test points as used for the flow resistance tests.

Contaminated air erosion. — A sample of the sheet, with backing material and supporting mechanisms appropriate to the design for the treatment installation, shall be formed into a tube of any convenient diameter and at least 6 inches long. Air contaminated with sand and dust particles shall be pumped through the tube. The sand and dust concentration shall be 4.4×10^{-5} pounds of solids per pound of air. The solids shall consist of crushed quartz of the following sizes:

Particle size, microns	Percent of particles finer than size indicated
1000	100
900	98-99
600	93-97
400	82-86
200	46-50
125	18-22
75	3-7

(Note that 1 micron equals about 0.00004 inch.)

The mean duct velocity through the tube shall be 1000 ft/sec. The test shall be conducted for 10 hours. No change in the airflow resistance or surface roughness of tensile strength shall be evident. It shall be permissible to clean the sample with a vacuum cleaner or by reverse flushing with air to dislodge particles trapped in the pores prior to making the airflow resistance tests.

Exposure to fluids. — Samples of the material shall be submerged for 7 days in "Skydrol" hydraulic fluid heated to 160°F. No change in airflow resistance, ultimate tensile strength or surface roughness shall be evident after the 7 days of continuous exposure.

Thermal Environment

Dry heat. — Samples of the material shall be exposed to +300°F air in an air-circulating oven. No change in airflow resistance, ultimate tensile

strength or surface roughness shall be evident after 48 hours of continuous exposure.

Heat with humidity. — Samples of the material shall be subjected to an environment with a 95-percent relative humidity at 100°F. No change in airflow resistance, ultimate tensile strength or surface roughness shall be evident after 7 days of continuous exposure.

Icing

A sample of the material shall be immersed in distilled water until saturated. It shall then be quick frozen to -65°F for 2 hours and then thawed to +60°F to melt away all ice. This cycle shall be repeated 100 times. The surface roughness, tensile strength, and airflow resistance shall be determined after the tests are complete. There shall be no change in airflow resistance, surface roughness or tensile strength.

Surface Weight Density

Weigh and measure the material and compute the surface weight density. For the thickness of the sheet, use the average of the values determined in Section 3.2.7.

REFERENCES

1. Miller, M. M.: Sound and Furor, the Jet Noise Suppression Age. SAE Transactions, vol. 65, 1957, pp. 595-607.

2. Jordan, L. R.; and Auble, C. M.: Development of the Suppressor and Thrust Brake for the DC-8 Airplane. SAE Transactions, vol. 67, 1959, pp. 524-531.

3. Walley, W.R.; and Gardner, R. N.: Sound Suppressor and Jet Reverser Effects on Aircraft Performance. SAE Paper No. 238C, October 10-14, 1960.

4. Adams, H. W.: Mechanical Engineer's Solution for Noise Suppression. ASME Paper No. 59-AV-30, March 9-12, 1959.

5. Kryter, K. D.: Scaling Human Reactions to the Sound from Aircraft. J. Acoust. Soc. Am., vol. 31, November 1959, pp. 1415-1429.

6. Little, J.W.: Human Response to Jet Engine Noises. Noise Control, vol. 7, May/June 1961, pp. 11-13.

7. Tyler, J.W.; and Sofrin, T.G.: Axial Flow Compressor Noise Studies. Trans. SAE, vol. 70, 1962, pp. 309-332.

8. Hetherington, R.: Compressor Noise Generated by Fluctuating Lift Resulting from Rotor-Stator Interaction. J. AIAA, vol. 1, February 1963, pp. 473-474.

9. Morfey, C.L.: Rotating Pressure Patterns in Ducts: Their Generation and Transmission. J. Sound Vib., vol. 1, January 1964, pp. 60-87.

10. Bragg, S. L.; and Bridge, R.: Noise from Turbojet Compressors. J. Roy. Aeronaut. Soc., vol. 68, January 1964, pp. 1-10.

11. Kilpatrick, D.A.; and Reid, D.T.: Transonic Compressor Noise. The Effect of Inlet Guide Vane-Rotor Spacing. National Gas Turbine Establishment Report R. 257, January 1964 (ASTIA No. AD 434124).

12. Griffiths, J.W.R.: The Spectrum of Compressor Noise of a Jet Engine. J. Sound Vib., vol. 1, April 1964, pp. 127-140.

13. Sharland, I.J.: Sources of Noise in Axial Flow Fans. J. Sound Vib., vol. 1, July 1964, pp. 302-322.

14. Bateman, D. A.; Chang, S. C.; Hulse, B.T.; and Large, J.B.: Compressor Noise Research. FAA Aircraft Development Service Technical Report, FAA ADS-31, January 1965.

15. Copeland, W. L.: Inlet Noise Studies for an Axial-Flow Single-Stage Compressor. NASA TN D-2615, 1965.

16. Crigler, J. L.; and Copeland, W. L.: Noise Studies of Inlet-Guide-Vane – Rotor Interaction of a Single-Stage Axial-Flow Compressor. NASA TN D-2962, September 1965.

17. Sivian, L. J.: Sound Propagation in Ducts Lined with Absorbing Materials. J. Acoust. Soc. Am., vol. 9, October 1937, pp. 135-140.

18. Morse, P. M.: The Transmission of Sound Inside Pipes. J. Acoust. Soc. Am., vol. 11, October 1939, pp. 205-210.

19. Rogers, R.: The Attenuation of Sound in Tubes. J. Acoust. Soc. Am., vol. 11, April 1940, pp. 480-484.

20. Sabine, Hale J.: The Absorption of Noise in Ventilating Ducts. J. Acoust. Soc. Am., vol. 12, July 1940, pp. 53-57.

21. Scott, R. A.: The Propagation of Sound Between Walls of Porous Material. Proc. Phys. Soc. London, vol. 58, 1946, pp. 358-368.

22. Zwikker, C.; and Kosten, C.W.: Sound Absorbing Materials. Elsevier Publishing Company, New York, 1949.

23. Bruel, P.V.: Sound Insulation and Room Acoustics. Chapman and Hall, Ltd., London, 1951.

24. Meyer, E.; Mechel, F.; and Kurtze, G.: Experiments on the Influence of Flow on Sound Attenuation in Absorbing Ducts. J. Acoust. Soc. Am., vol. 30, March 1958, pp. 165-174.

25. Beranek, L.L., ed.: Noise Reduction. McGraw-Hill Book Co., Inc., New York, 1960.

26. Mechel, F.; Mertens, P.; and Schilz, W.: Research on Sound Propagation in Sound Absorbent Ducts with Superimposed Airstreams. Vol. I, AMRL-TDR-62-140 (I), December 1962. See also Volumes II, III, and IV on AMRL-TDR-62-140 (II), (III), and (IV).

27. Piazza, R.S.: The Attenuation in Ducts Lined with Selective Structures. Acustica, vol. 15, 1965, pp. 402-407.

28. Tack, D.H.; and Lambert, R.F.: Influence of Shear Flow on Sound Attenuation in a Lined Duct. J. Acoust. Soc. Am., vol. 38, October 1965, pp. 655-666.

29. Strutt, J.W. (Lord Rayleigh): Theory of Sound. Vol. 2, Section 303, Dover Publications, Inc., New York, 1945.

30. Bies, D.A.; and Wilson, O.B., Jr.: Acoustic Impedance of a Helmholtz Resonator at Very High Amplitude. J. Acoust. Soc. Am., vol. 29, June 1957, pp. 711-714.

31. Spears, E. L.; and Wirt, L.S.: Gas Turbine Sound Attenuation, vol. I. AiResearch Manufacturing Co., Phoenix, Arizona, Report SD-5011-R4, July 1963.

32. Vershure, R.W.; and Wirt, L.S.: Gas Turbine Sound Attenuation, vol. II. AiResearch Manufacturing Co., Phoenix, Arizona, Report SD-5011-R4, October 1963.

33. Gebhardt, G. T.: Acoustical Design Features of the Boeing Model 727. J. Aircraft, vol. 2, July-August 1965, pp. 272-277.

34. Smith, A.M.O.; and Pierce, J.T.: Exact Solution of the Neumann Problem; Calculation of Non-Circulatory Plane and Axially Symmetric Flows About or Within Arbitrary Boundaries. Douglas Aircraft Company Report No. ES 26988, 25 April 1958.

35. Beranek, L.L.: Acoustic Measurements. John Wiley & Sons, Inc., New York, 1949.

36. Boone, D.W.: Use of Scottfelt Material for Sound Attenuating Gas Turbines. AiResearch Manufacturing Co., Phoenix, Arizona, Report No. GT-7413-R, 19 November 1964.

37. London, A.: The Determination of Reverberant Sound Absorption Coefficients from Acoustic Impedance Measurements. J. Acoust. Soc. Am., vol. 22, March 1950, pp. 263-269.

38. Anon.: Land Use Planning with Respect to Aircraft Noise. Tri-Service Manuals. Department of the Air Force Manual AFM 86-5, Department of the Army Technical Manual TM 5-365, Department of the Navy Manual NAVDOCKS P-98, 1 October 1964.

39. Anon.: Noise-Final Report. Wilson Committee on the Problem of Noise. Her Majesty's Stationery Office, London, July 1963, Cmnd. 2056.

40. Anon.: Standard Values of Atmospheric Absorption as a Function of Temperature and Humidity for Use in Evaluating Aircraft Flyover Noise. SAE Aerospace Recommended Practice, ARP 866, 1964.

TABLE I.—ABSORPTION COEFFICIENTS AND IMPEDANCE VALUES FROM NORMAL – INCIDENCE IMPEDANCE TUBE TESTS

Configurations		Frequency, Hz																																	
Flow resistance of fibermetal lining, cgs rayls (a)	Backing material (b)	1250				1600				2000				2500				3150				4000				5000				6300			
		α_N	$\frac{Z_A}{\rho_o c}$	$\frac{R_A}{\rho_o c}$	$\frac{X_A}{\rho_o c}$	α_N	$\frac{Z_A}{\rho_o c}$	$\frac{R_A}{\rho_o c}$	$\frac{X_A}{\rho_o c}$	α_N	$\frac{Z_A}{\rho_o c}$	$\frac{R_A}{\rho_o c}$	$\frac{X_A}{\rho_o c}$	α_N	$\frac{Z_A}{\rho_o c}$	$\frac{R_A}{\rho_o c}$	$\frac{X_A}{\rho_o c}$	α_N	$\frac{Z_A}{\rho_o c}$	$\frac{R_A}{\rho_o c}$	$\frac{X_A^c}{\rho_o}$	α_N	$\frac{Z_A}{\rho_o c}$	$\frac{R_A}{\rho_o c}$	$\frac{X_A}{\rho_o c}$	α_N	$\frac{Z_A}{\rho_o c}$	$\frac{R_A}{\rho_o c}$	$\frac{X_A}{\rho_o c}$	α_N	$\frac{Z_A}{\rho_o c}$	$\frac{R_A}{\rho_o c}$	$\frac{X_A}{\rho_o c}$
10	0.5-in. air	0.159	2.43	0.30	-2.42	0.236	1.88	0.30	-1.86	0.278	1.33	0.22	-1.30	0.397	0.98	0.24	-0.95	0.528	0.55	0.24	- 0.50	0.686	0.30	0.29	-0.09	0.750	0.44	0.36	0.25	0.626	0.86	0.39	0.76
10	1.0-in. air	0.309	1.21	0.23	-1.19	0.434	0.81	0.23	-0.76	0.555	0.45	0.23	-0.39	0.708	0.30	0.30	-0.02	0.657	0.47	0.30	0.37	0.599	1.11	0.47	1.00	0.378	3.90	1.90	3.42	0.281	—	2.88	—
10	2.0-in. air	0.620	0.35	0.25	-0.24	0.642	0.32	0.26	0.18	0.591	0.73	0.32	0.66	0.410	1.70	0.50	1.62	0.056	30.43	13.37	-27.36	0.500	0.68	0.25	-0.63	0.730	0.85	0.50	-0.69	—	—	—	—
25	0.5-in. air	0.252	3.05	0.75	-2.96	0.370	2.20	0.66	-2.10	0.534	1.82	0.79	-1.64	0.742	1.28	0.78	-1.00	0.835	1.14	0.86	- 0.74	0.947	0.74	0.70	-0.25	0.958	0.73	0.70	-0.18	0.808	1.00	0.68	0.74
25	1.0-in. air	0.615	1.30	0.60	-1.16	0.729	0.94	0.54	-0.77	0.875	0.68	0.57	-0.37	0.968	0.70	0.70	0.01	0.906	0.79	0.67	0.38	0.799	0.11	0.72	0.79	0.562	1.55	0.66	1.40	0.234	5.34	1.95	4.97
25	2.0-in. air	0.932	0.70	0.65	-0.26	0.911	0.57	0.56	-0.14	0.831	0.90	0.64	0.62	0.651	1.47	0.76	1.26	0.228	4.73	1.50	4.48	0.743	1.28	0.78	-1.02	0.966	0.93	0.77	0.52	0.298	2.78	0.76	2.68
25	0.5-in. CPF3-900	0.385	4.07	2.10	-3.49	0.553	2.81	1.70	-2.24	0.653	2.49	1.74	-1.78	0.773	1.84	1.38	-1.21	0.887	1.69	1.54	- 0.71	0.941	1.59	1.56	-0.26	0.929	1.71	1.70	0.18	0.846	1.72	1.46	0.89
25	1.0-in. CPF3-900	0.794	2.04	1.70	-1.13	0.868	1.90	1.76	-0.69	0.903	1.86	1.83	-0.26	0.885	2.03	2.02	0.10	0.870	2.11	2.10	0.14	0.842	2.29	2.26	0.22	0.811	2.53	2.51	0.24	0.825	2.39	2.35	-0.40
25	0.5-in. CPF3-900 plus 0.5-in. air	0.752	2.09	1.62	-1.32	0.881	1.53	1.31	-0.78	0.950	1.42	1.36	-0.38	0.951	1.56	1.56	-0.10	0.930	1.66	1.64	0.28	0.868	1.96	1.87	0.59	0.788	2.49	2.32	0.84	0.721	3.24	3.24	-0.01
25	0.5-in. air plus 0.5-in. CPF3-900	—	—	—	—	0.798	1.14	0.76	-0.85	0.921	0.99	0.84	-0.52	0.989	0.96	0.94	-0.19	0.987	1.00	0.98	0.20	0.945	1.16	1.05	0.50	0.878	1.59	1.38	0.79	0.848	1.66	1.38	0.92
25	0.5-in. fiberglass, 0.6 lb/ft^3	0.555	2.32	1.22	-2.06	0.702	1.85	1.19	-1.41	0.852	1.57	1.28	-0.90	0.915	1.44	1.30	-0.63	0.963	1.44	1.42	- 0.07	0.948	1.59	1.58	-0.05	0.898	1.93	1.92	-0.12	0.829	2.42	2.42	0.00
25	0.5-in. fiberglass, 1.2 lb/ft^3	0.644	2.24	1.44	-1.72	0.767	1.98	1.53	-1.26	0.880	1.79	1.64	-0.70	0.885	2.02	2.02	-0.14	0.881	2.06	2.06	- 0.04	0.863	2.16	2.15	-0.20	0.831	2.38	2.38	-0.22	0.863	2.25	2.24	0.12
25	1.0-in. fiberglass, 0.6 lb/ft^3	0.936	1.32	1.20	-0.54	0.976	1.31	1.30	-0.26	0.954	1.55	1.55	0.04	0.902	1.90	1.88	0.20	0.879	2.07	2.07	0.00	0.876	2.06	2.03	-0.05	0.874	2.09	2.08	-0.16	0.868	2.08	2.08	0.00
25	1.0-in. fiberglass, 1.2 lb/ft^3	0.868	2.12	2.11	-0.18	0.835	2.37	2.36	-0.10	0.794	2.57	2.52	-0.39	0.758	2.90	2.88	-0.17	0.800	2.57	2.54	- 0.41	0.840	2.29	2.26	-0.32	0.840	2.28	2.24	-0.23	0.835	2.29	2.24	-0.49
40	0.5-in. air	0.501	3.46	2.17	-2.68	0.642	2.22	1.41	-1.72	0.773	1.93	1.49	-1.23	0.856	1.90	1.73	-0.79	0.950	1.48	1.45	- 0.31	0.959	1.45	1.42	0.23	0.905	1.45	1.30	0.65	0.752	2.08	1.61	1.32
40	1.0-in. air	0.817	1.46	1.08	-0.98	0.941	1.08	0.97	-0.49	0.993	1.15	1.15	-0.09	0.970	1.28	1.24	0.31	0.911	1.51	1.38	0.62	0.799	1.78	1.38	1.11	0.605	2.43	1.51	1.91	0.209	5.41	1.76	5.10
40	2.0-in. air	0.974	1.39	1.38	-0.04	0.956	1.30	1.22	0.42	0.879	1.52	1.30	0.79	0.723	2.05	1.50	1.41	0.277	4.61	1.78	4.25	0.903	1.80	1.74	-0.44	0.846	1.26	0.95	0.83	0.334	3.13	1.18	2.86
40	0.5-in. CPF3-900	0.472	4.11	2.27	-2.92	0.598	2.98	1.44	-1.10	0.721	2.52	2.10	-1.52	0.773	2.62	2.44	-0.92	0.857	2.13	2.00	- 0.43	0.878	2.07	1.88	0.14	0.835	2.26	2.04	0.47	0.735	2.96	1.76	1.06
40	1.0-in. CPF3-900	0.732	2.49	2.30	-0.92	0.844	2.27	2.25	-0.32	0.846	2.29	2.29	-0.04	0.807	2.50	2.44	0.40	0.800	2.47	2.37	0.66	0.771	2.71	2.62	0.70	0.739	3.06	3.04	0.37	0.735	3.13	3.12	-0.01
40	0.5-in. CPF3-900 plus 0.5-in. air	0.788	2.30	2.06	-1.04	0.874	2.05	2.01	-0.36	0.892	1.98	1.98	-0.03	0.840	2.27	2.22	0.42	0.809	2.37	2.24	0.76	0.754	2.61	2.36	1.10	0.671	3.19	2.82	1.48	0.673	3.41	3.25	0.70
40	0.5-in. air plus 0.5-in. CPF3-900	0.798	2.07	1.65	-1.12	0.912	1.51	1.38	-0.62	0.954	1.53	1.52	-0.16	0.932	1.69	1.68	0.16	0.915	1.55	1.43	0.58	0.852	1.72	1.46	0.90	0.756	2.27	1.88	1.29	0.704	3.17	3.00	1.02
40	0.5-in. fiberglass, 0.6 lb/ft^3	0.655	2.70	2.01	-1.80	0.788	2.20	1.90	-1.11	0.861	2.06	1.98	-0.56	0.850	2.24	2.22	-0.28	0.865	2.13	2.11	0.20	0.831	2.25	2.14	0.58	0.769	2.75	2.67	0.58	0.682	3.52	3.46	-0.64
40	0.5-in. fiberglass, 1.2 lb/ft^3	0.708	2.63	2.16	-1.48	0.790	2.38	2.17	-0.96	0.829	2.40	2.38	-0.22	0.788	2.70	2.68	-0.22	0.792	2.59	2.52	0.58	0.771	2.84	2.84	-0.01	0.732	3.03	2.94	0.02	0.706	3.37	3.37	-0.01
40	1.0-in. fiberglass, 0.6 lb/ft^3	0.876	1.97	1.90	-0.51	0.911	1.85	1.84	0.05	0.861	2.17	2.16	0.17	0.794	2.46	2.32	-0.16	0.773	2.78	2.75	0.37	0.781	1.94	2.50	0.92	0.767	2.85	2.82	0.32	0.737	2.91	2.76	0.61
40	1.0-in. fiberglass, 1.2 lb/ft^3	0.771	2.74	2.67	-0.60	0.750	2.97	2.94	-0.40	0.706	3.32	3.28	0.46	0.695	3.47	3.46	0.12	0.730	3.08	2.99	- 0.58	0.760	2.86	2.80	0.00	0.728	3.11	3.04	-0.58	0.744	2.70	2.44	1.14
60	0.5-in. air	0.351	3.16	1.76	-2.59	0.492	2.19	1.44	-1.65	0.664	1.99	1.57	-1.21	0.777	1.90	1.67	-0.90	0.842	1.66	1.59	- 0.47	0.916	1.98	1.98	-0.11	0.891	2.49	2.44	-0.24	0.686	3.48	3.42	0.64
60	1.0-in. air	0.786	2.13	1.79	-1.15	0.908	1.61	1.50	-0.60	0.922	1.75	1.73	-0.23	0.881	2.04	2.02	0.15	0.876	2.06	2.04	0.26	0.749	2.86	2.74	0.79	0.558	4.85	4.74	-1.03	0.186	12.77	8.34	-9.44
60	2.0-in. air	0.905	1.88	1.88	-0.11	0.907	1.80	1.77	0.36	0.835	2.08	1.90	0.83	0.667	2.90	2.37	1.66	0.187	15.45	12.38	- 2.15	0.886	1.69	1.54	-0.70	0.760	2.87	2.38	-0.01	0.372	7.69	6.87	-3.47
60	0.5-in. CPF3-900	0.563	3.10	2.08	-2.30	0.715	2.24	1.68	-1.48	0.774	2.34	2.06	-1.12	0.791	2.35	2.14	-0.97	0.824	2.29	2.19	- 0.67	0.794	2.62	2.55	-0.41	0.723	3.04	2.91	-0.72	0.655	3.75	3.67	-0.74
60	1.0-in. CPF3-900	0.746	2.69	2.45	-1.11	0.809	2.39	2.31	-0.71	0.789	2.66	2.63	-0.37	0.763	3.11	3.11	-0.14	0.705	3.37	3.36	- 0.20	0.670	3.31	3.02	-1.36	0.648	2.93	2.28	-1.83	0.685	2.93	2.50	-1.52
60	0.5-in. CPF3-900 plus 0.5-in. air	0.756	2.60	2.36	-1.09	0.840	2.19	2.10	-0.62	0.823	2.45	2.44	-0.15	0.761	2.90	2.89	-0.25	0.724	3.19	3.16	0.39	0.642	3.94	3.90	-0.55	0.566	4.06	3.44	-2.15	0.642	2.80	1.82	-1.77
60	0.5-in. air plus 0.5-in. CPF3-900	0.794	2.29	2.05	-1.01	0.898	1.75	1.66	-0.57	0.893	1.96	1.94	-0.13	0.842	2.31	2.30	0.05	0.790	2.66	2.63	0.33	0.724	3.17	3.12	-0.15	0.642	3.50	3.13	-1.56	0.651	3.79	3.71	-0.79

[a] Fibermetal, nominal 0.040-in. thick, 0.004-in. diam fibers, type 347 stainless steel, reinforced on both sides

[b] Compressed open-cell polyurethane foam, type 3-900, 90 pores/lineal inch (before compression), 4.5 lb/ft^3

Fiberglass, type AA, nominal 0.00004-in. diam fibers, phenolic resin binder

TABLE II.—GENERAL ARRANGEMENT FOR TL TEST OUTLINES

Detailed outlines are given on succeeding pages for the fan-discharge and for the inlet duct transmission loss tests. These detailed outlines precede the tables that give the explanations for the configuration codes used to delineate the many different tests that were conducted; each of the detailed outlines follows the general arrangement and pattern given below. The general pattern describes first, the hardwall or baseline tests and then, the simplest or least complicated configuration with acoustically treated surfaces. The test runs with this configuration are arranged in a specific order. This order is maintained for each succeeding configuration tested.

I. All hardwall tests — reference or baseline runs.

II. First (simplest) configuration with acoustically treated surfaces.

- A. 25-rayl fibermetal surfaces
  - 1. One-inch-deep cavity filled with:
    - a. Air
    - b. Compressed polyurethane foam (CPF) type 3-900
    - c. CPF type 4-900
    - d. Ceramic fiber (CF) type 600 (fan-discharge ducts), or fiberglass, type AA (inlets)
  - 2. 1/2-inch-deep cavity filled with:
    - a. Air
    - b. CPF type 3-900
    - c. CPF type 4-900
    - d. CF type 600, or fiberglass
- B. 60-rayl fibermetal surfaces
  - 1. One-inch-deep cavity filled with:
    - a. Air
    - b. CPF type 3-900
    - c. CPF type 4-900
    - d. CF type 600, or fiberglass
  - 2. 1/2-inch-deep cavity filled with:
    - a. Air
    - b. CPF type 3-900
    - c. CPF type 4-900
    - d. CF type 600, or fiberglass

III. Second, or next more complex configuration.

The hardwall configurations had solid 0.05-in.-thick aluminum sheets rather than porous fibermetal surfaces. The porous surfaces were made

from a material with a nominal thickness of 0.040 inch. The fibers were made from type 347 stainless steel wire. A stainless steel boxweave screen was sintered into the material on both sides for reinforcement. The 25-rayl material was about 62% dense with a surface weight density of about 1.1 lb/ft^2; the 60-rayl material was about 72% dense and weighed about 1.3 lb/ft^2.

The open-cell compressed-polyurethane foam had a pore count of 90 pores per lineal inch before compression. The weight density of the type 3-900 material was about 5.4 lb/ft^3, while type 4-900 was about 7.2 lb/ft^3. The type 600 ceramic fiber weighed about 6 lb/ft^3. The type AA fiberglass was made from nominal 0.00004-in. diameter glass fibers with a phenolic resin binder and was supplied as 0.6 lb/ft^3 material in 1.0-in.-thick sheets.

Each of the test outlines indicates the runs that were made with a given duct configuration. For identification purposes, each run was assigned a configuration code. The configuration codes are explained in detail for each of the six duct systems in Tables IV, V, VI, XVII, XVIII, and XIX. These configuration codes are alpha-numerical symbols with the first symbol being a letter to indicate the duct test series (A through F), the second symbol being a number to indicate the run number (assigned in sequence), and the third symbol being a dash number to indicate the average throat velocity (from the highest velocity tested to the lowest). Thus, configuration code B23-4 represents the 23rd run with the 55% lightbulb inlet duct (configuration B) at the fourth highest duct velocity (which was 213 ft/sec in this case).

TABLE III . — TEST OUTLINE AND CONFIGURATIONS FOR FAN-DISCHARGE DUCT TESTS

Outline for fan-discharge duct tests	Configurations		
	Center duct -		End duct -
	blower system	vacuum system	blower system
I. Hardwall tests			
A. No splitter	—	F1	E1
B. No splitter but solid sheet aluminum laid over FM on the two circumferential walls	—	F2	—
C. Radial splitter	A1	F3	—
D. Radial and circumferential splitters	A2	F4	—
II. Tests with no splitter(s) installed			
A. 25-rayl FM on four walls			
1. One-in. deep cavity			
a. Air	—	F5	E2
2. 1/2-in. deep cavity			
a. Air	—	—	E3
b. CPF 3-900	—	F6	E4
c. CPF 4-900	—	—	E5
3. 1/4-in. deep cavity			
a. Air	—	—	E6
b. CPF 3-900	—	—	E7
C. 25-rayl FM on the two circumferential walls; sheet aluminum on two radial walls			
1. One-in. deep cavity			
a. Air: treatment area 841.5 $in.^2$	—	F7	—
2. 1/2-in. deep cavity			
a. Air	—	—	E8
b. CPF 3-900	—	—	E9
c. CPF 4-900	—	—	E10
3. Area variation with 1-in. air-filled cavity on the two circumferential walls; two radial walls hardwall. Circumferential walls were uncovered starting from inlet end.			
a. Solid aluminum sheet along 3/4 of duct length: treatment area 202.2 $in.^2$	—	F8	—
b. Solid aluminum sheet along 1/2 of duct length: treatment area 436.6 $in.^2$	—	F9	—
c. Solid aluminum sheet along 1/4 of duct length: treatment area 655.5 $in.^2$	—	F10	—
III. Tests with untreated, hardwall radial splitter installed			
A. 25-rayl FM on four walls			
1. One-in. deep cavity			
a. Air	A3	F11	—
b. CPF 3-900	A4	—	—
c. CPF 4-900	A5	—	—
d. Ceramic fiber	A6	—	—
2. 1/2-in. deep cavity			
a. Air	A7	—	—
b. CPF 3-900	A8	F12	—
c. CPF 4-900	A9	—	—
d. Ceramic fiber	A10	—	—
3. 1/4-in. deep cavity			
a. Air	A11	—	—
b. CPF 3-900	A12	—	—
B. 60-rayl FM on four walls			
1. One-in. deep cavity			
a. Air	A13	—	—
2. 1/2-in. deep cavity			
a. Air	A14	—	—
C. 25-rayl FM on the two circumferential walls; sheet aluminum on two radial walls			
2. 1/2-in. deep cavity			
a. Air	A15	—	—
b. CPF 3-900	A16	—	—
c. CPF 4-900	A17	—	—
d. Ceramic fiber	A18	—	—

TABLE III.—Concluded

Outline for fan-discharge duct tests	Configurations		
	Center duct-		End duct -
	blower system	vacuum system	blower system
D. 60-rayl FM on the two circumferential walls; sheet aluminum on two radial walls			
2. 1/2-in. deep cavity			
a. Air	A19	—	—
b. CPF 3-900	A20	—	—
c. CPF 4-900	A21	—	—
IV. Tests with radial splitter treated with 25-rayl FM over 1/2-in. air-filled cavity			
A. 25-rayl FM on four walls			
1. One-in. deep cavity			
c. CPF 4-900	A22	—	—
V. Tests with radial splitter treated with 25-rayl FM over 1/2-in. CPF 3-900 filled cavity			
A. 25-rayl FM on four walls			
1. One-in. deep cavity			
a. Air	—	F13	—
2. 1/2-in. deep cavity			
b. CPF 3-900	—	F14	—
VI. Test with radial and circumferential splitters installed: Radial splitter hardwall, circumferential splitter has 25-rayl FM over 1/2-in. air-filled cavity			
C. 25-rayl FM on the two circumferential walls; sheet aluminum on the two radial walls			
2. 1/2-in. deep cavity			
a. Air	A23	—	—
VII. Tests with radial and circumferential splitters installed: Radial splitter hardwall, circumferential splitter has 25-rayl FM over 1/2-in. CPF 3-900 filled cavity			
C. 25-rayl FM on the two circumferential walls; sheet aluminum on the two radial walls			
2. 1/2-in. deep cavity			
b. CPF 3-900	A24	—	—
VIII. Tests with radial and circumferential splitters installed: Radial splitter hardwall, circumferential splitter has 25-rayl FM over 1/2-in. ceramic-fiber-filled cavity			
C. 25-rayl FM on the two circumferential walls; sheet aluminum on the two radial walls			
2. 1/2-in. deep cavity			
d. Ceramic fiber	A25	—	—
IX. Test with radial and circumferential splitters installed: Radial splitter has 25-rayl FM over 1/2-in. CPF 4-900 filled cavity; circumferential splitter has 25-rayl FM over 1/2-in. air-filled cavity			
A. 25-rayl FM on four walls			
1. One-in. deep cavity			
c. CPF 4-900	A26	—	—
X. Tests with radial and circumferential splitters installed: Radial splitter has 25-rayl FM over 1/2-in. CPF 3-900 filled cavity; circumferential splitter also has 25-rayl FM over 1/2-in. CPF 3-900 filled cavity			
A. 25-rayl FM on four walls			
2. 1/2-in. deep cavity			
b. CPF 3-900	—	F15	—

TABLE IV . – EXPLANATION OF CONFIGURATION CODE FOR CENTER FAN-DISCHARGE DUCT TESTS

(Blower system runs)
(See figure 33a for dimensions and areas)
(Average throat velocity is 300 ft/sec for all tests)

Conf. Code	Description of configuration		Description of treatment	
	Number of walls treated	Splitter(s)	Walls	Splitter(s)
A1-2	4	Radial	Hardwall	Hardwall
A2-2	4	Radial and circumferential	Hardwall	Radial – hardwall; circumferential – hardwall
A3-2	4	Radial	25-rayl FM, 1-in. Air	Hardwall
A4-2	4	Radial	25-rayl FM, 1-in. CPF 3-900	Hardwall
A5-2	4	Radial	25-rayl FM, 1-in. CPF 4-900	Hardwall
A6-2	4	Radial	25-rayl FM, 1-in. CF	Hardwall
A7-2	4	Radial	25-rayl FM, 1/2-in. Air	Hardwall
A8-2	4	Radial	25-rayl FM, 1/2-in. CPF 3-900	Hardwall
A9-2	4	Radial	25-rayl FM, 1/2-in. CPF 4-900	Hardwall
A10-2	4	Radial	25-rayl FM, 1/2-in. CF	Hardwall
A11-2	4	Radial	25-rayl FM, 1/4-in. Air	Hardwall
A12-2	4	Radial	25-rayl FM, 1/4-in. CPF 3-900	Hardwall
A13-2	4	Radial	60-rayl FM, 1-in. Air	Hardwall
A14-2	4	Radial	60-rayl FM, 1/2-in. Air	Hardwall
A15-2	2	Radial	2 radial walls – hardwall; 2 circumferential walls – 25-rayl FM, 1/2-in. Air	Hardwall
A16-2	2	Radial	2 radial walls – hardwall; 2 circumferential walls – 25-rayl FM, 1/2-in. CPF 3-900	Hardwall
A17-2	2	Radial	2 radial walls – hardwall; 2 circumferential walls – 25-rayl FM, 1/2-in. CPF 4-900	Hardwall
A18-2	2	Radial	2 radial walls – hardwall; 2 circumferential walls – 25-rayl FM, 1/2-in. CF	Hardwall
A19-2	2	Radial	2 radial walls – hardwall; 2 circumferential walls – 60-rayl FM, 1/2-in. Air	Hardwall
A20-2	2	Radial	2 radial walls – hardwall; 2 circumferential walls – 60-rayl FM, 1/2-in. CPF 3-900	Hardwall
A21-2	2	Radial	2 radial walls – hardwall; 2 circumferential walls – 60-rayl FM, 1/2-in. CPF 4-900	Hardwall
A22-2	4	Radial	25-rayl FM, 1-in. CPF 4-900	25-rayl FM, 1/2-in. Air
A23-2	2	Radial and circumferential	2 radial walls – hardwall; 2 circumferential walls – 25-rayl FM, 1/2-in. Air	Radial – hardwall; circumferential – 25-rayl FM, 1/2-in. Air
A24-2	2	Radial and circumferential	2 radial walls – hardwall; 2 circumferential walls – 25-rayl FM, 1/2-in. CPF 3-900	Radial – hardwall; circumferential – 25-rayl FM, 1/2-in CPF 3-900
A25-2	2	Radial and circumferential	2 radial walls – hardwall; 2 circumferential walls – 25-rayl FM, 1/2-in. CF	Radial – hardwall; circumferential – 25-rayl FM, 1/2-in. CF
A26-2	4	Radial and circumferential	25-rayl FM, 1-in. CPF 4-900	Radial – 25-rayl FM, 1/2-in. CPF 4-900; circumferential – 25-rayl FM, 1/2-in. Air

TABLE V . — EXPLANATION OF CONFIGURATION CODE FOR CENTER FAN-DISCHARGE DUCT TESTS

(Vacuum system runs)

(See figure 33a for dimensions and areas)

Conf. code	Average throat velocity, ft/sec	Description of configuration		Description of treatment	
		Number of walls treated	Splitter(s)	Walls	Splitter(s)
(F1-2)[a]	300	4	—	Hardwall	—
(F3-2)	300	4	Radial	Hardwall	Hardwall
(F4-2)	300	4	Radial + circumferential	Hardwall	Radial–hardwall;circumferential–hardwall
F1-2	300	4	—	Hardwall	—
F1-3	100	4	—	Hardwall	—
F2-1	400	2	—	2 radial walls - hardwall; 2 circumferential walls - solid sheet - aluminum over FM	—
F2-2	300	2	—	2 radial walls - hardwall; 2 circumferential walls - solid sheet - aluminum over FM	—
F3-2	300	4	Radial	Hardwall	Hardwall
F3-3	100	4	Radial	Hardwall	Hardwall
F4-2	300	4	Radial + circumferential	Hardwall	Hardwall
F4-3	100	4	Radial + circumferential	Hardwall	Hardwall
F5-2	300	4	—	25 - rayl FM, 1-in. air	—
F5-3	100	4	—	25 - rayl FM, 1-in. air	—
F6-2	300	4	—	25 - rayl FM, 1/2-in. CPF 3-900	—
F6-3	100	4	—	25 - rayl FM, 1/2-in. CPF 3-900	—
F7-1	400	2	—	2 radial walls - hardwall; 2 circumferential walls - 25 - rayl FM, 1-in. air	—
F7-2	300	2	—	2 radial walls - hardwall; 2 circumferential walls - 25 - rayl FM, 1-in. air	—
F8-1	400	2	—	2 radial walls - hardwall; 2 circumferential walls - 25 - rayl FM, 1-in. air with solid sheet - aluminum along 3/4 of duct length	—
F8-2	300	2	—	2 radial walls - hardwall; 2 circumferential walls - 25 - rayl FM, 1-in. air with solid sheet - aluminum along 3/4 of duct length	—
F9-1	400	2	—	2 radial walls - hardwall; 2 circumferential walls - 25 - rayl FM, 1-in. air with solid sheet - aluminum along 1/2 of duct length	—
F9-2	300	2	—	2 radial walls - hardwall; 2 circumferential walls - 25 - rayl FM, 1-in. air with solid sheet - aluminum along 1/2 of duct length	—
F10-1	400	2	—	2 radial walls - hardwall; 2 circumferential walls - 25 - rayl FM, 1-in. air with solid sheet - aluminum along 1/4 of duct length	—
F10-2	300	2	—	2 radial walls - hardwall; 2 circumferential walls - 25 - rayl FM, 1-in. air with solid sheet - aluminum along 1/4 of duct length	—
F11-2	300	4	Radial	25 - rayl FM, 1-in. air	Hardwall
F11-3	100	4	Radial	25 - rayl FM, 1-in. air	Hardwall
F12-2	300	4	Radial	25 - rayl FM, 1/2-in. CPF 3-900	Hardwall
F12-3	100	4	Radial	25 - rayl FM, 1/2-in. CPF 3-900	Hardwall
F13-2	300	4	Radial	25 - rayl FM, 1-in. air	25-rayl FM, 1/2-in. CPF 3-900
F13-3	100	4	Radial	25 - rayl FM, 1-in. air	25-rayl FM, 1/2-in. CPF 3-900
F14-2	300	4	Radial	25 - rayl FM, 1/2-in. CPF 3-900	25-rayl FM, 1/2-in. CPF 3-900
F14-3	100	4	Radial	25 - rayl FM, 1/2-in. CPF 3-900	25-rayl FM, 1/2-in. CPF 3-900
F15-2	300	4	Radial + circumferential	25 - rayl FM, 1/2-in. CPF 3-900	Radial - 25-rayl FM, 1/2-in. CPF 3-900; circumferential - 25-rayl FM, 1/2-in. CPF 3-900
F15-3	100	4	Radial + circumferential	25 - rayl FM, 1/2-in. CPF 3-900	Radial - 25-rayl FM, 1/2-in. CPF 3-900; circumferential - 25-rayl FM, 1/2-in. CPF 3-900

[a]Configuration codes in parentheses represent background noise tests run with airflow only, transducers off

TABLE VI. – EXPLANATION OF CONFIGURATION CODE FOR END FAN–DISCHARGE DUCT TESTS

(Average throat velocity is 300 ft/sec for all tests, no splitters were used in any end duct tests)

Conf. code	Description of treatment
E1-2	4 walls, hardwall
E2-2	4 walls, 25-rayl FM, 1-in. Air
E3-2	4 walls, 25-rayl FM, 1/2-in. Air
E4-2	4 walls, 25-rayl FM, 1/2-in. CPF 3-900
E5-2	4 walls, 25-rayl FM, 1/2-in. CPF 4-900
E6-2	4 walls, 25-rayl FM, 1/4-in. Air
E7-2	4 walls, 25-rayl FM, 1/4-in. CPF 3-900
E8-2	2 circumferential walls, 25-rayl FM, 1/2 in. Air; 2 radial walls, hardwall
E9-2	2 circumferential walls, 25-rayl FM, 1/2-in. CPF 3-900; 2 radial walls, hardwall
E10-2	2 circumferential walls, 25-rayl FM, 1/2-in. CPF 4-900; 2 radial walls, hardwall

TABLE VII. – SOUND-PRESSURE LEVELS FROM CENTER FAN-DISCHARGE DUCT TESTS

(Blower system runs)

Conf. code (a)	Chamber number (b)	Sound-pressure level, dB re 0.0002 microbar						
		One-third octave-band center frequency, Hz						
		1600	2000	2500	3150	4000	5000	6300
A1-2	1	131.5	131.5	131.0	130.0	129.5	127.0	126.5
	2	119.0	117.0	115.0	113.0	110.0	106.5	104.5
A2-2	1	134.0	132.5	131.5	131.0	129.5	128.5	128.0
	2	119.0	117.0	114.5	113.0	109.5	106.0	103.5
A3-2	1	136.0	134.5	132.5	133.0	131.0	130.0	131.0
	2	109.0	103.5	99.5	97.5	95.0	93.0	92.0
A4-2	1	134.5	132.0	131.0	131.0	128.5	127.5	127.5
	2	103.5	101.5	99.0	98.5	96.5	93.5	92.0
A5-2	1	136.0	134.5	133.0	133.5	132.5	130.5	130.0
	2	106.0	102.5	100.5	100.5	98.0	95.0	93.0
A6-2	1	137.5	134.5	132.5	132.5	131.0	130.0	130.0
	2	115.5	110.5	105.5	103.0	99.0	96.0	94.0
A7-2	1	134.0	133.5	132.5	132.0	130.0	128.0	127.5
	2	114.5	112.0	108.0	104.5	99.5	95.5	92.0
A8-2	1	137.0	134.5	133.5	132.5	132.0	131.0	130.5
	2	114.0	106.5	101.0	98.5	97.0	95.0	94.0
A9-2	1	136.0	135.0	133.5	132.5	132.0	130.0	130.5
	2	110.5	106.0	100.0	98.5	97.0	95.5	94.0
A10-2	1	137.0	134.0	133.5	134.0	133.0	131.0	131.0
	2	114.0	109.5	105.5	103.5	100.0	96.0	95.0
A11-2	1	134.0	132.5	132.0	131.5	132.0	128.0	128.0
	2	115.0	114.0	110.0	108.0	102.5	97.5	93.5
A12-2	1	132.5	130.0	130.0	130.5	129.0	127.5	127.5
	2	112.0	107.0	102.0	98.0	93.5	90.0	89.0
A13-2	1	133.0	132.0	131.5	131.5	131.0	128.5	128.0
	2	108.5	106.0	103.5	101.5	98.0	94.5	93.5
A14-2	1	134.0	131.0	130.5	130.5	128.5	127.5	127.5
	2	114.0	109.0	106.0	103.5	99.0	97.5	92.5
A15-2	1	133.5	132.0	130.5	130.5	129.5	128.5	128.0
	2	115.5	112.0	108.5	106.5	101.5	98.0	98.0
A16-2	1	134.0	132.0	131.5	131.5	130.0	128.5	128.5
	2	112.5	106.5	101.5	100.5	99.0	97.0	95.5
A17-2	1	134.0	132.5	132.0	131.5	131.0	129.5	129.0
	2	112.0	106.0	101.0	101.0	99.0	97.5	96.5
A18-2	1	132.5	131.0	130.5	130.5	130.5	128.5	128.5
	2	113.5	107.5	105.0	103.5	100.0	96.5	94.5
A19-2	1	134.0	132.0	130.5	130.5	129.5	128.5	129.0
	2	117.0	112.0	109.0	106.5	101.5	98.0	97.0
A20-2	1	133.5	132.0	131.0	131.0	130.0	129.0	128.5
	2	113.5	108.5	104.5	103.0	101.0	98.0	97.0
A21-2	1	134.0	132.0	131.0	131.5	130.5	129.5	128.5
	2	114.0	108.0	105.0	104.0	101.0	99.0	97.5
A22-2	1	133.0	132.5	131.5	131.0	129.5	128.0	128.0
	2	103.5	101.5	99.0	98.0	94.5	92.0	90.5
A23-2	1	132.0	128.5	129.0	129.0	127.0	126.5	126.5
	2	115.0	111.0	107.0	102.5	97.0	94.0	92.5
A24-2	1	132.0	130.5	130.0	129.5	129.0	127.0	127.0
	2	111.0	104.0	97.5	94.5	93.5	92.5	91.5
A25-2	1	134.5	132.5	131.0	130.0	129.5	128.5	128.5
	2	112.5	109.0	104.0	100.5	96.0	93.5	92.5
A26-2	1	135.0	133.5	131.0	131.0	128.5	128.5	129.0
	2	107.5	104.0	99.0	95.0	92.0	89.5	88.5

[a]See table IV for explanation of configuration code

[b]Chamber number 1 is the upstream or sound source chamber, chamber number 2 is the downstream or sound receiver chamber

TABLE VIII. – SOUND PRESSURE LEVELS FROM CENTER FAN-DISCHARGE DUCT TESTS

(Vacuum system runs)

Conf. code (a)	Chamber number (b)	Sound-pressure level, dB re 0.0002 microbar						
		One-third octave-band center frequency, Hz						
		1600	2000	2500	3150	4000	5000	6300
(F1-2)	1	88.5	86.0	88.0	86.0	81.5	85.0	81.5
	2	98.0	94.5	93.0	90.0	87.0	84.5	85.5
(F3-2)	1	92.5	91.5	93.0	91.5	88.5	87.5	89.5
	2	100.5	94.5	93.5	92.0	88.0	86.0	85.5
(F4-2)	1	102.0	91.5	91.5	89.5	87.0	86.5	89.0
	2	102.0	95.5	93.0	90.5	87.0	86.0	85.5
F1-2	1	135.5	133.0	132.0	131.5	130.5	129.0	129.5
	2	124.0	119.5	118.0	117.0	114.5	110.0	108.5
F1-3	1	136.5	133.0	132.5	131.5	130.5	128.5	127.5
	2	123.5	119.5	117.0	115.0	112.5	109.5	106.5
F2-1	1	137.0	136.5	135.5	136.0	135.0	132.0	133.0
	2	124.0	121.5	120.0	119.0	116.0	112.0	110.0
F2-2	1	137.5	136.0	136.0	136.0	134.5	133.0	133.5
	2	123.5	121.0	120.0	118.5	116.0	112.0	109.0
F3-2	1	139.0	136.0	135.5	135.0	134.0	132.5	132.5
	2	123.0	118.0	116.5	114.5	112.0	109.5	108.5
F3-3	1	134.5	135.5	134.5	133.5	132.0	130.5	130.5
	2	120.0	119.0	117.0	114.5	111.5	109.0	107.0
F4-2	1	135.5	136.5	136.5	136.5	135.5	133.5	132.0
	2	119.0	118.5	117.0	115.5	113.5	108.5	107.5
F4-3	1	138.5	136.0	134.5	134.5	133.0	131.5	131.0
	2	123.5	118.5	116.0	114.0	111.5	108.5	106.0
F5-2	1	135.5	130.5	130.5	130.0	129.0	127.5	127.5
	2	109.5	101.5	99.0	97.5	96.0	94.5	95.0
F5-3	1	——	131.5	130.5	130.0	129.0	127.0	127.0
	2	——	101.0	96.5	96.0	95.0	93.0	93.5
F6-2	1	137.0	133.0	133.0	132.5	132.0	132.0	131.0
	2	112.0	104.0	99.5	97.5	96.0	94.5	93.5
F6-3	1	137.5	134.0	133.0	133.0	131.5	130.0	129.5
	2	110.5	101.5	96.0	95.5	95.0	93.5	92.5
F7-1	1	136.5	135.5	135.0	135.0	134.0	132.0	132.0
	2	116.0	112.0	109.0	108.0	106.0	104.0	103.0
F7-2	1	136.0	136.0	136.0	136.0	135.0	132.5	133.0
	2	112.5	110.0	107.0	106.0	105.0	101.5	102.0
F8-1	1	135.5	134.5	133.5	133.5	132.0	131.0	131.5
	2	122.0	120.0	118.0	115.0	113.5	111.0	109.0
F8-2	1	138.0	136.5	136.0	136.5	134.5	133.0	133.0
	2	121.0	118.5	117.0	115.5	113.0	110.0	108.0
F9-1	1	137.0	135.0	134.5	134.0	113.0	132.0	132.0
	2	119.5	115.5	113.0	112.0	109.0	107.5	106.5
F9-2	1	137.0	136.5	135.0	135.0	133.5	131.5	132.5
	2	119.0	115.0	113.0	112.0	110.0	107.5	106.0
F10-1	1	136.0	134.0	134.0	134.0	133.0	131.0	131.5
	2	118.0	114.0	110.5	109.5	107.5	105.5	104.5
F10-2	1	136.5	136.0	135.0	135.5	133.0	131.0	131.0
	2	116.5	113.0	109.0	108.5	107.5	105.0	103.0
F11-2	1	135.5	132.5	132.5	133.5	132.0	129.5	129.5
	2	110.5	104.5	101.0	100.5	98.0	95.0	95.0
F11-3	1	134.5	132.0	131.0	131.5	129.0	127.5	128.0
	2	113.5	104.5	100.0	98.5	97.0	94.5	93.0
F12-2	1	137.0	134.0	132.5	132.5	131.5	129.5	129.0
	2	111.0	102.5	98.5	97.0	96.0	94.5	93.5
F12-3	1	137.0	133.5	132.5	132.0	131.0	130.0	130.0
	2	113.0	107.5	101.0	99.5	97.5	96.0	95.5
F13-2	1	136.5	132.0	132.0	131.5	131.0	129.5	129.0
	2	112.5	103.0	100.5	99.0	96.5	94.5	94.5
F13-3	1	133.0	131.0	130.5	130.5	129.5	127.5	126.5
	2	109.5	100.5	97.5	96.0	95.5	92.5	92.0
F14-2	1	135.0	133.5	132.5	133.0	131.0	128.5	128.5
	2	110.0	102.5	97.0	95.5	95.0	93.0	92.0
F14-3	1	136.0	133.0	132.5	132.5	131.5	130.0	130.5
	2	111.5	105.5	100.0	98.0	96.5	94.5	94.0
F15-2	1	137.0	134.0	133.0	132.5	131.0	129.5	129.5
	2	110.5	101.5	96.0	92.5	92.0	91.0	88.5
F15-3	1	137.5	135.0	133.5	133.0	131.5	131.0	130.5
	2	113.5	104.0	98.0	95.5	93.0	92.5	91.5

[a] See table V for explanation of configuration code

[b] Chamber number 1 is the upstream or sound source chamber, chamber number 2 is the downstream or sound receiver chamber

TABLE IX. – SOUND-PRESSURE LEVELS FROM END FAN-DISCHARGE DUCT TESTS

Conf. code (a)	Chamber number (b)	Sound-pressure level, dB re 0.0002 microbar						
		8% narrow - band center frequency, Hz						
		1600	2000	2500	3150	4000	5000	6300
E1-2	1	131.5	129.0	128.0	128.5	127.5	126.5	126.5
	2	116.5	113.5	112.5	111.0	108.5	104.5	103.0
E2-2	1	129.0	128.5	128.0	128.0	127.5	126.0	126.0
	2	102.0	97.5	95.5	94.0	91.5	89.0	88.0
E3-2	1	128.5	128.0	128.0	128.5	128.0	126.0	126.5
	2	104.5	103.5	103.5	102.5	99.0	94.0	91.0
E4-2	1	132.5	131.0	130.0	129.0	129.0	126.5	126.5
	2	101.5	98.5	96.0	93.0	90.0	88.5	86.5
E5-2	1	130.5	129.0	129.5	129.0	128.5	126.5	126.5
	2	102.5	100.0	97.5	95.5	92.5	90.5	90.0
E6-2	1	129.5	128.5	128.0	128.5	128.0	125.5	125.5
	2	104.5	103.5	103.5	103.5	101.5	96.5	93.5
E7-2	1	130.0	129.5	129.0	128.5	128.5	126.5	126.5
	2	104.5	102.0	100.5	97.5	92.5	89.0	87.5
E8-2	1	127.5	127.0	127.5	128.0	127.0	125.5	125.0
	2	108.0	107.0	105.5	104.5	101.5	96.0	93.5
E9-2	1	129.5	131.0	129.5	128.5	129.0	126.5	126.5
	2	104.5	103.5	99.0	96.0	94.0	91.0	90.5
E10-2	1	127.5	125.5	125.5	128.0	127.5	126.0	125.5
	2	105.5	100.5	99.5	98.0	95.5	92.5	92.0

[a]See table VI for explanation of configuration code

[b]Chamber number 1 is the upstream or sound source chamber, chamber number 2 is the downstream or sound receiver chamber

TABLE X. – TRANSMISSION LOSS VALUES FROM CENTER FAN–DISCHARGE DUCT TESTS

(Blower system runs)

Conf. code (a)	Transmission loss, dB						
	One-third octave-band center frequency, Hz						
	1600	2000	2500	3150	4000	5000	6300
A1-2	12.5	14.5	16.0	17.0	19.5	20.5	22.0
A2-2	15.0	15.5	17.0	18.0	20.0	22.5	24.5
A3-2	27.0	31.0	33.0	35.0	36.0	37.0	39.0
A4-2	31.0	30.5	32.0	32.5	32.0	34.0	35.5
A5-2	30.0	32.0	32.5	33.5	34.5	35.5	37.0
A6-2	22.0	24.0	27.0	29.5	32.0	34.0	36.0
A7-2	19.5	21.5	24.5	27.5	30.5	32.5	35.5
A8-2	23.0	28.0	32.5	34.0	35.0	36.0	36.5
A9-2	25.5	29.0	33.5	34.0	35.0	34.5	36.5
A10-2	23.0	24.5	28.0	30.5	33.0	35.0	36.0
A11-2	19.0	18.5	22.0	23.5	29.5	30.5	34.5
A12-2	20.5	23.0	28.0	32.5	35.5	37.5	38.5
A13-2	24.5	26.0	28.0	30.0	33.0	34.0	34.5
A14-2	20.0	22.0	24.5	27.0	29.5	33.0	35.0
A15-2	18.0	20.0	22.0	24.0	28.0	30.5	30.0
A16-2	21.5	25.5	30.0	31.0	31.0	31.5	33.0
A17-2	22.0	26.5	30.5	30.5	32.0	32.0	32.5
A18-2	19.0	23.5	25.5	27.0	30.5	32.0	34.0
A19-2	17.0	20.0	21.5	24.0	28.0	30.5	32.0
A20-2	20.0	23.5	26.5	28.0	29.0	31.0	31.5
A21-2	20.0	24.0	26.0	27.5	29.5	30.5	31.0
A22-2	29.5	31.0	32.5	33.0	35.0	36.0	37.5
A23-2	17.0	17.5	22.0	26.5	30.0	32.5	34.0
A24-2	21.0	26.0	32.5	35.0	35.5	34.5	35.5
A25-2	22.0	23.5	27.0	29.5	33.5	35.0	36.0
A26-2	27.5	29.5	32.5	36.0	36.5	39.0	40.5

[a]See table IV for explanation of configuration code

TABLE XI. – TRANSMISSION LOSS VALUES FROM CENTER FAN–DISCHARGE DUCT TESTS

(Vacuum system runs)

Conf. code (a)	Transmission loss, dB						
	One-third octave-band center frequency, Hz						
	1600	2000	2500	3150	4000	5000	6300
F1-2	11.5	13.5	14.0	14.5	16.0	19.0	21.0
F1-3	13.0	13.5	15.5	16.5	18.0	19.0	21.0
F2-1	13.0	15.0	15.5	17.0	19.0	20.5	23.0
F2-2	14.0	15.0	16.0	17.5	18.5	21.0	24.5
F3-2	16.0	17.5	19.0	20.5	22.0	23.0	24.0
F3-3	14.5	16.5	17.5	19.0	20.5	21.5	23.5
F4-2	16.5	18.0	19.5	21.0	22.0	25.0	24.5
F4-3	15.0	17.5	18.5	20.5	21.5	23.0	25.0
F5-2	26.0	29.0	31.5	32.5	33.0	33.0	32.5
F5-3	——	30.5	34.0	34.0	34.0	34.0	33.5
F6-2	25.0	29.0	33.5	35.0	36.0	37.5	37.5
F6-3	27.0	32.5	37.0	37.5	36.5	36.5	37.0
F7-1	20.5	23.5	26.0	27.0	28.0	28.0	29.0
F7-2	23.5	26.0	29.0	30.0	30.0	31.0	31.0
F8-1	13.5	14.5	15.5	18.5	18.5	20.0	22.5
F8-2	17.0	18.0	19.0	21.0	21.5	23.0	25.0
F9-1	17.5	19.5	21.5	22.0	24.0	24.5	24.5
F9-2	18.0	21.5	22.0	23.0	23.5	24.0	26.5
F10-1	18.0	20.0	23.5	24.5	25.5	25.5	27.0
F10-2	20.0	23.0	26.0	27.0	25.5	26.0	28.0
F11-2	25.0	28.0	31.5	33.0	34.0	34.5	34.5
F11-3	21.0	27.5	31.0	33.0	32.0	33.0	35.0
F12-2	26.0	31.5	34.0	35.5	35.5	35.0	35.5
F12-3	24.0	26.0	31.5	32.5	33.5	34.0	34.5
F13-2	24.0	29.0	31.5	32.5	34.5	35.0	34.5
F13-3	23.5	30.5	33.0	34.5	34.0	35.0	34.5
F14-2	25.0	31.0	35.5	37.5	36.0	35.5	36.5
F14-3	24.5	27.5	32.5	34.5	35.0	35.5	36.5
F15-2	26.5	32.5	37.0	40.0	39.0	38.5	41.0
F15-3	24.0	31.0	35.5	37.5	38.5	38.5	39.0

[a]See table V for explanation of configuration code

TABLE XII. – TRANSMISSION LOSS VALUES FROM END FAN-DISCHARGE DUCT TESTS

Conf. code (a)	Transmission loss, dB						
	8% narrow - band center frequency, Hz						
	1600	2000	2500	3150	4000	5000	6300
E1-2	15.0	15.5	15.5	17.5	19.0	22.0	23.5
E2-2	27.0	31.0	32.5	34.0	36.0	37.0	38.0
E3-2	24.0	24.5	24.5	26.0	29.0	32.0	35.5
E4-2	31.0	32.5	34.0	36.0	39.0	38.0	40.0
E5-2	28.0	29.0	32.0	33.5	36.0	36.0	36.5
E6-2	25.0	25.0	24.5	25.0	26.5	29.0	32.0
E7-2	25.5	27.5	28.5	31.0	36.0	37.5	39.0
E8-2	19.5	20.0	22.0	23.5	25.5	29.5	31.5
E9-2	25.0	27.5	30.5	32.5	35.0	35.5	36.0
E10-2	22.0	25.0	26.0	30.0	32.0	33.5	33.5

[a]See table VI for explanation of configuration code

TABLE XIII. – ATTENUATION VALUES FROM CENTER FAN–DISCHARGE DUCT TESTS

(Blower system runs)

Conf. code (a)	Attenuation, dB						
	One-third octave-band center frequency, Hz						
	1600	2000	2500	3150	4000	5000	6300
A3-2	14.5	16.5	17.0	18.5	16.5	16.5	17.0
A4-2	18.5	16.0	16.0	15.5	12.5	13.5	13.5
A5-2	17.5	17.5	16.5	16.5	15.0	15.0	15.0
A6-2	9.5	9.5	11.0	12.5	12.5	13.5	14.0
A7-2	7.0	7.0	8.5	10.5	11.0	12.0	13.5
A8-2	10.5	13.5	16.5	17.0	15.5	15.5	14.5
A9-2	13.0	14.5	17.5	17.0	15.5	14.0	14.5
A10-2	10.5	10.0	12.0	13.5	13.5	14.5	14.0
A11-2	6.5	4.0	6.0	6.5	10.0	10.0	12.5
A12-2	8.0	8.5	12.0	15.5	16.0	17.0	16.5
A13-2	12.0	11.5	12.0	13.0	13.5	13.5	12.5
A14-2	7.5	7.5	8.5	10.0	10.0	12.5	13.0
A15-2	5.5	5.5	6.0	7.0	8.5	10.0	8.0
A16-2	9.0	11.0	14.0	14.0	11.5	11.0	11.0
A17-2	9.5	12.0	14.5	13.5	12.5	11.5	10.5
A18-2	6.5	9.0	9.5	10.0	11.0	11.5	12.0
A19-2	4.5	5.5	5.5	7.0	8.5	10.0	10.0
A20-2	7.5	9.0	10.5	11.0	9.5	10.5	9.5
A21-2	7.5	9.5	10.0	10.5	10.0	10.0	9.0
A22-2	17.0	16.5	16.5	16.0	15.5	15.5	15.5
A23-2	2.0	2.0	5.0	8.5	10.0	10.0	9.5
A24-2	6.0	10.5	15.5	17.0	15.5	12.0	11.0
A25-2	7.0	8.0	10.0	11.5	13.5	12.5	11.5
A26-2	12.5	14.0	15.5	18.0	16.5	16.5	16.0

[a]See table IV for explanation of configuration code

TABLE XIV. – ATTENUATION VALUES FROM CENTER FAN–DISCHARGE DUCT TESTS

(Vacuum system runs)

Conf. code (a)	Attenuation, dB						
	One-third octave-band center frequency, Hz						
	1600	2000	2500	3150	4000	5000	6300
F5-2	14.5	15.5	17.5	18.0	17.0	14.0	11.5
F5-3	——	17.0	18.5	17.5	16.0	15.0	12.5
F6-2	13.5	15.5	19.5	20.5	20.0	18.5	16.5
F6-3	14.0	19.0	21.5	21.0	18.5	17.5	16.0
F7-1	7.5	8.5	10.5	10.0	9.0	7.5	6.0
F7-2	9.5	11.0	13.0	12.5	11.5	10.0	6.5
F8-1	0.5	-0.5	0.0	1.5	-0.5	-0.5	-0.5
F8-2	3.0	3.0	3.0	3.5	3.0	2.0	0.5
F9-1	4.5	4.5	6.0	5.0	5.0	4.0	1.5
F9-2	4.0	6.5	6.0	5.5	5.0	3.0	2.0
F10-1	5.0	5.0	8.0	7.5	6.5	5.0	4.0
F10-2	6.0	8.0	10.0	9.5	7.0	5.0	3.5
F11-2	9.0	10.5	12.5	12.5	12.0	11.5	10.5
F11-3	6.5	11.0	13.5	14.0	11.5	11.5	11.5
F12-2	10.0	14.0	15.0	15.0	13.5	12.0	11.5
F12-3	9.5	9.5	14.0	13.5	13.0	12.5	11.0
F13-2	8.0	11.5	12.5	12.0	12.5	12.0	10.5
F13-3	9.0	14.0	15.5	15.5	13.5	13.5	11.0
F14-2	9.0	13.5	16.5	17.0	14.0	12.5	12.5
F14-3	10.0	11.0	15.0	15.5	14.5	14.0	13.0
F15-2	10.0	14.5	17.5	19.0	17.0	13.5	16.5
F15-3	9.0	13.5	17.0	17.0	17.0	15.5	14.0

[a]See table V for explanation of configuration code

TABLE XV. – ATTENUATION VALUES FROM END FAN-DISCHARGE DUCT TESTS

Conf. code (a)	Attenuation, dB						
	8% narrow - band center frequency, Hz						
	1600	2000	2500	3150	4000	5000	6300
E2-2	12.0	15.5	17.0	16.5	17.0	15.0	15.0
E3-2	9.0	9.0	9.0	8.5	10.0	10.0	12.5
E4-2	16.0	17.0	18.5	18.5	20.0	16.0	17.0
E5-2	13.0	13.5	16.5	16.0	17.0	14.0	13.5
E6-2	10.0	9.5	9.0	7.5	7.5	7.0	9.0
E7-2	10.5	12.0	13.0	13.5	17.0	15.5	16.0
E8-2	4.5	4.5	6.5	6.0	6.5	7.5	8.5
E9-2	10.0	12.0	15.0	15.0	16.0	13.5	13.0
E10-2	7.0	9.5	10.5	12.5	13.0	11.5	10.5

[a]See table VI for explanation of configuration code

TABLE XVI.–TEST OUTLINE AND CONFIGURATIONS FOR INLET DUCT TESTS

Outline for inlet-duct tests	Configurations		
	55%	75%	Standard
I. Hardwall	B1	D1	C1
II. Cowl surface treatment only, (all three panels)			
A. 25-rayl FM			
1. One-in. deep cavity			
a. Air	B2, B3	D2	C2
b. CPF 3-900	B4	——	——
c. CPF 4-900	B5, B6	——	——
d. 1/2-in. air, 1/2-in. CPF 4-900	B7	——	——
e. Fiberglass (FG)	B8	——	——
2. 1/2-in. deep cavity			
a. Air	B9, B10	——	——
b. CPF 3-900	B11	——	——
c. CPF 4-900	B12, B13	——	C3
B. 60-rayl FM			
1. One-in. deep cavity			
a. Air	B14	——	——
2. 1/2-in. deep cavity			
a. Air	B15	——	——
c. CPF 4-900	B16	——	——
III. Cowl and centerbody treated; all panels have same treatment			
A. 25-rayl FM			
1. One-in. deep cavity			
a. Air	——	D3	C4
c. CPF 4-900	B17	——	——
d. Fiberglass (FG)	B18, B19	——	——
2. 1/2-in. deep cavity			
b. CPF 3-900	——	D4	C5
c. CPF 4-900	B20	D5	C6
d. Fiberglass (FG)	B21, B22	——	——
B. 60-rayl FM			
1. One-in. deep cavity			
a. Air	——	D6	C7
2. 1/2-in. deep cavity			
c. CPF 4-900	B23	——	——
IV. Variations in area of treatment for one configuration: 1/2-in. CPF 4-900 under 25-rayl FM			
55% $107.2\ in^2$	B24	——	C8
108.9	B25	——	C9
216.1	B26	——	C10
313.7	B27	——	C11
420.9	B28	——	C12
526.7	B29	——	——
598.8	B30	——	——
633.9	B31	——	——
696.4	B32	——	——
Standard $47.6\ in^2$			
115.8			
163.4			
232.1			
279.7			

	Total area of treatment, in^2		
Cowl only	587.5	763.5	343.7
Cowl plus centerbody	803.6	1012.3	391.3

TABLE XVII.–EXPLANATION OF CONFIGURATION CODE FOR 55% LIGHTBULT INLET DUCT TESTS

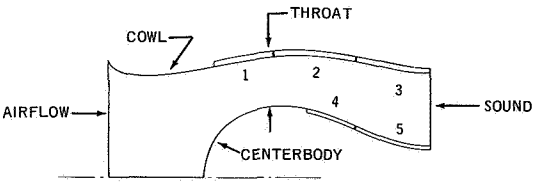

(See figure 33b for panel dimensions and areas)

Conf. code	Average throat velocity, ft/sec	Cowl surface treatment		Centerbody surface treatment	
		Description (a)	Panels (b)	Description (a)	Panels (b)
B1-1	465	Hardwall	—	Hardwall	—
B1-2	372	Hardwall	—	Hardwall	—
B1-3	286	Hardwall	↕	Hardwall	↕
B1-4	213	Hardwall	↕	Hardwall	↕
B1-5	137	Hardwall	↕	Hardwall	↕
B1-6	75	Hardwall	↕	Hardwall	↕
(B1-1)[c]	465	Hardwall	↕	Hardwall	↕
(B1-2)	372	Hardwall	↕	Hardwall	↕
(B1-3)	286	Hardwall	↕	Hardwall	↕
(B1-4)	213	Hardwall	—	Hardwall	↕
B2-1	465	25-rayl FM, 1-in. Air	1, 2, 3	Hardwall	↕
B2-2	372	25-rayl FM, 1-in. Air	1, 2, 3	Hardwall	↕
B3-1	465	25-rayl Al FM, 1-in. Air	1, 2, 3	Hardwall	↕
B3-2	372	25-rayl Al FM, 1-in. Air	1, 2, 3	Hardwall	↕
B4-1	465	25-rayl FM, 1-in. CPF 3-900	1, 2, 3	Hardwall	↕
B4-2	372	25-rayl FM, 1-in. CPF 3-900	1, 2, 3	Hardwall	↕
B5-1	465	25-rayl FM, 1-in. CPF 4-900	1, 2, 3	Hardwall	↕
B5-2	372	25-rayl FM, 1-in. CPF 4-900	1, 2, 3	Hardwall	↕
B6-1	465	25-rayl Al FM, 1-in. CPF 4-900	1, 2, 3	Hardwall	↕
B6-2	372	25-rayl Al FM, 1-in. CPF 4-900	1, 2, 3	Hardwall	↕
B7-1	465	25-rayl FM 1/2-in. Air, 1/2-in. CPF4-900	1, 2, 3	Hardwall	↕
B7-2	372	25-rayl FM 1/2-in. Air, 1/2-in. CPF4-900	1, 2, 3	Hardwall	↕
B8-1	465	25-rayl Al FM, 1-in. FG 1.2 lb/ft^3	1, 2, 3	Hardwall	↕
B8-2	372	25-rayl Al FM, 1-in. FG 1.2 lb/ft^3	1, 2, 3	Hardwall	↕
B9-1	465	25-rayl FM, 1/2-in. Air	1, 2, 3	Hardwall	↕
B9-2	372	25-rayl FM, 1/2-in. Air	1, 2, 3	Hardwall	↕
B10-1	465	25-rayl Al FM, 1/2-in. Air	1, 2, 3	Hardwall	↕
B10-2	372	25-rayl Al FM, 1/2-in. Air	1, 2, 3	Hardwall	↕
B11-1	465	25-rayl FM, 1/2-in. CPF 3-900	1, 2, 3	Hardwall	↕
B11-2	372	25-rayl FM, 1/2-in. CPF 3-900	1, 2, 3	Hardwall	↕
B12-1	465	25-rayl FM, 1/2-in. CPF 4-900	1, 2, 3	Hardwall	↕
B12-2	372	25-rayl FM, 1/2-in. CPF 4-900	1, 2, 3	Hardwall	↕
B12-3	286	25-rayl FM, 1/2-in. CPF 4-900	1, 2, 3	Hardwall	↕
B12-4	213	25-rayl FM, 1/2-in. CPF 4-900	1, 2, 3	Hardwall	↕
B12-5	137	25-rayl FM, 1/2-in. CPF 4-900	1, 2, 3	Hardwall	↕
B12-6	75	25-rayl FM, 1/2-in. CPF 4-900	1, 2, 3	Hardwall	↕
B13-1	465	25-rayl Al FM, 1/2-in. CPF 4-900	1, 2, 3	Hardwall	↕
B13-2	372	25-rayl Al FM, 1/2-in. CPF 4-900	1, 2, 3	Hardwall	↕
B14-1	465	60-rayl FM, 1-in. Air	1, 2, 3	Hardwall	↕
B14-2	372	60-rayl FM, 1-in. Air	1, 2, 3	Hardwall	↕
B15-1	465	60-rayl FM, 1/2-in. Air	1, 2, 3	Hardwall	—
B15-2	372	60-rayl FM, 1/2-in. Air	1, 2, 3	Hardwall	—

[a] Al FM = Aluminum fibermetal made from aluminum fibers, about 0.038-in. thick sheets, no screen reinforcing, about 60% dense and 0.33 lb/ft^2

[b] See sketch above for location of panels by number; panels not listed have solid sheet-aluminum surfaces

[c] Configuration codes in parentheses represent background noise tests run with airflow only, transducers off

TABLE XVII.—Concluded

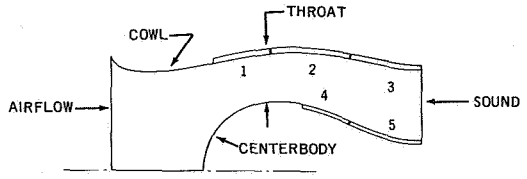

(See figure 33b for panel dimensions and areas)

Conf. code	Average throat velocity, ft/sec	Cowl surface treatment		Centerbody surface treatment	
		Description	Panels (a)	Description	Panels (a)
B16-1	465	60-rayl FM, 1/2-in. CPF 4-900	1, 2, 3	Hardwall	—
B16-2	372	60-rayl FM, 1/2-in. CPF 4-900	1, 2, 3	Hardwall	—
B17-1	465	25-rayl FM, 1-in. CPF 4-900	1, 2, 3	25-rayl FM, 1-in. CPF 4-900	4, 5
B17-2	372	25-rayl FM, 1-in. CPF 4-900	1, 2, 3	25-rayl FM, 1-in. CPF 4-900	4, 5
B18-1	465	25-rayl FM, 1-in. FG 0.6 lb/ft^3	1, 2, 3	25-rayl FM, 1-in. FG 0.6 lb/ft^3	4, 5
B18-2	372	25-rayl FM, 1-in. FG 0.6 lb/ft^3	1, 2, 3	25-rayl FM, 1-in. FG 0.6 lb/ft^3	4, 5
B19-1	465	25-rayl FM, 1-in. FG 1.2 lb/ft^3	1, 2, 3	25-rayl FM, 1-in. FG 1.2 lb/ft^3	4, 5
B19-2	372	25-rayl FM, 1-in. FG 1.2 lb/ft^3	1, 2, 3	25-rayl FM, 1-in. FG 1.2 lb/ft^3	4, 5
B20-1	465	25-rayl FM, 1/2-in. CPF 4-900	1, 2, 3	25-rayl FM, 1/2-in. CPF 4-900	4, 5
B20-2	372	25-rayl FM, 1/2-in. CPF 4-900	1, 2, 3	25-rayl FM, 1/2-in. CPF 4-900	4, 5
B20-3	286	25-rayl FM, 1/2-in. CPF 4-900	1, 2, 3	25-rayl FM, 1/2-in. CPF 4-900	4, 5
B20-4	213	25-rayl FM, 1/2-in. CPF 4-900	1, 2, 3	25-rayl FM, 1/2-in. CPF 4-900	4, 5
B20-5	137	25-rayl FM, 1/2-in. CPF 4-900	1, 2, 3	25-rayl FM, 1/2-in. CPF 4-900	4, 5
B20-6	75	25-rayl FM, 1/2-in. CPF 4-900	1, 2, 3	25-rayl FM, 1/2-in. CPF 4-900	4, 5
B21-1	465	25-rayl FM, 1/2-in. FG 1.2 lb/ft^3	1, 2, 3	25-rayl FM, 1/2-in. FG 1.2 lb/ft^3	4, 5
B21-2	372	25-rayl FM, 1/2-in. FG 1.2 lb/ft^3	1, 2, 3	25-rayl FM, 1/2-in. FG 1.2 lb/ft^3	4, 5
B22-1	465	25-rayl FM, 1/2-in. FG 2.4 lb/ft^3	1, 2, 3	25-rayl FM, 1/2-in. FG 2.4 lb/ft^3	4, 5
B22-2	372	25-rayl FM, 1/2-in. FG 2.4 lb/ft^3	1, 2, 3	25-rayl FM, 1/2-in. FG 2.4 lb/ft^3	4, 5
B23-1	465	60-rayl FM, 1/2-in. CPF 4-900	1, 2, 3	60-rayl FM, 1/2-in. CPF 4-900	4, 5
B23-2	372	60-rayl FM, 1/2-in. CPF 4-900	1, 2, 3	60-rayl FM, 1/2-in. CPF 4-900	4, 5
B23-3	286	60-rayl FM, 1/2-in. CPF 4-900	1, 2, 3	60-rayl FM, 1/2-in. CPF 4-900	4, 5
B23-4	213	60-rayl FM, 1/2-in. CPF 4-900	1, 2, 3	60-rayl FM, 1/2-in. CPF 4-900	4, 5
B23-5	137	60-rayl FM, 1/2-in. CPF 4-900	1, 2, 3	60-rayl FM, 1/2-in. CPF 4-900	4, 5
B23-6	75	60-rayl FM, 1/2-in. CPF 4-900	1, 2, 3	60-rayl FM, 1/2-in. CPF 4-900	4, 5
B24-1	465	Hardwall	—	25-rayl FM, 1/2-in. CPF 4-900	4
B24-2	372	Hardwall	—	25-rayl FM, 1/2-in. CPF 4-900	4
B25-1	465	Hardwall	—	25-rayl FM, 1/2-in. CPF 4-900	5
B25-2	372	Hardwall	—	25-rayl FM, 1/2-in. CPF 4-900	5
B26-1	465	Hardwall	—	25-rayl FM, 1/2-in. CPF 4-900	4, 5
B26-2	372	Hardwall	—	25-rayl FM, 1/2-in. CPF 4-900	4, 5
B27-1	465	25-rayl FM, 1/2-in. CPF 4-900	3	25-rayl FM, 1/2-in. CPF 4-900	5
B27-2	372	25-rayl FM, 1/2-in. CPF 4-900	3	25-rayl FM, 1/2-in. CPF 4-900	5
B28-1	465	25-rayl FM, 1/2-in. CPF 4-900	3	25-rayl FM, 1/2-in. CPF 4-900	4, 5
B28-2	372	25-rayl FM, 1/2-in. CPF 4-900	3	25-rayl FM, 1/2-in. CPF 4-900	4, 5
B29-1	465	25-rayl FM, 1/2-in. CPF 4-900	2, 3	25-rayl FM, 1/2-in. CPF 4-900	5
B29-2	372	25-rayl FM, 1/2-in. CPF 4-900	2, 3	25-rayl FM, 1/2-in. CPF 4-900	5
B30-1	465	25-rayl FM, 1/2-in. CPF 4-900	1, 2	25-rayl FM, 1/2-in. CPF 4-900	4, 5
B30-2	372	25-rayl FM, 1/2-in. CPF 4-900	1, 2	25-rayl FM, 1/2-in. CPF 4-900	4, 5
B31-1	465	25-rayl FM, 1/2-in. CPF 4-900	2, 3	25-rayl FM, 1/2-in. CPF 4-900	4, 5
B31-2	372	25-rayl FM, 1/2-in. CPF 4-900	2, 3	25-rayl FM, 1/2-in. CPF 4-900	4, 5
B32-1	465	25-rayl FM, 1/2-in. CPF 4-900	1, 2, 3	25-rayl FM, 1/2-in. CPF 4-900	5
B32-2	372	25-rayl FM, 1/2-in. CPF 4-900	1, 2, 3	25-rayl FM, 1/2-in. CPF 4-900	5

[a]See sketch above for location of panels by number; panels not listed have solid sheet-aluminum surfaces

TABLE XVIII. — EXPLANATION OF CONFIGURATION CODE FOR 75% LIGHTBULB INLET DUCT TESTS

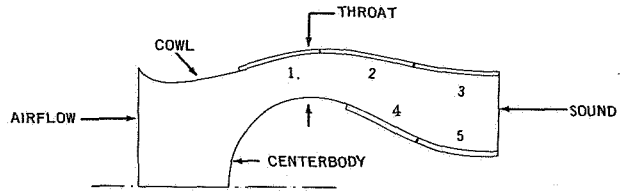

(See figure 33c for panel dimensions and areas)

Conf. code	Average throat velocity, ft/sec	Cowl surface treatment		Centerbody surface treatment	
		Description	Panels (a)	Description	Panels (a)
D1-1	465	Hardwall	—	Hardwall	—
D1-2	372	Hardwall	—	Hardwall	—
D1-3	286	Hardwall	↕	Hardwall	↕
D1-4	213	Hardwall	↕	Hardwall	↕
D1-5	137	Hardwall	↕	Hardwall	↕
D1-6	75	Hardwall	↕	Hardwall	↕
(D1-1)[b]	465	Hardwall	↕	Hardwall	↕
(D1-2)	372	Hardwall	↕	Hardwall	↕
(D1-3)	286	Hardwall	↕	Hardwall	↕
(D1-4)	213	Hardwall	↕	Hardwall	↕
(D1-5)	137	Hardwall	↕	Hardwall	↕
(D1-6)	75	Hardwall	—	Hardwall	↕
D2-1	465	25-rayl FM, 1-in. Air	1, 2, 3	Hardwall	—
D2-2	372	25-rayl FM, 1-in. Air	1, 2, 3	Hardwall	—
D3-1	465	25-rayl FM, 1-in. Air	1, 2, 3	25-rayl FM, 1-in. Air	4, 5
D3-2	372	25-rayl FM, 1-in. Air	1, 2, 3	25-rayl FM, 1-in. Air	4, 5
D4-1	465	25-rayl FM, 1/2-in. CPF 3-900	1, 2, 3	25-rayl FM, 1/2-in. CPF 3-900	4, 5
D4-2	372	25-rayl FM, 1/2-in. CPF 3-900	1, 2, 3	25-rayl FM, 1/2-in. CPF 3-900	4, 5
D5-1	465	25-rayl FM, 1/2-in. CPF 4-900	1, 2, 3	25-rayl FM, 1/2-in. CPF 4-900	4, 5
D5-2	372	25-rayl FM, 1/2-in. CPF 4-900	1, 2, 3	25-rayl FM, 1/2-in. CPF 4-900	4, 5
D5-3	286	25-rayl FM, 1/2-in. CPF 4-900	1, 2, 3	25-rayl FM, 1/2-in. CPF 4-900	4, 5
D5-4	213	25-rayl FM, 1/2-in. CPF 4-900	1, 2, 3	25-rayl FM, 1/2-in. CPF 4-900	4, 5
D5-5	137	25-rayl FM, 1/2-in. CPF 4-900	1, 2, 3	25-rayl FM, 1/2-in. CPF 4-900	4, 5
D5-6	75	25-rayl FM, 1/2-in. CPF 4-900	1, 2, 3	25-rayl FM, 1/2-in. CPF 4-900	4, 5
D6-1	465	60-rayl FM, 1-in. Air	1, 2, 3	60-rayl FM, 1-in. Air	4, 5
D6-2	372	60-rayl FM, 1-in. Air	1, 2, 3	60-rayl FM, 1-in. Air	4, 5

[a]See sketch above for location of panels by number; panels not listed have solid sheet-aluminum surfaces

[b]Configuration codes in parentheses represent background noise test run airflow only, transducers off

TABLE XIX. – EXPLANATION OF CONFIGURATION CODE FOR STANDARD DC-8 INLET DUCT TESTS

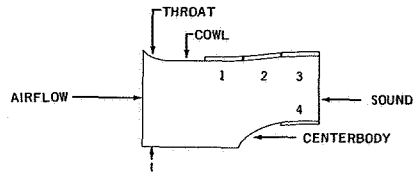

(See figure 33d for panel dimensions and areas)

Conf. code	Average throat velocity, ft/sec	Cowl surface treatment		Centerbody surface treatment	
		Description	Panels (a)	Description	Panels (a)
C1-1	358	Hardwall	—	Hardwall	—
C1-2	290	Hardwall	—	Hardwall	—
C1-3	225	Hardwall	↑	Hardwall	↑
C1-4	169	Hardwall	|	Hardwall	|
C1-5	110	Hardwall	|	Hardwall	|
C1-6	61	Hardwall	|	Hardwall	|
(C1-1)[b]	358	Hardwall	|	Hardwall	|
(C1-2)	290	Hardwall	|	Hardwall	|
(C1-3)	225	Hardwall	|	Hardwall	|
(C1-4)	169	Hardwall	|	Hardwall	|
(C1-5)	110	Hardwall	—	Hardwall	|
(C1-6)	61	Hardwall	—	Hardwall	|
C2-1	358	25-rayl FM, 1-in. Air	1, 2, 3	Hardwall	|
C2-2	290	25-rayl FM, 1-in. Air	1, 2, 3	Hardwall	↓
C3-1	358	25-rayl FM, 1/2-in. CPF 4-900	1, 2, 3	Hardwall	—
C3-2	290	25-rayl FM, 1/2-in. CPF 4-900	1, 2, 3	Hardwall	—
C4-1	358	25-rayl FM, 1-in. Air	1, 2, 3	25-rayl FM, 1-in. Air	4
C4-2	290	25-rayl FM, 1-in. Air	1, 2, 3	25-rayl FM, 1-in. Air	4
C5-1	358	25-rayl FM, 1/2-in. CPF 3-900	1, 2, 3	25-rayl FM, 1/2-in. CPF 3-900	4
C5-2	290	25-rayl FM, 1/2-in. CPF 3-900	1, 2, 3	25-rayl FM, 1/2-in. CPF 3-900	4
C6-1	358	25-rayl FM, 1/2-in. CPF 4-900	1, 2, 3	25-rayl FM, 1/2-in. CPF 4-900	4
C6-2	290	25-rayl FM, 1/2-in. CPF 4-900	1, 2, 3	25-rayl FM, 1/2-in. CPF 4-900	4
C6-3	225	25-rayl FM, 1/2-in. CPF 4-900	1, 2, 3	25-rayl FM, 1/2-in. CPF 4-900	4
C6-4	169	25-rayl FM, 1/2-in. CPF 4-900	1, 2, 3	25-rayl FM, 1/2-in. CPF 4-900	4
C6-5	110	25-rayl FM, 1/2-in. CPF 4-900	1, 2, 3	25-rayl FM, 1/2-in. CPF 4-900	4
C6-6	61	25-rayl FM, 1/2-in. CPF 4-900	1, 2, 3	25-rayl FM, 1/2-in. CPF 4-900	4
C7-1	358	60-rayl FM, 1-in. Air	1, 2, 3	60-rayl FM, 1-in. Air	4
C7-2	290	60-rayl FM, 1-in. Air	1, 2, 3	60-rayl FM, 1-in. Air	4
C8-1	358	Hardwall	—	25-rayl FM, 1/2-in. CPF 4-900	4
C8-2	290	Hardwall	—	25-rayl FM, 1/2-in. CPF 4-900	4
C9-1	358	25-rayl FM, 1/2-in. CPF 4-900	3	Hardwall	—
C9-2	290	25-rayl FM, 1/2-in. CPF 4-900	3	Hardwall	—
C10-1	358	25-rayl FM, 1/2-in. CPF 4-900	3	25-rayl FM, 1/2-in. CPF 4-900	4
C10-2	290	25-rayl FM, 1/2-in. CPF 4-900	3	25-rayl FM, 1/2-in. CPF 4-900	4
C11-1	358	25-rayl FM, 1/2-in. CPF 4-900	2, 3	Hardwall	—
C11-2	290	25-rayl FM, 1/2-in. CPF 4-900	2, 3	Hardwall	—
C12-1	358	25-rayl FM, 1/2-in. CPF 4-900	2, 3	25-rayl FM, 1/2-in. CPF 4-900	4
C12-2	290	25-rayl FM, 1/2-in. CPF 4-900	2, 3	25-rayl FM, 1/2-in. CPF 4-900	4

[a] See sketch above for location of panels by number; panels not listed have solid sheet-aluminum surfaces

[b] Configuration codes in parentheses represent background noise tests run with airflow only, transducers off

TABLE XX. – SOUND PRESSURE LEVELS FROM 55% LIGHTBULB INLET DUCT TESTS

Conf. code	Chamber number	Sound-pressure level, dB re 0.0002 microbar						
		One-third octave-band center frequency, Hz						
(a)	(b)	1600	2000	2500	3150	4000	5000	6300
B1-1	1	125.0	123.0	118.0	110.5	103.0	98.5	98.5
	2	138.5	136.5	133.0	127.0	120.5	115.5	115.0
B1-2	1	130.5	128.5	123.5	117.0	109.5	103.5	103.5
	2	143.0	140.5	137.0	131.5	124.5	119.0	118.0
B1-3	1	130.0	127.5	122.5	116.5	108.5	102.0	102.0
	2	143.5	140.5	137.0	132.0	124.5	119.5	118.0
B1-4	1	130.0	127.0	123.0	118.0	109.5	103.0	102.0
	2	143.0	140.0	137.0	131.0	124.5	119.5	118.0
B1-5	1	129.0	127.5	124.0	118.0	110.0	103.5	101.5
	2	143.0	140.0	136.0	130.5	124.0	118.5	117.0
B1-6	1	130.0	128.0	124.0	118.0	109.5	103.0	102.0
	2	143.0	140.0	136.5	130.5	124.0	118.5	117.0
(B1-1)	1	99.5	97.5	96.5	95.0	92.5	91.0	91.5
	2	104.0	102.5	100.5	98.5	95.0	92.5	92.0
(B1-2)	1	94.0	93.0	92.5	90.5	88.5	87.5	88.0
	2	101.5	100.5	97.0	94.5	91.0	89.0	88.0
(B1-3)	1	89.5	88.0	86.5	84.0	81.5	82.5	83.0
	2	98.0	96.0	93.0	89.5	85.0	82.5	81.5
(B1-4)	1	84.0	82.0	80.0	77.5	75.0	74.0	75.0
	2	95.0	92.5	90.0	85.5	80.0	67.0	67.0
B2-1	1	——	119.0	114.5	108.5	102.0	97.5	98.0
	2	——	139.0	135.0	129.5	123.5	118.5	117.5
B2-2	1	——	119.0	115.0	109.5	103.0	98.5	98.0
	2	——	139.0	135.5	130.0	123.5	118.5	117.0
B3-1	1	118.0	116.5	112.5	106.5	100.0	96.0	96.5
	2	139.0	136.5	133.0	127.5	121.5	115.5	115.0
B3-2	1	120.0	117.5	113.0	108.0	101.0	96.5	96.5
	2	139.5	137.0	134.0	128.5	122.0	116.5	115.5
B4-1	1	115.5	112.5	108.5	102.5	97.5	93.5	95.0
	2	139.5	137.5	135.0	125.0	121.0	116.0	115.5
B4-2	1	117.0	114.5	109.5	104.0	98.5	93.5	95.0
	2	139.5	136.5	133.5	128.5	122.0	116.5	115.5
B5-1	1	115.5	113.5	109.5	103.5	98.5	94.0	94.5
	2	138.5	135.5	133.0	127.0	120.5	115.5	114.5
B5-2	1	116.0	114.0	110.5	105.0	98.5	93.5	93.5
	2	137.5	134.5	133.0	127.5	121.0	116.0	114.5
B6-1	1	115.5	114.0	110.0	104.0	98.5	94.0	95.0
	2	139.0	136.0	133.0	127.0	120.5	115.5	114.5
B6-2	1	117.0	115.5	111.5	105.5	98.5	94.0	94.5
	2	137.0	136.5	133.5	127.0	121.0	116.0	115.0
B7-1	1	116.5	114.0	110.0	105.0	99.5	95.5	95.5
	2	139.5	136.0	132.5	127.5	121.0	116.0	114.5
B7-2	1	117.0	115.0	111.0	105.5	99.5	95.0	95.5
	2	139.5	136.5	133.0	128.5	122.0	117.0	115.5
B8-1	1	114.5	112.5	108.0	101.5	97.0	93.5	95.0
	2	136.0	133.5	130.5	124.5	118.5	114.5	114.5
B8-2	1	118.0	115.0	111.5	102.5	96.5	92.0	93.5
	2	137.5	134.5	131.0	127.5	119.5	114.5	114.5
B9-1	1	122.0	120.0	——	110.5	104.5	99.0	99.0
	2	140.0	138.0	——	128.0	122.0	116.5	115.0
B9-2	1	122.5	120.0	——	111.0	104.5	99.0	98.0
	2	140.0	137.5	——	128.5	122.5	117.5	115.5
B10-1	1	117.0	115.0	110.5	104.5	99.5	100.5	96.5
	2	137.0	134.0	131.0	124.5	118.5	119.5	114.5
B10-2	1	116.5	116.5	112.5	107.0	100.0	96.0	96.0
	2	137.0	134.0	130.5	125.5	119.5	115.0	114.5
B11-1	1	118.5	116.5	112.5	106.5	101.0	97.0	97.0
	2	139.5	137.5	134.5	128.5	122.0	117.0	115.0
B11-2	1	120.0	117.5	113.5	109.5	100.5	96.5	96.0
	2	140.0	137.5	134.0	128.5	122.5	117.5	115.0
B12-1	1	115.0	113.0	109.0	103.0	97.0	93.0	93.0
	2	138.5	136.5	133.0	127.0	120.5	115.5	114.0
B12-2	1	115.0	113.0	109.0	103.0	97.0	93.0	93.0
	2	138.5	136.5	133.0	127.0	120.5	115.5	114.0
B12-3	1	119.0	116.0	112.5	105.5	97.5	93.0	94.0
	2	140.0	137.0	134.0	128.5	122.0	117.0	115.5
B12-4	1	119.0	116.5	113.5	106.5	98.5	93.5	93.5
	2	140.0	136.5	133.5	128.0	122.0	117.0	115.0
B12-5	1	119.5	116.5	114.0	107.0	98.0	93.0	93.5
	2	140.0	136.5	133.5	127.5	121.0	116.0	114.5
B12-6	1	120.0	119.0	114.0	107.0	98.5	93.0	92.5
	2	139.0	136.0	133.0	127.5	121.0	115.5	114.0
B13-1	1	115.5	112.5	109.5	103.5	98.0	93.5	94.5
	2	138.5	136.0	133.0	127.5	121.0	115.5	115.0
B13-2	1	118.0	116.5	111.0	104.0	98.0	93.5	93.5
	2	139.5	136.5	133.5	128.0	121.5	116.5	115.0
B14-1	1	117.0	115.0	110.0	104.5	98.0	93.0	——
	2	139.0	136.0	131.5	126.0	118.5	113.5	111.5
B14-2	1	118.5	117.0	111.5	106.0	98.0	93.5	92.5
	2	139.0	135.5	132.0	125.5	118.5	114.0	111.5
B15-1	1	120.0	118.0	113.0	106.5	100.0	95.5	96.0
	2	139.5	136.5	133.0	127.5	120.5	115.5	115.5
B15-2	1	121.0	118.0	113.5	108.0	100.5	95.5	95.0
	2	140.0	137.0	133.0	128.0	121.0	116.5	114.0

Conf. code	Chamber number	Sound-pressure level, dB re 0.0002 microbar						
		One-third octave-band center frequency, Hz						
(a)	(b)	1600	2000	2500	3150	4000	5000	6300
B16-1	1	114.5	111.5	108.5	103.0	98.0	94.0	95.0
	2	139.5	136.5	132.5	127.5	121.0	116.5	115.0
B16-2	1	116.5	113.5	109.5	103.5	98.0	94.0	94.0
	2	139.5	136.5	133.0	128.0	121.5	117.0	115.5
B17-1	1	111.0	111.5	108.5	102.5	98.0	93.5	94.5
	2	136.5	136.0	133.0	127.0	121.0	115.5	115.0
B17-2	1	114.5	112.5	109.0	103.0	96.5	92.5	93.5
	2	139.0	136.5	133.0	128.0	121.5	116.0	115.0
B18-1	1	114.0	113.0	109.5	103.0	98.0	94.5	95.5
	2	138.0	135.5	131.5	125.0	118.5	113.5	112.5
B18-2	1	115.5	114.0	110.5	104.0	98.5	94.0	94.5
	2	137.5	135.0	132.0	126.0	119.5	114.0	112.5
B19-1	1	112.0	109.0	105.5	99.5	95.5	91.5	93.5
	2	136.5	134.0	131.0	124.5	119.0	114.5	115.0
B19-2	1	113.5	110.5	106.5	100.0	94.5	90.5	92.0
	2	137.0	134.5	131.0	125.5	117.5	115.5	115.0
B20-1	1	114.0	111.0	108.0	103.0	——	92.0	93.0
	2	140.0	137.0	133.5	128.5	——	116.5	114.0
B20-2	1	115.0	111.5	108.0	102.5	97.5	——	95.0
	2	140.0	137.5	134.0	128.5	122.5	——	115.0
B20-3	1	117.0	114.5	110.0	104.0	98.0	93.0	93.5
	2	139.5	137.5	134.5	128.5	123.5	117.5	116.0
B20-4	1	117.5	115.5	110.0	104.5	98.0	92.5	93.0
	2	139.5	137.0	134.0	128.5	122.5	116.5	115.0
B20-5	1	117.0	114.0	111.0	106.0	99.0	92.0	93.5
	2	139.5	136.0	133.5	128.0	122.0	116.0	115.0
B20-6	1	117.5	115.0	110.5	105.0	98.0	92.5	92.5
	2	139.5	136.5	133.5	128.0	122.0	116.0	114.5
B21-1	1	110.5	107.5	106.0	101.0	96.5	93.0	95.5
	2	139.0	135.5	134.0	128.5	122.0	117.5	118.0
B21-2	1	114.5	111.5	107.0	98.5	96.5	92.5	94.5
	2	139.0	136.5	135.5	128.5	122.5	118.0	117.5
B22-1	1	113.5	111.5	107.5	101.5	96.5	92.5	94.5
	2	139.5	136.5	133.5	127.5	122.0	117.5	117.0
B22-2	1	116.5	113.5	109.5	103.0	96.5	92.5	94.0
	2	139.5	137.0	133.5	128.5	122.5	118.0	117.5
B23-1	1	113.5	111.0	108.0	102.5	98.0	94.0	94.5
	2	138.5	136.5	133.5	127.5	121.5	116.0	115.0
B23-2	1	115.5	112.0	108.5	103.0	96.5	92.5	93.5
	2	139.0	136.5	133.0	127.5	121.5	116.0	114.5
B23-3	1	117.0	113.5	109.5	104.5	97.0	92.0	93.0
	2	139.0	136.5	133.0	127.5	122.0	116.5	115.0
B23-4	1	116.5	115.0	109.5	104.5	97.0	92.0	92.5
	2	139.0	136.5	133.5	128.0	122.0	116.0	114.5
B23-5	1	114.5	113.5	109.0	104.0	97.5	91.5	91.5
	2	139.0	136.0	135.0	128.0	121.5	115.5	114.0
B23-6	1	116.5	114.0	109.0	104.0	97.0	91.0	91.0
	2	139.0	136.0	135.0	127.5	121.5	115.5	113.5
B24-1	1	123.5	120.0	116.0	109.0	102.0	97.5	98.5
	2	139.5	136.5	133.5	127.5	121.0	116.5	115.5
B24-2	1	125.5	122.5	118.0	110.5	103.5	98.0	98.5
	2	140.0	137.0	133.5	128.0	122.0	116.5	115.5
B25-1	1	123.0	120.5	117.5	110.5	101.5	97.5	98.0
	2	137.0	136.5	135.5	127.5	121.0	116.0	115.0
B25-2	1	124.5	122.0	117.0	111.0	103.0	98.0	98.5
	2	139.5	137.0	133.5	127.5	122.0	116.5	115.5
B26-1	1	122.0	119.0	114.5	108.0	101.5	97.5	98.0
	2	138.0	135.5	132.0	127.0	120.5	116.0	115.5
B26-2	1	122.0	119.5	115.5	108.5	101.5	96.0	98.0
	2	138.5	135.5	132.0	126.5	120.0	115.5	115.0
B27-1	1	120.0	118.0	114.5	109.0	104.0	100.0	102.0
	2	139.0	137.0	134.0	129.0	123.5	118.5	118.0
B27-2	1	122.0	120.5	116.5	111.0	105.5	101.5	102.5
	2	139.5	137.0	134.0	129.0	124.0	119.5	118.5
B28-1	1	116.5	114.5	110.5	104.5	99.0	95.5	96.5
	2	137.5	135.0	131.5	126.0	120.0	115.5	115.0
B28-2	1	119.0	114.5	112.0	105.5	99.5	95.5	96.5
	2	138.0	135.5	131.5	125.5	120.0	115.0	115.0
B29-1	1	116.5	114.0	111:0	105.5	101.0	95.5	100.0
	2	138.0	135.5	132.5	127.5	122.5	118.0	118.0
B29-2	1	117.0	117.0	114.0	108.0	103.0	98.5	100.5
	2	137.0	136.5	133.5	128.5	123.0	118.5	117.5
B30-1	1	116.0	113.5	110.0	104.5	99.5	96.5	98.5
	2	138.5	136.0	133.5	128.5	122.5	118.0	117.5
B30-2	1	116.5	115.0	111.5	106.0	101.0	97.0	98.0
	2	138.5	136.5	133.5	128.5	122.5	118.5	119.5
B31-1	1	114.0	112.0	109.0	104.0	100.0	96.5	99.0
	2	139.0	136.0	133.5	128.5	122.5	118.0	117.5
B31-2	1	116.0	115.0	112.0	107.0	102.0	98.5	99.5
	2	139.0	136.5	133.5	128.5	123.0	118.5	118.0
B32-1	1	113.5	111.5	109.0	103.0	99.0	96.0	98.5
	2	138.0	136.0	133.0	127.5	122.5	118.0	118.0
B32-2	1	116.0	113.5	109.5	104.5	99.5	96.0	98.5
	2	138.5	136.0	133.5	128.0	122.0	118.5	117.5

[a] See Table XXII for explanation of configuration code

[b] Chamber number 1 is the upstream or sound receiver chamber, chamber number 2 is the downstream or sound source chamber

TABLE XXI. – SOUND-PRESSURE LEVELS FROM 75% LIGHTBULB INLET DUCT TESTS

Conf. Code (a)	Chamber number (b)	Sound-pressure level, dB re 0.0002 microbar, One-third octave-band center frequency, Hz						
		1600	2000	2500	3150	4000	5000	6300
D1-1	1	124.5	121.0	117.0	110.5	104.5	101.0	102.0
	2	140.5	138.0	135.5	129.5	123.5	119.0	116.0
D1-2	1	126.5	123.5	119.0	113.5	107.5	103.0	103.5
	2	141.5	139.0	135.5	130.0	124.0	118.5	118.0
D1-3	1	127.0	123.5	119.0	113.0	107.5	101.0	101.0
	2	139.5	137.0	133.5	128.5	123.5	118.5	117.0
D1-4	1	127.5	124.5	120.0	115.0	108.0	102.5	102.0
	2	140.5	137.5	134.0	129.0	123.5	118.5	117.0
D1-5	1	126.5	124.5	120.0	115.0	109.0	103.5	102.0
	2	140.0	137.5	133.5	129.0	123.0	118.0	116.5
D1-6	1	127.0	124.5	120.0	115.0	109.5	104.0	102.5
	2	139.5	137.0	133.0	128.5	122.5	117.5	116.5
(D1-1)	1	99.5	98.5	97.5	96.0	94.0	93.0	94.5
	2	104.0	103.0	101.0	99.0	97.0	95.0	94.0
(D1-2)	1	93.5	91.0	91.0	90.0	88.0	86.5	88.5
	2	101.0	99.0	96.0	93.0	90.0	88.0	88.0
(D1-3)	1	87.0	85.0	84.0	82.5	80.0	80.5	83.0
	2	97.5	94.5	92.0	89.0	84.5	81.5	81.0
(D1-4)	1	82.0	80.5	78.5	76.5	76.0	75.0	78.5
	2	94.0	92.0	89.5	85.0	80.0	77.5	79.0
(D1-5)	1	78.0	75.5	72.5	70.5	68.0	67.0	69.0
	2	91.0	89.0	86.0	82.0	76.0	71.0	69.0
(D1-6)	1	73.5	71.0	68.0	65.0	61.0	59.5	60.0
	2	87.0	85.0	81.5	77.0	71.0	66.5	62.5
D2-1	1	117.0	114.5	112.0	106.5	101.0	97.0	99.0
	2	138.5	136.5	133.5	128.5	122.0	117.5	117.0
D2-2	1	117.0	115.0	112.5	108.0	101.5	98.0	99.5
	2	136.5	133.0	130.5	125.5	120.0	115.0	114.0
D3-1	1	115.5	113.0	110.5	107.0	101.0	97.5	99.0
	2	139.5	136.5	133.0	129.0	122.5	119.0	118.0
D3-2	1	115.5	114.5	111.5	107.0	102.0	98.0	99.5
	2	137.5	135.0	132.0	127.0	121.5	117.0	116.0
D4-1	1	111.5	110.0	107.5	101.0	96.5	93.0	95.5
	2	141.0	138.0	134.5	129.5	123.0	118.5	118.0
D4-2	1	113.5	111.0	108.0	101.0	95.0	92.0	93.5
	2	141.5	138.5	135.5	130.0	123.5	119.0	117.5
D5-1	1	110.5	108.5	106.0	101.0	96.0	92.5	95.0
	2	141.0	138.5	135.0	129.5	123.5	119.0	118.5
D5-2	1	112.5	111.0	107.0	101.0	95.0	91.0	93.0
	2	141.5	139.0	136.0	130.0	124.0	119.0	118.0
D5-3	1	112.5	112.0	108.0	101.5	94.0	90.0	92.0
	2	141.5	139.0	136.0	131.0	125.0	120.5	119.0
D5-4	1	113.0	113.0	110.0	102.5	95.0	89.0	91.0
	2	142.5	139.0	136.0	131.0	124.5	119.5	118.0
D5-5	1	113.0	112.0	109.5	102.0	94.0	89.0	90.0
	2	141.5	139.0	135.5	130.5	124.0	119.0	117.5
D5-6	1	113.0	113.0	107.5	101.0	93.0	87.5	88.5
	2	141.5	138.5	135.5	129.5	123.5	117.5	116.0
D6-1	1	114.5	113.0	110.0	104.5	99.0	95.0	97.0
	2	141.0	138.0	134.5	130.0	123.5	118.5	118.5
D6-2	1	116.0	114.5	111.5	106.0	100.0	95.5	97.0
	2	140.5	137.5	134.5	130.0	124.0	119.0	118.0

[a] See table XVIII for explanation of configuration code

[b] Chamber number 1 is the upstream or sound receiver chamber, chamber number 2 is the downstream or sound source chamber

TABLE XXII. – SOUND-PRESSURE LEVELS FROM STANDARD DC-8 INLET DUCT TESTS

Conf. Code (a)	Chamber number (b)	Sound-pressure level, dB re 0.0002 microbar						
		One-third octave-band center frequency, Hz						
		1600	2000	2500	3150	4000	5000	6300
C1-1	1	124.5	125.5	121.0	114.5	107.5	103.0	103.0
	2	136.0	137.0	133.0	127.0	121.0	117.0	116.0
C1-2	1	129.0	128.0	124.5	118.5	110.0	104.0	103.0
	2	139.0	136.5	134.0	128.0	121.5	116.5	114.5
C1-3	1	128.5	127.0	123.0	118.5	111.0	104.0	104.0
	2	138.5	136.0	133.0	128.5	122.5	117.5	116.0
C1-4	1	130.5	128.5	124.0	118.5	111.5	105.5	104.5
	2	140.0	137.5	134.5	128.5	123.0	117.5	115.5
C1-5	1	130.5	128.0	125.0	119.5	113.0	106.5	104.5
	2	140.0	138.0	134.5	129.0	122.5	117.5	115.5
C1-6	1	129.5	127.5	124.0	118.0	112.0	105.5	103.5
	2	140.5	138.0	134.0	129.0	123.5	118.0	115.5
(C1-1)	1	98.0	96.5	95.5	95.0	94.5	94.5	96.5
	2	104.0	102.0	100.0	98.5	95.5	94.0	93.0
(C1-2)	1	92.5	91.5	91.5	91.0	90.5	90.5	91.5
	2	100.0	97.5	95.5	93.5	90.5	88.5	86.5
(C1-3)	1	88.5	88.5	87.5	87.5	86.0	85.5	87.5
	2	96.5	94.0	91.5	89.5	85.5	83.0	82.5
(C1-4)	1	84.5	83.5	83.0	81.5	80.0	80.5	81.5
	2	94.0	92.5	89.5	85.5	81.0	77.5	77.5
(C1-5)	1	81.5	79.5	76.5	74.5	71.5	70.0	70.5
	2	91.5	89.5	83.5	80.5	75.0	70.0	67.5
(C1-6)	1	77.0	75.5	72.5	69.5	64.5	61.5	61.5
	2	91.5	89.5	84.5	82.0	75.5	72.5	72.0
C2-1	1	125.0	123.0	119.5	114.0	107.5	102.5	101.0
	2	138.5	136.5	133.5	128.5	122.5	118.0	116.0
C2-2	1	128.0	124.5	121.0	115.0	110.5	103.0	103.0
	2	139.5	136.5	134.0	129.0	122.5	117.5	116.0
C3-1	1	122.0	119.0	115.0	110.5	103.5	99.0	101.0
	2	141.0	137.5	134.5	129.5	122.5	118.0	117.5
C3-2	1	124.5	121.5	117.5	111.5	104.5	100.5	100.5
	2	141.0	137.5	135.0	129.5	123.0	118.5	116.5
C4-1	1	127.0	124.5	120.0	113.5	107.5	102.5	103.0
	2	143.0	140.0	137.0	131.5	125.0	119.5	118.5
C4-2	1	128.0	126.0	122.5	116.0	108.0	102.5	102.5
	2	143.5	140.5	137.5	132.0	125.5	120.0	118.5
C5-1	1	124.5	122.0	118.5	112.0	106.5	102.0	102.5
	2	143.0	140.0	137.5	131.5	125.5	120.5	119.0
C5-2	1	126.5	124.0	120.5	114.0	107.0	102.0	102.0
	2	143.5	140.5	137.5	132.0	126.0	121.0	119.0
C6-1	1	121.5	119.0	112.0	108.0	103.0	98.5	99.0
	2	140.0	137.5	132.0	129.0	123.0	118.5	118.0
C6-2	1	123.5	120.5	117.5	111.0	104.0	99.5	99.0
	2	141.0	137.5	135.0	129.5	124.0	119.5	118.0
C6-3	1	124.0	121.0	118.0	112.0	104.5	98.5	98.5
	2	141.0	137.5	135.0	129.5	124.5	119.5	118.0
C6-4	1	125.0	122.5	119.0	113.0	106.0	99.5	98.5
	2	141.0	137.5	135.5	130.5	124.5	120.0	118.0
C6-5	1	125.0	122.0	118.0	112.5	105.5	99.0	97.5
	2	141.5	138.0	135.5	130.0	124.0	119.5	117.5
C6-6	1	124.0	121.5	118.0	112.5	106.0	100.0	98.0
	2	140.5	138.0	135.0	130.0	124.5	119.0	117.0
C7-1	1	126.5	123.5	119.5	113.5	107.5	103.0	103.0
	2	143.0	140.0	137.0	131.5	125.0	120.0	118.5
C7-2	1	128.0	125.5	121.5	115.5	108.0	103.0	103.0
	2	143.5	140.5	137.0	131.5	125.5	120.5	119.0
C8-1	1	127.0	124.5	120.5	113.5	106.5	103.5	103.5
	2	141.0	138.5	136.0	130.5	124.5	119.5	118.5
C8-2	1	128.0	126.5	122.0	115.5	108.0	102.5	102.0
	2	141.5	138.5	136.0	130.5	124.5	119.5	118.5
C9-1	1	125.5	123.0	119.0	112.5	106.0	101.5	102.0
	2	140.5	137.5	135.0	130.0	123.0	118.5	117.5
C9-2	1	127.5	124.5	120.5	114.5	107.5	102.5	103.0
	2	141.5	138.5	135.0	130.0	123.5	118.5	117.5
C10-1	1	124.5	122.0	117.5	111.5	105.5	101.0	102.0
	2	140.5	138.0	134.5	129.5	123.5	118.5	117.5
C10-2	1	126.5	123.0	119.5	113.0	106.5	101.5	102.0
	2	141.5	138.0	135.0	129.5	123.5	118.5	117.5
C11-1	1	124.5	121.0	117.0	——	105.0	100.5	101.5
	2	140.0	138.0	135.0	——	123.5	118.5	117.5
C11-2	1	126.5	123.0	119.0	112.5	106.0	101.5	102.0
	2	142.0	133.5	135.5	130.0	124.0	119.5	118.0
C12-1	1	123.0	120.0	116.0	110.5	104.5	100.5	101.5
	2	138.5	137.5	135.0	129.5	123.5	118.5	118.0
C12-2	1	125.5	121.5	118.5	112.0	105.5	101.0	101.5
	2	141.5	138.0	135.5	130.0	124.5	119.0	118.5

[a]See table XIX for explanation of configuration code

[b]Chamber number 1 is the upstream or sound receiver chamber, chamber number 2 is the downstream or sound source chamber

TABLE XXIII. — TRANSMISSION LOSS VALUES FROM 55% LIGHTBULB INLET DUCT TESTS

Conf. code	Transmission loss, dB						
	One-third octave-band center frequency, Hz						
(a)	1600	2000	2500	3150	4000	5000	6300
B1-1	13.5	13.5	15.0	16.5	17.5	17.0	16.5
B1-2	12.5	12.0	13.5	14.5	15.0	15.5	14.5
B1-3	13.5	13.0	14.5	15.5	16.0	17.5	16.0
B1-4	13.0	13.0	14.0	13.5	15.0	16.5	16.0
B1-5	14.0	12.5	12.0	12.5	14.0	15.0	15.5
B1-6	13.0	12.0	12.5	12.5	14.5	15.5	15.0
B2-1	——	20.0	20.5	21.0	21.5	21.0	19.5
B2-2	——	20.0	20.5	20.5	20.5	20.0	19.0
B3-1	21.0	20.0	20.5	21.0	21.5	19.5	18.5
B3-2	19.5	19.5	21.0	20.5	21.0	20.0	19.0
B4-1	24.0	25.0	26.5	22.5	23.5	22.5	20.5
B4-2	22.5	22.0	24.0	24.5	23.5	23.0	20.5
B5-1	23.0	22.0	23.5	23.5	22.0	21.5	20.0
B5-2	21.5	20.5	22.5	22.5	22.5	22.5	21.0
B6-1	23.5	22.0	23.0	23.0	22.0	21.5	19.5
B6-2	20.0	21.0	22.0	21.5	22.5	22.0	20.5
B7-1	23.0	22.0	22.5	22.5	21.5	20.5	19.0
B7-2	22.5	21.5	22.0	23.0	22.5	22.0	20.0
B8-1	21.5	21.0	22.5	23.0	21.5	21.0	19.5
B8-2	19.5	19.5	19.5	25.0	23.0	22.5	21.0
B9-1	18.0	18.0	——	17.5	17.5	17.5	16.0
B9-2	17.5	17.5	——	17.5	18.0	18.5	17.5
B10-1	20.0	19.0	20.5	20.0	19.0	19.0	18.0
B10-2	20.5	17.5	18.0	18.5	19.5	19.0	18.5
B11-1	21.0	21.0	22.0	22.0	21.0	20.0	18.0
B11-2	20.0	20.0	20.5	19.0	22.0	21.0	19.0
B12-1	23.5	23.5	24.0	24.0	23.5	22.5	21.0
B12-2	23.5	23.5	24.0	24.0	23.5	22.5	21.0
B12-3	21.0	21.0	21.5	23.0	24.5	24.0	21.5
B12-4	21.0	20.0	20.0	21.5	23.5	23.5	21.5
B12-5	20.5	20.0	19.5	20.5	23.0	23.0	21.0
B12-6	19.0	17.0	19.0	20.5	22.5	22.5	21.5
B13-1	23.0	23.5	23.5	24.0	23.0	22.0	20.5
B13-2	21.5	20.0	22.5	24.0	23.5	23.0	21.5
B14-1	22.0	21.0	21.5	21.5	20.5	20.5	——
B14-2	20.5	18.5	20.5	19.5	20.5	20.5	19.0
B15-1	19.5	18.5	20.0	21.0	20.5	20.0	19.5
B15-2	19.0	19.0	19.5	20.0	20.5	21.0	19.0
B16-1	25.0	25.0	24.0	24.5	23.0	22.5	20.0
B16-2	23.0	23.0	23.5	24.5	23.5	23.0	21.5

Conf. code	Transmission loss, dB						
	One-third octave-band center frequency, Hz						
(a)	1600	2000	2500	3150	4000	5000	6300
B17-1	25.5	24.5	24.5	24.5	23.0	22.0	20.5
B17-2	24.5	24.0	24.0	25.0	25.0	23.5	21.5
B18-1	24.0	22.5	22.0	22.0	20.5	19.0	17.0
B18-2	22.0	21.0	21.5	22.0	21.0	20.0	18.0
B19-1	24.5	25.0	25.5	25.0	23.5	23.0	21.5
B19-2	23.5	24.0	24.5	25.5	23.0	25.0	23.0
B20-1	26.0	26.0	25.5	25.5	——	24.5	21.0
B20-2	25.0	26.0	26.0	26.0	25.0	——	20.0
B20-3	22.5	23.0	24.5	24.5	25.5	24.5	22.5
B20-4	22.0	21.5	24.0	24.0	24.5	24.0	22.0
B20-5	22.5	22.0	22.5	22.5	23.0	24.0	21.5
B20-6	22.0	21.5	23.0	23.0	24.0	23.5	22.0
B21-1	28.5	28.0	28.0	27.5	25.5	24.5	22.5
B21-2	24.5	25.0	28.5	30.0	26.0	25.5	23.0
B22-1	26.0	25.0	26.0	26.0	25.5	25.0	22.5
B22-2	23.0	23.5	24.0	25.5	26.0	25.5	23.5
B23-1	25.0	25.5	25.5	25.0	23.5	22.0	20.5
B23-2	23.5	24.5	24.5	24.5	25.0	23.5	21.0
B23-3	22.0	23.0	23.5	23.0	25.0	24.5	22.0
B23-4	22.5	21.5	24.0	23.5	25.0	24.0	22.0
B23-5	24.5	22.5	26.0	24.0	24.0	24.0	22.5
B23-6	22.5	22.0	26.0	23.5	24.5	24.5	22.5
B24-1	16.0	16.5	17.5	18.5	19.0	19.0	17.0
B24-2	14.5	14.5	15.5	17.5	18.5	18.5	17.0
B25-1	14.0	16.0	18.0	17.0	19.5	18.5	17.0
B25-2	15.0	15.0	16.5	16.5	19.0	18.5	17.0
B26-1	16.0	16.5	17.5	19.0	19.0	18.5	17.5
B26-2	16.5	16.0	16.5	18.0	18.5	19.5	17.0
B27-1	19.0	19.0	19.5	20.0	19.5	18.5	16.0
B27-2	17.5	16.5	17.5	18.0	18.5	18.0	16.0
B28-1	21.0	20.5	21.0	21.5	21.0	20.0	18.5
B28-2	19.0	21.0	19.5	20.0	20.5	19.5	18.5
B29-1	21.5	21.5	21.5	22.0	21.5	20.5	18.0
B29-2	20.0	19.5	19.5	20.5	20.0	20.0	17.0
B30-1	22.5	22.5	23.5	24.0	23.0	21.5	19.0
B30-2	22.0	21.5	22.0	22.5	21.5	21.5	21.5
B31-1	25.0	24.0	24.5	24.5	22.5	21.5	18.5
B31-2	23.0	21.5	21.5	21.5	21.0	20.0	18.5
B32-1	24.5	24.5	24.0	24.5	23.5	22.0	19.5
B32-2	22.5	22.5	24.0	23.5	22.5	22.5	19.0

[a] See table XVII for explanation of configuration code

TABLE XXIV. – TRANSMISSION LOSS VALUES FROM 75% LIGHTBULB INLET DUCT TESTS

Conf. code (a)	Transmission loss, dB						
	One-third octave-band center frequency, Hz						
	1600	2000	2500	3150	4000	5000	6300
D1-1	16.0	17.0	18.5	19.0	19.0	18.0	14.0
D1-2	15.0	15.5	16.5	16.5	16.5	15.5	14.5
D1-3	12.5	13.5	14.5	15.5	16.0	17.5	16.0
D1-4	13.0	13.0	14.0	14.0	15.5	16.0	15.0
D1-5	13.5	13.0	13.5	14.0	14.0	14.5	14.5
D1-6	12.5	12.5	13.0	13.5	13.0	13.5	14.0
D2-1	21.5	22.0	21.5	22.0	21.0	20.5	18.0
D2-2	19.5	18.0	18.0	17.5	18.5	17.0	14.5
D3-1	24.0	23.5	22.5	22.0	21.5	21.5	19.0
D3-2	22.0	20.5	20.5	20.0	19.5	19.0	16.5
D4-1	29.5	28.0	27.0	28.5	26.5	25.5	22.5
D4-2	28.0	27.5	27.5	29.0	28.5	27.0	24.0
D5-1	30.5	30.0	29.0	28.5	27.5	26.5	23.5
D5-2	29.0	28.0	29.0	29.0	29.0	28.0	25.0
D5-3	29.0	27.0	28.0	29.5	31.0	30.5	27.0
D5-4	29.5	26.0	26.0	28.5	29.5	30.5	27.0
D5-5	28.5	27.0	26.0	28.5	30.0	30.0	27.5
D5-6	28.5	25.5	28.0	28.5	30.5	30.0	27.5
D6-1	26.5	25.0	24.5	25.5	24.5	23.5	21.5
D6-2	24.5	23.0	23.0	24.0	24.0	23.5	21.0

[a]See table XVIII for explanation of configuration code

TABLE XXV. — TRANSMISSION LOSS VALUES FROM STANDARD DC-8 INLET DUCT TESTS

Conf. code	Transmission loss, dB						
	One-third octave-band center frequency, Hz						
(a)	1600	2000	2500	3150	4000	5000	6300
C1-1	11.5	11.5	12.0	12.5	13.5	14.0	13.0
C1-2	10.0	8.5	9.5	9.5	11.5	12.5	11.5
C1-3	10.0	9.0	10.0	10.0	11.5	13.5	12.0
C1-4	9.5	9.0	10.5	10.0	11.5	12.0	11.0
C1-5	9.5	10.0	9.5	9.5	9.5	11.0	11.0
C1-6	11.0	10.5	10.0	11.0	11.5	12.5	12.0
C2-1	13.5	13.5	14.0	14.5	15.0	15.5	15 0
C2-2	11.5	12.0	13.0	14.0	12.0	14.5	13.0
C3-1	19.0	18.5	19.5	19.0	19.0	19.0	16.5
C3-2	16.5	16.0	17.5	18.0	18.5	18.0	16.0
C4-1	16.0	15.5	17.0	18.0	17.5	17.0	15.5
C4-2	15.5	14.5	15.0	16.0	17.5	17.5	16.0
C5-1	18.5	18.0	19.0	19.5	19.0	18.5	16.5
C5-2	17.0	16.5	17.0	18.0	19.0	19.0	17.0
C6-1	18.5	18.5	20.0	21.0	20.0	20.0	19.0
C6-2	17.5	17.0	17.5	18.5	20.0	20.0	19.0

Conf. code	Transmission loss, dB						
	One-third octave-band center frequency, Hz						
(a)	1600	2000	2500	3150	4000	5000	6300
C6-3	17.0	16.5	17.0	17.5	20.0	21.0	19.5
C6-4	16.0	15.0	16.5	17.5	18.5	20.5	19.5
C6-5	16.5	16.0	17.5	17.5	18.5	20.5	20.0
C6-6	16.5	16.5	17.0	17.5	18.5	19.0	19.0
C7-1	16.5	16.5	17.5	18.0	17.5	17.0	15.5
C7-2	15.5	15.0	15.5	16.0	17.5	17.5	16.0
C8-1	14.0	14.0	15.5	17.0	18.0	16.0	15.0
C8-2	13.5	12.0	14.0	15.0	16.5	17.0	16.5
C9-1	15.0	14.5	16.0	17.5	17.0	17.0	15.5
C9-2	14.0	14.0	14.5	15.5	16.0	16.0	14.5
C10-1	16.0	16.0	17.0	18.0	18.0	17.5	15.5
C10-2	15.0	15.0	15.5	16.5	17.0	17.0	15.5
C11-1	15.5	17.0	18.0	——	18.5	18.0	16.0
C11-2	15.5	15.5	16.5	17.5	18.0	18.0	16.0
C12-1	15.5	17.5	19.0	19.0	19.0	18.0	16.5
C12-2	16.0	16.5	17.0	18.0	19.0	18.0	17.0

[a]See table XIX for explanation of configuration code

TABLE XXVI.– ATTENUATION VALUES FROM 55% LIGHTBULB INLET DUCT TESTS

Conf. code (a)	Attenuation, dB: One-third octave-band center frequency, Hz						
	1600	2000	2500	3150	4000	5000	6300
B2-1	—	6.5	5.5	4.5	4.0	4.0	3.0
B2-2	—	8.0	7.0	6.0	5.5	4.5	4.5
B3-1	7.5	6.5	5.5	4.5	4.0	2.5	2.0
B3-2	7.0	7.5	7.5	6.0	6.0	4.5	4.5
B4-1	10.5	11.5	11.5	6.0	6.0	5.5	4.0
B4-2	10.0	10.0	10.5	10.0	8.5	7.5	6.0
B5-1	9.5	8.5	8.5	7.0	4.5	4.5	3.5
B5-2	9.0	8.5	9.0	8.0	7.5	7.0	6.5
B6-1	10.0	8.5	8.0	6.5	4.5	4.5	3.0
B6-2	7.5	9.0	8.5	7.0	7.5	6.5	6.0
B7-1	9.5	8.5	7.5	6.0	4.0	3.5	2.5
B7-2	10.0	9.5	8.5	8.5	7.5	6.5	5.5
B8-1	8.0	7.5	7.5	6.5	4.0	4.0	3.0
B8-2	7.0	7.5	6.0	10.5	8.0	7.0	6.5
B9-1	4.5	4.5	—	1.0	0.0	0.5	-0.5
B9-2	5.0	5.5	—	3.0	3.0	3.0	3.0
B10-1	6.5	5.5	5.5	3.5	1.5	2.0	1.5
B10-2	8.0	5.5	4.5	4.0	4.5	3.5	4.0
B11-1	7.5	7.5	7.0	5.5	3.5	3.0	1.5
B11-2	7.5	8.0	7.0	4.5	7.0	5.5	4.5
B12-1	10.0	10.0	9.0	7.5	6.0	5.5	4.5
B12-2	11.0	11.5	10.5	9.5	8.5	7.0	6.5
B12-3	7.5	8.0	7.0	7.5	8.5	6.5	5.5
B12-4	8.0	7.0	6.0	8.0	8.5	7.0	5.5
B12-5	6.5	7.5	7.5	8.0	9.0	8.0	5.5
B12-6	6.0	5.0	6.5	8.0	8.0	7.0	6.5
B13-1	9.5	10.0	8.5	7.5	5.5	5.0	4.0
B13-2	9.0	8.0	9.0	9.5	8.5	7.5	7.0
B14-1	8.5	7.5	6.5	5.0	3.0	3.5	—
B14-2	8.0	6.5	7.0	5.0	5.5	5.0	4.5
B15-1	6.0	5.0	5.0	4.5	3.0	3.0	3.0
B15-2	6.5	7.0	6.0	5.5	5.5	5.5	4.5
B16-1	11.5	11.5	9.0	8.0	5.5	5.5	3.5
B16-2	10.5	11.0	10.0	10.0	8.5	7.5	7.0
B17-1	12.0	11.0	9.5	8.0	5.5	5.0	4.0
B17-2	12.0	12.0	10.5	10.5	10.0	8.0	7.0
B18-1	10.5	9.0	7.0	5.5	3.0	2.0	0.5
B18-2	9.5	9.0	8.0	7.5	6.0	4.5	3.5
B19-1	11.0	11.5	10.5	8.5	6.0	6.0	5.0
B19-2	11.0	12.0	11.0	11.0	8.0	9.5	8.5
B20-1	12.5	12.5	10.5	9.0	—	7.5	4.5
B20-2	12.5	14.0	12.5	11.5	10.0	—	5.5
B20-3	9.0	10.0	10.0	9.0	9.5	7.0	6.5
B20-4	9.0	8.5	10.0	10.5	9.5	7.5	6.0
B20-5	8.5	9.5	10.5	11.0	9.0	9.0	6.0
B20-6	9.0	9.5	10.5	10.5	9.5	8.0	7.0
B21-1	15.0	14.5	13.0	11.0	8.0	7.5	6.0
B21-2	12.0	13.0	15.0	15.5	11.0	10.0	8.5
B22-1	12.5	11.5	11.0	9.5	8.0	8.0	6.0
B22-2	10.5	11.5	10.5	11.0	11.0	10.0	9.0
B23-1	11.5	12.0	10.5	8.5	6.0	5.0	4.0
B23-2	11.0	12.5	11.0	10.0	10.0	8.0	-6.5
B23-3	8.5	10.0	9.0	7.5	9.0	7.0	6.0
B23-4	9.5	8.5	10.0	10.0	10.0	7.5	6.0
B23-5	10.5	10.0	14.0	11.5	10.0	9.0	7.0
B23-6	9.5	10.0	13.5	11.0	10.0	9.0	7.5
B24-1	2.5	3.0	2.5	2.0	1.5	2.0	0.5
B24-2	2.0	2.5	2.0	3.0	3.5	3.0	2.5
B25-1	0.5	2.5	3.0	0.5	2.0	1.5	0.5
B25-2	2.5	3.0	3.0	2.0	4.0	3.0	2.5
B26-1	2.5	3.0	2.5	2.5	1.5	1.5	1.0
B26-2	4.0	4.0	3.0	3.5	3.5	4.0	2.5
B27-1	5.5	5.5	4.5	3.5	2.0	1.5	-0.5
B27-2	5.0	4.5	4.0	3.5	3.5	2.5	1.5
B28-1	7.5	7.0	6.0	5.0	3.5	3.0	2.0
B28-2	6.5	9.0	6.0	5.5	5.5	4.0	4.0
B29-1	8.0	8.0	6.5	5.5	4.0	3.5	1.5
B29-2	7.5	7.5	6.0	6.0	5.0	4.5	2.5
B30-1	9.0	9.0	8.5	7.5	5.5	4.5	2.5
B30-2	9.5	9.5	8.5	8.0	6.5	6.0	7.0
B31-1	11.5	10.5	9.5	8.0	5.0	4.5	2.0
B31-2	10.5	9.5	8.0	7.0	6.0	4.5	4.0
B32-1	11.0	11.0	9.0	8.0	6.0	5.0	3.0
B32-2	10.0	10.5	10.5	9.0	7.5	7.0	4.5

[a]See table XVII for explanation of configuration code

TABLE XXVII.– ATTENUATION VALUES FROM 75% LIGHTBULB INLET DUCT TESTS

Conf. code (a)	Attenuation, dB						
	One-third octave-band center frequency, Hz						
	1600	2000	2500	3150	4000	5000	6300
D2-1	5.5	5.0	3.0	3.0	2.0	2.5	4.0
D2-2	4.5	2.5	1.5	1.0	2.0	1.5	0.0
D3-1	8.0	6.5	4.0	3.0	2.5	3.5	5.0
D3-2	7.0	5.0	4.0	3.5	3.0	3.5	2.0
D4-1	13.5	11.0	8.5	9.5	7.5	7.5	8.5
D4-2	13.0	12.0	11.0	12.5	12.0	11.5	9.5
D5-1	14.5	13.0	10.5	9.5	8.5	8.5	9.5
D5-2	14.0	12.5	12.5	12.5	12.5	12.5	10.5
D5-3	16.5	13.5	13.5	14.0	15.0	13.0	11.0
D5-4	16.5	13.0	12.0	14.5	14.0	14.5	12.0
D5-5	15.0	14.0	12.5	14.5	16.0	15.5	13.0
D5-6	16.0	13.0	15.0	15.0	17.5	16.5	13.5
D6-1	10.5	8.0	6.0	6.5	5.5	5.5	7.5
D6-2	9.5	7.5	6.5	7.5	7.5	8.0	6.5

[a]See table XVIII for explanation of configuration code

TABLE XXVIII. – ATTENUATION VALUES FROM STANDARD DC-8 INLET DUCT TESTS

Conf. code (a)	Attenuation, dB						
	One-third octave-band center frequency, Hz						
	1600	2000	2500	3150	4000	5000	6300
C2-1	2.0	2.0	2.0	2.0	1.5	1.5	2.0
C2-2	1.5	3.5	3.5	4.5	0.5	2.0	1.5
C3-1	7.5	7.0	7.5	6.5	5.5	5.0	3.5
C3-2	6.5	7.5	8.0	8.5	7.0	5.5	4.5
C4-1	4.5	4.0	5.0	5.5	4.0	3.0	2.5
C4-2	5.5	6.0	5.5	6.5	6.0	5.0	4.5
C5-1	7.0	6.5	7.0	7.0	5.5	4.5	3.5
C5-2	7.0	8.0	7.5	8.5	7.5	6.5	5.5
C6-1	7.0	7.0	8.0	8.5	6.5	6.0	6.0
C6-2	7.5	8.5	8.0	9.0	8.5	7.5	7.5
C6-3	7.0	7.5	7.0	7.5	8.5	7.5	7.5
C6-4	6.5	6.0	6.0	7.5	7.0	8.5	8.5
C6-5	7.0	6.0	8.0	8.0	9.0	9.5	9.0
C6-6	5.5	6.0	7.0	6.5	7.0	6.5	7.0
C7-1	5.0	5.0	5.5	5.5	4.0	3.0	2.5
C7-2	5.5	6.5	6.0	6.5	6.0	5.0	4.5
C8-1	2.5	2.5	3.5	4.5	4.5	2.0	2.0
C8-2	3.5	3.5	4.5	5.5	5.0	4.5	5.0
C9-1	3.5	3.0	4.0	5.0	3.5	3.0	2.5
C9-2	4.0	5.5	5.0	6.0	4.5	3.5	3.0
C10-1	4.5	4.5	5.0	5.5	4.5	3.5	2.5
C10-2	5.0	6.5	6.0	7.0	5.5	4.5	4.0
C11-1	4.0	5.5	6.0	—	5.0	4.0	3.0
C11-2	5.5	7.0	7.0	8.0	6.5	5.5	4.5
C12-1	4.0	6.0	7.0	6.5	5.5	4.0	3.5
C12-2	6.0	8.0	7.5	8.5	7.5	5.5	5.5

[a]See table XIX for explanation of configuration code

NASA-Langley, 1968 — 28 CR-1056

"The aeronautical and space activities of the United States shall be conducted so as to contribute . . . to the expansion of human knowledge of phenomena in the atmosphere and space. The Administration shall provide for the widest practicable and appropriate dissemination of information concerning its activities and the results thereof."

—NATIONAL AERONAUTICS AND SPACE ACT OF 1958

NASA SCIENTIFIC AND TECHNICAL PUBLICATIONS

TECHNICAL REPORTS: Scientific and technical information considered important, complete, and a lasting contribution to existing knowledge.

TECHNICAL NOTES: Information less broad in scope but nevertheless of importance as a contribution to existing knowledge.

TECHNICAL MEMORANDUMS: Information receiving limited distribution because of preliminary data, security classification, or other reasons.

CONTRACTOR REPORTS: Scientific and technical information generated under a NASA contract or grant and considered an important contribution to existing knowledge.

TECHNICAL TRANSLATIONS: Information published in a foreign language considered to merit NASA distribution in English.

SPECIAL PUBLICATIONS: Information derived from or of value to NASA activities. Publications include conference proceedings, monographs, data compilations, handbooks, sourcebooks, and special bibliographies.

TECHNOLOGY UTILIZATION PUBLICATIONS: Information on technology used by NASA that may be of particular interest in commercial and other non-aerospace applications. Publications include Tech Briefs, Technology Utilization Reports and Notes, and Technology Surveys.

Details on the availability of these publications may be obtained from:

SCIENTIFIC AND TECHNICAL INFORMATION DIVISION
NATIONAL AERONAUTICS AND SPACE ADMINISTRATION
Washington, D.C. 20546